UNIVERSITY OF SOUTHAMPTON

FACULTY OF ENGINEERING AND APPLIED SCIENCE

DEPARTEMENT OF CIVIL ENGINNERING

THE COUPLING OF THE DIRECT BOUNDARY ELEMENT METHOD WITH THE FINITE ELEMENT DISPLACEMENT TECHNIQUE IN ELASTOSTATICS

by: PANOS GEORGIOU

A Thesis Submitted for the Degree of

Doctor of Philosophy

May 1981

CONTENTS

UNIVERSITY OF SOUTHAMPTON

FACULTY OF ENGINEERING AND APPLIED SCIENCE

DEPARTMENT OF CIVIL ENGINEERING

THE COUPLING OF THE DIRECT BOUNDARY ELEMENT METHOD WITH THE FINITE ELEMENT DISPLACEMENT TECHNIQUE IN ELASTOSTATICS

by: PANOS GEORGIOU

ABSTRACT

This work is concerned with the formation of an 'equivalent' stiffness matrix for a body, using a Direct Boundary Element Method approach, which only requires a surface discretisation. This 'equivalent' stiffness matrix may then be treated in the same way as a Finite Element, and coupled into a global Finite Element formulation.

The, thus derived, equivalent stiffness matrix is not found to exhibit the inherent symmetry properties generally expected of a stiffness formulation, and this problem is examined in depth. A simple symmetrisation process is adopted, the validity and accuracy of which is also examined in the context of the overall symmetry considerations.

The difficulties arising due to surface geometry discontinuities are also examined, and a technique is proposed for their solution. This is implemented for 2-Dimensional problems, but may readily be extended to 3-Dimensions.

3-Dimensional problems involving finite and semi-infinite regions are treated using constant Boundary Elements, and both constant and linear element formulations are presented for the 2-D case.

Finally an explicit formulation is presented for a 2-D half-space, loaded at the free surface, using constant, linear or quadratic elements, which does away with the necessity of numerical integration.

ACNOWLEDGEMENTS

I would like to thank my supervisor, Dr. C.A.Brebbia for his guidance during the course of this work. Thanks are also due to Joseph Telles, Luiz Wrobel, Mike Kavanagh, Roberto Nakaguma, Mike Bloom, Wilson Venturini, John Walters, Webe Mansur, Dr. James Nelson and Dr. Kolbane Bell who all provided, at various times, a very patient 'sounding board' for many of the ideas implemented in this work, and whose helpful criticism proved invaluable.

A special mention is deserved for my parents, Nicos and Anthoulla Georgiou, without whose very generous support, both moral and financial, this work would not have been possible.

Finally, I would like to thank Mrs. Hazel Paul for her expert and accurate typing of this thesis.

This research was carried out whilst in receipt of an SRC studentship.

NOTATION

$x_1\ x_2\ x_2$	Global cartesian coordinates
σ_{ij}	Stress components
$\underset{\sim}{\sigma}$	Stress vector
ε_{ij}	Strain components
$\underset{\sim}{\varepsilon}$	Strain vector
p_i, $\underset{\sim}{p}$	Traction, components and vector
u_i, $\underset{\sim}{u}$	Displacement, components and vector
b_i, $\underset{\sim}{b}$	Body forces, components and vector
n_i, $\underset{\sim}{n}$	Unit normal, components and vector
$C_{ijk\ell}$, $\underset{\sim}{C}$	Elastic compliances, tensor and matricial form
$D_{ijk\ell}$, $\underset{\sim}{D}$	Rigidity Coefficients, tensor and matricial form
E	Modulus of Elasticity
ν	Poisson Ratio
G	Shear Modulus
$f_{i,j}$	Derivative notation, $= \frac{\partial f_i}{\partial x_j}$
Ω	Volume of body for 3-D
	Area of body for 2-D - Domain
Γ	Boundary of body- Surface
Π	Energy functional
$L(u)$, $D(u)$ $S(u)$, $G(u)$	General linear differential operators
ε, ε_1, ε_2	Error functions
w	General weighting function
u^*_k, $\underset{\sim}{u}^*$	Fundamental Solution for displacements - component and matrical forms.
p^*_k, $\underset{\sim}{p}^*$	Fundamental Solution for Tractions - component and matricial forms
X	Source Point
Y	Field Point

r_i, $\underset{\sim}{r}$	Vector between Source point and Field point
r	Distance between Source point and Field point
α_i	Constants involved in 2-D Boussinesq Solution
$\underset{\sim}{\Psi}$, $\underset{\sim}{\Phi}$	Interpolation functions
ξ, η	Local coordinates
$c^i_{\ell k}$, $\underset{\sim}{c}^i$	Coefficients of free term relating to point 'i'
$\underset{\sim}{H}$, $\underset{\sim}{G}$	Global Boundary Element Matrices
$h^{ij}_{\ell k}$, $g^{ij}_{\ell k}$	Submatrices of $\underset{\sim}{H}$ and $\underset{\sim}{G}$ representing integrals of the influence at 'j' due to a source at 'i'
$\underset{\sim}{U}$	Global vector containing nodal values of displacements
$\underset{\sim}{P}$	Global Vector containing nodal vlues of tractions
$\underset{\sim}{F}$	Global Vector containing equivalent nodal forces
$\underset{\sim}{B}$	Global Vector containing nodal values of body forces
$\underset{\sim}{K}$	Finite Element type stiffness matrix
$\underset{\sim}{K}^u$	'Equivalent' Stiffness matrix derived from B.E.M. (generally unsymmetric)
$\underset{\sim}{K}^s$	Symmetrised form of $\underset{\sim}{K}^u$.
$\underset{\sim}{M}$	Matrix relating nodal values of traction to equivalent their equivalent nodal forces.

CHAPTER 1 - INTRODUCTION

In recent years, the Boundary Element Method (B.E.M.) has increasingly been presented as a powerful alternative to existing techniques for the solution of problems in continuum mechanics. (e.g. Brebbia [4], Cruse [8], Lachat and Watson [26]).

The Boundary Element Method involves the transformation of the governing differential equations within the domain under consideration, to an integral equation defined on the surface of the domain, thus enabling the reduction of the dimensionality of the problem by one. The surface may then be discretised into a number of 'elements' over which a polynomial form of the solution is assumed; this enables the evaluation of the relevant integrals, usually by some numerical process, resulting in a final system of linear algebraic equations. The advantages of the method are readily apparent and have been extensively discussed and demonstrated in the literature. (e.g. Cruse [13],[28], [40], Nakaguma [10], Tottenham [39]). As only the surface of the domain need be discretised, the resulting systems of equations are considerably smaller than those involving domain type solutions (e.g . Finite Elements,Finite Differences), and considerable savings can also be achieved in the time required for data preparation. A very important implication of the method is that there is no interpolation of the solution within the domain, and for a given solution on the surface, results at interior points involve no approximations.

The key to the method, in stress analysis applications, is the adoption of an analytical point load (fundamental) solution which is used to eliminate the domain integral from the formulation. The first such solution was developed by Lord Kelvin and following this, work by Flamant [15], Boussinesq [16], Melan [14], Mindlin [7], produced

solutions for semi-infinite domains in both 2 and 3 dimensions.

Some of the earliest work using boundary integral equations in elasticity was undertaken by the mathematician Muskhelishvili [47] as early as 1953. The late 60's saw work by Rizzo [34] in the analysis of 2 dimensional elastostatic problems and by Curse and Rizzo [45] in the analysis of transient elastodynamic problems, who used the boundary representation of the governing equations originally derived by Somigliana [50] in 1885.

In 1969 Cruse [13] presented a formulation for 3 dimensional elastostatic problems using the Kelvin fundamental solution and was to instigate what we know today as the 'Direct Boundary Element Method'. This work, however, employed elements over which the variables were assumed to be constant, but work soon followed postulating the use of localised shape functions to allow for higher order representation of the dependant variables (see Lachat [48]).

An alternative implementation of the Kelvin solution was first proposed by Kupradze [46] in 1965, thus establishing the foundations of the Indirect Boundary Element Method, but subsequent investigation has demonstrated the equivalence of the two techniques (e.g. see Brebbia and Butterfield [51]).

The last decade or so, has seen a great deal of research in the use of boundary element methods for the solution of problems in many fields of continuun mechanics and it is impossible to refer to all relevant or related works directly. As such for a more general background to developments and different applications of boundary element methods, the reader is referred to the bibliography at the end of this work.

There are however, many classes of problems, for which the B.E.M. is unsuitable, or for which its relative advantages over domain solutions (in particular, Finite Elements) are not sufficiently pronounced to outweight its disadvantages. The B.E.M. often involves a very time consuming numerical integration process and results in a system of equations, which although relatively small, is fully populated and unbanded. Problems with a large surface to volume ratio, or problems involving rapid variation of dependent parameters (e.g. material properties) may be more amenable to solutions using Finite Elements. Also, the B.E.M., is restricted to classes of problems for which fundamental (or point load) solutions are available, and this often makes the application to highly anisotropic fields very difficult. It would appear therefore, that an examination of Boundary and Finite Elements should be carried out from a point of view of compatibility rather than competitiveness.

The Finite Element Method (F.E.M.) is very well established and understood (e.g. see Brebbia [20], Zienkiewicz [30], [41]) and an extensive range of computer packages are readily available for its implementation.

Following some of the early work in Boundary Elements, more recent work has demonstrated the relationship between the B.E.M. and F.E.M., and it has been shown that they may both be derived as special cases of a much more general method - the Weighted Residual Technique (see Finlayson [6], Brebbia [11]). It is therefore possible to transform a Boundary Element formulation to an 'equivalent' Finite Element model, and vice-versa (e.g. see Brebbia and Georgiou [24]. Georgiou [43], Kelly [36]).

Given the establishment, wide acceptance, and ready availability of computer codes for the implementation of the F.E.M., it would be very useful to be able to treat a problem (or part, thereof) using Boundary Elements, where amenable, and transforming the formulation to an 'equivalent' stiffness relation, which may then readily be incorporated into an overall Finite Element system, in the usual way. It is this which is the objective of the present work.

In the last few years there has been a fair amount of work concerned with the combination of Finite and Boundary Element techniques (e.g. Zienkiewicz, Kelly and Bettess [29], [31], Fusco [42], Georgiou [43], [44] Mustoe [22], [36], [49], Shaw [52], [53]). However, the lack of symmetry of the Boundary Element method is also reflected in the fact that an 'equivalent' stiffness relation based on the B.E.M. is also unsymmetric. There have been several attempts to 'symmetrise' this 'equivalent' stiffness matrix, but the arguments presented to justify this are far from conclusive, and usually rest on the notion that any stiffness relation must be symmetric, from the first principles, and therefore any lack of symmetry is due to some 'error' in the formulation, for which some'correction' process is then employed.

The object of this work is to examine the general process of coupling a B.E.M. solution to an overall F.E. system, by forming the 'equivalent' stiffness matrix for the region under consideration, in the context of elastostatic problems. The properties of this 'equivalent' stiffness matrix are extensively tested for various

examples with particular emphasis on the symmetry aspect of the formulation. From this, it is hoped that a much clearer picture will emerge of the validity and accuracy of the formulation, together with a greater insight into the symmetric properties of stiffness relations, not only in relation to a B.E.M. based technique, but from a much more general viewpoint.

One of the main problems with the B.E.M., is that of sharp geometric discontinuities on the surface, which gave rise to discontinuous tractions at that point. Adequate provision for this situation can, for certain cases, present difficulties in solutions using the B.E.M. However, these difficulties are invariably encountered in the procedure of forming an 'equivalent' stiffness matrix and require special consideration. The difficulty is that the problem is ill-defined at such discontinuities, and extra equations are required in order to adequately include the effects of the discontinuity in the model, and to uniquely define the problem. The inclusion of these 'extra' equations can seriously affect the degree of symmetry (or lack thereof) exhibited by the final 'equivalent' stiffness matrix, and this is another key feature of the overall problem which is examined extensively in this work.

CHAPTER 2 gives a brief outline of the basic relations in linear elasticity which form the basis for the remainder of the work. By way of this, the notation and associated sign conventions are also introduced. Following this, the governing differential equations are derived from both static equilibrium criteria and variational energy considerations, and the equivalence of these processes is demonstrated. Finally the Weighted Residual Technique is presented, and it is shown that all the forms of the equilibrium

statements can be derived as special cases of this technique.

CHAPTER 3 begins by presenting the fundamental problems and their solutions for both 2 and 3-Dimensional problems. For bodies which have fully closed boundaries (either closed internal surfaces representing cavities, or closed external surfaces representing finite boundaries), the Kelvin solution is applicable, and the 2 and 3-Dimensional cases are quoted. For a 3-Dimensional half-space, the most general solution is that of Mindlin [7] and represents a point load acting in the interior of a 3-D semi-infinite space. (A special case of this, is for the load acting at the surface, known as the Boussinesq - Cerruti solution). The 2-Dimensional equivalents of the above are the solutions presented by Melan [14], and Flamant [15]. The Melan solution is not implemented in this work, but all the others are given in Chapter 3. Following this, Chapter 3 then goes on to formulate the B.E.M., and for completeness, a brief summary of the F.E.M. is also included.

CHAPTER 4 begins by demonstrating the relationship between the B.E.M. and F.E.M. and shows the basis of forming an 'equivalent' stiffness matrix using the B.E.M. formulation. Several examples are then implemented for the case of constant elements. 2-Dimensional problems are run using the Kelvin solution, and following the work of Nakaguma [10] some 3-D problems for both finite and semi-infinite domains are implemented.

CHAPTER 5 then proceeds to examine problems encountered with higher order elements - namely, those arising at geometric discontinuities. The problem is examined using a 2-Dimensional linear element formulation, but ideas involved can readily be extended to higher order elements and to 3-D. The corner problem is dealt with by supplying 'extra' equations at discontinuities, which were originally suggested by Chaudonneret [23]. A technique is developed which considers these 'extra' equations as additional boundary conditions imposed on the problem, and sets them up in the form of a series of 'rotation' matrices, reminiscent of the application of a set of linearly dependent constraints on a F.E.M. model. Unlike their straight forward imposition, this largely preserves the eventual symmetry of the formulation, and several examples are implemented to demonstrate the validity and accuracy of the 'equivalent' stiffness approach. Chapter 5 also includes a detailed discussion on the symmetry aspect, and presents arguments explaining the general 'lack' of symmetry from numerical, analytical and physical considerations.

CHAPTER 6 presents formulations for a 2-Dimensional half-space loaded at the free surface. Due to the fact that, for this case, all influences and effects are defined on a straight line (namely, the free surface), it is possible to perform all the relevant integrations analytically. These integrations are in fact performed for the cases of constant, linear and quadratic elements, thus enabling the explicit definition of the final linear algebraic equations, without any recourse to numerical integration. The behaviour of the formulations

is then tested with reference to several examples.

This work deals with the Finite Element displacement technique, as opposed to the force method, and therefore all the models considered have the global displacements as the primary system unknowns. As such, the numerical tests, comparisons, and the examples presented concentrate on the solutions obtained for displacements.

CHAPTER 2. GOVERNING RELATIONS

2.1 INTRODUCTION.

This chapter reviews the basic relations governing the theory of linear elasticity and defines the relationships between stresses, strains, displacements and tractions, which allow the mathematical definition of the problem. By way of this, the basic notation and sign convention for the remainder of this work is introduced, as well as leading to the definition of the governing equations of equilibrium.

Equilibrium conditions are then examined using energy considerations and the Principles of Virtual Work and Minimum Potential Energy are presented.

Finally, the Weighted Residual Technique is discussed, which is a general method used to formulate numerical solution schemes for differential equations. Many of the common techniques used in engineering can be shown to be special cases of this formulation.

2.2 BASIC RELATIONS IN ELASTOSTATICS

2.2.1 Components of Stress

In the general three-dimensional case the reference frame will be three mutually orthogonal cartesian axes denoted by x_1, x_2, x_3, or x_i ($i = 1, 3$). At any point within the body the state of stress may be defined by the second order tensor σ_{ij} ($i = 1, 3$; $j = 1, 3$) which denotes the stress on a small differential element acting on a face perpendicular to the axis x_i and in a direction parallel to the axis x_j (fig. 2.2.1). The stress

component σ_{ij} is considered positive when acting on the most positive x_i face in the positive x_j direction, or vice-versa.

The surface tractions will be denoted by the vector $\underset{\sim}{p}$ with components p_i $(i = 1, 3)$ considered positive when acting in the positive x_i direction.

The tangent plane at a point on the surface is defined by the unit normal at that point, $\underset{\sim}{n}$, with components n_i (fig. 2.2.2). By considering equilibrium of the trapezoidal element shown in fig. 2.2.2 it may readily be shown that the surface tractions and stresses are related as follows :

$$p_j = \sigma_{jk} n_k \qquad (2.2.1)$$

Where the usual summation convention for repeated indices applies.

2.2.2 Components of Strain

The state of strain at any point may be defined by the strain tensor ε_{ij}, and the displacements of any point, by the vector u_i. If the deformations are small, such that $u_{i,j}^2$ is insignificant compared to $u_{i,j}$ (the subscript $,_j$ denotes the partial derivative $\frac{\partial}{\partial x_j}$) then the strain displacement relations are linear and may be expressed as follows :

$$\varepsilon_{ij} = \frac{1}{2}(u_{i,j} + u_{j,i}) \qquad (2.2.2)$$

It is important to note that both the stress and strain tensors are symmetric and hence for the 3-Dimensional case there are only six independent components and for the 2-Dimensional case there are three such independent components.

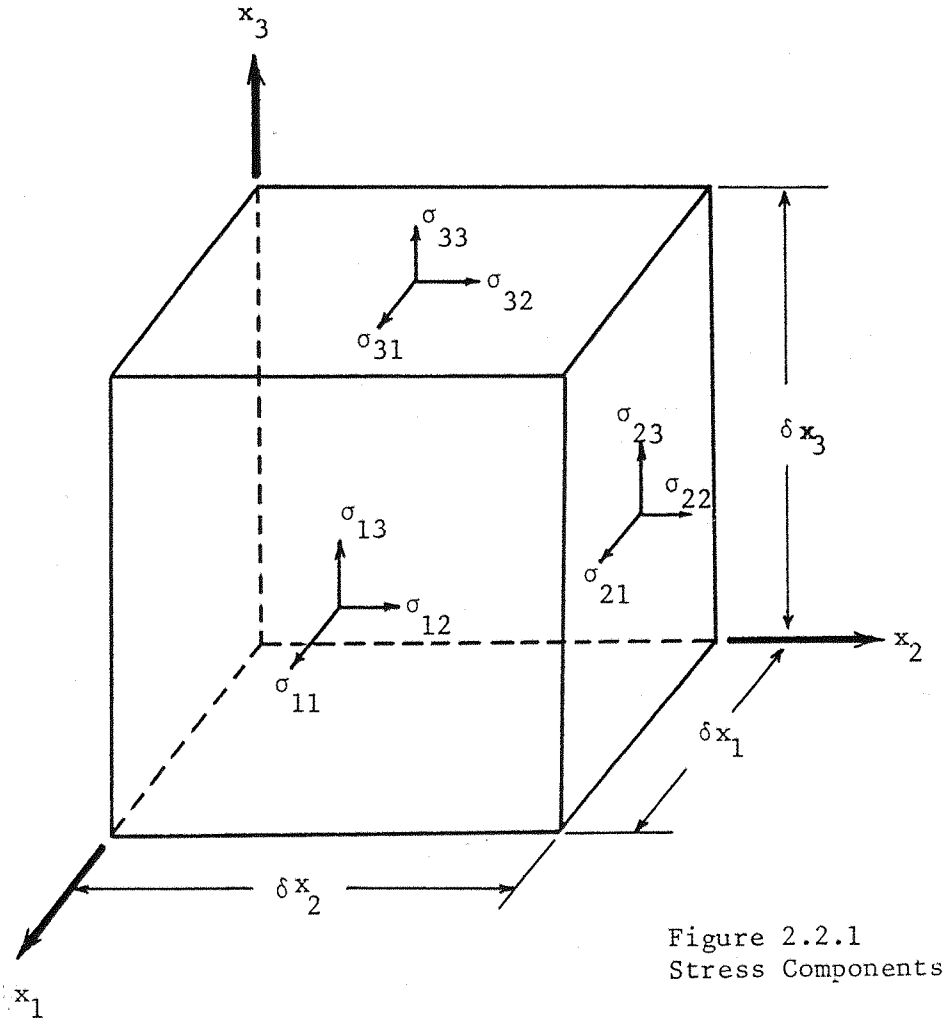

Figure 2.2.1
Stress Components.

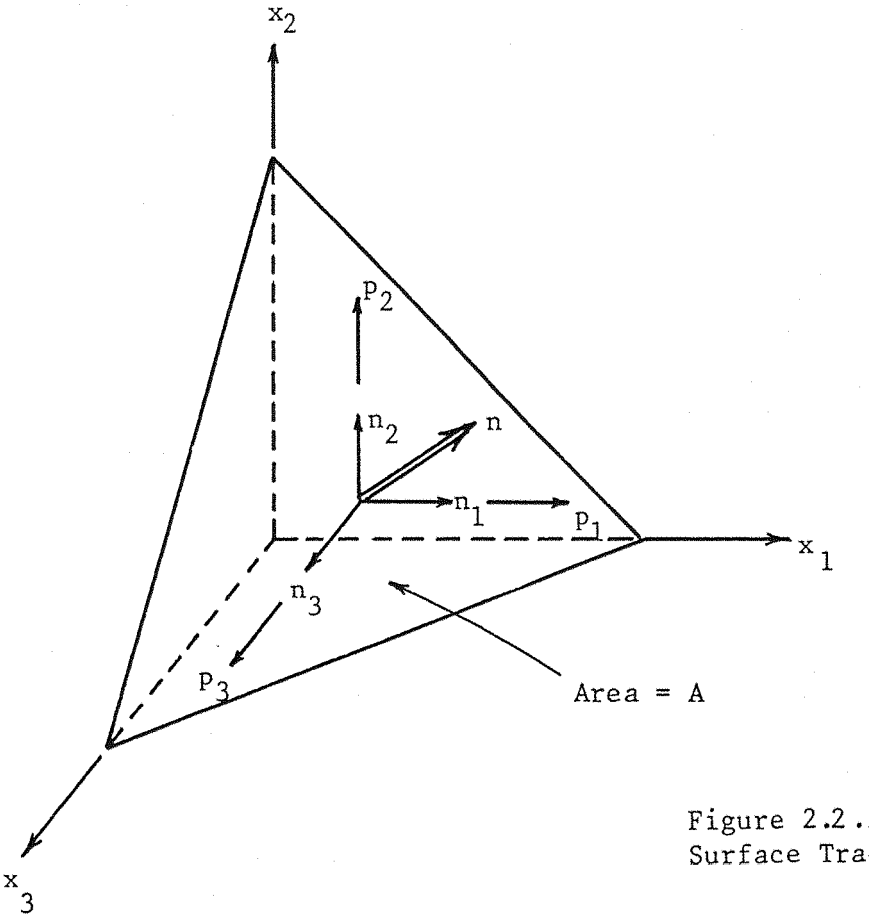

Figure 2.2.2
Surface Tractions.

2.2.3 Stress-Strain Relations

GENERAL STRESS-STRAIN RELATIONS

For a linearly elastic material, the most general form of Hooke's law may be expressed in tensor notation as

$$\varepsilon_{ij} = C_{ijk\ell}\sigma_{k\ell} \tag{2.2.3a}$$

this may also be written in matrix form :

$$\begin{bmatrix} \varepsilon_{11} \\ \varepsilon_{22} \\ \varepsilon_{33} \\ 2\varepsilon_{12} \\ 2\varepsilon_{13} \\ 2\varepsilon_{23} \end{bmatrix} = \begin{bmatrix} c_{11} & c_{12} & c_{13} & c_{14} & c_{15} & c_{16} \\ & c_{22} & c_{23} & c_{24} & c_{25} & c_{26} \\ & & c_{33} & c_{34} & c_{35} & c_{36} \\ & & & c_{44} & c_{45} & c_{46} \\ & \text{SYM} & & & c_{55} & c_{56} \\ & & & & & c_{66} \end{bmatrix} \times \begin{bmatrix} \sigma_{11} \\ \sigma_{22} \\ \sigma_{33} \\ \sigma_{12} \\ \sigma_{13} \\ \sigma_{23} \end{bmatrix} \tag{2.2.3b}$$

or $$\underset{\sim}{\varepsilon} = \underset{\sim}{C}\ \underset{\sim}{\sigma} \tag{2.2.3c}$$

The inverse relationship of equation (2.2.3) may be written

$$\sigma_{ij} = D_{ijk\ell}\,\varepsilon_{k\ell} \tag{2.2.4a}$$

or, in matrix notation

$$\underset{\sim}{\sigma} = \underset{\sim}{D}\ \underset{\sim}{\varepsilon} \tag{2.2.4b}$$

The terms c_{ij} are called the 'elastic compliances' and d_{ij} the rigidity coefficients'.

For a general anisotropic material (i.e. no symmetry in the

material properties) the elements of the matrix $\underset{\sim}{C}$ (and correspondingly, $\underset{\sim}{D}$), shown in equations (2.2.3) and (2.2.4) are all non-zero and not interelated, hence there are 21 independent material constants.

In practice, however, real materials exhibit various forms of symmetry in their material behaviour, which reduces the number of independent constants in the stress-strain relations for that material. A method for determining the form of the stress-strain relations in such a case is as follows : When the material exhibits an elastic symmetry then there are at least two sets of reference frames which are, in fact, equivalent due to the symmetry, say x_i and x_i^1. The total energy potential may be expressed in terms of the stress components σ_{ij} and σ_{ij}^1 and, of course, the elastic compliances, and will have the same form in both systems, as they are, in fact, equivalent. The stresses σ_{ij}^1 may be transformed to the x_i system using simple stress transformation, and hence the coefficients of the terms describing the two energy potentials may be equated. Many of the terms c_{ij} will disappear, depending on the type of symmetry involved.

For a material which has three orthogonal planes of symmetry (orthotropic), corresponding to the planes containing the coordinate axes, the matrix $\underset{\sim}{C}$ takes the following form, containing nine independent constants.

$$\underset{\sim}{C} = \begin{bmatrix} c_{11} & c_{12} & c_{13} & & & \\ & c_{22} & c_{23} & & 0 & \\ & & c_{33} & & 0 & \\ & & & c_{44} & 0 & \\ & \text{SYM} & & & c_{55} & \\ & & & & & c_{66} \end{bmatrix} \qquad (2.2.5)$$

If a material has only one plane of symmetry, say the $x_1 - x_2$ plane, (a necessary condition for reduction of a problem to 2-Dimensions), then the following elements are also non-zero :

$$c_{14},\ c_{24},\ c_{34},\ c_{56} \neq 0 \qquad (2.2.6)$$

The most symmetric case is that of an orthotropic material where the properties in each of the planes of symmetry are identical. This is called an 'isotropic' material, and the number of independent constants needed to define the stress-strain relations reduce to two ; - E, the Youngs Modulus, and ν , the poisson ratio. The matrices $\underset{\sim}{C}$ and $\underset{\sim}{D}$ now take the following form :

$$\underset{\sim}{C} = \frac{E}{2(1+\nu)} \begin{bmatrix} c_1 & c_2 & c_2 & & & \\ & c_1 & c_2 & & & \\ & & c_1 & & & \\ & & & 1 & & \\ & & & & 1 & \\ \text{SYM} & & & & & 1 \end{bmatrix} \qquad c_1 = \frac{2(1-\nu)}{(1-2\nu)}, \quad c_2 = \frac{2\nu}{(1-2\nu)}$$

$$\underset{\sim}{D} = \frac{1}{E} \begin{bmatrix} 1 & -\nu & -\nu & & & \\ & 1 & -\nu & & & \\ & & 1 & & & \\ & & & 2(1+\nu) & & \\ & & & & 2(1+\nu) & \\ \text{SYM} & & & & & 2(1+\nu) \end{bmatrix} \qquad (2.2.8)$$

PLANE STRESS AND PLANE STRAIN

Plane stress problems are ones in which the body under consideration is planar, lying in the x_1-x_2 plane with a relatively very small dimension in the x_3 direction; all body forces act in the plane of the body and are independent of x_3, and the applied forces and tractions are also planar and act on the edge of the body. In such a case, $\sigma_{33} = \sigma_{23} = \sigma_{13} = 0$ on the surfaces of the plate, and without significant error, may be assumed zero throughout the thickness. It is also reasonable to assume that the remaining stress components σ_{12}, σ_{11}, σ_{22} remain constant throughout the thickness, i.e. are independent of x_3.

It should be noted that although $\sigma_{33} = 0$, the transverse displacement $u_3 \neq 0$, hence $\varepsilon_{33} \neq 0$ and may be calculated using the stress strain relations.

Plane strain problems occur at the other extreme of geometry, when the x_3 dimension is very large compared to x_1 and x_2. The conditions that all applied forces, tractions and body forces act in the $x_1 - x_2$ plane and are independent of x_3, still apply, and the remaining initial condition for plane strain is that $u_3 = 0$.

In this case it may be assumed that u_1 and u_2 are independent of x_3 and this is equivalent to specifying $\varepsilon_{33} = \varepsilon_{13} = \varepsilon_{23} = 0$.

Note that $\sigma_{33} \neq 0$ and may be calculated using the stress strain relations.

For any two-dimensional problem, the $x_1 - x_2$ plane must be a plane of symmetry by definition, and for a general case, the stress-strain

relations are given by :

$$\begin{bmatrix} \varepsilon_{11} \\ \varepsilon_{22} \\ \varepsilon_{33} \\ 2\varepsilon_{12} \\ 2\varepsilon_{13} \\ 2\varepsilon_{23} \end{bmatrix} = \begin{bmatrix} c_{11} & c_{12} & c_{13} & c_{14} & & \\ & c_{22} & c_{23} & c_{24} & & \\ & & c_{33} & c_{34} & & \\ & & & c_{44} & & \\ \text{SYM} & & & & c_{55} & c_{56} \\ & & & & & c_{66} \end{bmatrix} \times \begin{bmatrix} \sigma_{11} \\ \sigma_{22} \\ \sigma_{33} \\ \sigma_{12} \\ \sigma_{13} \\ \sigma_{23} \end{bmatrix} \qquad (2.2.9)$$

Note that initial strain components have been omitted for simplicity but may be easily incorporated by considering the strain vector $\underset{\sim}{\varepsilon}$ to be the difference between the total and initial strains.

For the plane stress case σ_{33} is set to zero in equation (2.2.9) resulting in,

$$\begin{bmatrix} \varepsilon_{11} \\ \varepsilon_{22} \\ 2\varepsilon_{12} \end{bmatrix} = \begin{bmatrix} c_{11} & c_{12} & c_{14} \\ & c_{22} & c_{24} \\ & & c_{44} \end{bmatrix} \times \begin{bmatrix} \sigma_{11} \\ \sigma_{22} \\ \sigma_{12} \end{bmatrix} \qquad (2.2.10)$$

or,

$$\underset{\sim}{\varepsilon} = \underset{\sim}{C}^{\sigma}\ \underset{\sim}{\sigma}$$

Inverting (2.2.10),leads to

$$\underset{\sim}{\sigma} = \underset{\sim}{D}^{\sigma}\ \underset{\sim}{\varepsilon} \qquad (2.2.11)$$

Where $\underset{\sim}{C}^{\sigma}$, $\underset{\sim}{D}^{\sigma}$ denote the elastic compliances and rigidity coefficients for the plane stress case, and $\underset{\sim}{C}^{\varepsilon}$ and $\underset{\sim}{D}^{\varepsilon}$ for the plane strain case.

For the plain strain case, σ_{33} is not conveniently zero and must be eliminated from equation (2.2.9).

$$\sigma_{33} = (c_{13}\,\sigma_{11} + c_{23}\,\sigma_{22} + c_{34}\,\sigma_{12}) \quad \frac{-1}{c_{33}} \qquad (2.2.12)$$

Substitution of σ_{33} in equation (2.2.9), yields the expression for $\underset{\sim}{C}^{\varepsilon}$, and upon inversion, $\underset{\sim}{D}^{\varepsilon}$.

For an orthotropic material (one in which the axes of symmetry correspond to the x_1 and x_2 axes) the stress strain relations may be expressed explicitly in terms of the material constants :

Equation (2.2.11) may be expressed as (plane stress)

$$\begin{bmatrix} \sigma_{11} \\ \sigma_{22} \\ \sigma_{12} \end{bmatrix} = \begin{bmatrix} \frac{E_{11}}{(1-n\nu_{21}^2)} & \frac{\nu_{21}\,E_{11}}{(1-n\nu_{21}^2)} & 0 \\ & \frac{E_{11}}{n(1-n\nu_{21}^2)} & 0 \\ & & G_{12} \end{bmatrix} \times \begin{bmatrix} \varepsilon_{11} \\ 2\varepsilon_{22} \\ 2\varepsilon_{12} \end{bmatrix}$$

Where $n = \dfrac{E_{11}}{E_{22}}$

And for an isotropic material $E_{11} = E_{22} = E$;

$$\nu_{21} = \nu \qquad (2.2.14)$$

$$G_{12} = \frac{E}{2(1+\nu)}$$

Resulting in the expression for $\underset{\sim}{D}^{\sigma}$

$$\underset{\sim}{D}^{\sigma} = \begin{bmatrix} \frac{E}{1-\nu^2} & \frac{\nu E}{1-\nu^2} & 0 \\ \text{SYM} & \frac{E}{(1-\nu^2)} & 0 \\ & & G \end{bmatrix} \qquad (2.2.15)$$

By carrying out the process of first eliminating σ_{33} from the explicit form of the stress-strain relations and setting $\varepsilon_{33} = 0$, the equivalent relations for the plane strain case are obtained. $\underset{\sim}{D}^{\varepsilon}$ is found to have the same form as (2.2.15) in terms of E' and ν', where

$$E' = \frac{E}{(1-\nu^2)} \qquad (2.2.16)$$

$$\nu' = \frac{\nu}{1-\nu}$$

Hence the same formulation for the solution of any 2-dimensional problem may be used, by simply adjusting the material constants according to equation (2.2.16) when the plane strain case is required.

2.3 EQUILIBRIUM CONDITIONS

2.3.1 Equilibrium Equations in Terms of Stresses and Displacements.

Referring to Fig. 2.2.1, consider the force acting in the x_1 direction due to σ_{11}. The force will be : (variation of σ_{11} with respect to x_1) × (increment in x_1 direction) × (area on which the stress acts). Hence force due to σ_{11} is given by :

$$\left(\frac{\partial \sigma_{11}}{\partial x_1}\right) (\delta x_1) (\delta x_2\ \delta x_3)$$

Considering all stresses acting in the x_1 direction, and denoting b_1 as the body force per unit volume acting in the x_1 direction, then equilibrium in the x_1 direction requires :

$$\frac{\partial \sigma_{11}}{\partial x_1} + \frac{\partial \sigma_{21}}{\partial x_2} + \frac{\partial \sigma_{31}}{\partial x_3} + b_1 = 0 \qquad (2.3.1)$$

Similar equations may be written for equilibrium in the x_2 and x_3 coordinate directions. The three equations may now be written :

$$\sigma_{jk,j} + b_k = 0 \quad , \qquad (i,j = 1,2,3) \qquad (2.3.2)$$

By considering rotational equilibrium about each of the coordinate axes in turn, it is immediately shown that

$$\sigma_{ij} = \sigma_{ji} \quad , \quad i \neq j \qquad (2.3.3)$$

(This is, in fact, the reason why the stress tensor is symmetric).

Equations (2.3.2) define equilibrium for any elastic body, in terms of stresses, and are applicable to both the 2 and 3-dimensional cases.

For an isotropic material, Hookes law, (equations (2.2.3) and (2.2.4)) may be written :

$$\sigma_{ij} = \lambda\ \varepsilon_{kk}\ \delta_{ij} + 2\ G\ \varepsilon_{ij} \qquad (2.3.4)$$

where

$$G = \frac{E}{2(1+\nu)} \qquad (2.3.5)$$

$$\lambda = \frac{\nu E}{(1+\nu)(1-2\nu)} \qquad (2.3.6)$$

and δ_{ij} is the Kronecker Delta

$$\delta_{ij} = 1 \qquad i = j$$
$$\delta_{ij} = 0 \qquad i \neq j \tag{2.3.7}$$

By using the strain displacement relations (2.2.2), the stresses (2.3.4) may be expressed in terms of displacements :

$$\sigma_{ij} = \lambda u_{k,k}\, \delta_{ij} + G(u_{i,j} + u_{j,i}) \tag{2.3.8}$$

Using equation (2.3.8), the equilibrium equations (2.3.2) may also be expressed in terms of displacements, resulting in the well known Navier Equations of equilibrium.

$$\frac{1}{(1-2\nu)}\, u_{i,ij} + u_{j,ii} + \frac{1}{G}\, b_j = 0 \tag{2.3.9}$$

As all of the compatibility conditions relating stresses, strains, and displacements have now been included, equations (2.3.9) uniquely define the problem, providing 3 equations for the 3 unknown displacements at any point.

2.3.2 Energy Formulations

THE PRINCIPLE OF VIRTUAL WORK

Consider a body enclosing the domain Ω with a surface Γ (Fig. 2.3.1) and with boundary conditions as follows :

$$u_i(S) = \bar{u}_i(S) \quad , \quad S \in \Gamma_1 \tag{2.3.10}$$

$$p_i(S) = \bar{p}_i(S) \quad , \quad S \in \Gamma_2 \tag{2.3.11}$$

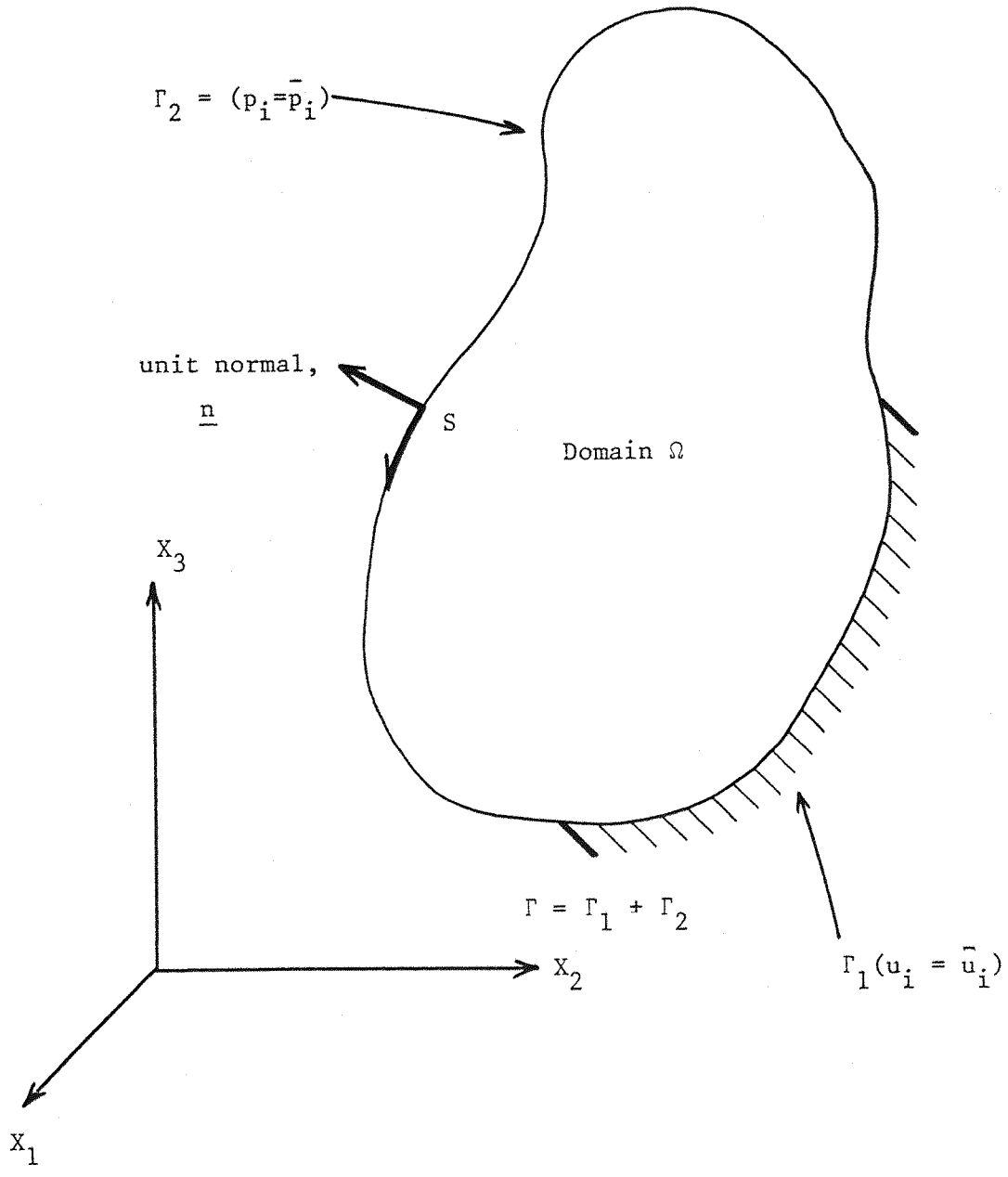

Figure 2.3.1 General Problem Definition.

The boundary, Γ, will be considered as the sum $\Gamma_1 + \Gamma_2$, where Γ_1 is the part of the boundary where the essential (or geometric) boundary conditions are applied (equation (2.3.10)), and Γ_2 where the natural (or mechanical) boundary conditions are applied (equation (2.3.11)).

Now, let the body undergo any small virtual displacements δu_i such that on the surface Γ_1 the geometric boundary conditions are identically satisfied and $\delta u_i = 0$. Corresponding to these displacements, the internal strains will also undergo small variations :

$$\delta\varepsilon_{ij} = \frac{1}{2}\left[(\delta u_i)_{,j} + (\delta u_j)_{,i}\right] \tag{2.3.12}$$

The work done by the internal stresses is given by :

$$\int_\Omega \sigma_{ij}\ \delta\varepsilon_{ij}\ d\Omega = \frac{1}{2}\int_\Omega \sigma_{ij}\left[(\delta u_i)_{,j} + (\delta u_j)_{,i}\right] d\Omega \tag{2.3.13}$$

Now,

$$\int_\Omega \sigma_{ij}(\delta u_i)_{,j}\ d\Omega = I_1 - I_2 \tag{2.3.14}$$

where,

$$I_1 = \int_\Omega (\sigma_{ij}\ \delta u_i)_{,j}\ d\Omega \tag{2.3.15}$$

$$I_2 = \int_\Omega \delta u_i\ \sigma_{ij,j}\ d\Omega \tag{2.3.16}$$

For a vector function F (with components F_i) in a closed domain Ω, with boundary Γ, Gauss theorem states that :

$$\int_\Omega F_{j,j}\ d\Omega = \int_\Gamma F_j\ n_j\ d\Gamma \tag{2.3.17}$$

Hence,

$$I_1 = \int_\Gamma \sigma_{ij}\, n_j\, \delta u_i \, d\Gamma \qquad (2.3.18)$$

and using equation (2.2.1)

$$I_1 = \int_\Gamma p_i\, \delta u_i \, d\Gamma \qquad (2.3.19)$$

Also, from equations (2.3.2) the term $\sigma_{ij,j}$ in equation (2.3.16) for I_2, may be replaced by $-b_i$, and hence the work done by the internal stresses becomes :

$$\int_{\Gamma_2} \bar{p}_i\, \delta u_i \, d\Gamma + \int_\Omega b_i\, \delta u_i \, d\Omega \qquad (2.3.20)$$

(noting that $\delta u_i = 0$ on Γ_1).

Hence the Principle of Virtual Work may be expressed:

$$\int_\Omega \sigma_{ij}\, \delta\varepsilon_{ij} \, d\Omega = \int_{\Gamma_2} \bar{p}_i\, \delta u_i \, d\Gamma + \int_\Omega b_i\, \delta u_i \, d\Omega \qquad (2.3.21)$$

The linearity of the material behaviour has not been imposed on the above equation and hence it is completely general in that sense. Also, by introducing the strain displacement relations (equations (2.2.2)) into (2.3.21), and performing an analysis as above, the equilibrium equations (2.3.2) may be derived. (see [9]).

THE PRINCIPLE OF MINIMUM POTENTIAL ENERGY

The Principle of Minimum Potential Energy is another of the well-known theorems in solid mechanics, and requires that the total potential of a body in equilibrium, usually expressed as some energy functional, is stationary with respect to some generalised degrees of freedom. [9].

The potential energy of the system depicted by Fig. 2.3.1 may be written as,

$$\Pi = \int_{\Omega} \frac{1}{2} \sigma_{ij} \, \varepsilon_{ij} \, d\Omega - \int_{\Omega} b_i \, u_i \, d\Omega - \int_{\Gamma_2} \bar{p}_i \, u_i \, d\Gamma \tag{2.3.22}$$

and for equilibrium

$$\delta \Pi = 0 \tag{2.3.23}$$

Now

$$\delta \Pi = \int_{\Omega} \frac{1}{2} \delta\sigma_{ij} \, \varepsilon_{ij} \, d\Omega + \int_{\Omega} \frac{1}{2} \sigma_{ij} \, \delta\varepsilon_{ij} \, d\Omega - \int_{\Omega} b_i \, \delta u_i \, d\Omega - \int_{\Gamma_2} \bar{p}_i \, \delta u_i \, d\Gamma \tag{2.3.24}$$

Because of the symmetry of the rigidity coefficients which relate the stresses, σ_{ij} , and the strains, ε_{ij}, (equation (2.2.4)), it may readily be shown that the first two terms in equation (2.3.24) are equal and hence, equations (2.3.23) and (2.3.24) yield equation (2.3.21) - The Principle of Virtual Work.

MIXED FORMULATIONS

The above energy formulations have been based on the fact that the essential boundary conditions (those defining displacements on Γ_1) are identically satisfied, and hence the virtual displacements are assumed zero on this part of the boundary. This leads to displacement type models where all the applied forces are defined and the unknowns are the displacements on the Γ_2 part of the boundary.

However, if the model is of a mixed type, where there are both displacements and tractions unknown on the surface then both

parts of the boundary have to be considered. As the displacement boundary conditions are now not identically satisfied, and hence, there is a contribution to the total potential energy due to this part of the boundary. The most widely known mixed principle is given by the Reissner functional, which includes an extra term in the total potential energy functional (equation (2.3.22)), corresponding to the work done on the Γ_1 part of the boundary, (see [9]). The Reissner energy functional is given by :

$$\Pi_R = \int_\Omega \frac{1}{2}\,\sigma_{ij}\,\varepsilon_{ij}\,d\Omega - \int_\Omega b_i\,u_i\,d\Omega - \int_{\Gamma_2} \bar{p}_i\,u_i\,d\Gamma + \int_{\Gamma_1} p_i(\bar{u}_i - u_i)\,d\Gamma \tag{2.3.25}$$

The variation of the extra term is,

$$\int_{\Gamma_1} \delta p_i(\bar{u}_i - u_i)\,d\Gamma - \int_{\Gamma_1} p_i\,\delta u_i\,d\Gamma$$

Thus the Principle of Virtual Work now takes the modified form :

$$\int_\Omega \sigma_{ij}\,\delta\varepsilon_{ij}\,d\Omega = \int_{\Gamma_2} \bar{p}_i\,\delta u_i\,d\Gamma + \int_{\Gamma_1} p_i\,\delta u_i\,d\Gamma - \int_{\Gamma_1} (u_i - \bar{u}_i)\delta p_i\,d\Gamma + \int_\Omega b_i\,\delta u_i\,d\Omega \tag{2.3.26}$$

2.3.3 The Weighted Residual Technique

Consider the general linear differential operator $L(u)$ in Ω , which must satisfy the equation

$$L(u) - b = 0 \quad \text{in} \quad \Omega \tag{2.3.27}$$

with boundary conditions

$$S(u) = r \quad \text{on} \quad \Gamma_1$$
$$G(u) = q \quad \text{on} \quad \Gamma_2 \tag{2.3.28}$$

where the total boundary $\Gamma = \Gamma_1 + \Gamma_2$, and S and G are differential operators giving the essential and natural boundary conditions, respectively.

If an approximate solution 'u' is now introduced, this will not exactly satisfy equations (2.3.27) and (2.3.28) and there will be a resultant error involved. The errors involved may be defined as follows :

$$\begin{aligned} \varepsilon &= L(u) - b \neq 0 \\ \varepsilon_1 &= S(u) - r \neq 0 \\ \varepsilon_2 &= G(u) - q \neq 0 \end{aligned} \tag{2.3.29}$$

The inner product of two functions f_1 and f_2 is defined as

$$\langle f_1, f_2 \rangle_\Omega = \int_\Omega f_1 \, f_2 \, d\Omega \tag{2.3.30}$$

A general method of minimising the errors (2.3.29) is to distribute them, by defining a weighting function w, such that the following relationship is satisfied. (For further reading, see [4], [5], [6]).

$$\langle \varepsilon, w \rangle_\Omega = \langle \varepsilon_2, S(w) \rangle_{\Gamma_2} - \langle \varepsilon_1, G(w) \rangle_{\Gamma_1} \tag{2.3.31}$$

or $$\langle L(u) - b, w \rangle_\Omega = \langle G(u) - q, S(w) \rangle_{\Gamma_2} - \langle S(u) - r, G(w) \rangle_{\Gamma_1} \tag{2.3.32}$$

This may be considered the starting point for a wide variety of weighted residual techniques, such as Finite Differences, Method of Moments, Collocation Method, Galerkin technique etc. (see [5]).

The Finite Difference technique is simply derived by taking w, the weighting function in equation (2.3.32), to be the dirac delta, replacing the derivatives by finite difference expressions, and identically satisfying all boundary conditions.

The well known original Galerkin technique assumes a weighting function w, which is the same type of function as the solution, u. However this requires that the assumed function be of high enough order to allow for the existence of the derivatives imposed by the differential operators. These continuity requirements may be relaxed by lowering the order of the function space of which u and w must be sub-sets. This is achieved by integrating (2.3.32) by parts, obtaining what is known as a 'weak' formulation.

Noting that, for a self adjoint operator, $L(u)$, integrating by parts a sufficient number of times,

$$\begin{aligned} \langle L(u), w\rangle_{\Omega} = &- \langle D(u), D(w)\rangle_{\Omega} \\ &+ \langle G(u), S(w)\rangle_{\Gamma} \end{aligned} \tag{2.3.33}$$

(where, D is a differential operator) equation (2.3.32) then becomes,

$$\begin{aligned} \langle D(u), D(w)\rangle_{\Omega} = &\langle q, S(w)\rangle_{\Gamma_2} + \langle S(u) - r, G(w)\rangle_{\Gamma_1} \\ &+ \langle G(u), S(w)\rangle_{\Gamma_1} + \langle b, w\rangle_{\Omega} \end{aligned} \tag{2.3.34}$$

where u may now be of lower order, but w of higher order, than the functions necessarily required by (2.3.32).

Equation (2.3.34) may now be used as the basis for the Galerkin type Finite Element technique as u and w may be chosen to be of the same order. It is important to note that by considering the

equilibrium equations and boundary conditions for the elasticity problem (equations (2.3.2),(2.3.10), (2.3.11)) as a particular case of the equations (2.3.27) and (2.3.28), and by choosing the weighting, w, to correspond to some virtual displacement field, then equation (2.3.34) corresponds exactly to the general Principle of Virtual displacements given by equation (2.3.26) in the previous section.

Finally, equation (2.3.34) may be further integrated by parts until the original operator, L, now operates on w as opposed to u. (This is still assuming L is self-adjoint). If w is then chosen such that $L(w) = 0$, the problem is reduced to integrals only on the boundary, (other than the body force terms). A convenient choice for w, is that which forces w to satisfy the fundamental problem of a point source, given by the equation

$$L(w^*) + \delta_i = 0 \tag{2.3.35}$$

where δ_i is the dirac delta function representing a point source at 'i', and w^* is the corresponding response field within the domain, given by the solution of (2.3.35). Now the term

$$\langle u, L(w^*)\rangle_\Omega = \langle u, -\delta_i\rangle_\Omega = -u^i \tag{2.3.36}$$

where u^i is the value of the variable u, at the source point 'i'. Hence, equation (2.3.34) becomes :

$$c^i u^i + \langle r, G(w^*)\rangle_{\Gamma_1} + \langle S(u), G(w^*)\rangle_{\Gamma_2} = \langle q, S(w^*)\rangle_{\Gamma_2} + \langle G(u), S(w^*)\rangle_{\Gamma_1} + \langle b, w^*\rangle_\Omega \tag{2.3.37}$$

where $c^i = 1$ for the point i inside Ω

$c^i = 0$ for the point i outside Ω

When the point 'i' is on the boundary of the domain, then the value of c^i is not trivial for the general case, but this problem will be discussed in much greater detail in Chapter 3.

2.3.4 Discussion

This section has reviewed some of the fundamental relations for determining the stress state of a body in equilibrium under some applied loading. The equations of equilibrium were shown to be equivalent to statements of Virtual Work or Minimum Potential Energy, and furthermore these were shown to be special cases of a much more general technique - that of Weighted Residuals. (For further reading, see [11], [12]).

CHAPTER 3 - THE BOUNDARY ELEMENT AND FINITE ELEMENT FORMULATIONS

3.1 INTRODUCTION

This Chapter begins by defining the fundamental problems of a point load in a homogeneous elastic space - both infinite and semi-infinite - and presents the relevant solutions for displacements and stresses.

This fundamental solution is then used to reduce the governing equations of equilibrium, defined on the domain of the problem, to a form which involves only integrals on its boundary.

These equations may be solved numerically by dividing the boundary into a discrete number of elements and assuming interpolation functions for the unknowns, similar to those used in Finite Elements. This gives rise to the Boundary Element Method (BEM).

A brief description of the Finite Element Method (FEM) is included, and is shown to have a common basis with the BEM.

Finally a brief description is included of the computer implementation of the Boundary Element Method for the 2-Dimensional linear element case.

3.2 THE FUNDAMENTAL PROBLEMS FOR INFINITE AND SEMI-INFINITE DOMAINS

3.2.1 The Kelvin Problem - Infinite Space

THE 3-DIMENSIONAL CASE.

Consider the problem depicted in Fig. 3.2.1 within a domain Ω ; a unit point load is applied at the source point X

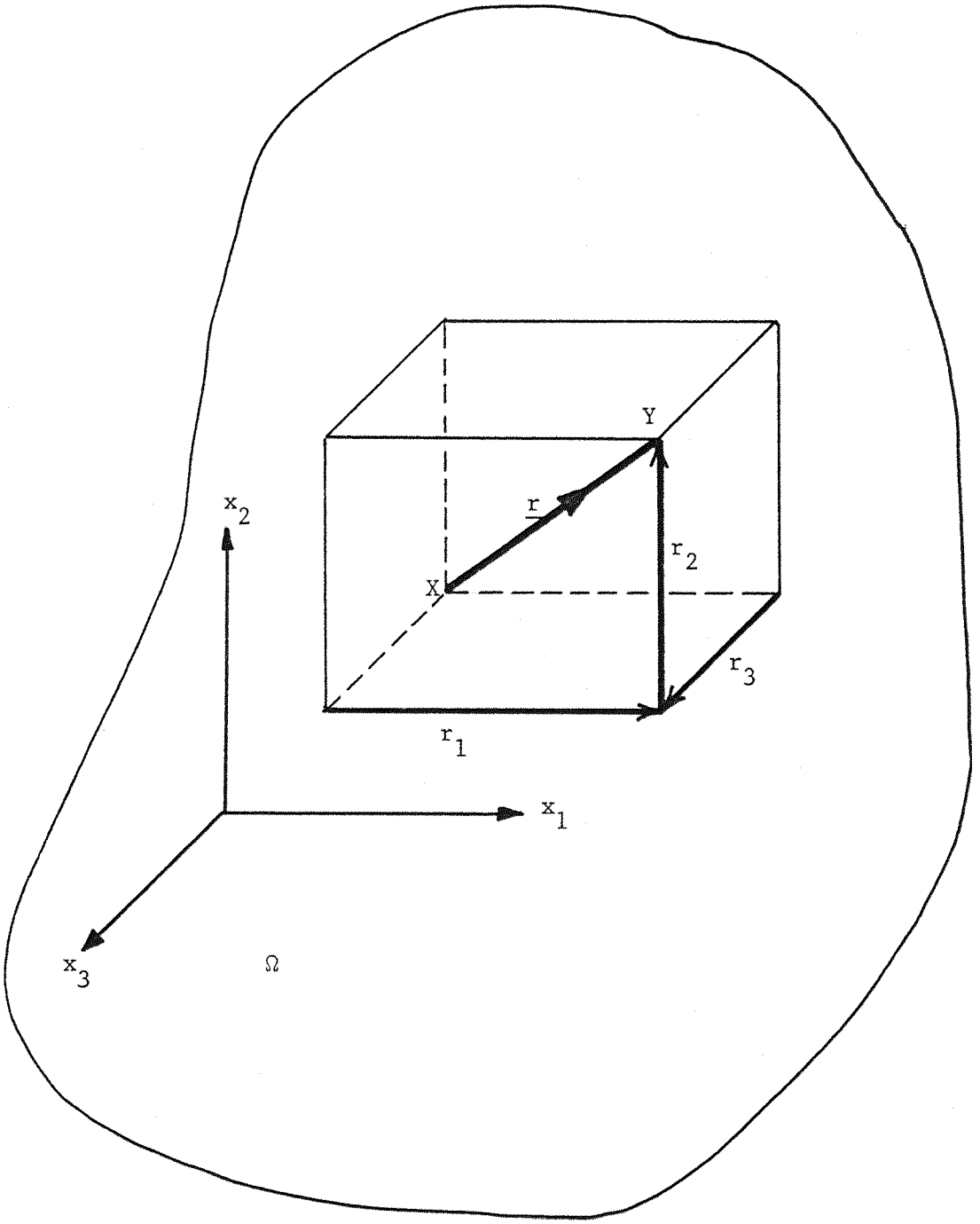

Ω represents the Infinite Domain

$X = X(x_i)$ denotes the source point

$Y = Y(x_i)$ denotes the field point.

Figure 3.2.1. Kelvins Problem. Force acting in a 3-Dimensional infinite space.

and the corresponding displacements and stresses are sought at some field point Y . The solution of this problem was originally achieved by Kelvin and is readily available in the literature ([1], [2], [3]). Cruse [4] gives the expressions for the displacements and tractions, using an indicial notation consistent with the notation being used in this work.

Consider a unit load applied at a source point X in the 'k' direction (k = 1,2,3) and the effect of this source at some field point Y , on the surface of the domain (defined by the unit normal $\underset{\sim}{n}$), and at a distance r from X (Figs.3.2.2). The displacements and tractions at Y are given by $u^*_{\ell k}$ and $p^*_{\ell k}$ respectively. The subscript 'ℓ' refers to the direction of the source (at X), and the subscript 'k' refers to the direction of the response, (at Y). (This notation is clearly shown in Figs. 3.2.2). The expressions for the fundamental solutions are :

$$u^*_{\ell k} = \frac{1}{16\pi G(1-\nu)r}\left[(3-4\nu)\ \delta_{\ell k} + r_{,\ell}\ r_{,k}\right] \qquad (3.2.1)$$

$$p^*_{\ell k} = \frac{1}{8\pi(1-\nu)\ r^2}\left[\frac{\partial r}{\partial n}\left[(1-2\nu)\ \delta_{\ell k} + 3r_{,\ell}\ r_{,k}\right] - (1-2\nu)\left[r_{,\ell}\ n_k - r_{,k}\ n_\ell\right]\right] \qquad (3.2.2)$$

where:

G is the Shear Modulus

ν is the Poisson ratio

$\delta_{\ell k}$ is the kronecker delta;

$\delta_{\ell k} = 1 \quad \ell = k$

$\delta_{\ell k} = 0 \quad \ell \neq k$

r is the distance between the source point and the field point i.e. :

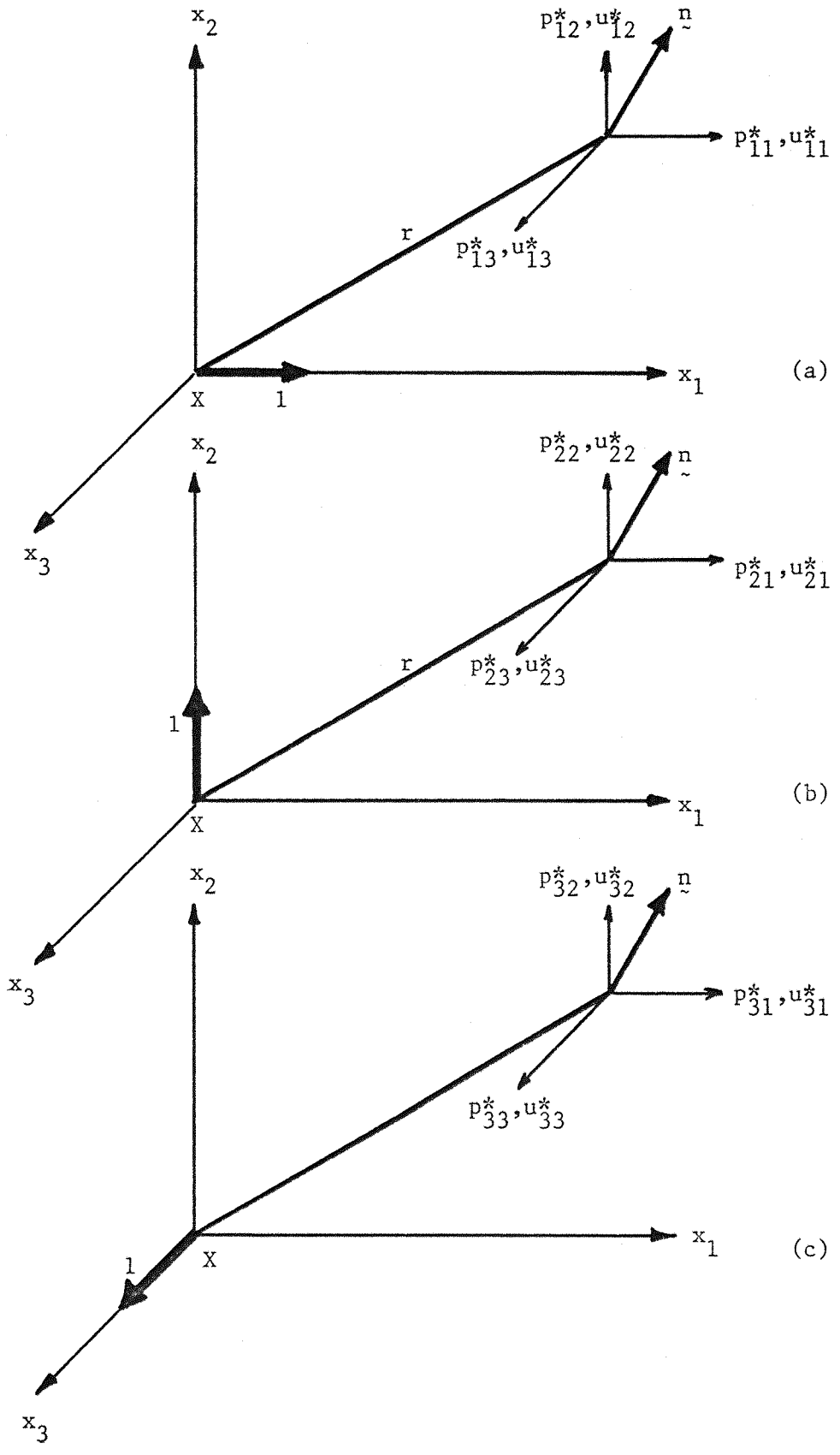

Figure 3.2.2. Definition of the displacement and traction tensor $u^*_{\ell k}$ and $p^*_{\ell k}$

$$r = \left[\sum_{j=1}^{3} (Y_j - X_j)^2 \right]^{\frac{1}{2}} \qquad (3.2.3)$$

and $r_{,i}$ represents the derivative of r, in the 'i' direction with respect to the field point, Y.

hence, $$r_{,i} = \frac{\partial r}{\partial Y_i} = \frac{1}{2} \left[\sum_{j=1}^{3} (Y_j - X_j)^2 \right]^{-\frac{1}{2}} 2(Y_i - X_i) \qquad (3.2.4)$$

$$r_{,i} = \frac{Y_i - X_i}{r} = \frac{r_i}{r}$$

THE TWO DIMENSIONAL CASE

The analogous 2-Dimensional solution is given by :

$$u^*_{\ell k} = \frac{1}{8\pi G(1-\nu)} \left[(3-4\nu) \ln \left(\frac{1}{r}\right) \delta_{\ell k} + r_{,\ell}\, r_{,k} \right] \qquad (3.2.5)$$

$$p^*_{\ell k} = \frac{1}{4\pi(1-\nu)r} \left[\frac{\partial r}{\partial n} \left[(1-2\nu)\, \delta_{\ell k} + 2 r_{,\ell}\, r_{,k} \right] - (1-2\nu) \left[r_{,\ell}\, n_k - r_{,k}\, n_\ell \right] \right] \qquad (3.2.6)$$

This solution is for the plane strain case, but a formulation based on this may be used to solve plane stress problems by adjusting the material constants according to equations (2.2.16).

3.2.2 Semi-Infinite Space Solutions

THE THREE DIMENSIONAL CASE

A 3-Dimensional semi-infinite space occupies the domain $-\infty < x_1 < \infty$, $-\infty < x_2 < \infty$, $0 < x_3 < \infty$ i.e. is bounded by the surface $x_3 = 0$, which is traction free. The most general solution, for a point load within the domain (see Fig. 3.2.3) is given by MINDLIN [7]. The Boussinesq-Cerruti solution [2], for the fundamental problem of the load acting at the free surface, although developed

earlier, can be derived as a special case of Mindlin by setting $c = 0$ (Fig. 3.2.3). Also by allowing $c \to \infty$, the Kelvin solution is obtained.

The general Mindlin solution, [7], was developed, implemented, and tested extensively by NAKAGUMA [10]. The solution lacks symmetry with respect to the three coordinate axes, and as such cannot conveniently be expressed using a neat tensor notation. However, for reasons of completeness and easy reference, the explicit form of the solution for the displacements and stresses are quoted in Appendix B. The Boussinesq-Cerruti solution, however, is very simple, as only the response on the free surface is required for its implementation with the BEM. Also, the free surface is traction free (by definition), so only the fundamental displacements on the surface need be defined. These are given by :

$$
\begin{aligned}
u^*_{11} &= K\left[(1-\nu) + \nu\, r^2_{,1}\right] \\
u^*_{12} &= K\,\nu\, r_{,1}\, r_{,2} \\
u^*_{13} &= K\,(0.5-\nu)\, r_{,1} \\
u^*_{22} &= K\left[(1-\nu) + \nu\, r^2_{,2}\right] \\
u^*_{23} &= K\,(0.5-\nu)\, r_{,2} \\
u^*_{33} &= K\,(1-\nu)
\end{aligned}
\qquad (3.2.7)
$$

where $K = \dfrac{1}{2\pi G\, r}$,

and

$$
\begin{aligned}
u^*_{21} &= u^*_{12} \\
u^*_{32} &= -\,u^*_{23} \\
u^*_{31} &= -\,u^*_{13}
\end{aligned}
$$

THE TWO DIMENSIONAL CASE

The 2-Dimensional problems analogous to the above are depicted in Figs. 3.2.4 and 3.2.5, the domain under consideration bounded by the x_2 axis (i.e. $x_1 = 0$). The general solution was first devised by MELAN [14], and again may be obtained from Mindlin by integrating the solution for a point load, to form a solution for a line load, and performing the relevant coordinate transformations. A special case of this solution, is again, when the load is applied at the free surface. This solution was first devised for a point load perpendicular to the surface, FLAMANT [15], and subsequently modified by BOUSSINESQ [16], for the general case of an inclined load at the surface.

This solution is given by TIMOSHENKO [1], in terms of polar coordinates, r , θ. For a point load P , applied at the origin, the position of the field point, Y , is defined by its distance from the origin, r , and the angle it subtends from the line of action of the force, θ ; (see Fig. 3.2.5).

The stresses at Y are given by :

$$\sigma_r = -\frac{2P}{\pi r}\cos\theta$$

$$\sigma_\theta = 0 \qquad (3.2.8)$$

$$\sigma_{r\theta} = 0$$

and these may be integrated to yield the radial and tangential displacements (u and v , respectively), given by :

$$u = -\frac{2P}{\pi E}\cos\theta\,\ln(r) - \frac{(1-\nu)P}{\pi E}\,\theta\sin\theta + A\sin\theta + B\cos\theta \qquad (3.2.9a)$$

$$v = \frac{2\nu P}{\pi E}\sin\theta + \frac{2P}{\pi E}\ln(r)\sin\theta - \frac{(1-\nu)P}{\pi E}\,\theta\cos\theta + \frac{(1-\nu)P}{\pi E}\sin\theta + A\cos\theta - B\sin\theta + Cr \qquad (3.2.9b)$$

where A, B, C are constants of integration and must be determined from the physical constraints of the problem. In order to facilitate the implemention of this solution, using the BEM, equations (3.2.9) must be specialised for the case of the field point Y lying on the free surface, $x_1 = 0$, and written in terms of the rectangular coordinate system x_1, x_2.

For the case of P acting vertically (in the x_1 direction), we can assume that the constraint is such that there is no lateral displacement along the x_1 axis, i.e. $v = 0$ for $\theta = 0$. This yields $A = C = 0$. Furthermore we must restrain the system from a rigid body translation and thus assume zero vertical displacement at some point on the x_1 axis, at a distance, d, say, from the origin. We then find

$$B = \frac{2P}{\pi E}\ln(d) \qquad (3.2.10)$$

For the case of P acting horizontally, an anti-symmetric condition applies; $v_{\theta=0} = v_{\theta=\pi}$ and $u_{\theta=0} = -u_{\theta=\pi}$. To prevent a rigid body translation we fix the horizontal displacements at the surface at some distance, b, say from the origin. The constants of integration then become :

$$A = \frac{(1-\nu)}{2E}$$

$$B = \frac{2}{\pi E} \ln(b) \qquad (3.2.11)$$

$$C = 0$$

Again denoting $u^*_{\ell k}$ as the displacement in the 'k' direction (at the field point), due to a unit load in the 'ℓ' direction, (at the source point), the solution (3.2.9) may be specialised for the free surface, and expressed as follows

$$\begin{aligned} u^*_{11} &= \alpha_1 - \alpha_2 \ln(r) \\ u^*_{12} &= - \lambda \alpha_3 \\ u^*_{21} &= + \lambda \alpha_3 \\ u^*_{22} &= \alpha_4 - \alpha_2 \ln(r) \end{aligned} \qquad (3.2.12)$$

where, $\lambda = + 1$ for the field point , Y , lying on the positive x_2 side

and $\lambda = - 1$ for the field point, Y , lying on the negative x_2 side.

and where $\alpha_i (i = 1, 4)$ are constants given by :

$$\begin{aligned} \alpha_1 &= \frac{1}{\pi E} \left[2 \ln(d) - (1+\nu)\right] \\ \alpha_2 &= \frac{2}{\pi E} \\ \alpha_3 &= \frac{(1-\nu)}{2E} \\ \alpha_4 &= \frac{2}{\pi E} \ln(b) \end{aligned} \qquad (3.2.13)$$

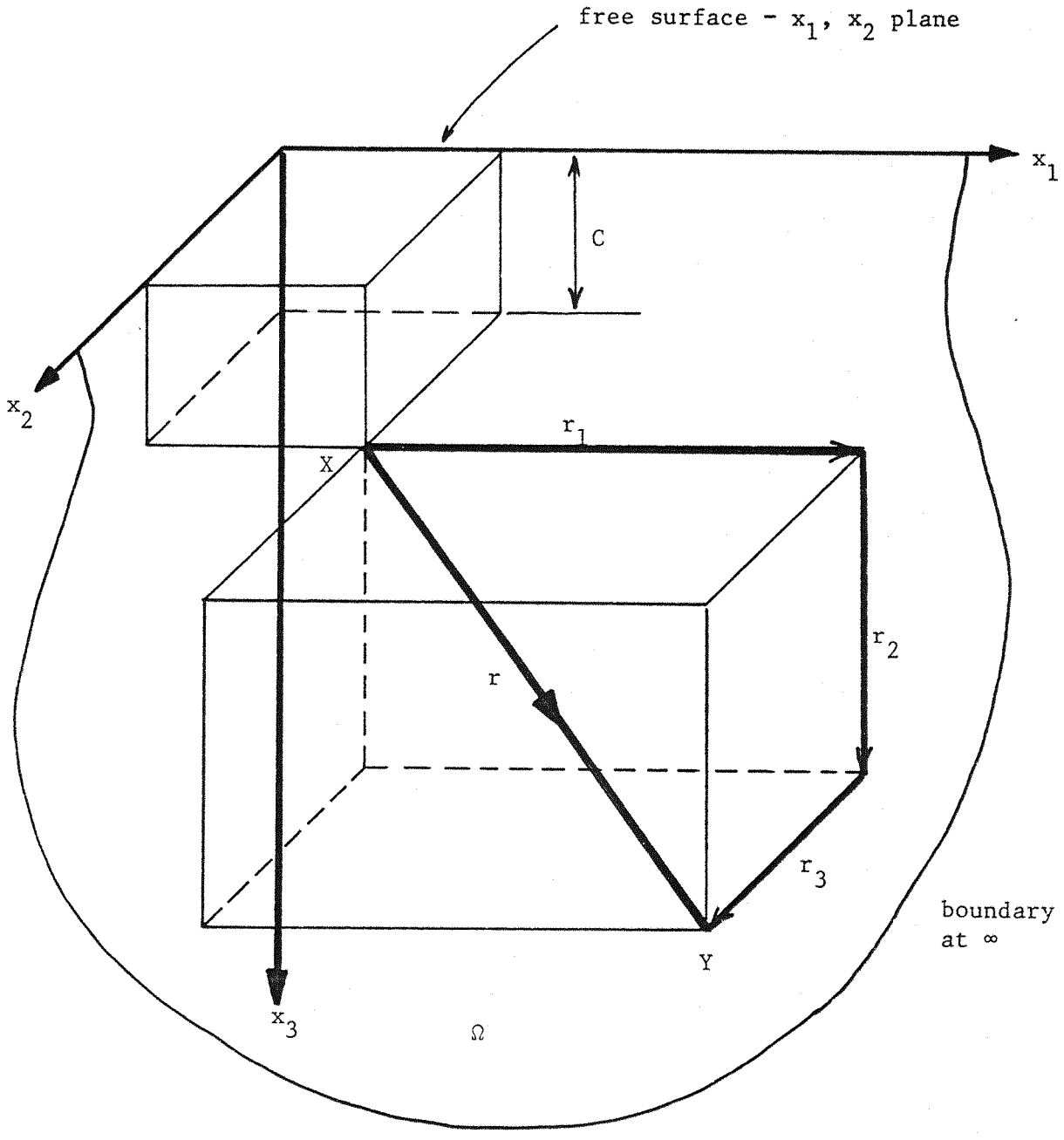

Ω ($x_3 > 0$) represents the semi-infinite domain

X denotes the source point

Y denotes the field point

Figure 3.2.3. The Mindlin Problem. Force acting in the interior of a 3-Dimensional semi-infinite space.

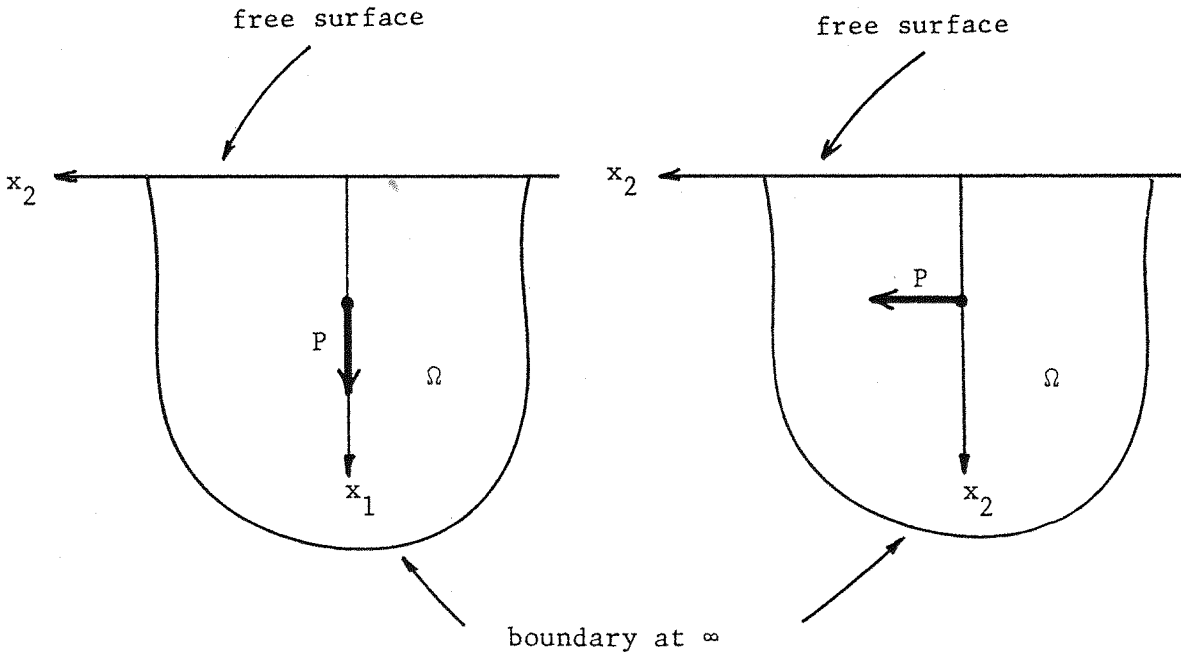

Figure 3.2.4. The Melan Problem - Force acting in the interior of a 2-Dimensional semi-infinite space.

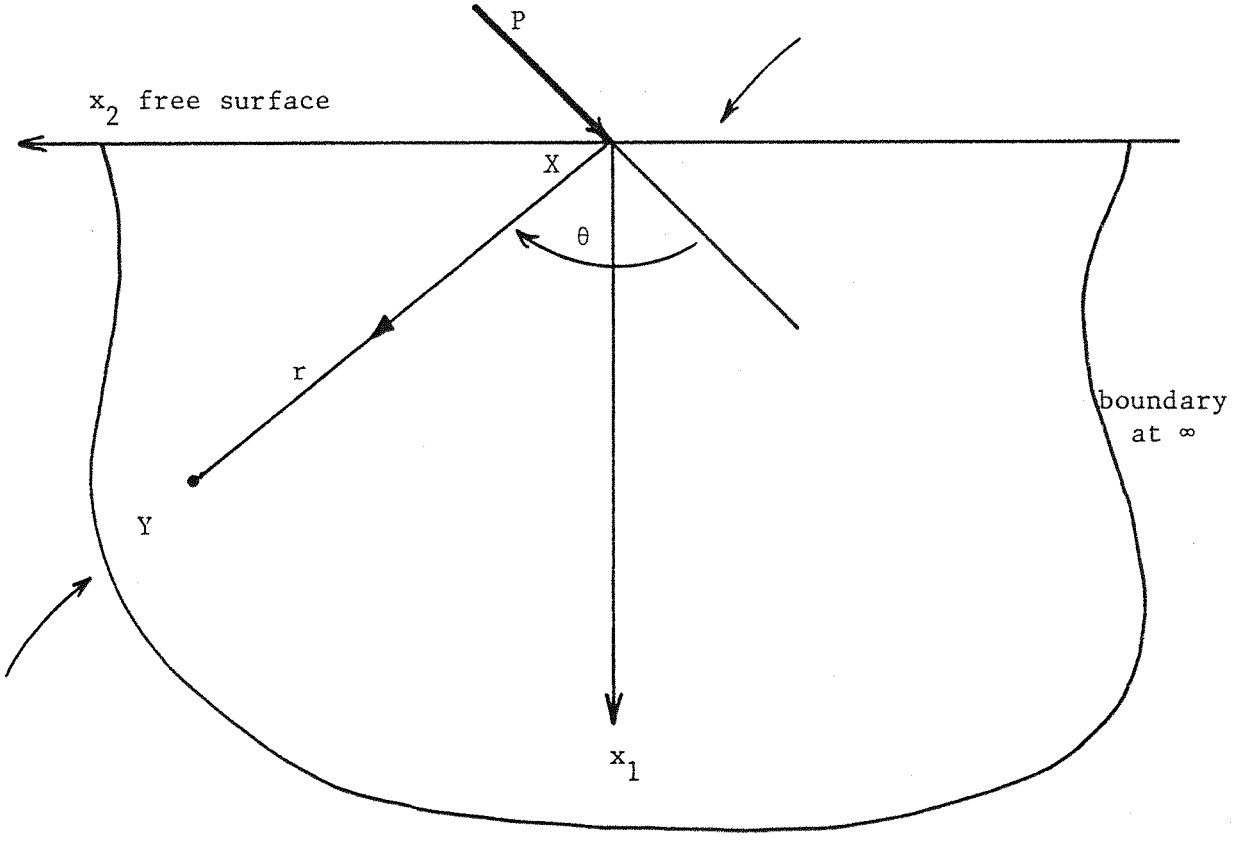

Figure 3.2.5. The Bouosinesq Problem. Inclined force acting at the free surface of a 2-Dimensional semi-infinite space.

It is important to note that the displacements cannot be defined absolutely, only in relation to some chosen fixed datum :- thus the constants b and d can be chosen quite arbitrarily and not affect the relative values of the displacements, upon which the values of the stresses depend.

3.3 REDUCTION OF THE EQUILIBRIUM EQUATIONS TO A BOUNDARY INTEGRAL FORM

3.3.1 Boundary Integral Equation for an Interior Point

Referring to Fig. 2.3.1 we require the solution of the equilibrium equations

$$\sigma_{jk,j} + b_k = 0 \quad , \quad \text{in} \quad \Omega \tag{3.3.1}$$

with boundary conditions

$$\begin{aligned} u_i &= \bar{u}_i \quad \text{on} \quad \Gamma_1 \\ p_i &= \bar{p}_i \quad \text{on} \quad \Gamma_2 \end{aligned} \tag{3.3.2}$$

For an assumed solution, u_k , the error is minimized by the weighted residual statement (2.3.31), which can now be written in the terms of this particular problem as,

$$\begin{aligned} \int_\Omega (\sigma_{jk,j} + b_k) u_k^* \, d\Omega = & \int_{\Gamma_2} (p_k - \bar{p}_k) u_k^* \, d\Gamma \\ & + \int_{\Gamma_1} (\bar{u}_k - u_k) p_k^* \, d\Gamma \end{aligned} \tag{3.3.3}$$

where u_k^*, p_k^* are interpreted as weighting functions.
p_k^* and u_k^* are related by virtue of the fact that p_k^* is the traction distribution on the boundary corresponding to the displacement field u_k^* .

Integrating equation (3.3.3) by parts and using equations (2.2.1) and (2.2.2), we have

$$\int_\Omega b_k\, u_k^*\, d\Omega - \int_\Omega \sigma_{jk}\, \varepsilon_{jk}^*\, d\Omega = -\int_{\Gamma_1} p_k\, u_k^*\, d\Gamma + \int_{\Gamma_1} (\bar{u}_k - u_k) p_k^*\, d\Gamma - \int_{\Gamma_2} \bar{p}_k\, u_k^*\, d\Gamma \tag{3.3.4}$$

At this stage we see that by interpreting the weighting functions (denoted by *) as a small virtual displacement field δu_k and its corresponding strain and traction field, $\delta\varepsilon_{jk}$, δp_k, equation (3.3.4) becomes the Principle of Virtual Work (equation (2.3.26)) corresponding to the generalised Reissner Energy functional (equation (2.3.25)). Furthermore, by assuming that the boundary conditions are identically satisfied on the Γ_1 part of the boundary, and that the virtual displacements on this part of the boundary are zero, equation (3.3.4) reduces to the special case of the Principle of Virtual Work (equation (2.3.21)), which is used as the starting expression for the Finite Element Method.

Now, making use of Betti's theorem

$$\int_\Omega \sigma_{jk}\, \varepsilon_{jk}^*\, d\Omega = \int_\Omega \sigma_{jk}^*\, \varepsilon_{jk}\, d\Omega \tag{3.3.5}$$

and again integrating equation (3.3.4) by parts, we have,

$$\int_\Omega b_k\, u_k^*\, d\Omega + \int_\Omega \sigma_{jk,j}^*\, u_k\, d\Omega = -\int_{\Gamma_2} \bar{p}_k\, u_k^*\, d\Gamma - \int_{\Gamma_1} p_k\, u_k^*\, d\Gamma + \int_{\Gamma_1} \bar{u}_k\, p_k^*\, d\Gamma + \int_{\Gamma_2} u_k\, p_k^*\, d\Gamma \tag{3.3.6}$$

or in general,

$$- \int_{\Omega} \sigma^*_{jk,j} \, u_k \, d\Omega + \int_{\Gamma} p^*_k \, u_k \, d\Gamma$$
$$= \int_{\Gamma} u^*_k \, p_k \, d\Gamma + \int_{\Omega} b_k \, u^*_k \, d\Omega \qquad (3.3.7)$$

We now interpret the weighting field $(\sigma^*_{jk}, u^*_k, p^*_k)$ as the solution to the fundamental problem, for a single unit point load acting at 'i' . This problem is represented by the equation

$$\sigma^*_{jk,j} + \Delta^i_\ell = 0 \qquad (3.3.8)$$

where Δ^i_ℓ represents a point load at 'i' acting in the 'ℓ' direction.

For each point 'i' , within the domain Ω , the domain integral in equation (3.3.7) becomes, $- u^i$, giving,

$$u^i_\ell + \int_{\Gamma} p^*_{\ell k} \, u_k \, d\Gamma = \int_{\Gamma} u^*_{\ell k} \, p_k \, d\Gamma + \int_{\Omega} u^*_{\ell k} \, b_k \, d\Omega \qquad (3.3.9)$$

where, u^i represents the displacement at 'i' in the 'ℓ' direction.

and, $u^*_{\ell k}, p^*_{\ell k}$ are the fundamental solutions for displacements and tractions, representing the response in the 'k' direction due to a unit load (at 'i'), in the 'ℓ' direction. (see section 3.2).

Equation (3.3.9) is the well known Somigliana identity, giving the displacements of any point 'i' , within the domain Ω , in terms of the displacements and tractions on the boundary of the domain, Γ .

An alternative derivation of the Somigliana identity (see, [8]), is to write Bettis theorem as :

$$\int_{\Omega} \left(u_j \, D_{jk} \, (u_k^*) - u_j^* \, D_{jk} \, (u_k)\right) d\Omega$$

$$= \int_{\Gamma} (u_j \, p_j^* - u_j^* \, p_j) d\Gamma \qquad (3.3.10)$$

Which is equivalent to writing the equilibrium equations (3.3.5) in terms of displacements and integrating both sides by parts. (It is interesting to note that (3.3.10) corresponds to Greens second theorem). D_{jk} is the differential operator of the Navier equilibrium equations (2.3.9), in terms of displacements.

$$D_{jk}(u_j) = \frac{1}{1-2\nu} u_{j,jk} + u_{k,jj} = 0 \qquad (3.3.11)$$

The first term in equation (3.3.10) becomes $-u_j^i$, as u_k^* is the fundamental solution ; The second term of equation (3.3.10) represents the distribution of the error in the assumed solution, u_k , weighted by a function, u_k^* , and summed over the domain. Setting this term equal to zero implies the minimisation of this error in an average sense over the domain Ω. Equation (3.3.10) then results, in the Somigliana identity (3.3.9). (The body force terms have been omitted for simplicity).

Although the weighted residual formulation appears more cumbersome than the second alternative, the processes are equivalent, as the general weighted residual statement simply starts at a degree of integration further back; It should be noted that we are still using a weighted residual concept in the argument used to set the second term of equation (3.3.10) equal to zero. The more general formulation presented in the first part of this section has the

advantage of enveloping the Finite Element technique in addition to showing how the Boundary Element method can be thought of as a special case of a much more general process for the numerical solution of differential equations.

3.3.2 Boundary Integral Equation for a Boundary Point.

The Somigliana identity (equation (3.3.9)) is valid for the source point 'i' inside the domain Ω. When this point is moved to the boundary, Γ, the integrals involved in equation (3.3.9) become singular at 'i' and must be evaluated in the Gauchy Principle Value sense. Consider the body augmented by a small hemisphere, radius ε, centred at 'i', such that the boundary is now made up of $\Gamma_{\Gamma-\varepsilon} + \Gamma_{\varepsilon}$, and the point 'i' now lies within the domain of this augmented body. (See Fig. 3.3.1).

The boundary integrals of equation (3.3.9) may now be considered as the sum $\int_{\Gamma_{\Gamma-\varepsilon}} + \int_{\Gamma_{\varepsilon}}$ and evaluated at the limit as $\varepsilon \to 0$. The evaluation of the term $\int_{\Gamma_{\varepsilon}}$ is facilitated by employing a spherical system of coordinates (Fig. 3.3.2); details of the integration are given here for the 3-Dimensional Kelvin solution. (See [5]).

Consider the first integral in equation (3.3.9) as two parts:

$$\int_{\Gamma} u_k \, p^*_{\ell k} \, d\Gamma = \int_{\Gamma_{\Gamma-\varepsilon}} u_k \, p^*_{\ell k} \, d\Gamma + \int_{\Gamma_{\varepsilon}} u_k \, p^*_{\ell k} \, d\Gamma \qquad (3.3.12)$$

let :

$$I = \lim_{\varepsilon \to 0} \int_{\Gamma_{\varepsilon}} u_k \, p^*_{\ell k} \, d\Gamma \qquad (3.3.13)$$

Substituting for $p^*_{\ell k}$ from equation (3.2.2),

$$I = \lim_{\varepsilon \to 0} \left[- \int_{\Gamma_\varepsilon} u_k \left\{ \frac{\partial r}{\partial n} \left[(1-2\nu)\ \delta_{\ell k} + 3r,_\ell\ r,_k \right] \right.\right.$$

$$\left.\left. - (1-2\nu)\ \left[r,_\ell\ n_k - r,_k\ n_\ell \right] \right\} \frac{d\Gamma}{8\pi(1-\nu)r^2} \right] \tag{3.3.14}$$

Now, for the particular case of the hemispherical region

$$\frac{\partial r}{\partial x_i} = \frac{r_i}{r} = n_i = e_i \tag{3.3.15}$$

Where, e_i are the projections of the unit normal vector on the x_i coordinate axes. The second term in equation (3.3.14) becomes,

$$r,_\ell\ r,_k - r,_k\ r,_\ell = 0$$

Noting the fact that $\frac{dr}{dn} = 1$, equation (3.3.14) may now be written,

$$I = \lim_{\varepsilon \to 0} \left[- \int_{\Gamma_\varepsilon} u_k \left[(1-2\nu)\ \delta_{\ell k} + 3r,_\ell\ r,_k \right] \frac{d\Gamma}{8\pi(1-\nu)r^2} \right] \tag{3.3.16}$$

and expanding (3.3.16) for the instance when $\ell = 1$,

$$I = \lim_{\varepsilon \to 0} \left[- \int_{\Gamma_\varepsilon} \left[u_1^i\ (1-2\nu) + 3u_1^i\ e_1 e_1 + 3u_2^i\ e_1 e_2 + 3u_3^i\ e_1 e_3 \right] \right.$$

$$\left. \frac{\sin\theta\ d\theta\ d\phi}{8\pi(1-\nu)} \right] \tag{3.3.17}$$

The integral is now independent of r and may be expressed in terms of θ and ϕ only.

$$I = - \int_0^{2\pi} \int_0^{\pi/2} u_1^i(1-2\nu) + 3u_1^i \sin^2\theta \cos^2\phi + 3u_2^i \sin^2\theta \cos\phi \sin\phi$$

$$3u_3^i \sin\theta \cos^2\phi\ \frac{\sin\theta\ d\theta\ d\phi}{8\ (1-\nu)} \tag{3.3.18}$$

'I' is now reduced to integrals of a standard form which may readily be evaluated to yield the following result:

$$I = \frac{-\left[(1-2\nu)2\pi + 2\pi\right]u_1^i}{8\pi(1-\nu)} \qquad (3.3.19)$$

hence, $$I = \frac{-4(1-\nu)}{8(1-\nu)}\, u_1^i = -\frac{1}{2}\, u_1^i$$

The same result applies for $\ell = 2$ and $\ell = 3$, giving the combined result as :

$$I = \lim_{\varepsilon \to 0} \int_{\Gamma_\varepsilon} u_k\, p^*_k\, d\Gamma = -\frac{1}{2}\, u_\ell^i \qquad (3.3.20)$$

The second integral in the Somigliana identity (3.3.9) may be written

$$\int_\Gamma p_k\, u^*_{\ell k}\, d\Gamma = \int_{\Gamma - \Gamma_\varepsilon} p_k\, u^*_{\ell k}\, d\Gamma + \int_{\Gamma_\varepsilon} p_k\, u^*_{\ell k}\, d\Gamma \qquad (3.3.21)$$

The fundamental solution for $u^*_{\ell k}$ (equation 3.2.1)) is of the order $\frac{1}{r}$ as opposed to $\frac{1}{r^2}$ for $p^*_{\ell k}$, and when transforming to spherical coordinates, there remains a factor 'r' in the numerator, i.e.

$$I = \lim_{\varepsilon \to 0} \left[\int_{\Gamma\varepsilon} f(\phi, \theta)\, r\, d\phi\, d\theta \right] \qquad (3.3.22)$$

Hence the term disappears in the limit of $\varepsilon \to 0$, and therefore, this integral does not introduce a new term to the Somigliana identity.

The same analysis may be applied for the 2-Dimensional Kelvin solution and in fact yields the same result.

The Somigliana identity may now be written for any point 'i'

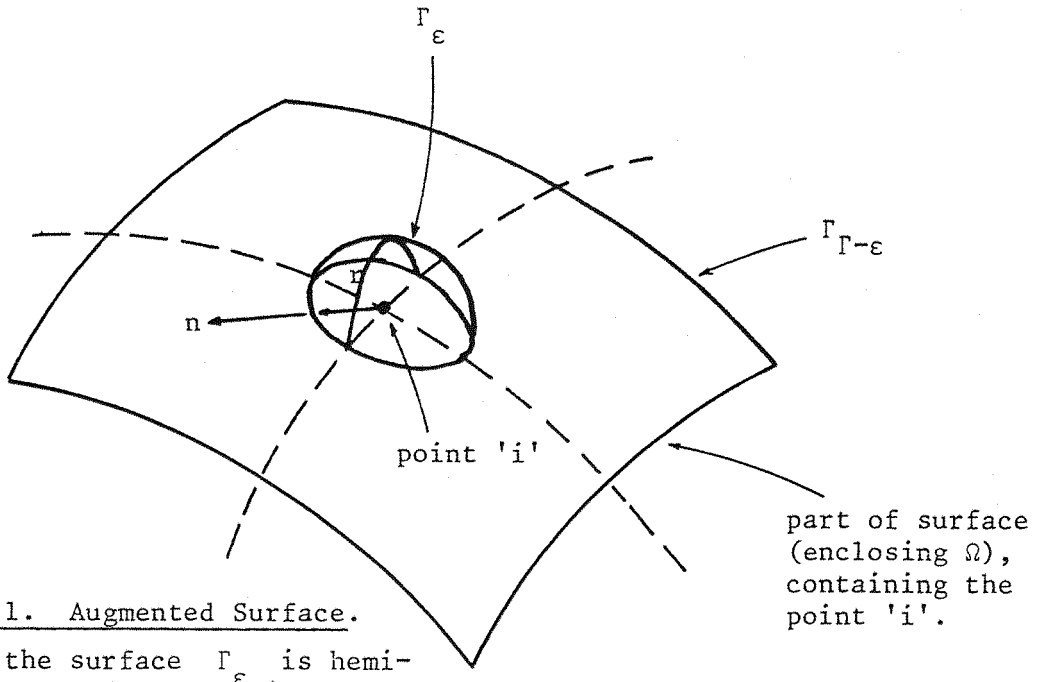

Figure 3.3.1. Augmented Surface.

(Note : As the surface Γ_ε is hemispherical, r and n are in the same direction i.e. $\frac{\partial r}{\partial n} = 1$)

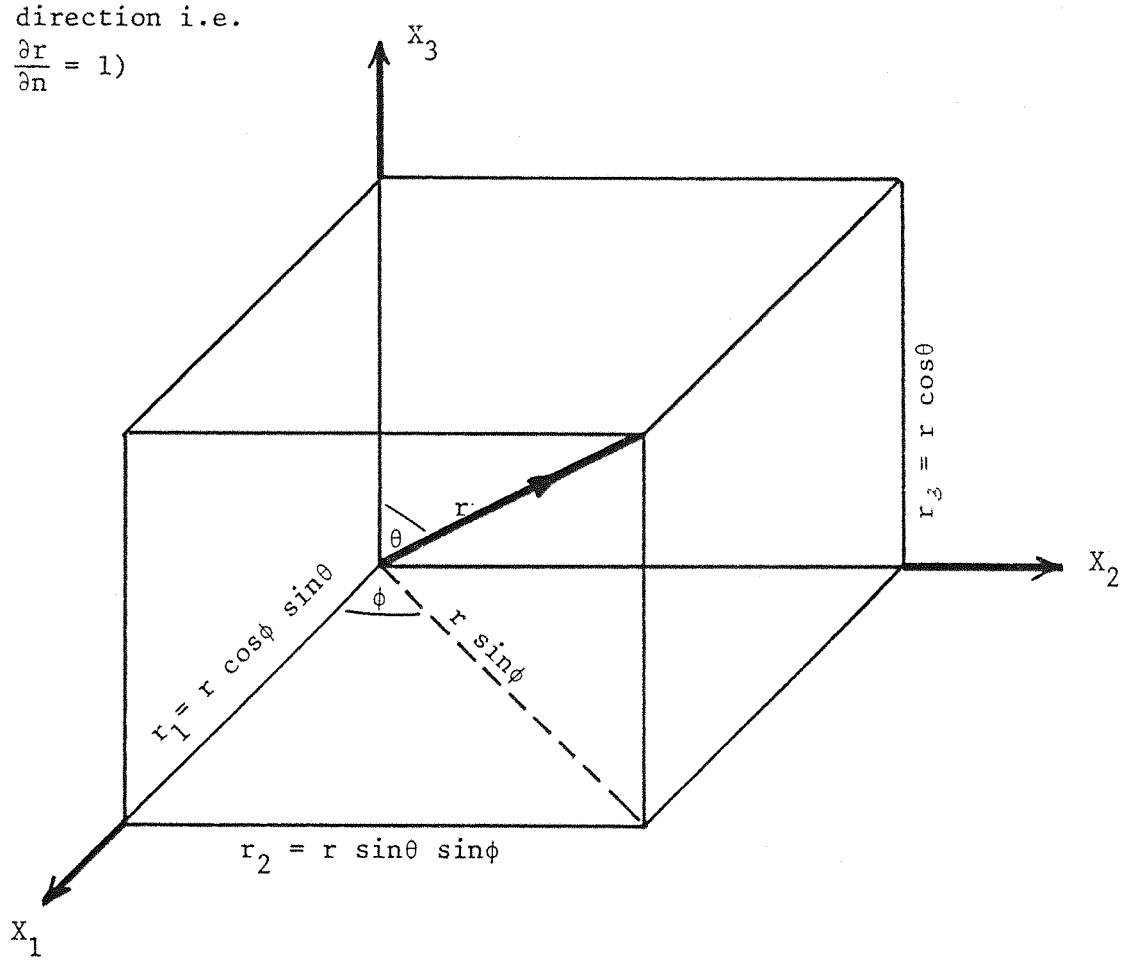

Figure 3.3.2. Definition of Spherical Coordinates

on the boundary.

$$c^i_{\ell k}\, u^i_k + \int_\Gamma p^*_{\ell k}\, u_k \, d\Gamma = \int_\Gamma u^*_{\ell k}\, p_k \, d\Gamma + \int_\Omega u^*_{\ell k}\, b_k \, d\Omega \qquad (3.3.23)$$

where $c^i_{\ell k} = \frac{1}{2}\,\delta_{\ell k}$ for a closed body (Kelvin solution), and with 'i' lying on a smooth surface Γ. The analogous situation for the semi-infinite space fundamental solutions are examined in depth by NAKAGUMA [10] and equation (3.3.23) is valid for all cases with the following provisos on $c^i_{\ell k}$.

(i) For infinite and semi-infinite solutions, 'i' ε Ω

$$c^i_{jk} = \delta_{jk} \qquad (3.2.24a)$$

(ii) For infinite and semi-infinite solutions 'i' ε Γ

$$c^i_{jk} = \frac{1}{2}\,\delta_{jk} \qquad (3.2.24b)$$

(iii) For semi-infinite solution 'i' ε Γ (Γ is now the free surface)

$$c^i_{jk} = \delta_{jk} \qquad (3.2.24c)$$

For the case when the source point 'i' does not lie on a smooth part of the boundary calculation of the term $c^i_{\ell k}$ can become very complicated. This situation is usually dealt with using rigid body motion considerations and will be discussed later, in section 3.4.

3.3.3 Solution for an Internal Point

Once the complete solution on the boundary is achieved, the response at any interval point is readily available by making use of the Somigliana identity (equation (3.3.9)). We have, for

for any internal point 'i' , the displacement in the 'ℓ' direction, given by :

$$u_\ell^i = \int_\Gamma u^*_{\ell k}\, p_k \, d\Gamma - \int_\Gamma p^*_{\ell k}\, u_k \, d\Gamma + \int_\Omega b_k \, u^*_{\ell k} \, d\Omega \qquad (3.3.25)$$

The stress at 'i' can be obtained by differentiation, and for an isotropic material, using the Kelvin solution, the solution is given by : (see [5]).

$$\sigma_{ij} = \int_\Gamma D_{kij}\, p_k \, d\Gamma - \int_\Gamma S_{kij}\, u_k \, d\Gamma + \int_\Omega D_{kij}\, b_k \, d\Omega \qquad (3.3.26)$$

where :

$$D_{kij} = \frac{1}{r^\alpha} \left\{ (1-2\nu) \left[\delta_{ki}\, r_{,j} + \delta_{kj}\, r_{,i} - \delta_{ij}\, r_{,k} \right] + \beta\, r_{,i}\, r_{,j}\, r_{,k} \right\} \frac{1}{4\alpha(1-\nu)} \qquad (3.3.27)$$

$$S_{kij} = \frac{1}{r^\beta} \left\{ \beta \frac{\partial r}{\partial n} \left[(1-2\nu)\, \delta_{ij}\, r_{,k} + \nu(\delta_{ik}\, r_{,j} + \delta_{jk}\, r_{,i}) - \gamma\, r_{,i}\, r_{,k} \right] + \beta\nu \left[n_i\, r_{,j}\, r_{,k} + n_j\, r_{,i}\, r_{,k} \right] + (1-2\nu) \left[\beta n_k\, r_{,i}\, r_{,j} + n_j\, \delta_{ik} + n_i\, \delta_{jk} \right] - (1-4\nu)\, n_k\, \delta_{ij} \right\} \frac{1}{4\pi(1-\nu)\alpha} \qquad (3.3.28)$$

This solution applies to both the two and three dimensional cases:

For 2-D $\alpha = 1$, $\beta = 2$, $\gamma = 4$

For 3-D $\alpha = 2$, $\beta = 3$, $\gamma = 5$

3.4 THE BOUNDARY ELEMENT METHOD

As most of the applications presented in this work are 2-Dimensional, the following matrix formulation will be described for problems in two dimensions. However the process involved can be readily extended to the 3-Dimensional case.

At this point it is convenient to write the Somigliana identity (equation (3.3.25)) in a matrix notation :

Define $\underset{\sim}{u}^*$ as a 2×2 matrix with elements $u^*_{\ell k}$, $(\ell, k = 1, 2)$, and $\underset{\sim}{p}^*$, similarly, with elements $p^*_{\ell k}$ i.e.

$$\underset{\sim}{p}^* = \begin{bmatrix} p^*_{11} & p^*_{12} \\ p^*_{21} & p^*_{22} \end{bmatrix} \quad ; \quad \underset{\sim}{u}^* = \begin{bmatrix} u^*_{11} & u^*_{12} \\ u^*_{21} & u^*_{22} \end{bmatrix} \tag{3.4.2}$$

The unknown displacements and tractions, and the known body forces, (u_k, p_k, b_k) may be written as vectors:

$$\underset{\sim}{u} = \begin{Bmatrix} u_1 \\ u_2 \end{Bmatrix} \quad ; \quad \underset{\sim}{p} = \begin{Bmatrix} p_1 \\ p_2 \end{Bmatrix} \quad ; \quad \underset{\sim}{b} = \begin{Bmatrix} b_1 \\ b_2 \end{Bmatrix} \tag{3.4.2}$$

The Somigliana identity, equation (3.3.25) can then be expressed in matrix form as,

$$\underset{\sim}{c}^i \, \underset{\sim}{u}^i + \int_\Gamma \underset{\sim}{p}^* \, \underset{\sim}{u} \, d\Gamma = \int_\Gamma \underset{\sim}{u}^* \, \underset{\sim}{p} \, d\Gamma + \int_\Omega \underset{\sim}{u}^* \, \underset{\sim}{b} \, d\Omega \tag{3.4.3a}$$

or

$$\underset{\sim}{c}(S) \, \underset{\sim}{u}(S) + \int_\Gamma \underset{\sim}{p}^*(S,Q) \, \underset{\sim}{u}(Q) \, d\Gamma(Q)$$

$$= \int_\Gamma u^*(S,Q) \, p(Q) \, d\Gamma(Q)$$

$$+ \int_\Omega \underset{\sim}{u}^*(S, q) \, \underset{\sim}{b}(q) \, d\Omega(q) \tag{3.4.3b}$$

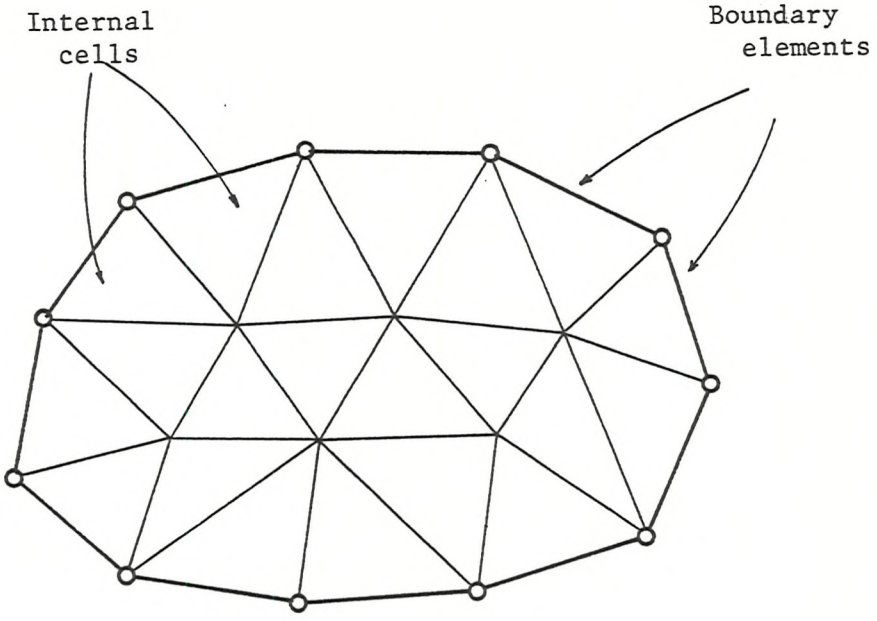

Figure 3.4.1. Body divided into boundary elements and internal cells.

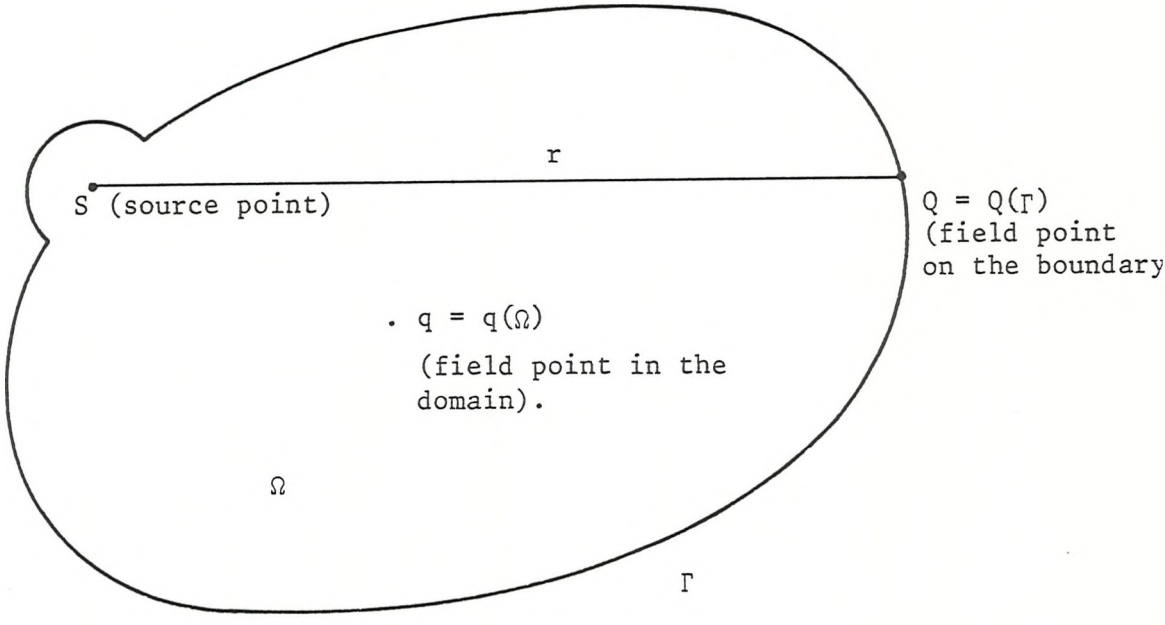

Fig. 3.4.2 Notation for the Somigliana identity.

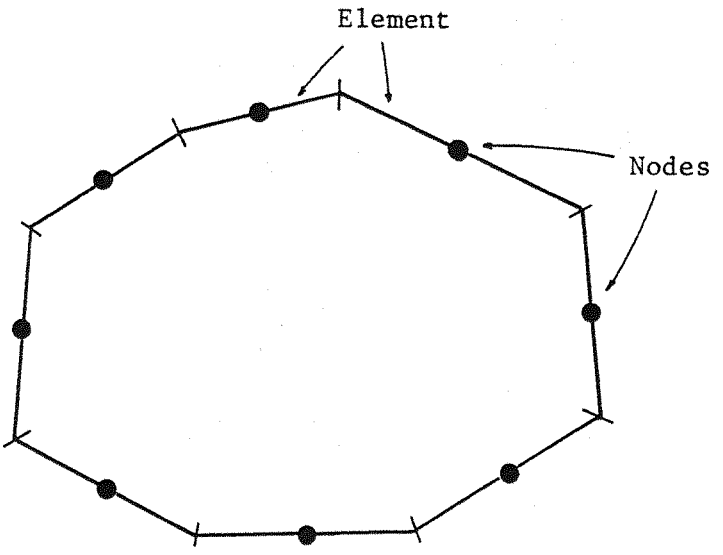

(a) Constant elements

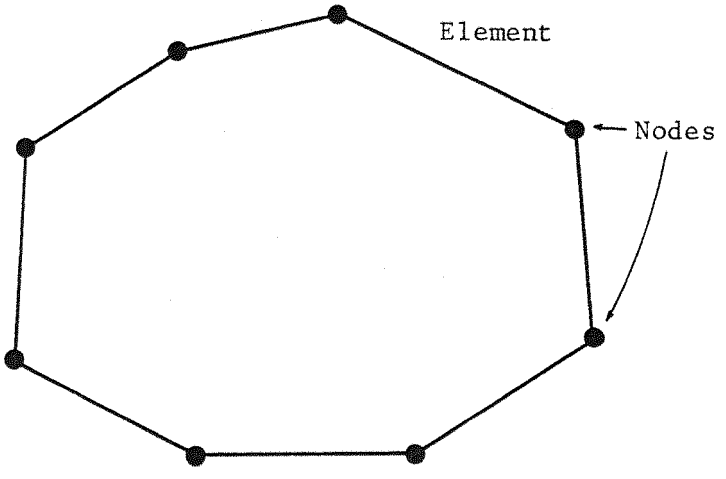

(b) Linear elements

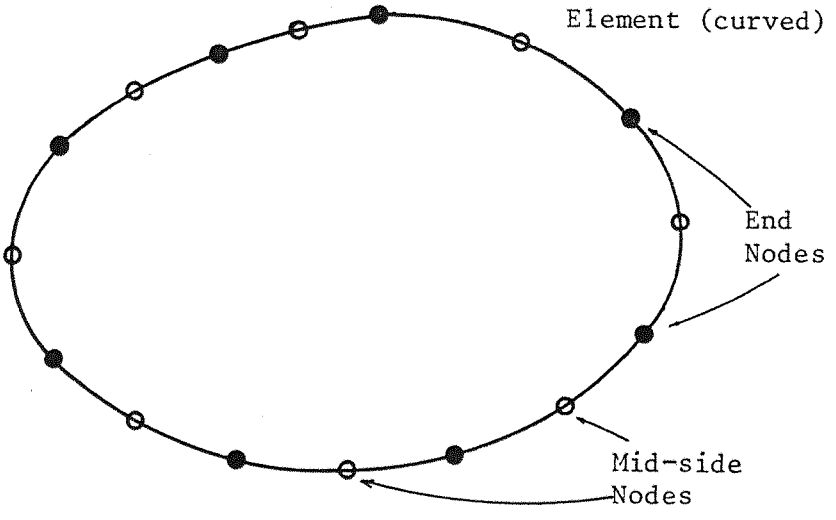

(c) Quadratic elements

Figure 3.4.3 Two dimensional body divided into boundary elements.

where S is the source point

Q is a field point on the boundary Γ

q is a field point in the domain Ω

(see Fig. 3.4.2)

The type of notation in equation (3.4.3b) is more complete and found commonly in the literature, however, for convenience, the simpler notation of equation (3.4.3a) will be retained in this work. The boundary may now be divided into a discrete number of elements with defined nodal points, and the domain divided into cells for the numerical evaluation of the body force term in equation (3.4.3). See figure 3.4.1

Consider the case of the boundary values of $\underset{\sim}{u}$ and $\underset{\sim}{p}$ given by some interpolation functions, such that;

$$\underset{\sim}{u} = \underset{\sim}{\Phi}^T \underset{\sim}{u}^n$$

$$\underset{\sim}{p} = \underset{\sim}{\Psi}^T \underset{\sim}{p}^n \qquad (3.4.4)$$

where, $\underset{\sim}{u}^n$ and $\underset{\sim}{p}^n$ are the nodal values of displacements and tractions.

The simplest possible elements are those for which $\underset{\sim}{u}$ and $\underset{\sim}{p}$ are constant over the element and consist of a straight line with a central node. (Fig. 3.4.3(a)). The value of $\underset{\sim}{p}$ and $\underset{\sim}{u}$ over the whole element is taken as constant and equal in value to that at the node. In general $\underset{\sim}{u}$ and $\underset{\sim}{p}$ can have any variation (Figs. 3.4.3) simply by choosing the appropriate interpolation functions $\underset{\sim}{\Phi}$ and $\underset{\sim}{\Psi}$. These functions are standard interpolation functions similar to those used in Finite Element formulations, the main difference being that they vary only along the boundary Γ as opposed to over the domain Ω, which in fact lessens their complexity. In order to find the body

force terms the domain has to be divided into a series of cells (Fig. 3.4.1), or internal elements, however, in contrast to finite elements this process does not introduce any additional internal unknowns.

Substituting equation (3.4.4) into the matrix equation (3.4.3), we can write for each particular node, 'i' :

$$\underset{\sim}{c}^{i}\ \underset{\sim}{u}^{i} + \sum_{\ell=1}^{NE} \left\{ \int_{\Gamma_\ell} \underset{\sim}{p}^{*}\ \underset{\sim}{\Phi}^{T}\, d\Gamma \right\} \underset{\sim}{u}^{n} = \sum_{\ell=1}^{NE} \left\{ \int_{\Gamma_\ell} \underset{\sim}{u}^{*}\ \underset{\sim}{\Psi}^{T}\, d\Gamma \right\} \underset{\sim}{p}^{n} + \sum_{k=1}^{M} \left\{ \int_{\Omega_k} \underset{\sim}{u}^{*}\ \underset{\sim}{b}\, d\Omega \right\} \tag{3.4.5}$$

where: NE is the number of boundary elements

M is the number of internal cells

Γ_ℓ is the surface of the 'ℓ' boundary element

Ω_k is the area of the 'k' internal cell.

For the general case of an element with 'n' nodes the integrals in equation (3.4.5) will be of the form:

$$\int_{\Gamma_\ell} \left[\phi_1\ \phi_2 \cdots \phi_n\right] \underset{\sim}{p}^{*}\, d\Gamma$$

$$\int_{\Gamma_\ell} \left[\psi_1\ \psi_2 \cdots \psi_n\right] \underset{\sim}{u}^{*}\, d\Gamma \tag{3.4.6}$$

The products $\phi_i\ \underset{\sim}{p}^{*}$ and $\psi_i\ \underset{\sim}{u}^{*}$ (i= 1,n) are evaluated numerically, usually employing some local homogeneous system of coordinates for the interpolation functions, and using a one dimensional Gauss Quadrature scheme. Details of the interpolation functions and integration scheme are readily available in the literature (e.g. see [5]), and will be briefly discussed in Section 3.6.

Evaluation of expressions (3.4.6) and (3.4.5) produce, for each element, a set of submatrices :

$$\left[h_{\ell k}^{i p_1} \quad h_{\ell k}^{i p_2} \ldots . h_{\ell k}^{i p_n} \right]$$

and (3.4.7)

$$\left[g_{\ell k}^{i p_1} \quad g_{\ell k}^{i p_2} \ldots . g_{\ell k}^{i p_n} \right]$$

where; $h_{\ell k}^{i j_m}$ and $g_{\ell k}^{i j_m}$ are 2×2 submatrices

$(k, \ell = 1, 2)$

'i' refers to the source point

and p_m refers to the 'm'th node of element 'p' , over which the integration is being carried out.

These submatrices may then be assembled into global matrices $\underset{\sim}{H}$ and $\underset{\sim}{G}$ such that contributions at a node common to two elements are added together. For a particular node 'i' , this will produce a set of equations (2, for the 2-D case) in the $\underset{\sim}{H}$ and $\underset{\sim}{G}$ matrices, and when this process is carried out for all nodes, equation (3.4.5) may now be written :

$$\underset{\sim}{C} \; \underset{\sim}{U} + \hat{\underset{\sim}{H}} \; \underset{\sim}{U} = \underset{\sim}{G} \; \underset{\sim}{P} + \underset{\sim}{B} \qquad (3.4.8)$$

Where $\underset{\sim}{U}$ and $\underset{\sim}{P}$ are global vectors containing the displacements and tractions at the NN nodes on the boundary, and $\underset{\sim}{B}$ is a vector containing the values of the body forces at the internal nodes.

Let us now call :

$$h_{\ell k}^{ij} = \hat{h}_{\ell k}^{ij} \qquad \text{for} \quad i \neq j \qquad (3.4.9)$$

$$h_{\ell k}^{ij} = \hat{h}_{\ell k}^{ij} + c_{\ell k}^{i} \qquad \text{for} \quad i = j \qquad (3.4.10)$$

hence, equation (3.4.8) may now be written

$$\underset{\sim}{H}\ \underset{\sim}{U} = \underset{\sim}{G}\ \underset{\sim}{P} + \underset{\sim}{B} \qquad (3.4.11)$$

Note that N1 values of displacements and N2 values of tractions (N = N1 + N2) are known on the boundary, and hence in the $\underset{\sim}{U}$ and $\underset{\sim}{P}$ vectors, there remain N unknowns, which may all be gathered into a left hand side vector $\underset{\sim}{X}$; after reordering the equations, we obtain;

$$\underset{\sim\sim}{A}\underset{\sim}{X} = \underset{\sim}{F} + \underset{\sim}{B} \qquad (3.4.12)$$

Equation (3.4.12) may now be solved to yield all remaining unknown displacements and tractions on the boundary. Equations (3.2.26) and (3.2.27) may now be implemented to yield the solution at any internal point.

It should be noted that in the general case of using linear or higher order elements, the nodes do not necessarily lie on a smooth boundary, and as such the diagonal submatrices of $\underset{\sim}{H}$ (i.e. $h^{ii}_{k\ell}$) cannot be calculated using equation (3.4.10). However this may be overcome using rigid body motion considerations:

For a closed body with zero applied tractions undergoing a rigid body translation, equation (3.4.11) becomes:

$$\underset{\sim}{H}\ \underset{\sim}{U} = 0 \qquad (3.4.13)$$

(body forces have been omitted for simplicity).

In order for equation (3.4.13) to be satisfied for a unit translation in each of the coordinate directions in turn, the sum of the submatrices corresponding to each node 'i' must be zero. i.e.

$$\sum_{j=1}^{NN} h_{\ell k}^{ij} = \underset{\sim}{0} \qquad (3.4.14)$$

Hence, once the off diagonal submatrices of the $\underset{\sim}{H}$ matrix are known, the diagonal terms may be calculated by a simple summation. For infinite or semi-infinite regions, the boundary at infinity must be considered in order to allow the 'body' to undergo a rigid translation. The terms in the $\underset{\sim}{H}$ matrix will now consist of two integrals :-

$$\int_{\Gamma} p_{\ell k}^{*} \, d\Gamma + \int_{\Gamma_{\infty}} p_{\ell k}^{*} \, d\Gamma$$

The second integral may be evaluated analytically, to produce an extra contribution in equation (3.4.14), i.e.

$$\sum_{j=1}^{NN} h_{\ell k}^{ij} = \underset{\sim}{\beta}_{\ell k} \qquad (3.4.15)$$

For an infinite region using the Kelvin Solution, the Γ_{∞} surface is taken as a sphere of infinite radius and has been evaluated, yielding the result $\underset{\sim}{\beta}_{\ell k} = \underset{\sim}{\delta}_{\ell k}$ ([26], [27]). Similarly for a semi-infinite problem, using a Mindlin or Boussinesq Solution, the additional surface is considered as a hemi-sphere of infinite radius, and again gives $\underset{\sim}{\beta}_{\ell k} = \underset{\sim}{\delta}_{\ell k}$. ([10]).

3.5 THE FINITE ELEMENT FORMULATION

This work will be concerned with the Finite Element Displacement Method (FEM) and, as such, a brief description of the formulation will be given here. Full details are readily available in the literature (e.g. [19], [20]).

Consider a body as shown in Fig. 2.3.1 in which the equation

$$\sigma_{jk,j} + b_k = 0 \tag{3.5.1}$$

must be satisfied, with boundary conditions

$$\begin{aligned} p_i &= \bar{p}_i \quad \text{on} \quad \Gamma_2 \\ u_i &= \bar{u}_i \quad \text{on} \quad \Gamma_1 \end{aligned} \tag{3.5.2}$$

If we assume that the displacement boundary conditions on Γ_1 are identically satisfied then the Weighted Residual Statement (equation (2.3.31)) may be written,

$$\int_\Omega (\sigma_{jk,j} + b_k)\, u^*_k \, d\Omega = \int_{\Gamma_2} (p_k - \bar{p}_k)\, u^*_k \, d\Gamma \tag{3.5.3}$$

and integrating by parts, we have,

$$\int_\Omega \sigma_{jk}\, \varepsilon^*_{jk} \, d\Omega = \int_{\Gamma_2} \bar{p}_k\, u^*_k \, d\Gamma + \int_\Omega b_k\, u^*_k \, d\Omega \tag{3.5.4}$$

which is in fact the Principle of Virtual Work derived in section 2.3.2 (equation (2.3.21)); ε^*_{jk} and u^*_k are any mutually compatible, virtual strain-displacement fields. Equation (3.5.4) may be written in matrix notation as:

$$\begin{aligned} \int_\Omega \underset{\sim}{\varepsilon}^{*,T}\, \underset{\sim}{\sigma} \, d\Omega &= \int_{\Gamma_2} \underset{\sim}{u}^{*,T}\, \underset{\sim}{p} \, d\Gamma \\ &+ \int_\Omega \underset{\sim}{u}^{*,T}\, \underset{\sim}{b} \, d\Omega \end{aligned} \tag{3.5.5}$$

We now divide the domain into a discrete number of 'Finite Elements' and assume that over each element, the variation of $\underset{\sim}{u}$ and $\underset{\sim}{u}^*$ can be approximated using their values at the nodes of each element and a set of interpolation functions - the same for both. i.e.

$$\underset{\sim}{u} = \underset{\sim}{\phi}^T \underset{\sim}{u}^n$$

$$\underset{\sim}{u}^* = \underset{\sim}{\phi}^T \underset{\sim}{u}^{*n} \tag{3.5.6}$$

Differentiating these displacements, (equation (2.2.2)), the strains may be expressed as :

$$\underset{\sim}{\varepsilon}^* = \underset{\sim}{B}\ \underset{\sim}{u}^{*n} \tag{3.5.7}$$

and the stress-strain relations (equation (2.2.4)) give,

$$\underset{\sim}{\sigma} = \underset{\sim}{D}\ \underset{\sim}{\varepsilon} = \underset{\sim}{D}\ \underset{\sim}{B}\ \underset{\sim}{u}^n \tag{3.4.8}$$

The tractions on the boundary are interpolated as,

$$\underset{\sim}{p} = \underset{\sim}{\Psi}^T \underset{\sim}{p}^n \tag{3.5.9}$$

and the body forces,

$$\underset{\sim}{b} = \underset{\sim}{\Phi}^T \underset{\sim}{b}^n \tag{3.5.10}$$

Substituting (3.5.6) - (3.5.10) in equation (3.5.5) and replacing the integrals by a summation over the elements,

$$\underset{\sim}{u}^{*n,T} \sum^{NE} \left(\int_{\Omega_e} \underset{\sim}{B}^T \underset{\sim}{D}\ \underset{\sim}{B}\ d\Omega \right) \underset{\sim}{u}^n = u^{*n,T} \sum^{NS} \left(\int_{\Gamma_\ell} \underset{\sim}{\Phi}\ \underset{\sim}{\Psi}^T\ d\Gamma \right) \underset{\sim}{p}^n + u^{*n,T} \sum^{NE} \left(\int_{\Omega_e} \underset{\sim}{\Phi}\ \underset{\sim}{\Phi}^T\ d\Omega \right) \underset{\sim}{b}^n \tag{3.5.11}$$

where NE is the number of elements in Ω

and NS is the number of boundary segments on Γ .

or

$$\underset{\sim}{K}\ \underset{\sim}{U} = \underset{\sim}{F} + \underset{\sim}{D} \tag{3.5.12}$$

where $\underset{\sim}{K}$ is the global stiffness matrix obtained by assembling the element contributions ($\underset{\sim}{K}_e = \int_{\Omega_e} B^T D B \, d\Omega$) in the normal way.

$\underset{\sim}{U}$ is the global vector of displacements

$\underset{\sim}{F}$ is the global vector of equivalent nodal loads -obtained by weighting the distribution of tractions as shown in the second term of equation (3.5.11)

and $\underset{\sim}{D}$ is a vector containing the influence of the body forces (known), given by the third term of equation (3.5.11).

The displacement boundary conditions may now be imposed on equations (3.5.12) and the system solved to yield the remaining unknown displacements.

3.6 COMPUTER IMPLEMENTATION OF THE BOUNDARY ELEMENT METHOD

3.6.1 General Structure of Program

This section will give a brief description of the computer program developed (using linear elements), as a basis for the 2-Dimensional formulations described in this work.

(Chapter 4 will include some 3-Dimensional applications using constant elements; the program developed for this part of the work is very similar in structure to that of the 2-D case, the main differences being in the description of the element geometry and in the numerical integration scheme employed. This part of the program was largely based on the work of NAKAGUMA [10] and all relevant details pertaining to these aspects are fully documented in the above reference. As such they will not be repeated here).

The macro flow chart of the program is shown in Fig. 3.6.1.

The MAIN program is used to define the work areas required to solve the problem :

Several 1-Dimensional arrays required are :

X : stores the x coordinate of each node

Y : stores the y coordinate of each node

FLAG : contains 2 flags for each node (one for each coordinate direction) defining the type of boundary condition. (Integer array).

: FLAG = 0 indicates the displacement is prescribed.

FLAG = 1 indicates the traction is prescribed.

VALUE : Contains the two prescribed values of either displacement or traction at each node (one in each coordinate direction).

RHSV : Right hand side vector of the final system of equations. (See equation (3.4.12)).

One 2-Dimensional array is required :

A(N,N) : used to store the left hand side coefficients of the final system of equations (see equation (3.4.12)).

(N is the order of the system, = {Total number of nodes} × 2.)

The MAIN program then calls the routines as shown in Fig. 3.6.1.

The INPUT routine reads in all the parameters necessary to define the problem :- The number of nodes, and then for each node, in each coordinate direction :-

(i) the global coordinate; (X, Y)

(ii) the flag defining the type of boundary condition; (FLAG)

(iii) the value of the prescribed boundary condition; (VALUE).

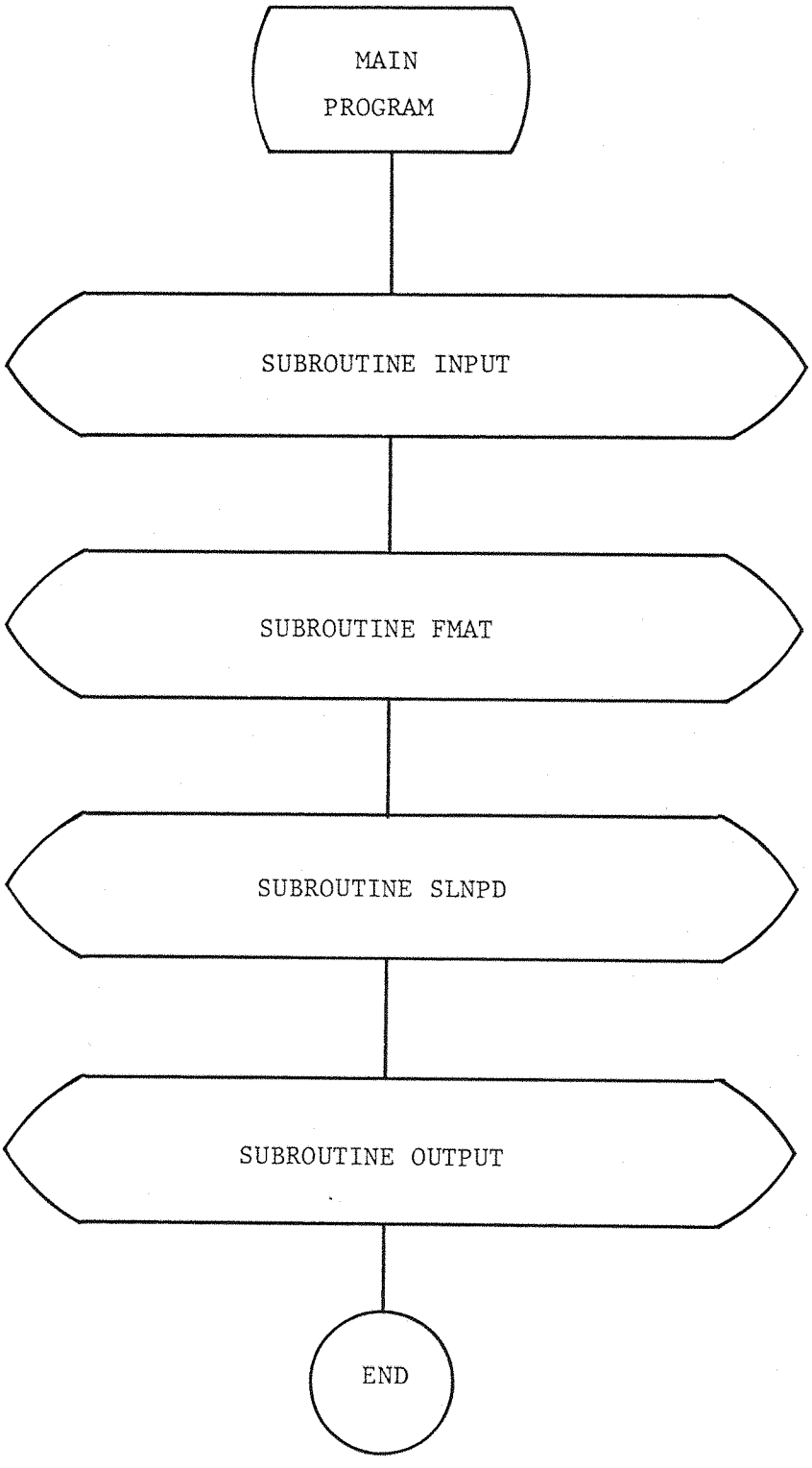

Figure 3.6.1 Macro flow chart used as a basis for the implementation of the B.E.M.

The routine, FMAT forms the final system of equations (3.4.12).

For node I, the routine loops on each element forming the integrals shown in equation (3.4.5). (The details of the integration process will be shown in the following section). For each element two sets of terms (see expression (3.4.7)) will be formed, (as there are 2 nodes per element) and are stored in local work areas H(L,K,J), G(L,K,J). J takes the value 1 for the first node of the element and 2 for the second node. (H and G dimensioned (2,2,2))

For each node of the element (J = 1,2) and for the response in each coordinate direction (K = 1, 2) the FLAG is tested. If the traction is prescribed then H(L, K, J) is assembled in the global matrix A , (L = 1, 2, for each coordinate direction at node I), and G(L, K, J) is multiplied by the known VALUE and assembled in RHSV. If the displacement is prescribed then the product of H(L, K, J) and VALUE is placed in RHSV (with a sign change) and G(L, K, J) is assembled in the matrix A (again with a sign change).

This process is repeated for each node I in turn, and hence all the rows of the left hand side coefficient matrix are formed together with the corresponding terms in the right hand side vector.

The routine SLNPD is a standard solver using Guass Elimination and is fed the left hand side coefficient matrix and the right hand side vector of a general non-symmetric, unbanded set of linear equations. After the elimination process, RHSV is returned containing the solution vector.

The OUTPUT routine sorts out the solution vector into displacements and tractions by checking the values in FLAG, and outputs the results.

3.6.2 Numerical Integration

For each node 'i' , on the boundary, the Somigliana identity in its discretised form (equation (3.4.5)) requires the evaluation (for each element), of the terms:

$$\int_{\Gamma_\ell} \underset{\sim}{p^*}\ \underset{\sim}{\phi}^T\, d\Gamma \quad \text{and} \quad \int_{\Gamma_\ell} \underset{\sim}{u^*}\ \underset{\sim}{\phi}^T\, d\Gamma \tag{3.6.1}$$

To facilitate the process a local coordinate ξ is used, which varies between + 1 and - 1 at the 2 ends of the element. (see Fig. 3.6.2(a)). The shape functions can now be expressed :

$$\begin{aligned} \phi_1 &= \frac{1}{2}(1 - \xi) \\ \phi_2 &= \frac{1}{2}(1 + \xi) \end{aligned} \tag{3.6.2}$$

The integrals in expressions (3.6.1) are performed using a 4-point Gauss integration scheme. The sample points are placed symmetrically along the element (see Fig. 3.6.2(b)) with local coordinates

$$\begin{aligned} \xi_4 &= -\xi_1 = 0.86113631 \\ \xi_3 &= -\xi_2 = 0.33998104 \end{aligned} \tag{3.6.3}$$

and corresponding weightings,

$$\begin{aligned} W_4 &= W_1 = 0.34785485 \\ W_2 &= W_2 = 0.65214515 \end{aligned} \tag{3.6.4}$$

the integrals (3.6.1), for each source node 'i' may now be expressed :

$$\int_{\Gamma_\ell} \underset{\sim}{p^*}\, \phi_1 \, d\Gamma = \hat{h}^{i1}_{\ell k} = \sum_{n=1}^{4} p^*_{\ell k}(\xi_n)\, \phi_1(\xi_n)\, W_n\, L \qquad (a)$$

$$\int_{\Gamma_\ell} \underset{\sim}{p^*}\, \phi_2 \, d\Gamma = \hat{h}^{i2}_{\ell k} = \sum_{n=1}^{4} p^*_{\ell k}(\xi_n)\, \phi_2(\xi_n)\, W_n\, L \qquad (b)$$

$$\int_{\Gamma_\ell} \underset{\sim}{u^*}\, \phi_1 \, d\Gamma = g^{i1}_{\ell k} = \sum_{n=1}^{4} u^*_{\ell k}(\xi_n)\, \phi_1(\xi_n)\, W_n\, L \qquad (c)$$

$$\int_{\Gamma_\ell} \underset{\sim}{u^*}\, \phi_2 \, d\Gamma = g^{i2}_{\ell k} = \sum_{n=1}^{4} u^*_{\ell k}(\xi_n)\, \phi_2(\xi_n)\, W_n\, L \qquad (d)$$

(3.6.5)

The expressions $p^*_{\ell k}$ and $u^*_{\ell k}$ are the fundamental solutions given in section 3.2. The value of the fundamental solution at each integration point 'n' can be defined in terms of the coordinates of the node 'i' and the end nodes of the element under consideration.

For a more refined integration scheme, the local coordinates and appropriate weightings are readily available in the literature. (e.g. [37]).

For the special case of the source node being coincident with one of the end nodes of the element under consideration, the terms $g^{i1}_{\ell k}$ and $g^{i2}_{\ell k}$ may be calculated analytically. These terms will contribute to the dominant diagonal coefficients of the $\underset{\sim}{G}$ matrix, and as the fundamental solution becomes singular at the source node, an exact analytic answer for the integrals is desirable; this is relatively simple as the variable of the fundamental solution only varies along the line of integration. Although the expressions are long and complicated, all the integrals reduce to standard forms; as such, only the resulting expressions are given here :

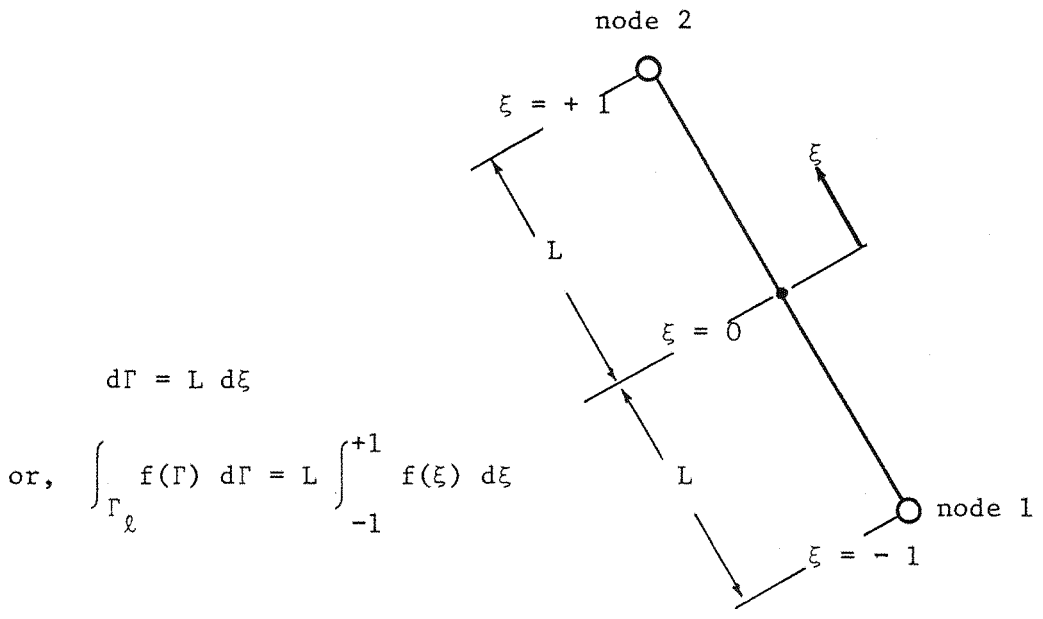

$$d\Gamma = L\, d\xi$$

$$\text{or,} \quad \int_{\Gamma_\ell} f(\Gamma)\, d\Gamma = L \int_{-1}^{+1} f(\xi)\, d\xi$$

(a) local coordinate, ξ ,

Numerical integration point 'k',
local coordinate ξ_k
weighting W_k

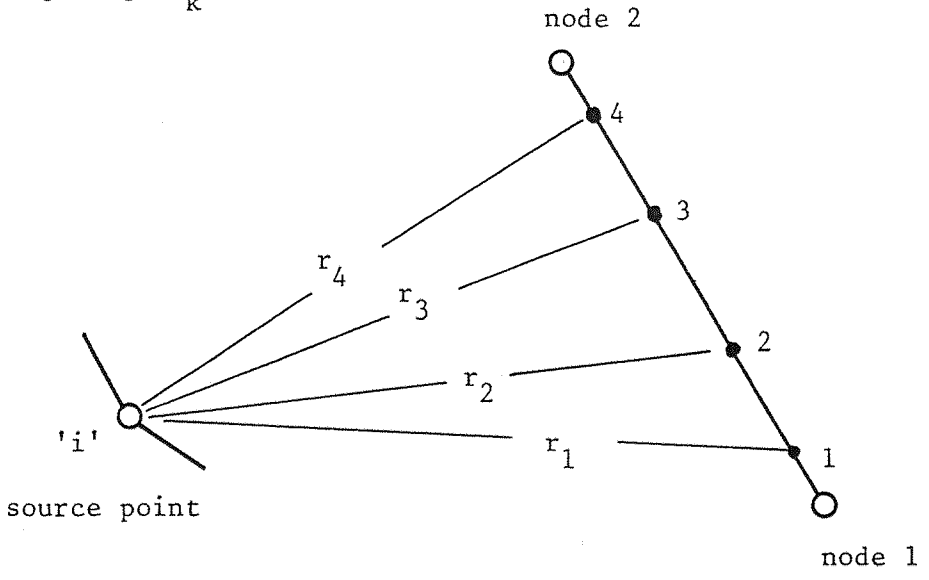

(b) Numerical integration

Figure 3.6.2. Local coordinates and numerical integration along an element with a linear variation.

$$g^{ij}_{mk} = \ell c_1 \, c_2 \left\{ \frac{\alpha}{2} - \ln(\ell) \right\} + \frac{\ell^2 m}{\ell} c_2 \quad \text{for} \quad m = k \tag{3.6.7}$$

$$g^{ij}_{mk} = \frac{\ell_1 \, \ell_2 \, c_2}{\ell} \quad \text{for} \quad m \neq k \tag{3.6.8}$$

where :

$$c_1 = (3 - 4\nu)$$

$$c_2 = \frac{1}{16\pi G(1-\nu)}$$

ℓ = length of the element

ℓ_1 = projection of element on the x_1 coordinate axes

ℓ_2 = projection of element on the x_2 coordinate axis

$\alpha = 3$ for $i = j$

$\alpha = 1$ for $i \neq j$

Remember, the diagonal submatrices of the H matrix are calculated by rigid body motion considerations as discussed at the end of section 3.4. As both the $\underset{\sim}{H}$ and $\underset{\sim}{G}$ matrices are not stored before any re-ordering is carried out, when the element contributions for each set of rows 'i' (i.e. $h^{ij}_{k\ell}$) are calculated, a running total of their sums must be kept, so that after the completion of each set of rows, equation (3.4.15) may be applied to compute the diagonal submatrices.

CHAPTER 4 - 2 AND 3-DIMENSIONAL PROBLEMS USING CONSTANT ELEMENTS

4.1 INTRODUCTION

This Chapter will give a general outline of the technique used for combining Finite and Boundary Element solutions. The common basis of the two techniques has been fully demonstrated in Chapter 3, and this is used (in section 4.2) to enable a linking of the two methods. Two approaches are available : the first is to form an 'equivalent' stiffness matrix for the Boundary Element region, which may then be thought of as simply an additional element in an overall F.E. system; and the second approach entails converting the F.E. part of the solution into a Boundary Element form, and solving the problem as an overall B.E.M. system.

This work is predominantly concerned with the formation of an 'equivalent' stiffness approach and as such we will concentrate on the first of the above two alternatives. However using both techniques in order to demonstrate their equivalence.

The'equivalent' stiffness formulation is implemented for several examples using constant Boundary Elements. This is relatively simple, as the discontinuity problems exhibited at corners, do not arise in this case.

The stiffness matrix obtained using the 'equivalent' stiffness approach, $\underset{\sim}{K}^{u}$, is not inherently symmetric, and a simple technique has been proposed to form a symmetric matrix $\underset{\sim}{K}^{s}$. Comparisons of the solutions obtained using both $\underset{\sim}{K}^{u}$ and $\underset{\sim}{K}^{s}$ are performed.

Unlike the B.E.M., the 'equivalent' stiffness approach is a

displacement technique and does not immediately yield the solution for surface tractions (or reactions). However, once the displacements are obtained the surface tractions are readily obtained by substitution into the original Boundary Element equations. As such, the examples presented here concentrate on the displacements, which are of primary importance.

Some F.E.M./B.E.M. combination examples are run for the 2-D case. However no standard Finite Element package was readily available to facilitate such examples in 3-D, and once the behaviour of the 'equivalent' stiffness matrix had been established, it was decided that combination examples would have served only in a purely demonstrational capacity, and did not warrant the time needed to develop the necessary computer package.

4.2 MATHEMATICAL BASIS FOR THE COUPLING OF FINITE AND BOUNDARY ELEMENTS

In the previous Chapter, both the B.E.M. and F.E.M., have been shown to have a common basis for their formulation; and it is this common basis which allows the relationship between them to become apparent, and thus a linking of the two methods is possible.

The final expressions for the B.E.M. and F.E.M. are repeated here for completeness (see sections 3.4 and 3.5).

The B.E.M. results in,

$$\underset{\sim}{H}\,\underset{\sim}{U} = \underset{\sim}{G}\,\underset{\sim}{P} + B \qquad (4.2.1)$$

The F.E.M. results in,

$$\underset{\sim}{K}\,\underset{\sim}{U} = \underset{\sim}{F} + \underset{\sim}{D} \qquad (4.2.2)$$

The relationship between the two is readily established by examining the relationship between the vectors $\underset{\sim}{P}$ and $\underset{\sim}{F}\cdot\underset{\sim}{P}$ contains the values of the nodal tractions on the boundary and $\underset{\sim}{F}$ contains their equivalent nodal forces.

The vector $\underset{\sim}{F}$ arises from the term representing the work done by the applied tractions $\bar{p}_k$ in the statement of the Principle of Virtual Work as does the vector $\underset{\sim}{P}$ (see equations (3.3.7) and (3.5.4)); i.e. the term,

$$\int_\Gamma u_k^* \, p_k \, d\Gamma \tag{4.2.3}$$

The discretised form of this term, (see equation (3.5.11)), gives,

$$\underset{\sim}{F} = \sum_{\Gamma=1}^{NS} \left(\int_{\Gamma_\ell} \underset{\sim}{\phi} \, \underset{\sim}{\psi}^T \, d\Gamma \right) \underset{\sim}{P} \tag{4.2.4}$$

or

$$\underset{\sim}{F} = \underset{\sim}{M} \, \underset{\sim}{P} \tag{4.2.5}$$

Where $\underset{\sim}{M}$ is a matrix formed by evaluating the expression $\int_\Gamma \underset{\sim}{\phi} \, \underset{\sim}{\psi}^T \, d\Gamma$ on each boundary segment, and assembling the contributions into $\underset{\sim}{M}$ in the same way as the stiffness matrix, $\underset{\sim}{K}$, is built up.

Hence equation (4.2.2) becomes

$$\underset{\sim}{K} \, \underset{\sim}{U} = \underset{\sim}{M} \, \underset{\sim}{P} + \underset{\sim}{D} \tag{4.2.6}$$

which is now of the same form as equation (4.2.1)

Consider a problem consisting of two domains Ω^1, Ω^2 joined by an interface Γ^I, and which makes use of a finite element formuation in Ω^2 and a boundary element formulation in Ω^1 (Fig. 4.2.1).

In order to join the two parts we apply compatability and equilibrium conditions along the interface Γ_I , i.e.

$$\underset{\sim}{U}_I^1 = \underset{\sim}{U}_I^2 \tag{4.2.7}$$

$$\underset{\sim}{P}_I^1 + \underset{\sim}{P}_I^2 = 0 \tag{4.2.8}$$

where, $\underset{\sim}{U}_I^\ell$, $\underset{\sim}{P}_I^\ell$ refer to the displacements and tractions on the interface Γ_I for the region ℓ ($\ell = 1, 2$) .

We now have 2 alternatives as to how to approach the problem. We may develop the boundary element region Ω^1 as an equivalent finite element, assemble the effective stiffness matrix with those of the finite elements of region Ω^2 and solve the overall system as a stiffness problem. Alternatively we can consider Ω^1 and Ω^2 as if they were both boundary element formulations.

APPROACH 1.

Using the first approach, we can transform equation (4.2.1) by inverting $\underset{\sim}{G}$, such that

$$\underset{\sim}{G}^{-1}(\underset{\sim}{H}\underset{\sim}{U} - \underset{\sim}{B}) = \underset{\sim}{P} \tag{4.2.9}$$

and premultiply by the matrix $\underset{\sim}{M}$ described by equation (4.2.5), giving

$$(\underset{\sim}{M}\underset{\sim}{G}^{-1}\ \underset{\sim}{H})\underset{\sim}{U} - (\underset{\sim}{M}\underset{\sim}{G}^{-1}\ \underset{\sim}{B}) = \underset{\sim}{M}\ \underset{\sim}{P} \tag{4.2.10}$$

We can now define

$$\underset{\sim}{K}^u = \underset{\sim}{M}\underset{\sim}{G}^{-1}\ \underset{\sim}{H} \tag{4.2.11}$$

$$\underset{\sim}{D}' = \underset{\sim}{M}\underset{\sim}{G}^{-1}\ \underset{\sim}{B} \tag{4.2.12}$$

$$\underset{\sim}{F}' = \underset{\sim}{M}\ \underset{\sim}{P} \tag{4.2.13}$$

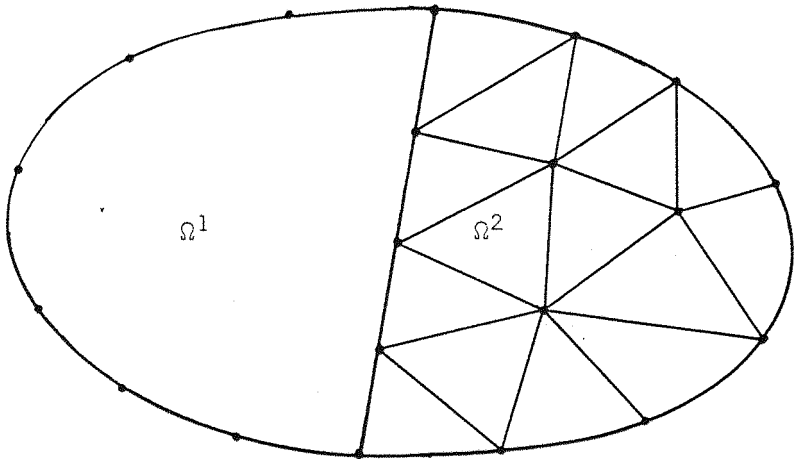

(a) Body divided into Boundary and Finite Element

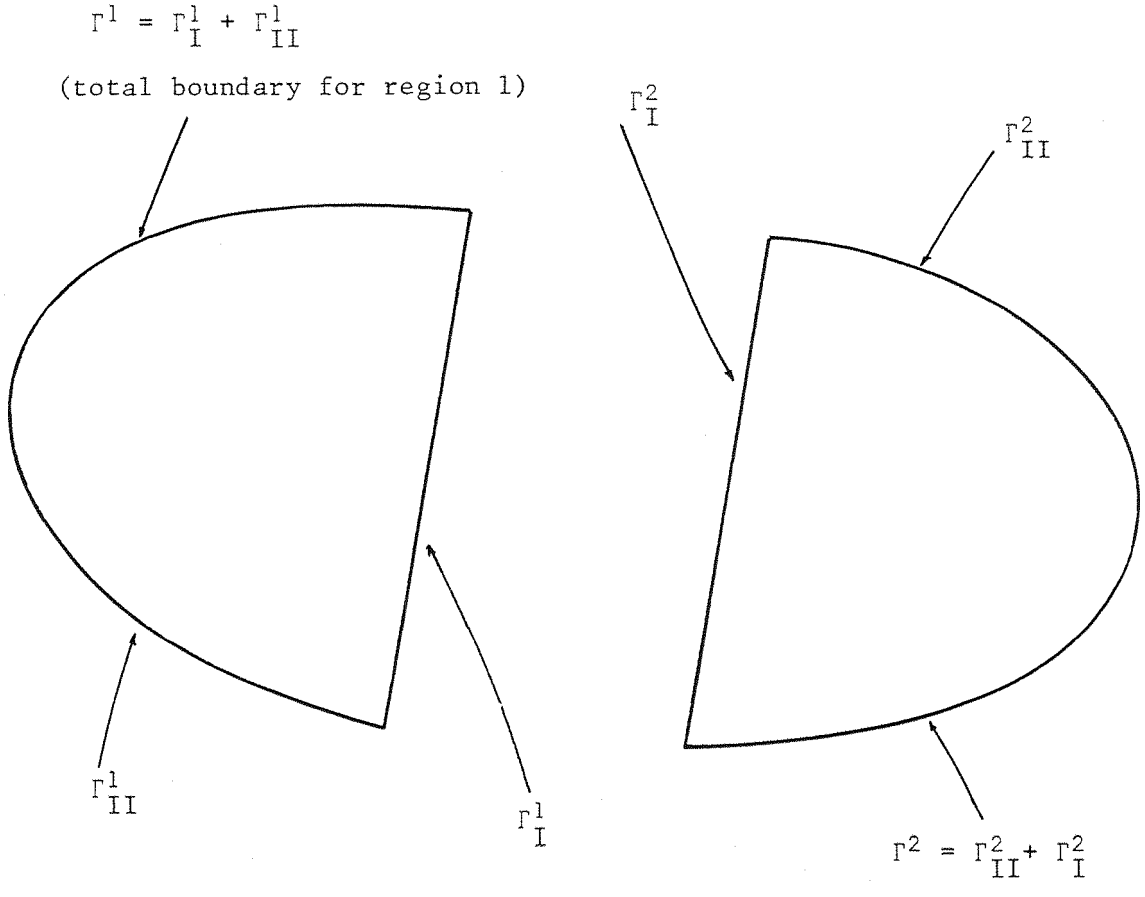

(b) Labelling of the boundary segments for the combination problem.

Figure 4.2.1 The Combination Problem.

Hence equation (4.2.10) has the following Finite Element form

$$\underset{\sim}{K}^{u}\ \underset{\sim}{U} = \underset{\sim}{F}' + \underset{\sim}{D}' \qquad (4.2.14)$$

Although equation (4.2.14) is in fact a stiffness type relation, the coefficient matrix $\underset{\sim}{K}^{u}$ is not symmetric, in the general case. The numerical reason for this, is that the integration process for forming the starting equations (4.2.1) is not a symmetric one. If the domain under consideration could be described by a regular polyhedron with one element on each side, then the symmetrical way in which the problem is set up would be reflected in the symmetrical way in which the integrations would be carried out, and symmetric matrices would ensue. However, for a general problem elements are not of equal length or at equivalent inclination to each other.

Figure 4.2.2 clearly demonstrates how the integration over element B from a source at A is not equivalent to the integration over element A from a source at B .

The lack of symmetry arising from the different lengths of the elements is scaled out to a large degree when the $\underset{\sim}{M}$ matrix is introduced into the formulation (equation 4.2.10). However this is not exact and there still remains the unsymmetric inclination of elements towards each other. It was found that the degree of unsymmetry is very slight and when the matrix is symmetrised using the equation,

$$\underset{\sim}{K}^{s} = \frac{1}{2}(\underset{\sim}{K}^{u} + \underset{\sim}{K}^{u,T}) \qquad (4.2.15)$$

the solution using the now symmetric matrix $\underset{\sim}{K}^{s}$ gives very good answers, especially for the 2-Dimensional case.

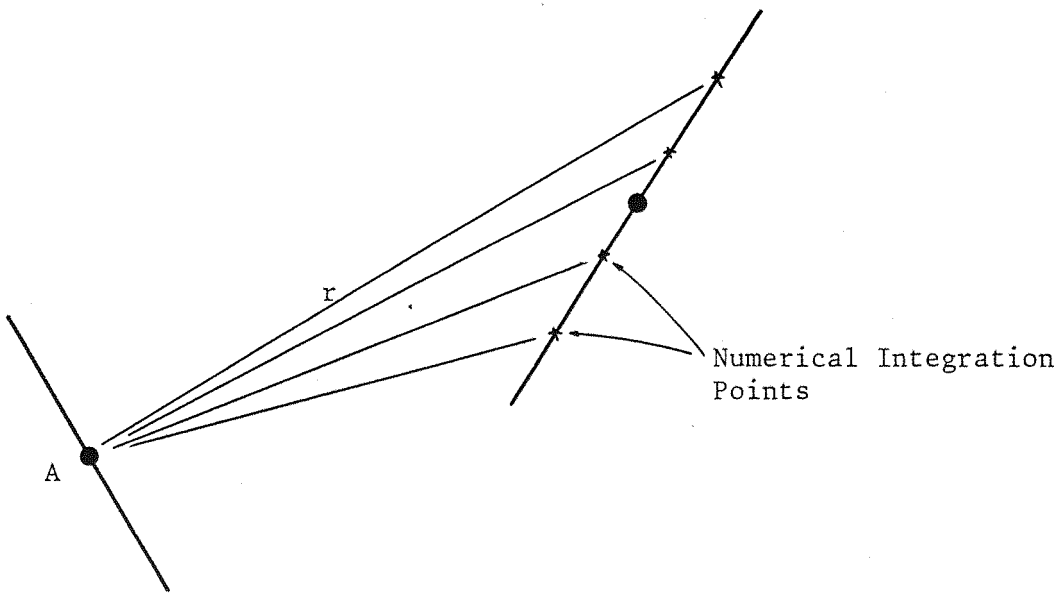

(a) Integration over element B , due to a source at A .

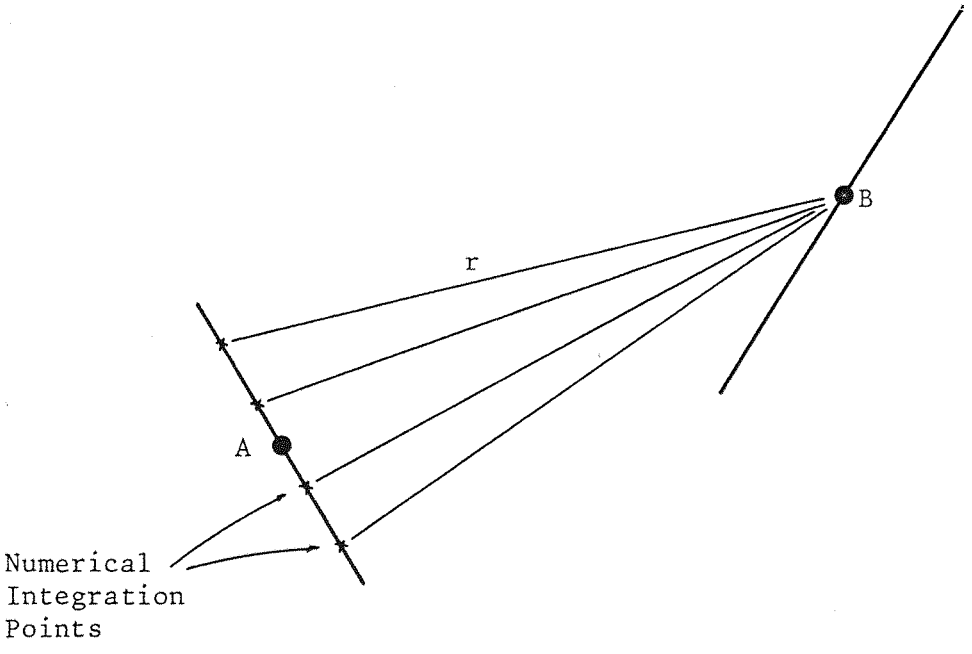

(b) Integration over element A , due to a source at B .

Figure 4.2.2 Reciprocal Integrations for Two Elements.

The whole problem of the symmetry aspect is analysed in much greater depth in Chapter 5, when higher order elements are also considered. As such any arguments which are applicable here, are fully encompassed in later discussions, and the reader is referred to Section 5.7.

The lack of symmetry due to the integration process is more pronounced for 3-Dimensional problems, and as such, the 3-D examples are run using both $\underset{\sim}{K}^{u}$ and $\underset{\sim}{K}^{s}$ in order to examine the effect of the symmetisation process.

APPROACH 2.

Using the second approach, mentioned above, for combining the two methods, we can consider region 2 as a boundary element type region.

For region 1 we can write,

$$\begin{bmatrix} \underset{\sim}{H}^{1} & \underset{\sim I}{H}^{1}_{I} \end{bmatrix} \begin{Bmatrix} \underset{\sim}{U}^{1} \\ \underset{\sim I}{U}^{1}_{I} \end{Bmatrix} = \begin{bmatrix} \underset{\sim}{G}^{1} & \underset{\sim I}{G}^{1}_{I} \end{bmatrix} \begin{Bmatrix} \underset{\sim}{P}^{1} \\ \underset{\sim I}{P}^{1}_{I} \end{Bmatrix} + \underset{\sim}{B}^{1} \qquad \text{(a)} \tag{4.2.16}$$

and for region 2,

$$\begin{bmatrix} \underset{\sim}{K}^{2} & \underset{\sim I}{K}^{2}_{I} \end{bmatrix} \begin{Bmatrix} \underset{\sim}{U}^{2} \\ \underset{\sim I}{U}^{2}_{I} \end{Bmatrix} = \begin{bmatrix} \underset{\sim}{M}^{2} & \underset{\sim I}{M}^{2}_{I} \end{bmatrix} \begin{Bmatrix} \underset{\sim}{P}^{2} \\ \underset{\sim I}{P}^{2}_{I} \end{Bmatrix} + \underset{\sim}{D}^{2} \qquad \text{(b)}$$

By writing $\underset{\sim I}{P}_{I} = \underset{\sim I}{P}^{1}_{I} = - \underset{\sim I}{P}^{2}_{I}$ and $\underset{\sim I}{U}_{I} = \underset{\sim I}{U}^{1}_{I} = \underset{\sim I}{U}^{2}_{I}$

we automatically satisfy conditions (4.2.7) and (4.2.8), and equations (4.2.16 a) and (4.2.16 b) can be rearranged as follows,

$$\begin{bmatrix} \underset{\sim}{H}^1 & \underset{\sim}{H}^1_I & -\underset{\sim}{G}^1_I \end{bmatrix} \begin{Bmatrix} \underset{\sim}{U}^1 \\ \underset{\sim}{U}_I \\ \underset{\sim}{P}_I \end{Bmatrix} = \begin{bmatrix} \underset{\sim}{G}^1 \end{bmatrix} \begin{Bmatrix} \underset{\sim}{P}^1 \end{Bmatrix} + \underset{\sim}{B}^1 \qquad (4.2.17)$$

and

$$\begin{bmatrix} \underset{\sim}{K}^2 & \underset{\sim}{K}^2_I & \underset{\sim}{M}^2_I \end{bmatrix} \begin{Bmatrix} \underset{\sim}{U}^2 \\ \underset{\sim}{U}_I \\ \underset{\sim}{P}_I \end{Bmatrix} = \begin{bmatrix} \underset{\sim}{M}^2 \end{bmatrix} \begin{Bmatrix} \underset{\sim}{P}^2 \end{Bmatrix} + \underset{\sim}{D}^2 \ . \qquad (4.2.18)$$

Writing these two equations together, as a single matrix equation, we have

$$\begin{bmatrix} \underset{\sim}{H}^1 & \underset{\sim}{H}^1_I & -\underset{\sim}{G}^1_I & 0 \\ 0 & \underset{\sim}{K}^2_I & \underset{\sim}{M}^2_I & \underset{\sim}{K}^2 \end{bmatrix} \begin{Bmatrix} \underset{\sim}{U}^1 \\ \underset{\sim}{U}_I \\ \underset{\sim}{P}_I \\ \underset{\sim}{U}^2 \end{Bmatrix} = \begin{bmatrix} \underset{\sim}{G}^1 & 0 \\ 0 & \underset{\sim}{M}^2 \end{bmatrix} \begin{Bmatrix} \underset{\sim}{P}^1 \\ \underset{\sim}{P}^2 \end{Bmatrix} + \begin{Bmatrix} \underset{\sim}{B}^1 \\ \underset{\sim}{D}^1 \end{Bmatrix} \qquad (4.2.19)$$

Notice that on the boundary of the finite element region Ω^2 , only the displacements on Γ_1 have to be prescribed, whilst on the boundary of Ω^2 we prescribe the displacements or tractions and consequently need to re-order the equations.

The advantage of the second approach is that it does not require an inversion.

This second approach is the same as the technique used for solving problems with sub-regions using the B.E.M. If we use a Boundary Element formulation for region 2, equation (4.2.19) is applicable when the submatrices $\underset{\sim}{K}^2$, $\underset{\sim}{K}^2_I$, $\underset{\sim}{M}^2$, $\underset{\sim}{M}^2_I$ are replaced by $\underset{\sim}{H}^2$, $\underset{\sim}{H}^2_I$, $\underset{\sim}{G}^2$, $\underset{\sim}{G}^2_I$, respectively.

4.3 TWO-DIMENSIONAL PROBLEMS USING CONSTANT ELEMENTS

EXAMPLE 1.

As a test of the 'equivalent' stiffness formulation, and of the coupling of Finite and Boundary Elements, a T-shaped plate problem was considered, as shown in Fig. 4.3.1. The domain is divided into two regions, the first of which is discretised into normal Finite Elements (linear strain triangles), and the second using constant Boundary Elements, (Fig. 4.3.1(a)). The $\underset{\sim}{H}$ and $\underset{\sim}{G}$ matrices for the boundary region are used to form an 'equivalent' stiffness matrix, $\underset{\sim}{K}^S$, and this is assembled with the element contributions from region 1 to form a global stiffness matrix for the system.

Region 2 was first considered separately as a check on the validity of the idea of formulating an 'equivalent' stiffness matrix. The domain was discretised and loaded, as shown in Fig. 4.3.1 (b). This region was firstly analysed using the B.E.M., i.e. the $\underset{\sim}{H}$ and $\underset{\sim}{G}$ matrices were formed, mixed boundary conditions applied, and the equations then re-ordered and solved to yield the unknown displacements and tractions. (Method 1). Secondly, the matrix $\underset{\sim}{K}^S$ was formed, and the stiffness system $\underset{\sim}{K}^S \underset{\sim}{U} = \underset{\sim}{F}$ was solved to yield the unknown displacements . (Method 2). The displacements along the top face are shown in Table 4.3.1, and their agreement clearly demonstrates the validity of $\underset{\sim}{K}^S$ representing the 'equivalent' stiffness of the system. Differences in the solution do not occur until the 4th or 5th significant figure.

The equivalent stiffness matrix for region 2 was then assembled with the finite elements of region 1 (Fig. 4.3.1 (a)) to form the overall system $\underset{\sim}{K}\,\underset{\sim}{U} = \underset{\sim}{F}$. The results are shown as Approach 1 in Table 4.3.2. A program to implement the second of the two alternatives combination procedures (i.e. the equivalent boundary element approach) equation (4.2.19) was then developed. The matrix $\underset{\sim}{M}$ is formed by integration around the perimeter of the finite element region and the $\underset{\sim}{M}$, $\underset{\sim}{K}$, $\underset{\sim}{H}$, $\underset{\sim}{G}$ matrices are broken down and reassembled in an overall system as given by equation (4.2.19). The equations are then reordered and solved, and the results are shown as Approach 2 in Table 4.3.2.

Two loading cases were considered, the first being a uniformly distributed vertical load equal to 4.0 on the top edge, producing a symmetrical problem, and the second included a concentrated horizontal load equal to 3.0 on the top corner node (see Figure 4.3.1 (a)).

In order to make a comparative study, the system was also analysed as a whole, using both the finite element and boundary element techniques. The meshes used are shown in Figures 4.3.2 (c) and 4.3.2. (d), and the results obtained for displacements are also tabulated in Table 4.3.2.

This application shows the validity of developing an equivalent stiffness matrix from a boundary element formulation. The example also demonstrates that either of the two different combination approaches - equivalent finite elements or the equivalent boundary elements approach - can be equally well applied to solve the problem.

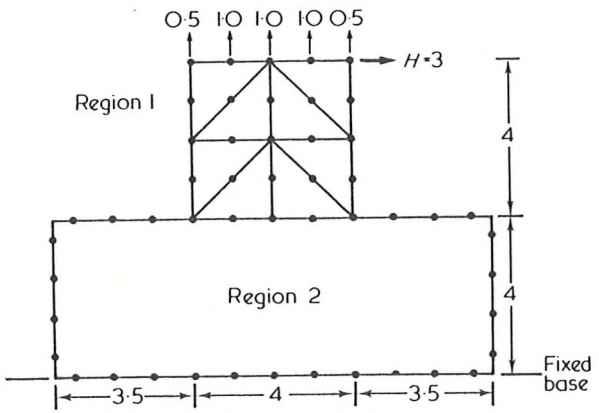

(a) Combination Problem.

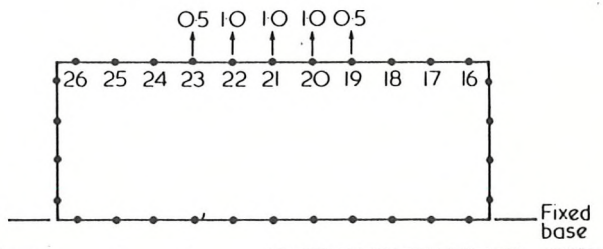

(b) Boundary Element region

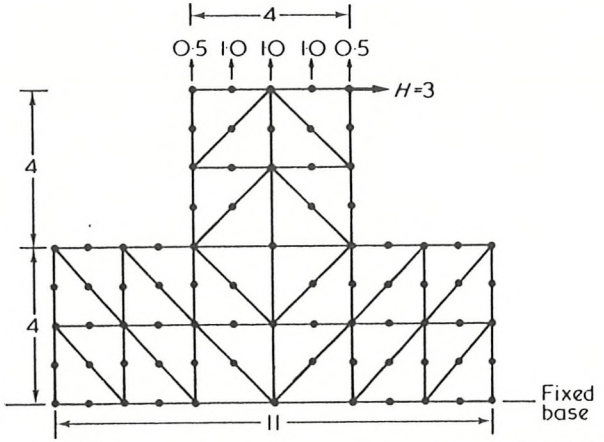

(c) Finite Element Mesh

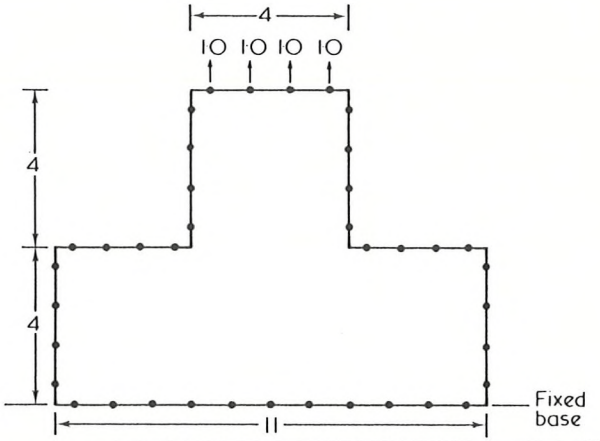

(d) Boundary Element Mesh.

Figure 4.3.1 T-Shaped Plate Problem - Example 1.

Node	Displacements	
	Method 1	Method 2
16	0.070	0.071
17	0.224	0.224
18	0.549	0.549
19	1.304	0.304
20	1.605	1.605
21	1.684	1.684

$$E = 2 \times 10^5 \quad \nu = 0.2$$

Table 4.3.1 Displacements in the direction of the load for Boundary Element region of Example 1. (Fig. 4.3.1 (b)).

EXAMPLE 2.

This example consists of a rectangular plate resting on a large semi-circular foundation (Fig. 4.3.2 (a)). In this section,. the Kelvin solution is used for the bounded Boundary Element region (Fig. 4.3.2. (b)).

It should be noted that by using a half-space fundamental solution in the Boundary Element formulation, only the discretisation of the loaded (or interface) segment is required. A formulation based on the Bousinesq solution is presented in Chapter 6. This example serves as a useful demonstration of the coupling technique, and facilitates comparison with a Finite Element model, which also requires a bounded domain.

Approach 1		Approach 2		Finite Element Method		Boundary Element Method
Displ. u_1	Displ. u_2	Displ. u_1	Displ. u_2	Displ. u_1	Displ. u_2	Average vertical displacement u_2
-3.59	33.50	-3.59	33.50	-3.50	33.40	
-1.35	30.91	-1.35	30.91	-1.35	30.84	
0.00	32.66	0.00	32.66	0.00	32.62	33.00
1.35	30.91	1.35	30.91	1.35	30.84	
3.59	33.50	3.59	33.50	3.59	33.40	
211.56	-58.66	211.55	-58.67	213.19	-58.58	
183.06	-0.83	183.05	0.83	184.67	-0.79	
165.86	36.36	165.85	36.36	167.43	36.27	-
161.48	62.32	161.48	62.33	163.17	62.12	
162.33	97.40	162.32	97.41	164.06	97.20	

(Note: The concentrated load, H , cannot be represented accurately in the boundary element method with constant elements).

$E = 2 \times 10^5$, $\nu = 0.2$

Table 4.3.2. Displacement profile along the loaded nodes of the T-shaped plate - Example 1.

The foundation part of the problem is first considered separately. A large F.E. mesh is used to discretise this region (Fig. 4.3.3. (b)), and a uniform strip loading is applied along the interface elements. This F.E. solution gives a maximum displacement at the centre of 64.8×10^{-6}.

The B.E.M. discretisation was then used and the 'equivalent' stiffness matrix $\underset{\sim}{K}^{s}$ was formed. The solution of this 'equivalent' Finite Element system yields a maximum central displacement of 66.2×10^{-6}.

The above answers are in good agreement with the analytical solution, fora strip loading on a semi-infinite half-space,given by Timoshenko [1], of 71.5×10^{-6}. The numerical solutions are expectedly lower bounds, as there is an artificial restraint imposed by the inclusion of the boundary. It is interesting to note that the B.E.M. based solution gives a slightly better answer than the classical F.E.M., although the B.E.M. uses only a constant interpolation for displacements, as opposed to a quadratic interpolation, used in the F.E.M. model. This is because the B.E.M. based formulation imposes no restriction on the displacement variation within the domain, only on the boundary; and as such the domain discretisation of the F.E.M. introduces an additional artificial stiffness in the model.

The overall problem was then run using the 'equivalent' stiffness matrix $\underset{\sim}{K}^{s}$ for region 2. Two loading cases were used, and the vertical displacements obtained at the top of the cantilever type structure are compared.

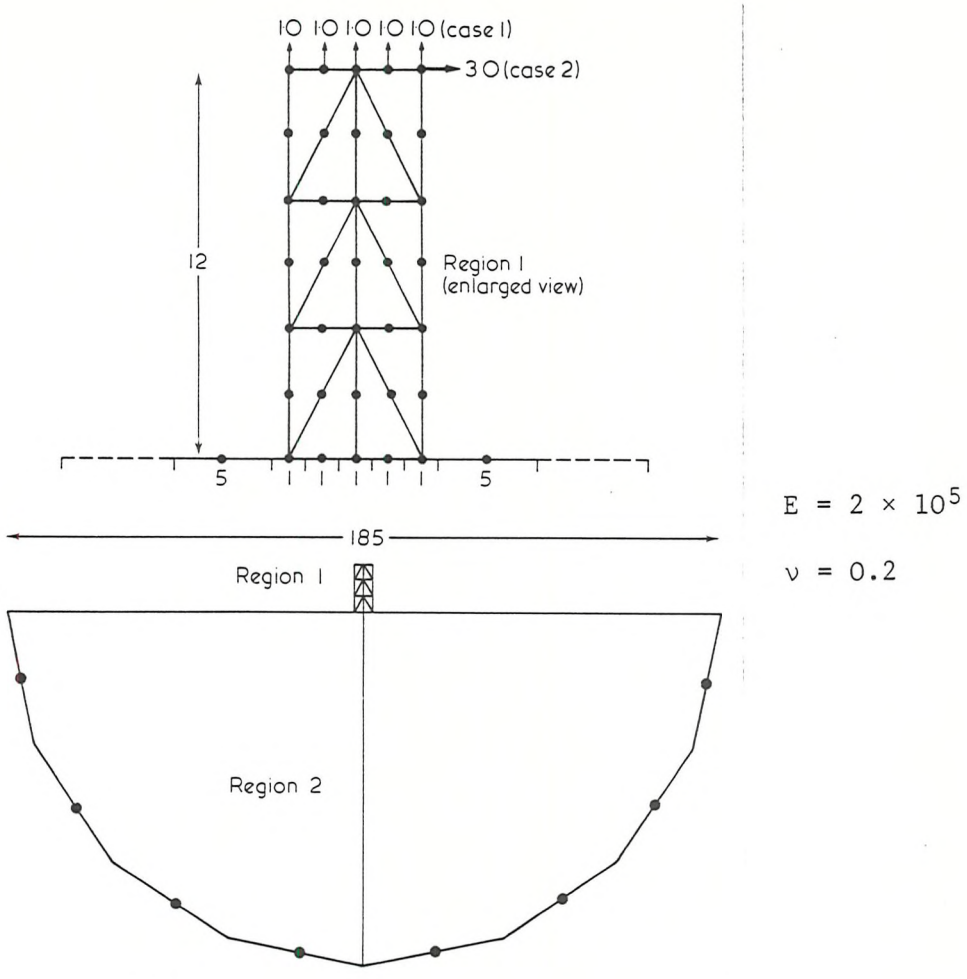

(a) Finite and Boundary Element Combination Mesh.

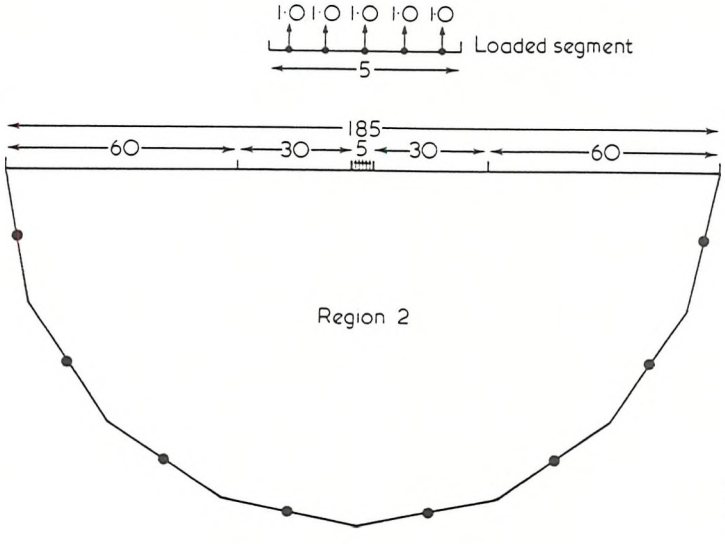

(b) Boundary Element mesh for foundation part of problem.

Figure 4.3.2 Structure resting on a large foundation. Discretisation for coupling problem.

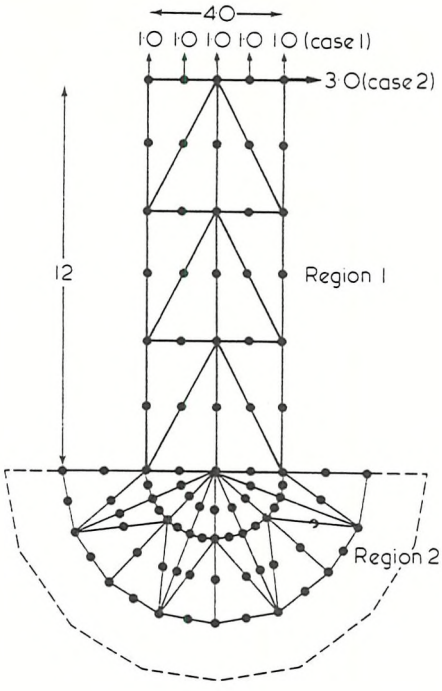

(a) Structure

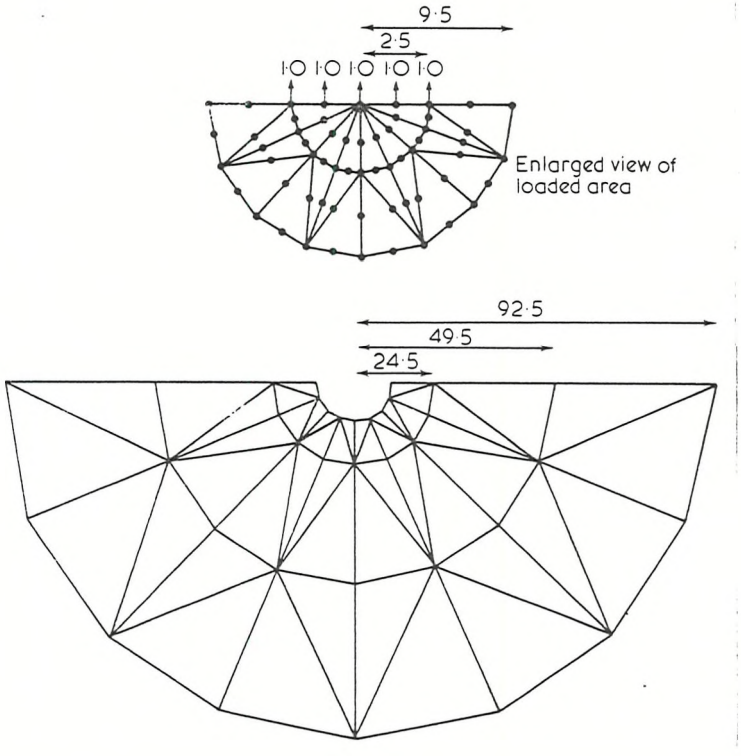

(b) Foundation

Figure 4.3.3. Structure resting on a large foundation Finite Element Mesh.

	Finite Element Method	Combination Method
Load Case 1	1.41	1.40
	1.34	1.33
	1.32	1.32
	1.34	1.33
	1.41	1.40
Load Case 2	- 3.39	- 3.55
	- 0.97	- 1.05
	1.35	1.35
	3.61	3.70
	6.00	6.17

Displacements $\times 10^{-4}$

Table 4.3.3. Vertical displacements along the top of the Cantilever - Example 2.

4.4 THREE-DIMENSIONAL PROBLEMS USING CONSTANT ELEMENTS

A three-dimensional constant element program, based on the work of NAKAGUMA [10], was developed and used to examine the behaviour of the 'equivalent' stiffness formulation for several examples of three-dimensional problems.

4.4.1 Finite Domains. Kelvin Solution

EXAMPLE 1. CUBE UNDER UNIFORM COMPRESSION

A cube of side length 4 is loaded with a uniform traction of 1/unit area on opposing faces. Due to symmetry, only one eighth

of the cube need be considered with appropriate boundary conditions, Fig. 4.4.1 . Each face is divided in 8 triangular elements, and the face $x_3 = 0$ is loaded in the x_3 direction.

The problem was first run using the normal B.E.M. The matrices $\underset{\sim}{K}^u$ and $\underset{\sim}{K}^s$ were then formed, and the system solved as a stiffness problem. As expected the solution obtained using $\underset{\sim}{K}^u$ is the same as the normal B.E.M. (The same equations are being solved in both instances; the only difference being the way the boundary conditions are applied, and the solution procedure). The only differences occur in the 4th or 5th significant figures, which are due to rounding errors.

The displacements in the direction of the load, for different values of x_3 , are given in Table 4.4.1.

The solution given by $\underset{\sim}{K}^u$ is expectedly a little lower than the exact solution, due to the artificial stiffness imposed on the system by the constant elements. The solution obtained using $\underset{\sim}{K}^s$ definitely introduces an error, and this seems to be of greater magnitude than with 2-Dimensional problems. This again is to be expected as the degree of unsymmetry due to the unsymmetric reciprocal integration process is more marked in 3-Dimensions. The error is as much as 15 - 20% in one or two of the displacements in the non-principal directions (i.e. x_1 and x_2), but if taken as a proportion of the maximum displacement is only 2 - 3%.

The relatively large differences (compared to the 2-D examples of the previous section) are due to the fact that typical distances between elements are of the same order of magnitude, as the representative dimensions of the elements themselves. This causes the unsymmetric

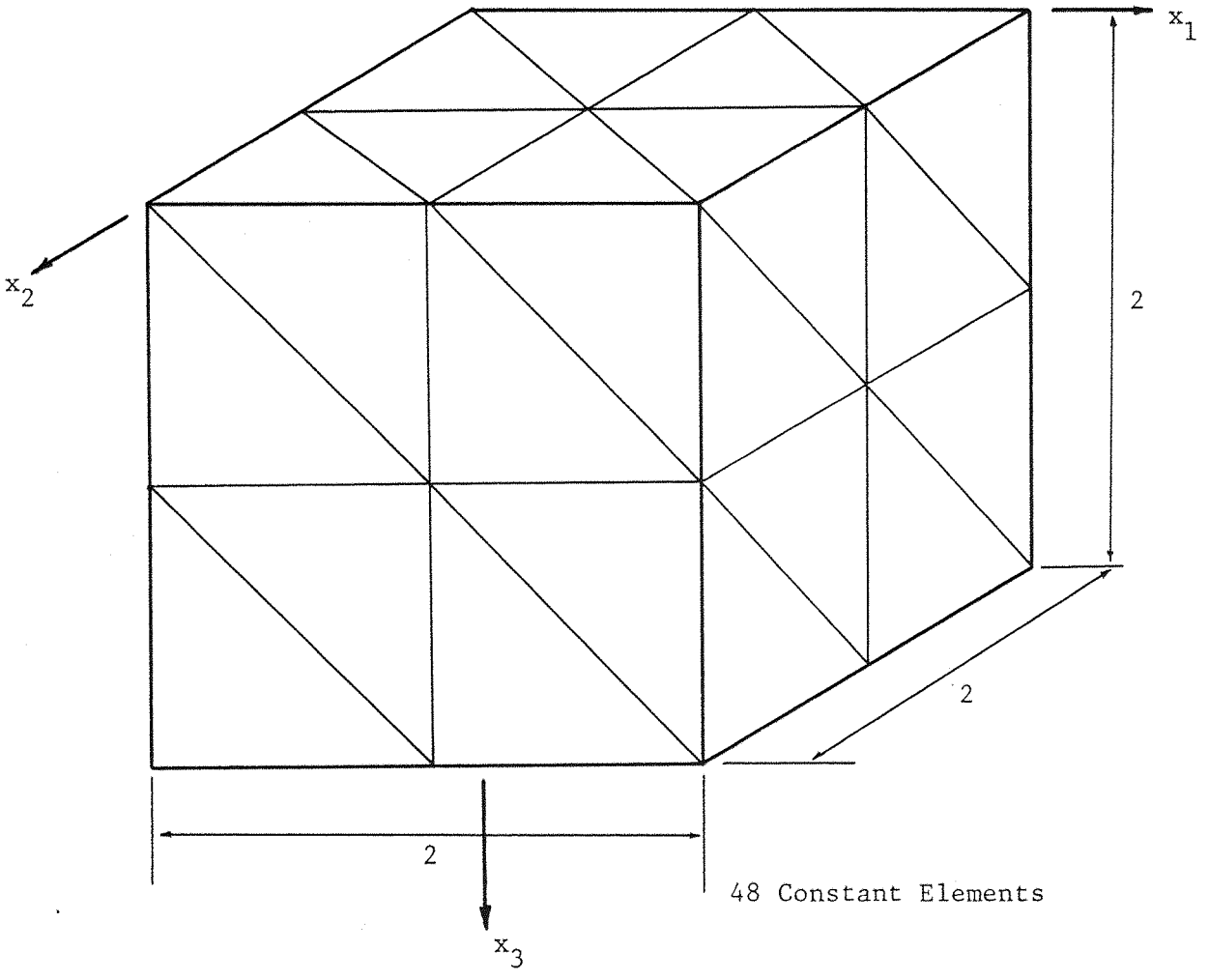

Boundary Conditions : face $x_1 = 0$, $u_1 = 0$

$x_2 = 0$, $u_2 = 0$

$x_3 = 2$, $u_3 = 0$

Figure 4.4.1 Cube under uniform Compression.

effect due to the inclination of the elements towards each other to have a more pronounced effect on the values of the integrals.

x_3	EXACT SOLUTION	B.E.M., and 'equivalent' stiffness method, using $\underset{\sim}{K}^u$	'Equivalent' stiffness method, using $\underset{\sim}{K}^s$
0.0	2.0	1.9760	2.0081
0.3333	1.6667	1.6416	1.5444
0.6667	1.3333	1.3025	1.2921
1.3333	0.6667	0.6657	0.6796
1.6667	0.3333	0.3274	0.3638

Table 4.4.1 Displacements in the Direction of the Load for a Cube under Uniform Compression.

EXAMPLE 2. THICK CYLINDER UNDER INTERNAL PRESSURE

As a further example of a 3-D application, a thick cylinder under internal pressure was analysed. The problem description and discretisation is depicted in Fig. 4.4.2, (only a 90^o sector need be considered, due to symmetry). In order to faciliate comparisons of displacements with an exact solution, all displacements in the axial direction of the cylinder were set equal to zero. The 3-D problem then corresponds to the 2-D plane strain case, for which the stress distribution is readily available (e.g. TIMOSHENKO, [1]).By integrating these stresses, the analytical solution for the displacements is obtained.

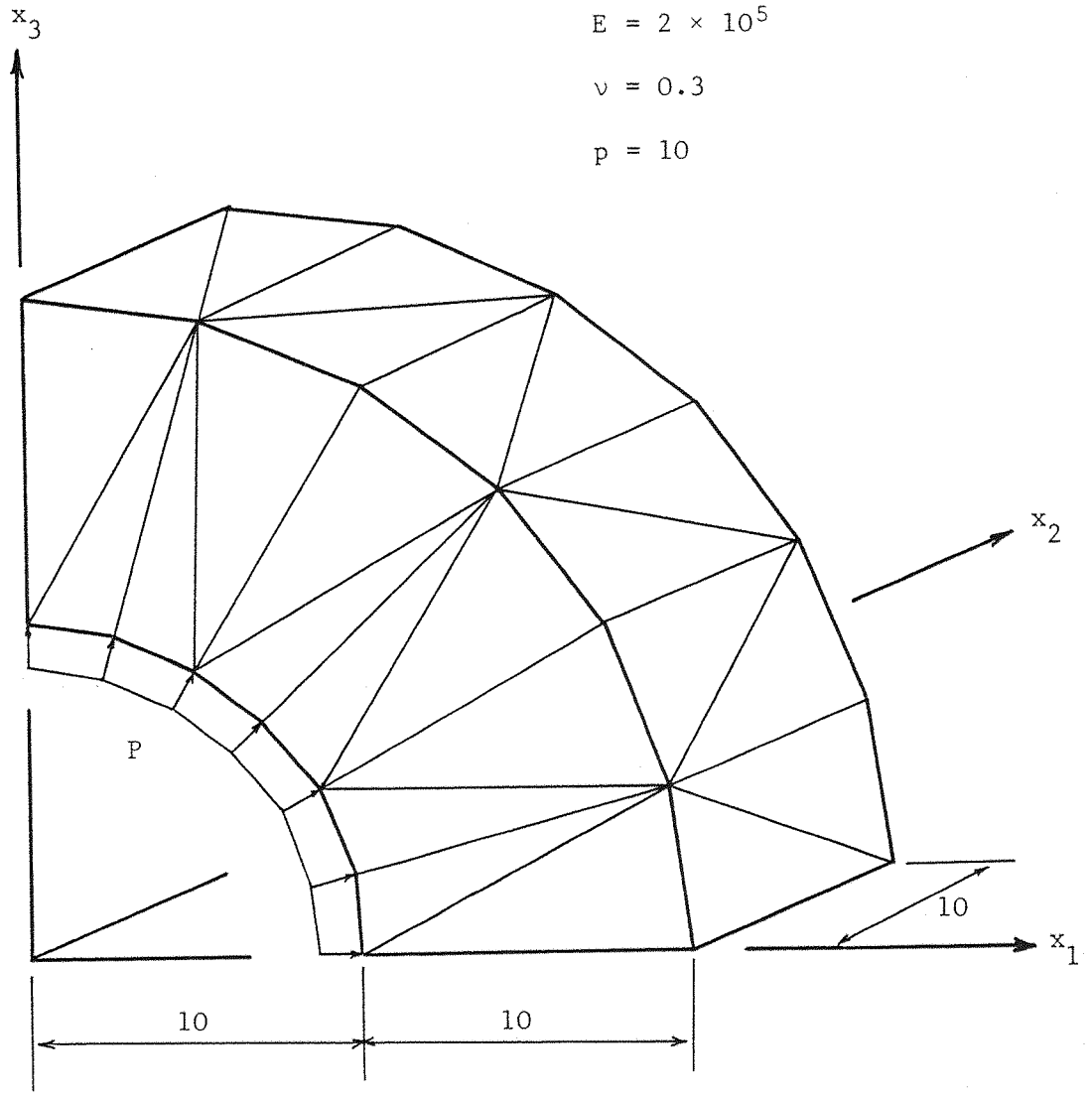

Figure 4.4.2 Thick cylinder under internal pressure.

In order to obtain an idea of the level of accuracy available from the constant element formulation, the problem was first run as a normal B.E.M. system. The same mesh was then used for a run using the 'equivalent' stiffness approach. (Both the unsymmetric and symmetrised stiffness matrices were formed - $\underset{\sim}{K}^u$ and $\underset{\sim}{K}^s$ - and boundary conditions applied as in the usual Finite Element displacement technique). Table 4.4.2 gives a comparison of the results obtained, which are in good agreement. As expected, the B.E.M. and the solution obtained using $\underset{\sim}{K}^u$ are the same, and are a lower bound on the exact solution. Although the solution obtained using $\underset{\sim}{K}^s$ is closer to the exact solution, this is only due to the fact that the error introduced by the symmetrisation process happens to shift the solution in that direction. (The 'equivalent' stiffness solution can only be as accurate as the Boundary Element solution on which it is based).

It should be noted that when comparing the solution obtained using $\underset{\sim}{K}^u$ and $\underset{\sim}{K}^s$, the degree of the differences in the solution depends on the relative size of the displacement components, so that the relatively large discrepancies occur in the relatively small components of displacement. e.g. say that at a particular point, the displacement in the x_3 direction is 10 times as large as the displacement in the x_1 direction; then the difference in solution, obtained using $\underset{\sim}{K}^s$ as opposed to $\underset{\sim}{K}^u$, may be 2 - 3% in the x_3 direction, but as much as 20 - 30% in the x_1 direction. This is definitely a numerical problem and needs to be studied in further quantitative detail. However, these relatively large errors in the small components of the solution become insignificant compared to the

dominant terms, as can be seen by the good agreement of the radial components of displacement given in Table 4.4.2.

Radius	Radial displacements, $u_r \times 10^{-4}$				σ_c	
			'Equivalent' K			
	EXACT	B.E.M.	$\underset{\sim}{K}^u$	$\underset{\sim}{K}^s$	EXACT	B.E.M.
10.0	9.53	9.38	9.38	9.68		
13.33	7.65	7.26	7.26	7.41	10.84	11.02
16.67	6.64	6.29	6.29	6.40	8.13	8.22
20.0	6.07	5.93	5.93	6.13		

Table 4.4.2 Solutions for thick cylinder under internal pressure.

4.4.2 Semi-infinite Domains. Mindlin Solution

The explicit form of the fundamental solution is given in Appendix B, and for details of the numerical integration scheme used, see NAKAGUMA [10]. Similar physical examples as those presented in [10] are run, firstly serving as a useful check on the program and secondly facilitating comparisons between the 'equivalent' stiffness formulation and the Direct Boundary Element Method.

EXAMPLE 1. HALF-SPACE WITH SURFACE LOADING.

In this example a semi-infinite, three dimensional half-space carries a uniformly distributed load on a circular area at the surface. As such the Bousinesq-Cerruti fundamental solution is applicable, easily derived as a special case of the Mindlin formulae

by setting the term 'c' equal to zero. (See Chapter 3 and Appendix B).

In this case only the loaded segment of the free surface need be discretised, but in order to examine more general aspects of the solution, additional elements were used on non-loaded areas. The circular loaded area (of radius 1.) is approximated by a hexagon, comprised of six triangles.

The problem was first run using a mesh discretising a circular area of radius 10, as shown in Fig. 4.4.3. The additional elements serve to give the displacement profile outside the loaded segment, and also enable the use of the Kelvin solution, for comparison.

The problem was first run using the normal B.E.M., employing, in turn, the Mindlin and Kelvin fundamental solutions, and the vertical displacement profile at the surface is compared to the analytical solution in Fig. 4.4.4. (The exact solution for a distributed load is used for $r = 0$, but at other values of r, this requires a complex evaluation of some elliptic integrals (see [1]), and so, the solution was taken as that for the load concentrated at the origin, for $r > 2$).

The Mindlin solution is in excellent agreement with the analytical solution; this is to be expected as the Mindlin solution inherently assumes a traction free surface. The Kelvin solution is also in good agreement, but gives slightly smaller answers for displacements, due to the fact that an artificial stiffness is introduced into the model by cutting off the mesh on the surface at a finite radius.

The problem was then run by forming the 'equivalent' stiffness matrices $\underset{\sim}{K}^u$ and $\underset{\sim}{K}^s$, and solving the problem as a Finite Element type displacement model. The displacements obtained using $\underset{\sim}{K}^u$ are the same as those for the B.E.M., and these are compared to the solution obtained using $\underset{\sim}{K}^s$, in Table 4.4.1. As expected, $\underset{\sim}{K}^u$, exhibits a lack of symmetry, mainly due to the differing sizes of the elements (their odd orientation to each other also contributes a small effect), but this assymmetry is very slight, as can be seen by the small differences introduced in the results when using $\underset{\sim}{K}^s$.

With using the Mindlin solution, elements only on the loaded segments are required and need not be interconnected. As a check on the level of unsymmetry due to the differing sizes of the elements, the same problem was run again using elements of equal size placed unconnected, on the x_1 and x_2 axis, as shown in Fig. 4.4.5. The Mindlin solution was used, and, as expected, the B.E.M. and $\underset{\sim}{K}^u$ solutions agreed exactly with the previous run. A comparison of radial and vertical displacement components on the surface, obtained using $\underset{\sim}{K}^u$ and $\underset{\sim}{K}^s$, is given in Table 4.4.2. As can be seen, any differences do not occur until about the 5th significant figure, showing that the degree of unsymmetry in $\underset{\sim}{K}^u$ is very minor indeed.

EXAMPLE 2. CYLINDRICAL CAVITY IN A HALF-SPACE

A cylindrical cavity, with its axis parallel to x_3 carries a uniformly distributed load, as shown in Fig. 4.4.6. The developed surface of the cylinder, discretised into 36 Boundary Elements, is shown in Fig. 4.4.7. Although the use of the Mindlin solution does not necessitate discretisation of the free surface, Boundary Elements

were in fact placed on the surface : this enables comparison with the Kelvin solution, and also allows examination of the response at the surface, using the 'equivalent' stiffness approach, which is important as this surface could form the interface of some combination problem. The Boundary Element mesh used to discretise the free surface is shown in Fig. 4.4.8.

For both the Kelvin and Mindlin solutions, the problem was first run using the B.E.M., and then the 'equivalent' stiffness matrices $\underset{\sim}{K}^{u}$ and $\underset{\sim}{K}^{s}$ were formed, and the problem solved in its stiffness form. The displacement profiles obtained for the free surface are given in Tables 4.4.3. Table 4.4.4 compares the vertical displacements of the top and bottom faces of the cylindrical cavity for all the runs.

The results for this problem again exhibit the expected behaviour. Solutions obtained using $\underset{\sim}{K}^{u}$ are the same as for the B.E.M., the very slight differences being attributable to the different numerical process of solving the equations. The Kelvin solution gives smaller values of displacements, but this stiffness is expected, as the semi-infinite boundaries of the physical problem are not accounted for, as with the Mindlin solution. The differences in the solutions between $\underset{\sim}{K}^{u}$ and $\underset{\sim}{K}^{s}$ are again present and are due to the error introduced in the symmetrisation process. The magnitude of these errors are of the order of 3 - 4%, less for the most dominant values (i.e. at the loaded face), than the least dominant.

The above results clearly demonstrate that there definitely exists a lack of unsymmetry in the 'equivalent' stiffness matrix $\underset{\sim}{K}^{u}$, which is independent of the type of fundamental solution used, and

the degree of which relies on the relative sizes of the elements and their orientation towards each other.

However, if for economy reasons, a symmetric 'equivalent' stiffness matrix is demanded, then the cost, in terms of the lost accuracy, seems to be of a quite acceptable degree for most engineering applications.

Radius	MINDLIN SOLUTION		KELVIN SOLUTION	
	$\underset{\sim}{K}^u$	$\underset{\sim}{K}^s$	$\underset{\sim}{K}^u$	$\underset{\sim}{K}^s$
0.5773	1.4426	1.4441	1.3785	1.3821
1.5773	0.4996	0.5245	0.4894	0.5146
2.2555	0.3410	0.3478	0.3322	0.3414
3.8982	0.1944	0.1962	0.1901	0.1928
4.8365	0.1563	0.1573	0.1503	0.1525
7.1357	0.1057	0.1062	0.1000	0.1018
8.3873	0.0899	0.0900	0.0817	0.0847

Vertical Displacements $\times 10^{-3}$

Table 4.4.1 Half-space with Surface Loading; Comparison of displacement profile obtained using $\underset{\sim}{K}^u$ and $\underset{\sim}{K}^s$

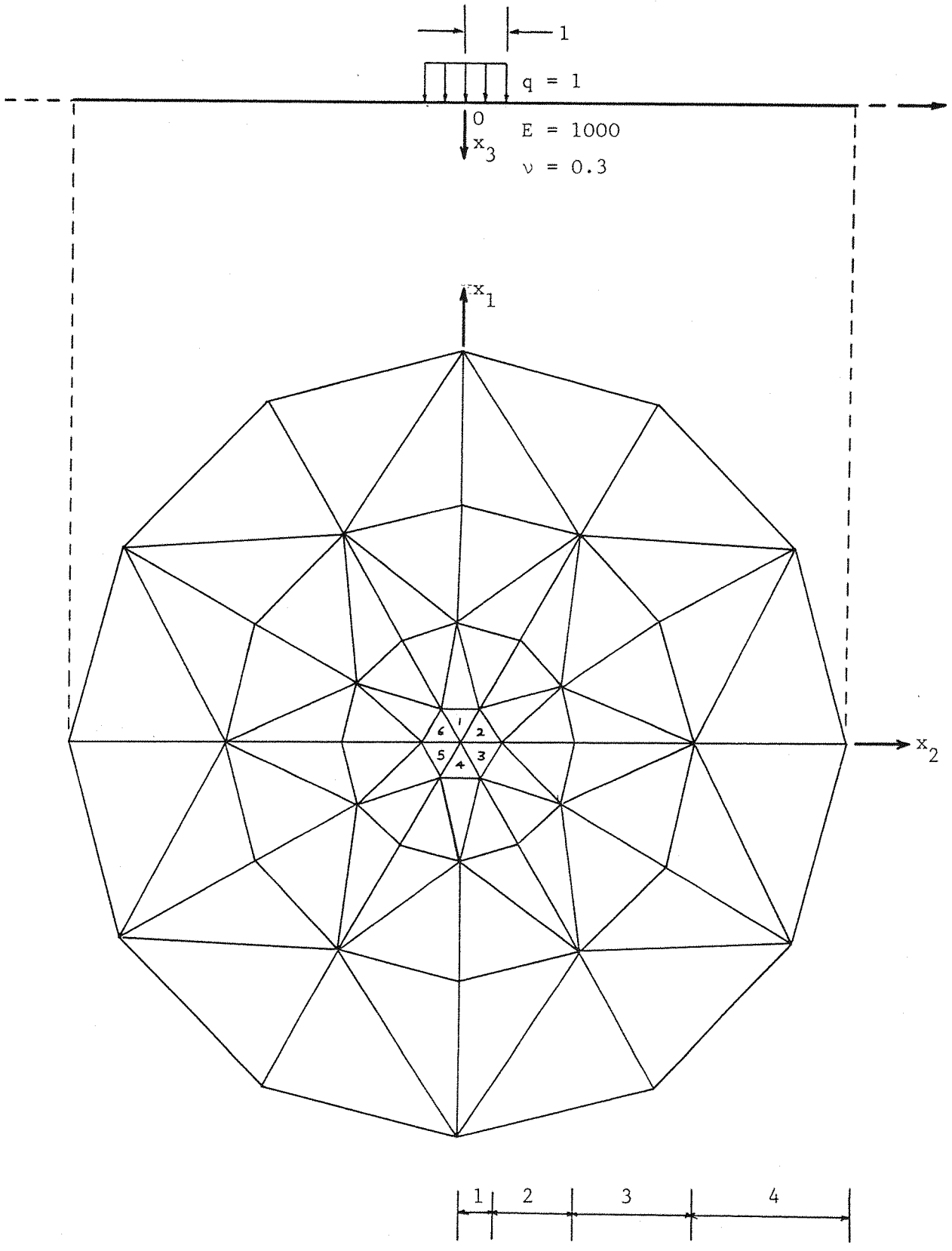

Figure 4.4.3 Half-space Loaded over Circular Area
(72 Elements - Elements 1 - 6, loaded)

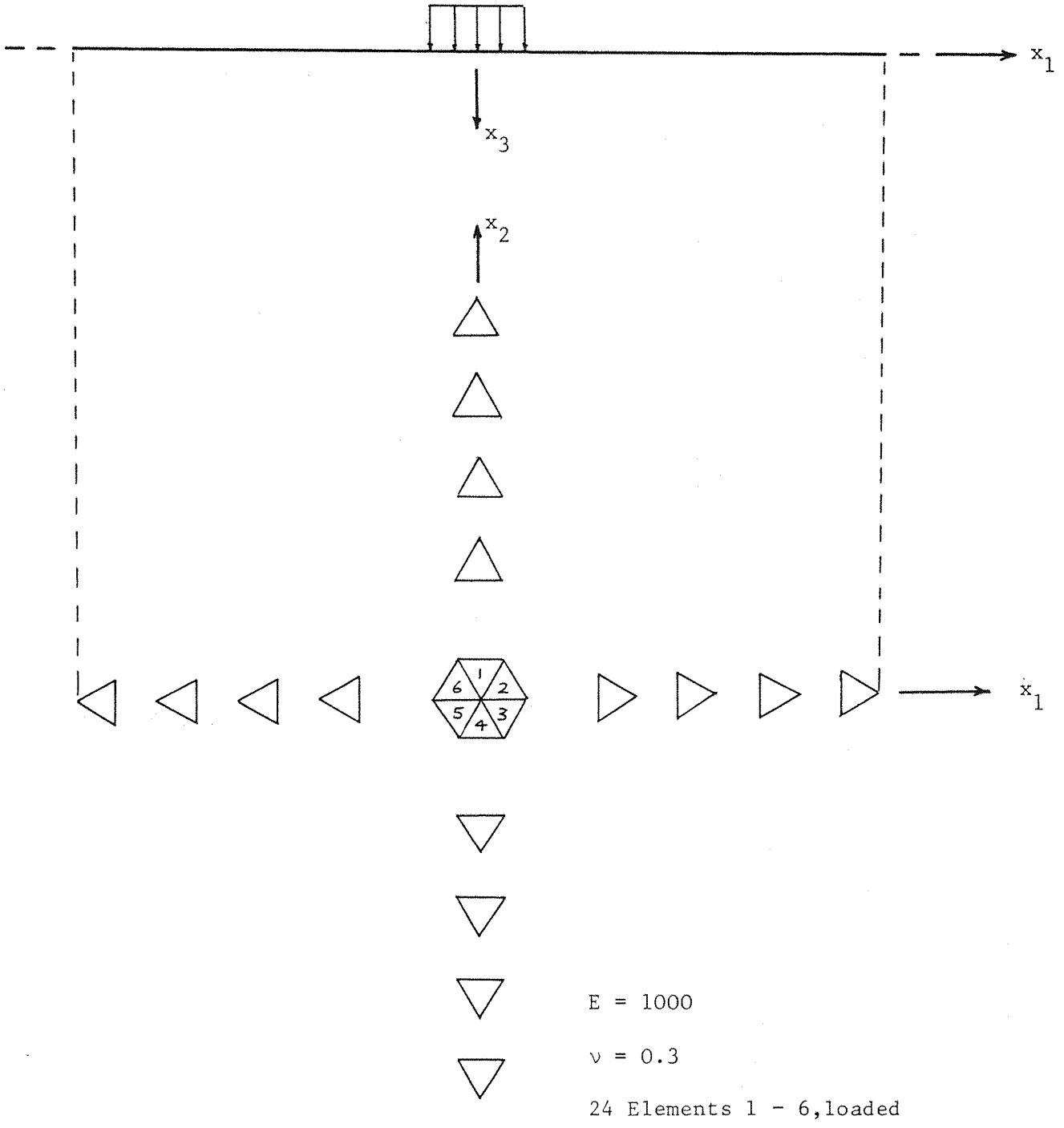

Figure 4.4.5 Mesh for half-space, using equal size elements.

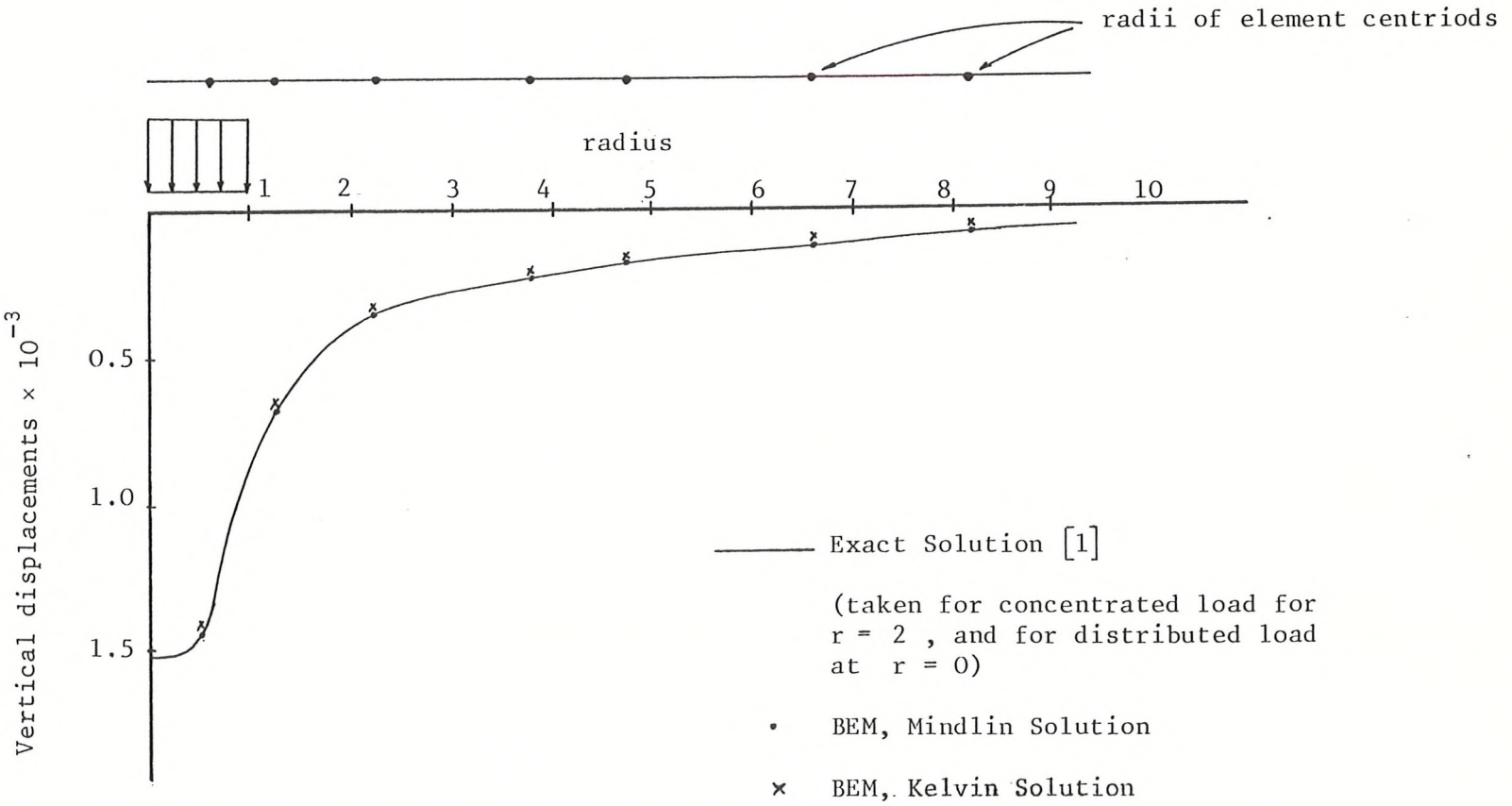

Figure 4.4.4 Half-Space with surface loading; displacement profile on free surface. (72 elements).

Radius	Displacements $\times 10^{-3}$, using $\underset{\sim}{K}^u$		Displacements $\times 10^{-3}$, using $\underset{\sim}{K}^s$	
	radial	vertical	radial	vertical
0.5773	-0.07574	1.44262	-0.07540	1.44263
1.1547	-0.18371	0.71514	-0.18432	0.71497
2.8867	-0.07448	0.26408	-0.07446	0.26402
4.6187	-0.04655	0.16374	-0.04655	0.16374
6.3507	-0.03386	0.11881	-0.03386	0.11880
8.0827	-0.02660	0.09325	-0.02660	0.09325

Table 4.4.2 Half-space solution using $\underset{\sim}{K}^u$ and $\underset{\sim}{K}^s$, for mesh of equal sized elements.

Radius	B.E.M.	'Equivalent' Stiffness $\underset{\sim}{K}^u$	$\underset{\sim}{K}^s$
0.2887	5.730	5.727	5.914
0.9553	5.587	5.588	5.770
1.3213	5.453	5.451	5.616
2.6547	4.737	4.738	4.892
3.2647	4.360	4.359	4.427
5.4313	3.169	3.169	3.240
6.9333	2.572	2.572	2.617

(a) Mindlin Solution

Table 4.4.3 Half-Space with a cylindrical Cavity. Free Surface vertical Displacements ($\times 10^{-2}$)

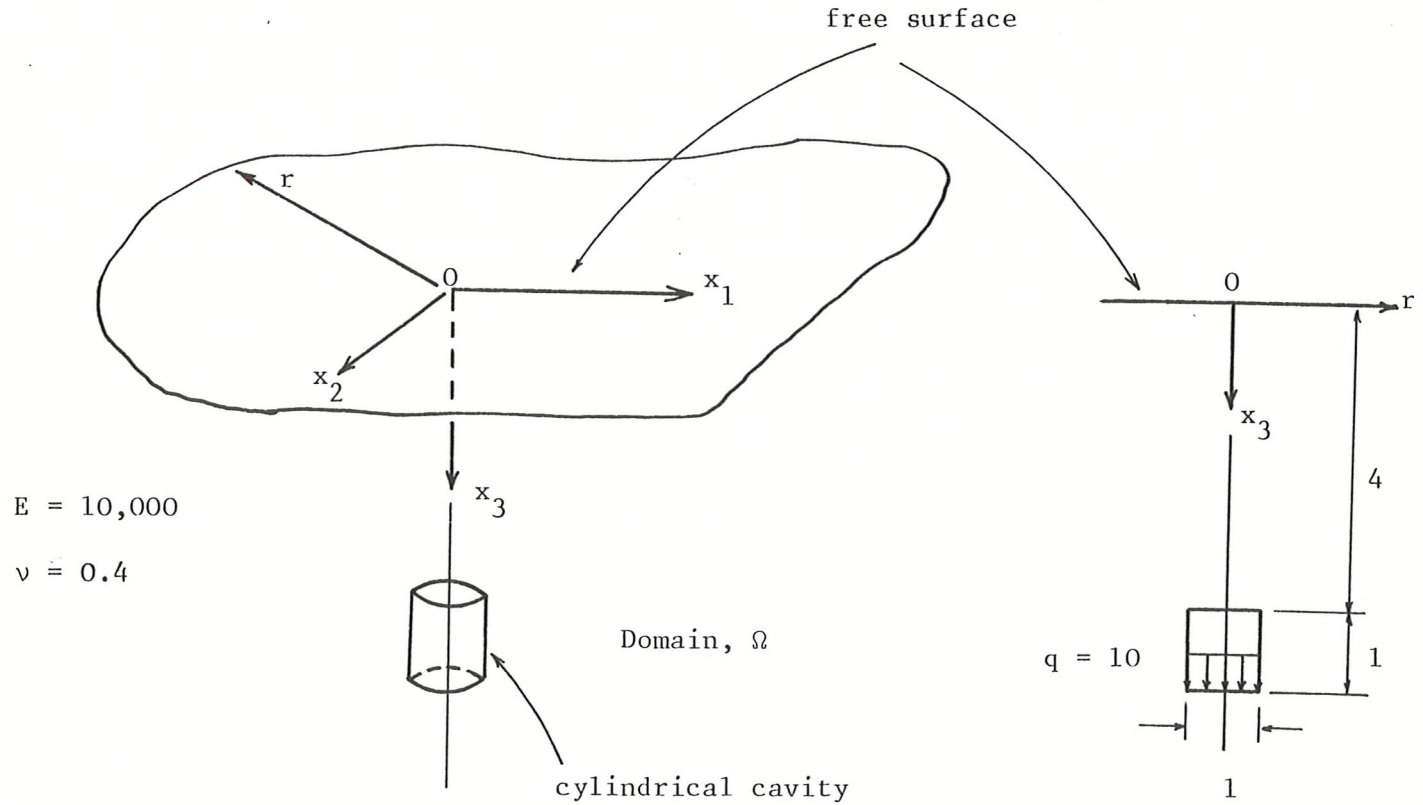

Figure 4.4.6 Half-Space with a Cylindrical Cavity

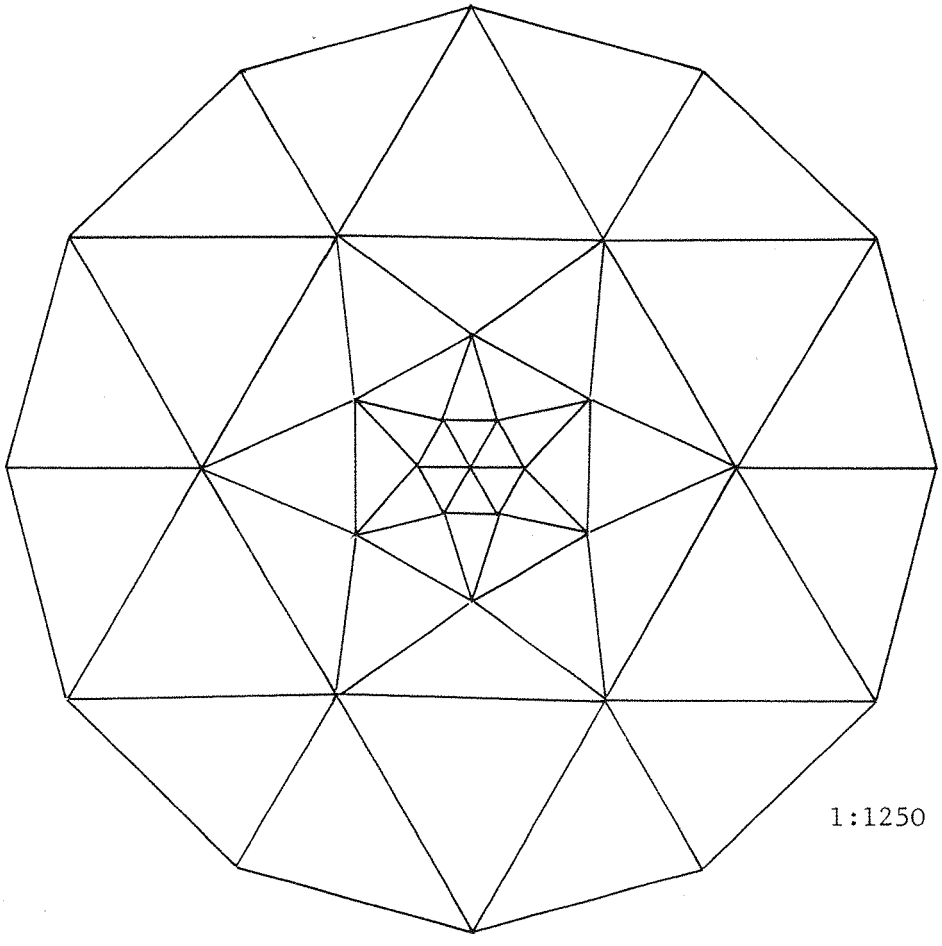

Figure 4.4.8 Boundary Element Mesh for the Surface

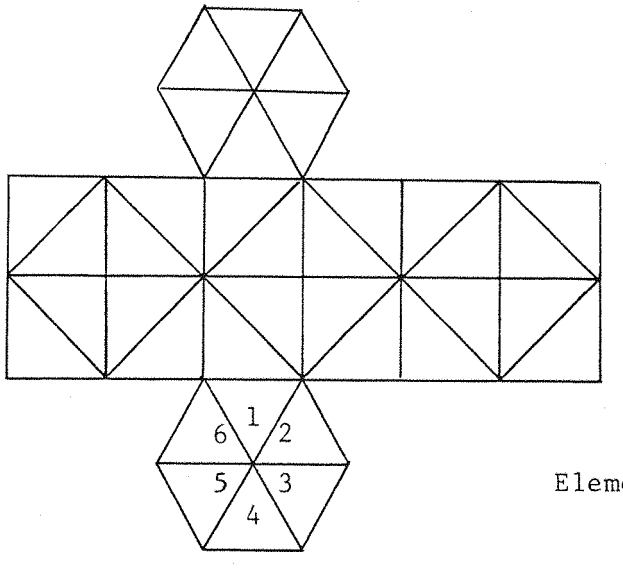

Elements 1 - 6 loaded

Figure 4.4.7 Developed Boundary Element Mesh for Cavity

Radius	B.E.M.	'Equivalent' Stiffness $\underset{\sim}{K}^{u}$	$\underset{\sim}{K}^{s}$
0.2287	5.607	5.604	5.406
0.9553	5.452	5.451	5.272
1.3213	5.291	5.291	5.150
2.6547	4.593	4.592	4.468
3.2647	4.215	4.214	4.093
5.4313	3.035	3.035	2.989
6.9333	2.424	2.424	2.390

(b) Kelvin Solution

Table 4.4.3 Half-Space with a cylindrical Cavity. Free Surface vertical Displacements ($\times 10^{-2}$).

	B.E.M.		'Equivalent' Stiffness			
			$\underset{\sim}{K}^{u}$		$\underset{\sim}{K}^{s}$	
	Top	Bottom	Top	Bottom	Top	Bottom
Kelvin	0.086	0.557	0.087	0.557	0.081	0.563
Mindlin	0.096	0.570	0.096	0.570	0.088	0.591

Table 4.4.4 Half-Space with a cylindrical Cavity. Vertical displacements of Top and Bottom faces of cylinder.

CHAPTER 5

2-D PROBLEMS WITH TRACTION DISCONTINUITIES

5.1 INTRODUCTION

This Chapter will deal with the problem of forming an 'equivalent' stiffness matrix based on the Boundary Element Method, and using higher order elements (i.e. higher than constant elements). The use of higher order elements entails the placing of nodes at geometric discontinuities on the boundary at which discontinuities of the surface tractions often exist, and this aspect requires special attention for accurate modelling of the problem.

The above difficulties are discussed in depth and a formulation is presented, for the 2-Dimensional linear element case, which overcomes these problems to a very large degree. The ideas in this formulation may readily be extended to the 3-Dimensional problem, and the inclusion of higher order elements presents no further difficulties once the discontinuity problem at the ends of the elements is adequately dealt with.

Several examples, testing the behaviour of the thus derived 'effective' stiffness matrix are presented and finally several combination problems are run as an overall finite element displacement type model.

This chapter also includes a discussion of the symmetric properties of stiffness relations, in particular those derived from a Boundary Element formulation. The reasons for lack of symmetry in certain cases are analysed and considered in the context of classical Finite Element interpretations of the physical systems concerned.

5.2 SURFACE TRACTION DISCONTINUITIES

Consider a general problem of the mixed type, where displacement boundary conditions are defined on Γ_1 and traction boundary conditions

are defined on Γ_2 . The discretisation of the surface using linear or higher order elements will entail nodes positioned at geometric discontinuities on the surface at which points the tractions are different on the two elements adjacent to the node. (e.g. nodes B-G, fig. 5.2.1). In principle, at such nodes, there are three sets of variables :- (i) the displacement vector, (ii) the traction components on the first element; (iii) the traction components on the second element.

At this point a notation is introduced which will facilitate the mathematical definition of the problem : Consider a geometric discontinuity existing at a node 'i' with adjacent nodes 'i-1' and 'i+1', linking two elements 'j' and 'j+1' , as shown in Fig. 5.2.2. Define the vectors $\underset{\sim}{u}^i$ and $\underset{\sim}{p}^{i,m}$ as follows :

$$\underset{\sim}{u}^i = \begin{Bmatrix} u_1^i \\ u_2^i \end{Bmatrix} \quad ; \quad \underset{\sim}{p}^{i,m} = \begin{Bmatrix} p_1^{i,m} \\ p_2^{i,m} \end{Bmatrix} \tag{5.2.1}$$

where :

u_k^i is the displacement component in the 'k'(k=1,2) direction, at node 'i' .

$p_k^{i,m}$ is the traction component in the 'k' direction on the 'm'th element at the'i'th node. (m = j, j + 1)

ℓ_j is the length of element 'j'.

In general the discontinuity problem is overcome using the concept of a 'double node'. The 'extra' node at any such discontinuity point gives rise to an extra set of equations in the final system (equations (3.4.11)) thus allowing for the consideration of the 'extra' traction. Only one of the three variables need be defined by the boundary conditions, at a discontinuous node, and the remaining two

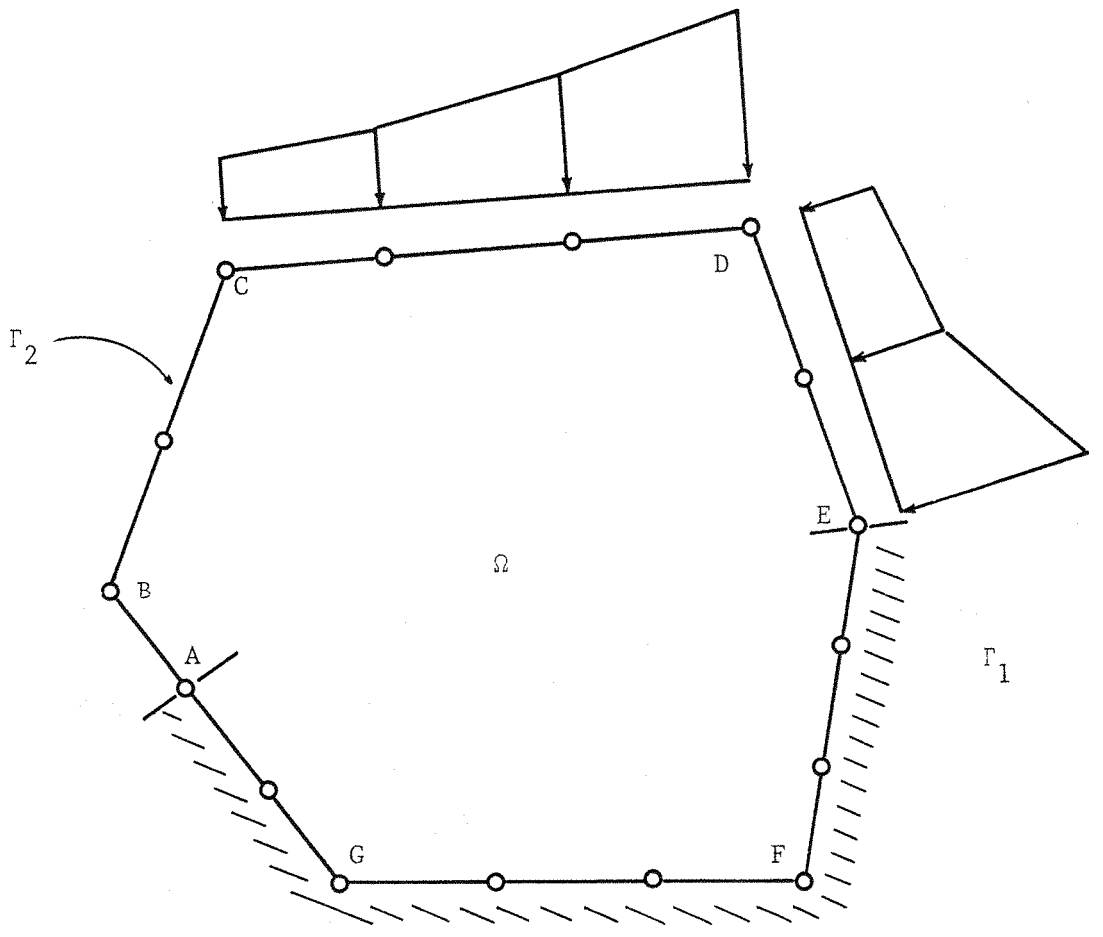

Figure 5.2.1 General problem demonstrating traction discontinuities.

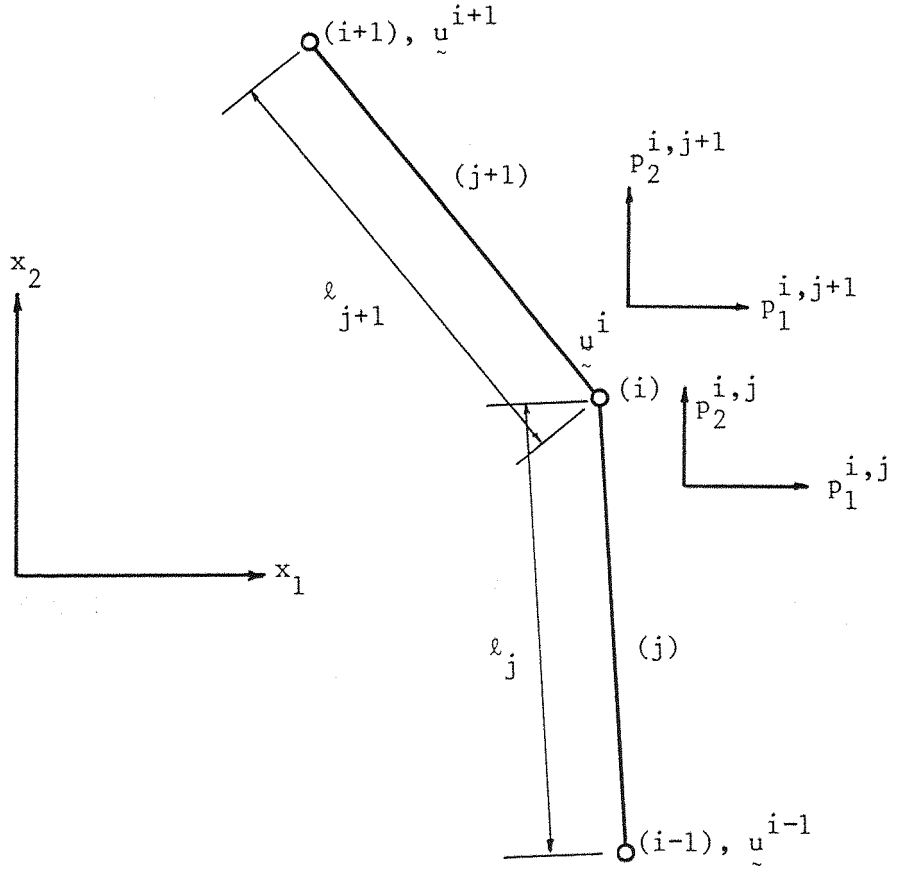

Figure 5.2.2 Definition of Discontinuity Problem

will be yielded by the solution of the equations, as there are two equations corresponding to that point.

However, the rows of the $\underset{\sim}{H}$ and $\underset{\sim}{G}$ matrices (equations (3.4.11)) corresponding to the double points are identical -other than the diagonal submatrices of $\underset{\sim}{H}$, due to the $\underset{\sim}{c}^i$ term in equation (3.4.8). The system of equations is represented diagrammatically in Fig. 5.2.3, showing the double set of equations for one particular point 'i'.

Consider points such as 'B, C, D', Fig. (5.2.1) at which both tractions (i.e. $\underset{\sim}{p}^{i,1}$ and $\underset{\sim}{p}^{i,2}$) are known.

There is no interchange of the columns H_m^i and G_m^i in order to form the final system, and solution of the equations will yield the value of u^i .

For points such as 'E' (Fig. 5.2.1) where $\underset{\sim}{p}^{i,2}$ is unknown, the columns H_2^i are added to H_1^i forming H^i , and these columns are now interchanged with G_2^i (corresponding to the unknown $\underset{\sim}{p}^{i,2}$), so that all the unknowns are on the left hand side of the equations. The columns originally occupied by the H^i terms (and their corresponding rows) are now superfluous and may be replaced by dummy equations - i.e. zero's everywhere, with unity on the leading diagonal.

For points such as 'A' , (Fig. 5.2.1) where $\underset{\sim}{p}^{i,1}$ is unknown, the same applies except that the columns G_1^i are now interchanged as opposed to G_2^i .

It should be noted that the actual inclusion of these extra sets of equations is not necessary and the same effect as that described above may be accomplished by modifying the elemental contributions to

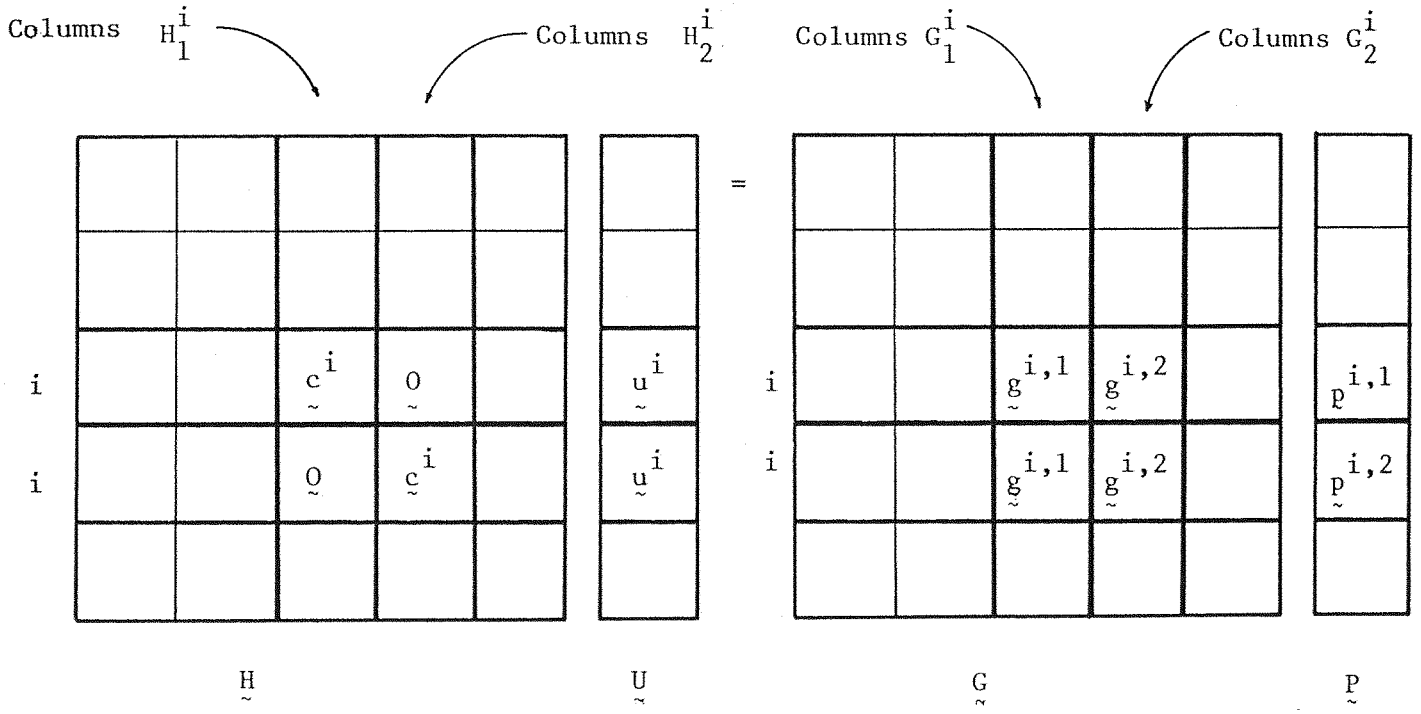

$g^{i,m}$ is the 2 × 2 submatrix of G contributed by the integration over the m'th element (m = 1,2) adjacent to node 'i'.

Figure 5.2.3 Diagrammatic representation of H and G matrices, using double nodes.

the $\underset{\sim}{G}$ matrix in the assembly process. The $\underset{\sim}{H}$ matrix may be assembled in the normal way, as the $\underset{\sim}{u}^i$ vector is unique, thus forming only one set of equations for that point, and adding the contributions at node 'i' due to the 2 adjoining elements. For nodes where the displacements are prescribed, these may be immediately used to multiply out the corresponding columns and added to the right hand side. The $\underset{\sim}{G}$ matrix need not be formed as such; the contributions corresponding to known tractions being multiplied out and added to the right hand side vector, and the contributions corresponding to the unknown tractions being assembled in the appropriate columns of the left hand side matrix. A final system with all the unknowns on the left hand side is then achieved (equation 3.4.12).

There is, however, one special case where the above technique breaks down. If at the discontinuous node the boundary conditions are not mixed, and only the displacements are prescribed (e.g. nodes 'G' and 'F'. Fig. 5.2.1) then there are two sets of independent unknown tractions, corresponding to that point, ($\underset{\sim}{p}^{i,1}$, $\underset{\sim}{p}^{i,2}$). If both the columns G_1^i and G_2^i are interchanged with the columns H_i^1 and H_1^2 , then the final left hand side coefficient matrix will contain two sets of identical rows and thus the solution will be singular. Clearly, the problem is that there are two sets of unknown tractions at that point and only one set of independent equations corresponding to it, giving rise to more unknowns than equations.

This unfortunately, is a problem which arises when trying to formulate the 'equivalent' stiffness matrix using the Boundary Element Method. The technique always requires the inversion of the $\underset{\sim}{G}$ matrix (see equation (3.6.11)) and the two sets of identical rows arising for each discontinuity clearly prohibits this.

A simple way of overcoming this problem is to ignore the discontinuity and only consider a single node. The formulation will then assume a continuous traction, and this effect has been observed to only cause a local error in the solution. (e.g. Lachat and Watson [26]). This can be acceptable, especially for a fine mesh, but if the elements are not particularly small compared to the whole surface, and if there are many such nodes, then the solution can be quite false; especially if the discontinuities are quite sharp. Also, in a general combination problem; refining the Boundary Element mesh around discontinuities in order to reduce the local effect entails the refining of the adjoining Finite Element mesh to allow matching of the nodes, and this may lead to a substantial increase in the total number of nodes. Furthermore, if an accurate appraisal of the stresses around the discontinuity is required, then this technique is clearly unsuitable.

Other attempts have been made to overcome this problem, and Mustoe [5], proposes two. The first is to simply move the double nodes away from the actual discontinuity either side of the point involved, and modify the interpolation functions along those elements accordingly. This seems to give acceptable results as a Boundary Element technique, but problems of matching a Finite Element mesh around that point will be incurred. Alternatively Mustoe [22] presents a formulation based on weighting the Somigliana identity (equation 3.3.25)) with the interpolation functions used for the displacements and tractions. This, in effect, means that each equation is formed by applying a distributed source at around a node, (as opposed to a point source), and integrating the effect of this around the boundary. This substantially increases the amount of numerical integration involved but has the advantage of allowing for inclusion of the discontinuities

by applying discontinuous sources at the double nodes. This technique certainly seems interesting and warrants further investigation.

A further alternative was first suggested by Chaundoneret [23] in which an independent set of equations is derived for any such double point. For the case of two dimensional elastostatics, two extra equations for each point are required. The first of these expresses the symmetry of the stress tensor at this point and relates the surface tractions to the normals of each element. The second equation relates the discontinuous tractions and the boundary normals to the displacements at the discontinuity and at its two adjacent nodes. This is, in fact, a simple 'finite difference' type of equation expressing the invariance of the trace of the strain tensor at that point. This set of independent equations may then be used to replace one of the non-independent sets (see Fig. 5.2.3), and thus allow inversion of the $\underset{\sim}{G}$ matrix. (See also Wardle and Crotty, [25]).

The formulation presented in this Chapter will be based on the use of these 'extra' independent equations for any double node. The actual mechanics of the implementation of these 'extra' equations (hereafter referred to as the 'Corner Condition') is very important as far as the symmetry of the final system is concerned; also their implementation must be such, that the final system is reduced to only one set of equations for any double point,in order to allow matching with a finite element mesh.

5.3 DERIVATION OF THE CORNER CONDITION

The following derivation was first presented by Chaudoneret [23], but will be detailed here for completeness, as well as introducing a notation for its further implementation in the formation of an

'equivalent' stiffness matrix for the system.

Consider two elements, 'j' and 'j+1' which meet at a node 'i'. Their incidences are measured by the angles θ_j and θ_{j+1}, respectively, considered positive when measured in the anti-clockwise sense from the positive x_1 global coordinate axis. The discontinuous outward unit normals at 'i' are denoted by the vectors, $\underset{\sim}{n}^{i,j}$ and $\underset{\sim}{n}^{i,j+1}$. The geometry is depicted in Fig. 5.3.1 (in the diagram the elements are not joined for reasons of clarity).

Figures 5.3.2 (a) and (b) show a differential surface element, and the acting stresses, along 'j' and 'j+1' respectively. The lengths of the sides of these differential elements are given by the components of the respective unit normals, as shown in the diagram.

Equilibrium of the two differential elements in each of the coordinate directions yield the following relationship between the internal stresses at 'i' and the surface tractions :

$$\begin{bmatrix} p_1^{i,j+1} \\ p_1^{i,j} \\ p_2^{i,j+1} \\ p_2^{i,j} \end{bmatrix} = \begin{bmatrix} n_1^{i,j+1} & n_2^{i,j+1} & & \\ n_1^{i,j} & n_2^{i,j} & \underset{\sim}{0} & \\ & & n_1^{i,j+1} & n_2^{i,j+1} \\ \underset{\sim}{0} & & n_1^{i,j} & n_2^{i,j} \end{bmatrix} \begin{bmatrix} \sigma_{11} \\ \sigma_{21} \\ \sigma_{12} \\ \sigma_{22} \end{bmatrix} \qquad (5.3.1)$$

Equations (5.3.1) are valid for the unit normals lying in any of the four quadrants of the global axes x_1 and x_2. These equations may now be inverted to yield :

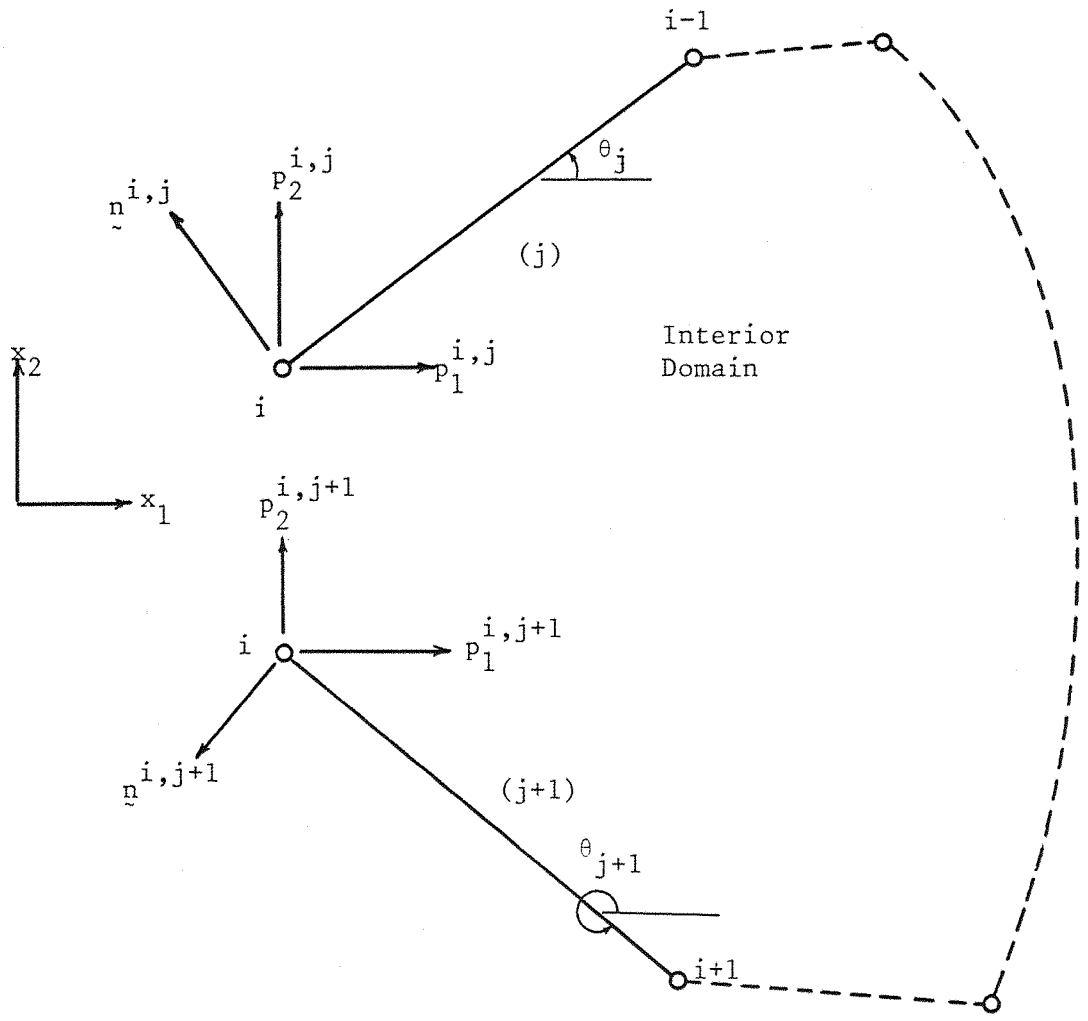

Figure 5.3.1 Notation for Corner Condition

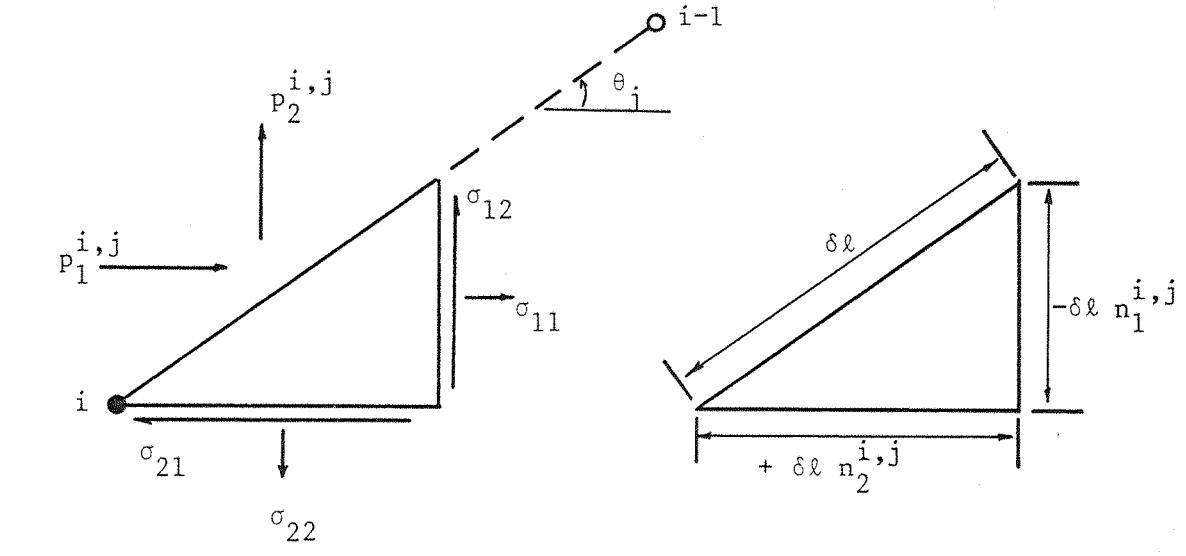

(a) Element j

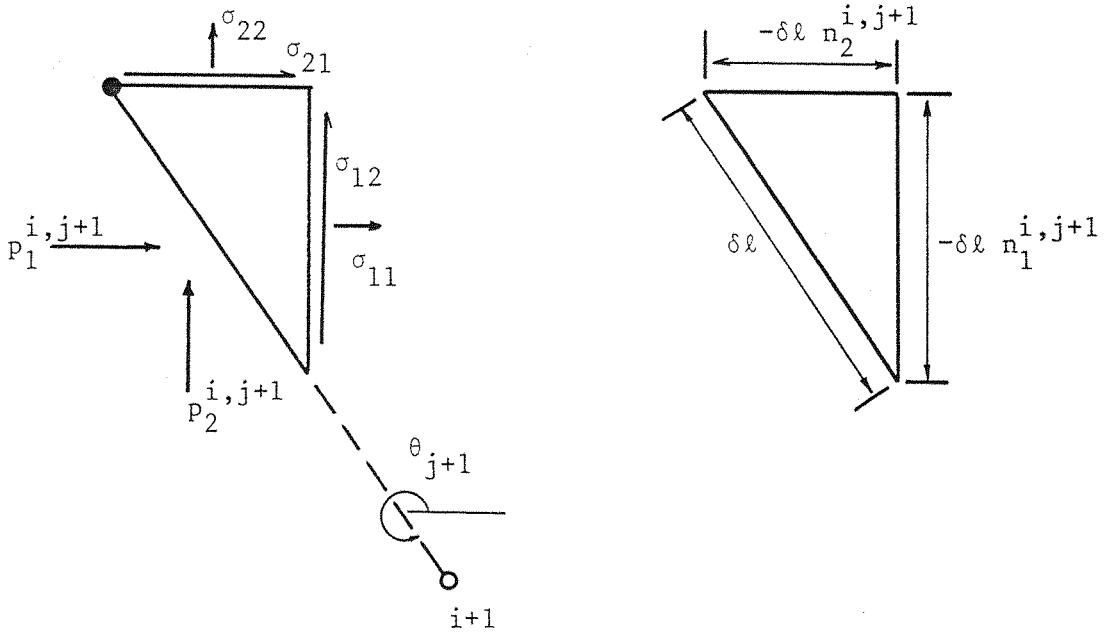

(b) Element j+1

Figure 5.3.2 Tractions and stresses on the two elements adjacent to the discontinuous node.

$$\begin{bmatrix} \sigma_{11} \\ \sigma_{21} \\ \sigma_{12} \\ \sigma_{22} \end{bmatrix} = \frac{1}{D} \begin{bmatrix} n_2^{i,j} & -n_2^{i,j+1} & & \\ -n_1^{i,j} & n_1^{i,j+1} & \underset{\sim}{0} & \\ & & n_2^{i,j} & -n_2^{i,j+1} \\ & \underset{\sim}{0} & -n_1^{i,j} & n_1^{i,j+1} \end{bmatrix} \begin{bmatrix} p_1^{i,j+1} \\ p_1^{i,j} \\ p_2^{i,j+1} \\ p_2^{i,j} \end{bmatrix} \qquad (5.3.2)$$

where $$D = n_2^{i,j+1}\, n_1^{i,j} - n_1^{i,j+1}\, n_2^{i,j} \qquad (5.3.3)$$

When the angle between the two elements is 0 or $\pi/2$, equation (5.3.3) gives $D = 0$, the thus equations (5.3.2) are not valid. This is to be expected, as in this case, a discontinuous traction at 'i' entails a stress singularity at that point, thus prohibiting unique definition of the stress tensor.

From equations (5.3.2), the symmetry of the stress tensor ($\sigma_{12} = \sigma_{21}$) requires that :

$$\begin{bmatrix} n_1^{i,j} & n_2^{i,j} \end{bmatrix} \begin{bmatrix} p_1^{i,j+1} \\ p_2^{i,j+1} \end{bmatrix} + \begin{bmatrix} -n_1^{i,j+1} & -n_2^{i,j+1} \end{bmatrix} \begin{bmatrix} p_1^{i,j} \\ p_2^{i,j} \end{bmatrix} = 0 \qquad (5.3.4)$$

Consider two sets of reference axis - (Z, T), and , (X, Y) - originating at 'i' , as shown in Fig. 5.3.3. The state of stress and strain at 'i' may then be expressed with reference to either sets of axes, and for a unique state of strain the trace of the strain tensor remains invariant. i.e. ;

$$\varepsilon_{XX} + \varepsilon_{YY} = \varepsilon_{ZZ} + \varepsilon_{TT} \qquad (5.3.5)$$

This is an expression of the bulk constantancy of volume of the material.

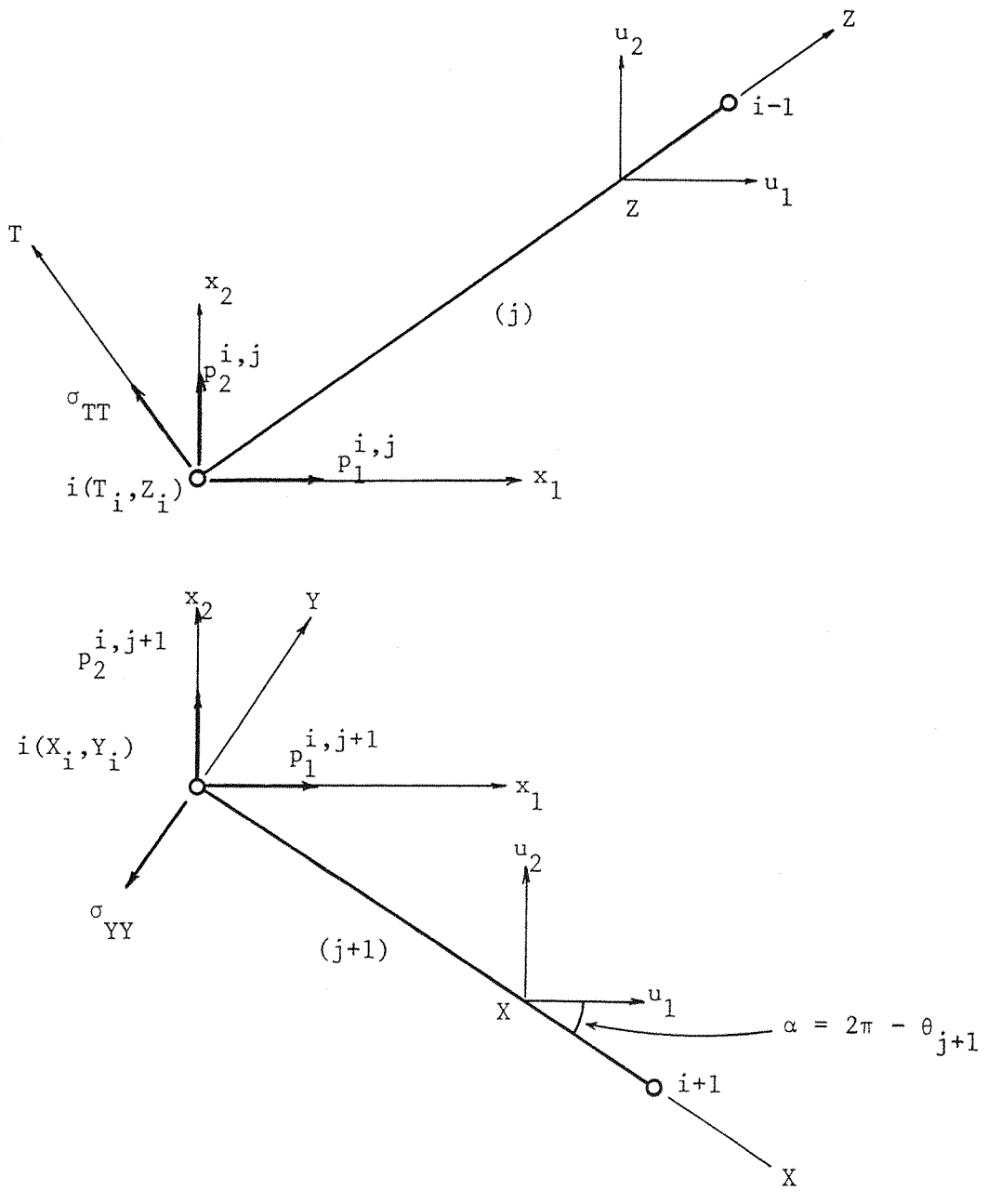

Figure 5.3.3 Coordinate reference systems at a geometric discontinuity.

Now consider the displacement at any point, X, along the element 'j+1' in the global x_1, x_2 reference system. Assuming a linear variation,

$$u_k = u_k^i + \frac{u_k^{i+1} - u_k^i}{\ell_{j+1}} (X - X_i) \quad , \; k = 1,2, \tag{5.3.6}$$

The component of the displacement along the X axis is given by :

$$u_X = u_1 \cos\theta_{j+1} + u_2 \sin\theta_{j+1} \tag{5.3.7}$$

Using equations (5.3.6) we may now differentiate (5.3.7) to obtain the strain ε_{XX}

$$\varepsilon_{XX} = \frac{\partial u_X}{\partial X} = \frac{u_1^{i+1} - u_1^i}{\ell_{j+1}} \cos\theta_{j+1} + \frac{u_2^{i+1} - u_2^i}{\ell_{j+1}} \sin\theta_{j+1} \tag{5.3.8}$$

Similarly, by considering the element 'j', the strain ε_{ZZ} may be expressed as follows :

$$\varepsilon_{ZZ} = \frac{\partial u_Z}{\partial Z} = \frac{u_1^{i-1} - u_1^i}{\ell_j} - \cos\theta_j + \frac{u_2^{i-1} - u_1^{i-1}}{\ell_j} - \sin\theta_j \tag{5.3.9}$$

Now, consider the relationship between the stress tensors and the tractions at 'i' . Along element 'j+1'.

$$- \sigma_{YY} = p_2^{i,j+1} \cos\alpha + p_1^{i,j+1} \sin\alpha$$

or

$$\sigma_{YY} = p_1^{i,j+1} \sin\theta_{j+1} - p_2^{i,j+1} \cos\theta_{j+1} \tag{5.3.10}$$

and similarly along element 'j' :

$$\sigma_{TT} = p_1^{i,j} \sin\theta_j - p_2^{i,j+1} \cos\theta_j \tag{5.3.11}$$

Introducing Hooke's Law, for the (X,Y) system

$$\sigma_{YY} = E_1 \varepsilon_{YY} + E_2 \varepsilon_{XX} \tag{5.3.12}$$

and for the (Z,T) system

$$\sigma_{TT} = E_1 \varepsilon_{TT} + E_2 \sigma_{ZZ} \tag{5.3.13}$$

where $$E_1 = \frac{1}{E(1-\nu^2)} \; ; \; E_2 = \frac{\nu}{E(1-\nu^2)}$$

Subtracting equation (5.3.13) from (5.3.12)

$$\frac{1}{E_2}(\sigma_{YY} - \sigma_{TT}) = \frac{E_1}{E_2}(\varepsilon_{YY} - \varepsilon_{TT}) + (\varepsilon_{XX} - \varepsilon_{ZZ}) \tag{5.3.14}$$

Equation (5.3.5) may be written :

$$0 = (\varepsilon_{YY} - \varepsilon_{TT}) + (\varepsilon_{XX} - \varepsilon_{ZZ}) \tag{5.3.15}$$

and subtracting (5.3.15) from (5.3.14) we have

$$\sigma_{YY} - \sigma_{TT} = 2G(\varepsilon_{YY} - \varepsilon_{TT}) \tag{5.3.16}$$

where

$$2G = (E_1 - E_2) = \frac{E}{(1+\nu)}$$

Now expressions for σ_{YY}, σ_{TT}, ε_{YY}, ε_{TT} are given by equations (5.3.8) - (5.3.11), and on substitution into equation (5.3.16), we have :

$$\begin{bmatrix} -\sin\theta_j & \cos\theta_j \end{bmatrix} \begin{bmatrix} p_1^{i,j} \\ p_2^{i,j} \end{bmatrix} + \begin{bmatrix} \sin\theta_{j+1} & -\cos\theta_{j+1} \end{bmatrix} \begin{bmatrix} p_1^{i,j+1} \\ p_2^{i,j+1} \end{bmatrix} =$$

$$\frac{2G}{\ell_j} \begin{bmatrix} -\cos\theta_j & -\sin\theta_j \end{bmatrix} \begin{bmatrix} u_1^{i-1} \\ u_2^{i-1} \end{bmatrix} + \frac{2G}{\ell_{j+1}} \begin{bmatrix} -\cos\theta_{j+1} & -\sin\theta_{j+1} \end{bmatrix} \begin{bmatrix} u_1^{i+1} \\ u_2^{i+1} \end{bmatrix}$$

$$+ 2G \left[\left(\frac{\cos\theta_j}{\ell_j} + \frac{\cos\theta_{j+1}}{\ell_{j+1}} \right) \left(\frac{\sin\theta_j}{\ell_j} + \frac{\sin\theta_{j+1}}{\ell_{j+1}} \right) \right] \begin{bmatrix} u_1^i \\ u_2^i \end{bmatrix}$$

(5.3.17)

Equation (5.3.17) expresses the invariance of the trace of the strain tensor using a finite difference type approximation to describe the strains, based on a linear variation along an element. A more refined approximation could be developed by assuming a higher order interpolation of the displacements along an element.

Equations (5.3.17) and (5.3.4) may now be used to provide the additional equations for the definition of the extra set of tractions at any discontinuity.

It is convenient for the further implementation of these equations to express them in a matrix notation. The variables involved are the nodal values of displacements and tractions at the discontinuity and adjacent points, and the incidences of the elements and their normals; Defining X_k^m as the projection of the m'th element (m=j,j+1) on the x_k'th global coordinate axis, divided by the length of the element, then equations (5.3.17) and (5.3.4) may be written :

$$\underset{\sim}{T1}\ \underset{\sim}{p}^{i,j} + \underset{\sim}{T2}\ \underset{\sim}{p}^{i,j+1} = \underset{\sim}{T3}\ \underset{\sim}{u}^{i-1} + \underset{\sim}{T4}\ \underset{\sim}{u}^{i+1} + \underset{\sim}{T5}\ \underset{\sim}{u}^{i} \qquad (5.3.18)$$

where :

$$T1 = \begin{bmatrix} -X_2^j & +X_1^j \\ +X_2^{j+1} & -X_1^{j+1} \end{bmatrix}$$

$$T2 = \begin{bmatrix} +X^{j+1} & -X_1^{j+1} \\ -X_1^j & -X_1^{j+1} \end{bmatrix}$$

$$T3 = \frac{2G}{\ell_j} \begin{bmatrix} -X_1^j & -X_2^j \\ 0 & 0 \end{bmatrix}$$

$$T4 = \frac{2G}{\ell_{j+1}} \begin{bmatrix} -X_1^{j+1} & -X_2^{j+1} \\ 0 & 0 \end{bmatrix}$$

$$T5 = 2G \begin{bmatrix} \left(\frac{X_1^j}{\ell_j} + \frac{X_1^{j+1}}{\ell_{j+1}} \right) & \left(\frac{X_2^j}{\ell_j} + \frac{X_2^{j+1}}{\ell_{j+1}} \right) \\ 0 & 0 \end{bmatrix} \qquad (5.3.19)$$

and $G = \frac{E}{2(1+\nu)}$, the shear modulus.

(Note : G is invariant for the cases of plane stress and plane strain).

5.4 IMPLEMENTATION OF THE CORNER CONDITION IN THE BOUNDARY ELEMENT METHOD

For any discontinuous point a double node may be employed, giving rise to two sets of equations, as shown diagramatically in Fig. 5.2.3. If the boundary conditions are such that the displacement is prescribed and both sets of tractions are unknown, then equation

(5.3.18) provides the extra, necessary relationship between the tractions and neighbouring displacements. This equation may be used to replace one the repeated equations arising from the double node and thus render the system solvable.

In practice, however, the use of a double node and twin sets of equations for discontinuous points is not necessary, as the same effect may be achieved in the assembly process of the equations. This will be demonstrated below using as an example the case of linear elements.

Consider the formation of the equation for point 'k' . We apply a point source at 'k' and integrate the corresponding fundamental solution (weighted by the appropriate shape functions) around the boundary. Figure 5.4.1 represents the situation when integrating along two elements, ('j' and 'j+1') at whose intersection, (point 'i') there exists a traction discontinuity. We seek to form the appropriate set of rows, for point 'k' , in the $\underset{\sim}{H}$ and $\underset{\sim}{G}$ matrices of equation (3.4.11). If we had a double node at 'i', with two sets of rows and columns in the $\underset{\sim}{H}$ and $\underset{\sim}{G}$ matrices, then the terms corresponding to node 'i' would be;

a) On the left hand side of the equations :

$$\underset{\sim}{h}^{k(j)_2}\,\underset{\sim}{u}^{i} + \underset{\sim}{h}^{k(j+1)_1}\,\underset{\sim}{u}^{i} \qquad (5.4.1)$$

b) On the right hand side of the equations :

$$\underset{\sim}{g}^{k(j)_2}\,\underset{\sim}{p}^{i,j} + \underset{\sim}{g}^{k(j+1)_1}\,\underset{\sim}{p}^{i,j+1} \qquad (5.4.2)$$

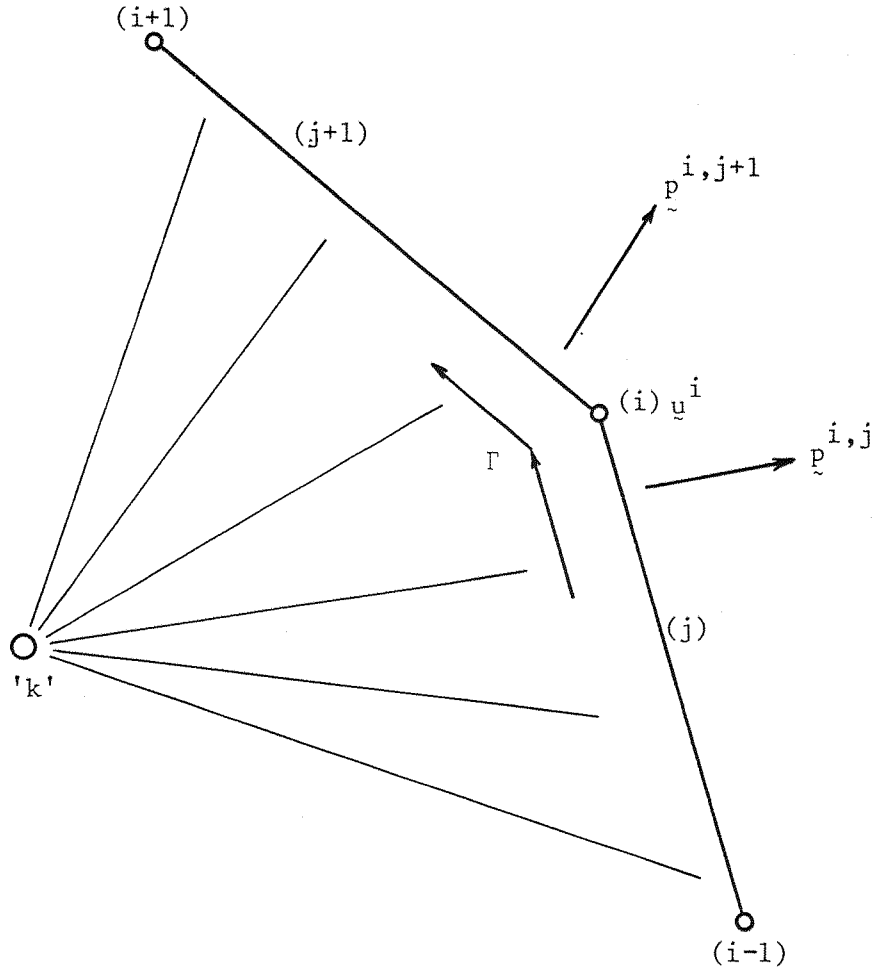

Figure 5.4.1 Integration around a discontinuity.

where $\underset{\sim}{h}^{kp_m}$ and $\underset{\sim}{g}^{kp_m}$ are 2 × 2 submatrices of $\underset{\sim}{H}$ and $\underset{\sim}{G}$ respectively, and represent the contribution of the integration at the m'th node of the p'th element due to a source at 'k' .

If we now only use one set of rows and columns for point 'i', we assemble allowing for only one variable at 'i' . There are 3 cases :

(i) For the case where the discontinuous tractions $(\underset{\sim}{p}^{i,j}, \underset{\sim}{p}^{i,j+1})$ are known :

The displacement, $\underset{\sim}{u}^{i}$, is unique and thus the sum

$$\underset{\sim}{h}^{k(j)_2} + \underset{\sim}{h}^{k(j+1)_1} \qquad (5.4.3)$$

is assembled in k'th rows and i'th columns of $\underset{\sim}{H}$.

The corresponding contributions to the $\underset{\sim}{G}$ matrix (expression (5.4.2)) need not be assembled, as all the terms are known and may be multiplied out and added to the right hand side vector of the final set of equations (3.4.12).

(ii) For the case when the displacement, $\underset{\sim}{u}^{i}$, and one of the tractions (either $\underset{\sim}{p}^{i,j}$ or $\underset{\sim}{p}^{i,j+1}$) are known.

In this case the displacement is used to multiply both the $\underset{\sim}{h}$ contributions (expression 5.4.3) to form a term in the right hand side vector, as does the known traction with its corresponding $\underset{\sim}{g}$ contribution. The remaining unknown traction becomes an unknown in the left hand side vector, and its corresponding $\underset{\sim}{g}$ sub-matrix is placed in the appropriate column of the left hand side coefficient matrix.

(iii) For the case when only the displacements, $\underset{\sim}{u}^i$, are known:

In this case both tractions ($\underset{\sim}{p}^{i,j}$, $\underset{\sim}{p}^{i,j+1}$) are unknown and we require the additional relationship provided by the 'Corner Condition' (equation (5.3.18)) in order to uniquely define the problem. Consider the integration performed over the element 'j' (Fig. 5.4.1), which will produce the following elemental contributions for assembling in $\underset{\sim}{H}$ and $\underset{\sim}{G}$.

$$\begin{bmatrix} \underset{\sim}{h}^{kj}{}_1 & \underset{\sim}{h}^{kj}{}_2 \end{bmatrix} \begin{bmatrix} \underset{\sim}{u}^{i-1} \\ \underset{\sim}{u}^{i} \end{bmatrix} = \begin{bmatrix} \underset{\sim}{g}^{kj}{}_1 & \underset{\sim}{g}^{kj}{}_2 \end{bmatrix} \begin{bmatrix} \underset{\sim}{p}^{i-1,j} \\ \underset{\sim}{p}^{i,j} \end{bmatrix} \qquad (5.4.4)$$

+ terms due to integration along the rest of the elements.

We may now write equation (5.3.18) as :

$$\underset{\sim}{p}^{i,j} = - \hat{\underset{\sim}{T}}2 \; \underset{\sim}{p}^{i,j+1} + \hat{\underset{\sim}{T}}3 \; \underset{\sim}{u}^{i-1} + \hat{\underset{\sim}{T}}4 \; \underset{\sim}{u}^{i+1} + \hat{\underset{\sim}{T}}5 \; \underset{\sim}{u}^{i}$$

where

$$\begin{aligned} \hat{\underset{\sim}{T}}2 &= \underset{\sim}{T1}^{-1} \; \underset{\sim}{T2} \\ \hat{\underset{\sim}{T}}3 &= \underset{\sim}{T1}^{-1} \; \underset{\sim}{T3} \\ \hat{\underset{\sim}{T}}4 &= \underset{\sim}{T1}^{-1} \; \underset{\sim}{T4} \\ \hat{\underset{\sim}{T}}5 &= \underset{\sim}{T1}^{-1} \; \underset{\sim}{T5} \end{aligned} \qquad (5.4.5)$$

Substituting equation (5.4.5) into (5.4.4), we have :

$$\begin{bmatrix} \hat{\underset{\sim}{h}}^{kj}{}_1 & \hat{\underset{\sim}{h}}^{kj}{}_2 \end{bmatrix} \begin{bmatrix} \underset{\sim}{u}^{i-1} \\ \underset{\sim}{u}^{i} \end{bmatrix} + \begin{bmatrix} \underset{\sim}{E} \end{bmatrix} \begin{bmatrix} \underset{\sim}{u}^{i+1} \end{bmatrix} = \begin{bmatrix} \hat{\underset{\sim}{g}}^{kj}{}_1 & \hat{\underset{\sim}{g}}^{kj}{}_2 \end{bmatrix} \begin{bmatrix} \underset{\sim}{p}^{i-1,j} \\ \underset{\sim}{p}^{i,j+1} \end{bmatrix} \qquad (5.4.6)$$

where

$$\hat{\underset{\sim}{h}}^{kj_1} = \underset{\sim}{h}^{kj_2} - \underset{\sim}{g}^{kj_2}\,\hat{\underset{\sim}{T}}3 \qquad (a)$$

$$\hat{\underset{\sim}{h}}^{kj_2} = \underset{\sim}{h}^{kj_2} - \underset{\sim}{g}^{kj_2}\,\hat{\underset{\sim}{T}}5 \qquad (b)$$

$$\underset{\sim}{E} = - \underset{\sim}{g}^{kj_2}\,\hat{\underset{\sim}{T}}4 \qquad (c) \qquad (5.4.7)$$

$$\hat{\underset{\sim}{g}}^{kj_2} = - \underset{\sim}{g}^{kj_2}\,\hat{\hat{\underset{\sim}{T}}}2 \qquad (d)$$

$$\hat{\underset{\sim}{g}}^{kj_1} = \underset{\sim}{g}^{kj_1} \qquad (e)$$

These modified contributions to the $\underset{\sim}{H}$ and $\underset{\sim}{G}$ matrices (denoted by $\hat{\underset{\sim}{h}}$ and $\hat{\underset{\sim}{g}}$) may then be assembled in the normal way, and we are left with only one traction $(\underset{\sim}{p}^{i,j+1})$ to work with in the equations. $\underset{\sim}{E}$ is an additional 2×2 submatrix which is added in the columns of $\underset{\sim}{H}$ corresponding to node 'i + 1'. The equations may now be solved, yielding a solution for $\underset{\sim}{p}^{i,j+1}$, which may then be substituted in equation (5.3.18) to compute the remaining traction $\underset{\sim}{p}^{i,j}$.

The above process may be shown to be equivalent to employing a double node, replacing one of the sets of equations by (5.3.18), and then proceeding to eliminate the rows and columns corresponding to this equation by linear row and column operations on the matrices. Although the technique above may seem complicated and cumbersome, this is partly due to the necessary number of small matrices within the formulation, and also the indicial notation, necessary to distinguish between the relevant parameters, which appears awkward; however, definition of the 'Corner Condition' (equation 5.3.18) is very simple, as it only depends on the coordinates of the discontinuous node, and its neighbours; once these matrices have been defined, the computation

of the modified contributions to the $\underset{\sim}{H}$ and $\underset{\sim}{G}$ matrices (5.4.6) is in fact very simple, and may be programmed directly using equations (5.4.7).

5.5 FORMING AN 'EQUIVALENT' STIFFNESS MATRIX

5.5.1 General Remarks

The formulation outlined here is based on the technique outlined in section 3.6 and involves the inversion of the $\underset{\sim}{G}$ matrix. With the use of double nodes for a discontinuity this matrix is singular; however, upon inclusion of the extra 'Corner Condition' equations, the singularities are removed. The formulation must be developed with certain important considerations in mind : the final stiffness type relation must contain only one set of equations corresponding to each point in order to allow matching to a Finite Element mesh; and also, the final right hand side vector, containing the equivalent nodal loads must be formed considering the accumulative effect of both tractions at a discontinuous node, in order to give the correct nodal load at that point. Finally, consideration for the degree of symmetry of the final equations must be made : Chaudonneret[23] presents a formulation which gives good results for the simple test cases published, however the 'equivalent' stiffness matrix is very unsymmetric. A similar approach to [23] was originally attempted in the early stages of this work and similar results were obtained. Upon consideration of the problem, the inclusion of this extra 'Corner Condition' can be thought of as a necessary boundary condition on the problem, reminiscent of the imposition of a set of linearly dependent constraints on a classical Finite Element type model. This type of boundary condition usually takes the form of a

a linear dependence between a sub-set of the displacements and hence this equation must also be satisfied by the final solution; as such the equation relating the prescribed displacements must be included in the stiffness matrix of the system. The classical Finite Element formulation produces an inherently symmetric stiffness matrix, $\underset{\sim}{K}$; however if a linear constraint of this type is simply used to replace a non-independent equation in the Finite Element system,

$$\underset{\sim}{K}\ \underset{\sim}{U} = \underset{\sim}{F} \tag{5.5.1}$$

then the symmetry of $\underset{\sim}{K}$ is destroyed. As a result the linear constraints are usually written in terms of a rotation matrix $\underset{\sim}{R}$, such that

$$\underset{\sim}{U} = \underset{\sim}{R}\ \underset{\sim}{U} \tag{5.5.2}$$

where equations (5.5.2) contain the necessary boundary conditions, and may be substituted in equation (5.5.1) to yield

$$\bar{\underset{\sim}{K}}\ \underset{\sim}{U} = \bar{\underset{\sim}{F}} \tag{5.5.3}$$

where

$$\bar{\underset{\sim}{K}} = \underset{\sim}{R}^{T}\ \underset{\sim}{K}\ \underset{\sim}{R}$$

$$F = \underset{\sim}{R}^{T}\ \underset{\sim}{F}$$

The final coefficient matrix $\bar{\underset{\sim}{K}}$ thus retains symmetry.

The problem of imposing the extra 'Corner Condition' in the formation of an 'equivalent' stiffness matrix using the BEM is similar to the Finite Element problem described above, except that the linear constraint also relates surface tractions to a set of displacements. (equation (5.3.18)). A formulation was thus developed based on the idea of setting up the necessary constraints as a set of rotation matrices and imposing these on the Boundary Element system. The details of this formulation are given below.

5.5.2 Matrix Formulation

The ensuing formulation will use the following notation :

$\underset{\sim}{U}$, $\underset{\sim}{P}$, $\underset{\sim}{F}$ are vectors containing values of the displacements, tractions, nodal forces, respectively at each node. (a set of two values for any node, and two sets for any double node.)

$\hat{\underset{\sim}{U}}$, $\hat{\underset{\sim}{P}}$, $\hat{\underset{\sim}{F}}$ are vectors containing only one set of values for any double node.

$\hat{\underset{\sim}{U}}$ will contain one set of values, u^i, for point 'i'

$\hat{\underset{\sim}{P}}$ will contain $\underset{\sim}{p}^{i,j+1}$ at point i

$\hat{\underset{\sim}{F}}$ will contain $\underset{\sim}{f}^i$, total equivalent force, at point 'i'.

NN = order of overall system = (total number of nodes) × (number of degrees of freedom at each node).

NI = order of reduced system = (number of independent nodes) × (number of degrees of freedom at each node).

The standard B.E.M. formulation, with the inclusion of double nodes, yields,

$$\underset{\sim}{H}\ \underset{\sim}{U} = \underset{\sim}{G}\ \underset{\sim}{P} \tag{5.5.4}$$

The 'Corner Condition', equation (5.3.18), may be written in the form given by equation (5.4.5), and this may be expressed for the whole system as

$$\underset{\sim}{P} = \underset{\sim p}{R}\ \hat{\underset{\sim}{P}} + \underset{\sim u}{R}\ \hat{\underset{\sim}{U}} \tag{5.5.5}$$

where, $\underset{\sim p}{R}$ and $\underset{\sim u}{R}$ are rotation matrices of order NN × NI and contain equation (5.4.5) for each double node, on the rows corresponding to $\underset{\sim}{p}^{i,j}$. These matrices are depicted diagrammatically in Fig. 5.5.1

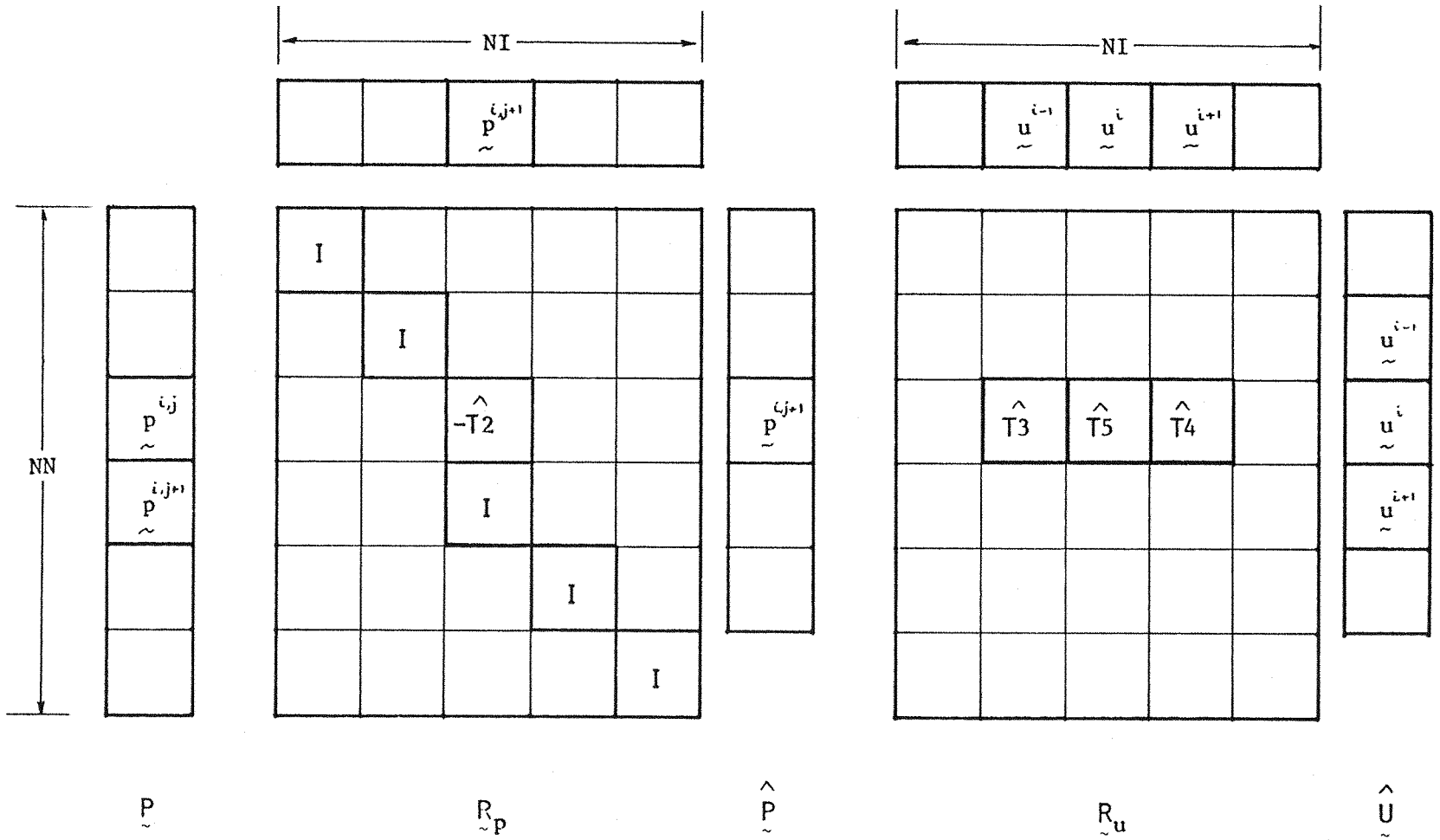

($R_{\sim u}$ and $R_{\sim p}$ are null other than the 2×2 submatrices shown).

Figure 5.5.1 Diagrammatic representation of the 'Corner Condition' written within global rotation matrices. (equations (5.4.5)).

and show the 2 × 2 submatrices for one particular double node, 'i'. (The column vectors, $\hat{\underset{\sim}{P}}$ and $\hat{\underset{\sim}{U}}$, are also shown above the matrices in order to clarify the positions of the relevant terms in the $\underset{\sim}{R}_u$ and $\underset{\sim}{R}_p$ matrices. 'I' is the unit matrix of order 2).

The condition of a unique set of displacements at any double point may be written :

$$\underset{\sim}{U} = \underset{\sim}{R}_d \, \hat{\underset{\sim}{U}} \tag{5.5.6}$$

The condition that the total equivalent nodal force at any double point, 'i', is the sum $\underset{\sim}{f}^{i,j} + \underset{\sim}{f}^{i,j+1}$ may be written :

$$\hat{\underset{\sim}{F}} = \underset{\sim}{R}_d^T \, \underset{\sim}{F} \tag{5.5.7}$$

For reasons of clarity, the form of the matrix $\underset{\sim}{R}_d$ (equations (5.5.6) and (5.5.7)) is depicted diagrammatically in Fig. 5.5.2.

The relationship between the equivalent nodal forces and the surface tractions may be written (see equation (3.6.5)):

$$\underset{\sim}{F} = \underset{\sim}{M} \, \underset{\sim}{P} \tag{5.5.8}$$

Using equation (5.5.4), substituting for $\underset{\sim}{P}$ from equation (5.5.5), and premultiplying by $\underset{\sim}{R}_d^T$, we have

$$(\underset{\sim}{R}_d^T \, \underset{\sim}{H} \, \underset{\sim}{R}_d - \underset{\sim}{R}_d^T \, \underset{\sim}{G} \, \underset{\sim}{R}_u) \, \hat{\underset{\sim}{U}} = (\underset{\sim}{R}_d^T \, \underset{\sim}{G} \, \underset{\sim}{R}_p) \, \hat{\underset{\sim}{P}} \tag{5.5.9}$$

or

$$\hat{\underset{\sim}{K}} \, \hat{\underset{\sim}{U}} = \hat{\underset{\sim}{P}} \tag{5.5.10}$$

where :

$$\hat{\underset{\sim}{K}} = (\underset{\sim}{G} \, \underset{\sim}{R}_p)^{-1} (\underset{\sim}{H} \, \underset{\sim}{R}_d - \underset{\sim}{G} \, \underset{\sim}{R}_u) \tag{5.5.11}$$

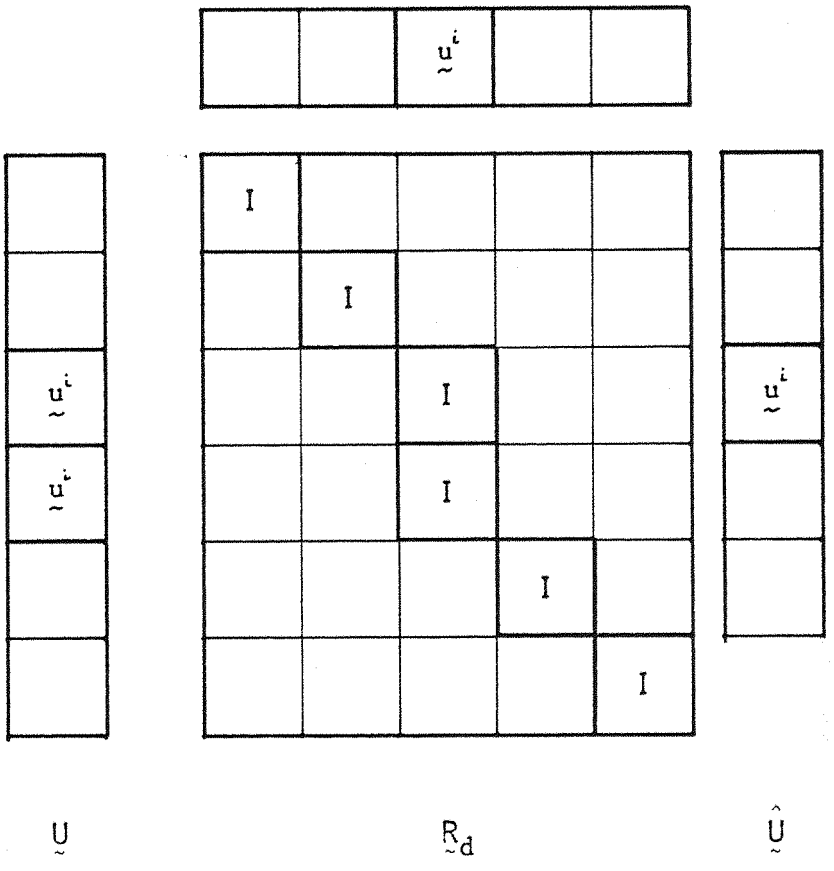

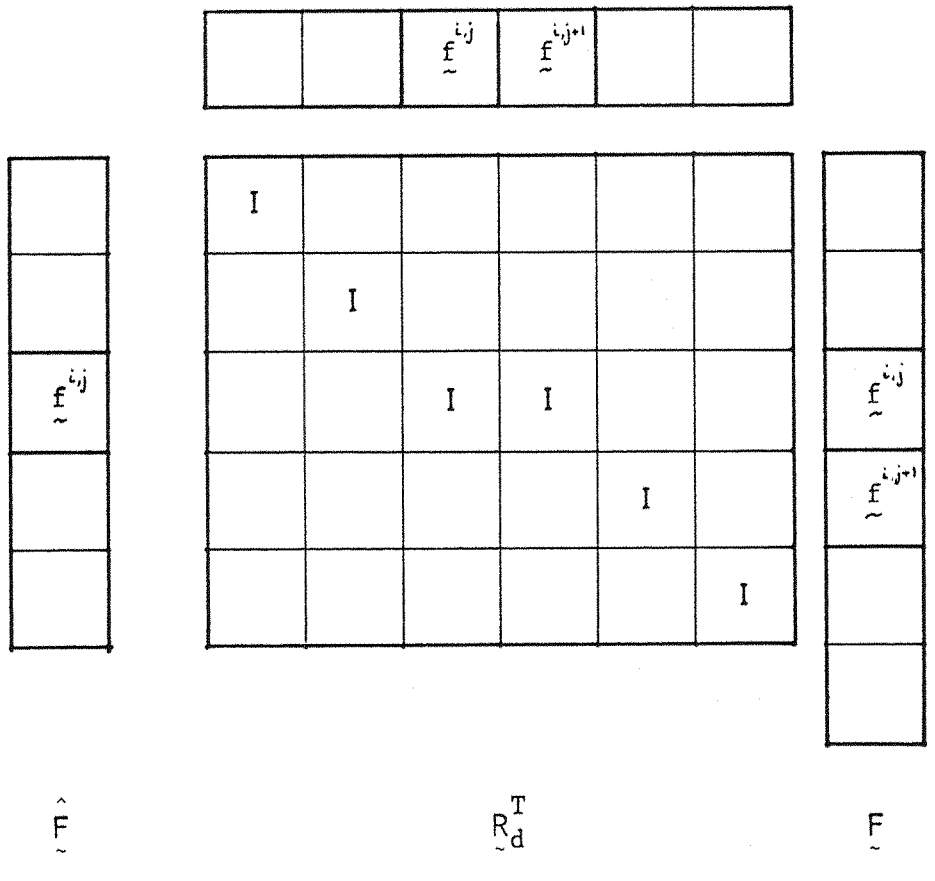

Figure 5.5.2 Diagrammatic representation of equations (5.5.6) and (5.5.7).

Using equation (5.5.8), substituting for $\underset{\sim}{P}$ from equation (5.5.5), and premultiplying by $\underset{\sim}{R}_d^T$, we have :

$$\underset{\sim}{R}_d^T \underset{\sim}{F} = (\underset{\sim}{R}_d^T \underset{\sim}{M} \underset{\sim}{R}_p) \hat{\underset{\sim}{P}} + (\underset{\sim}{R}_d^T \underset{\sim}{M} \underset{\sim}{R}_u) \hat{\underset{\sim}{U}} \tag{5.5.12}$$

which, from equation (5.5.7) gives

$$\hat{\underset{\sim}{F}} = \underset{\sim}{R}_1 \hat{\underset{\sim}{P}} + \underset{\sim}{R}_2 \hat{\underset{\sim}{U}} \tag{5.5.13}$$

where,

$$\underset{\sim}{R}_1 = (\underset{\sim}{R}_d^T \underset{\sim}{M} \underset{\sim}{R}_p)$$

and $$\underset{\sim}{R}_2 = (\underset{\sim}{R}_d^T \underset{\sim}{M} \underset{\sim}{R}_u) \tag{5.5.14}$$

writing equation (5.5.10) as

$$\underset{\sim}{R}_1 \hat{\underset{\sim}{K}} \hat{\underset{\sim}{U}} = \underset{\sim}{R}_1 \hat{\underset{\sim}{P}} \tag{5.5.15}$$

and substituting equation (5.5.15) into (5.5.13), we have,

$$\hat{\underset{\sim}{F}} = \underset{\sim}{R}_1 \hat{\underset{\sim}{K}} \hat{\underset{\sim}{U}} + \underset{\sim}{R}_2 \hat{\underset{\sim}{U}} \tag{5.5.16}$$

or

$$\underset{\sim}{K}^u \hat{\underset{\sim}{U}} = \hat{\underset{\sim}{F}} \tag{5.5.17}$$

where $$\underset{\sim}{K}^u = (\underset{\sim}{R}_1 \hat{\underset{\sim}{K}} + \underset{\sim}{R}_2) \tag{5.5.18}$$

This final relationship between the equivalent nodal loads and the nodal displacements, (equation (5.5.17)) is a stiffness relationship, and $\underset{\sim}{K}^u$ is the 'equivalent' stiffness matrix of the system. The superscript 'u' denotes the fact that this matrix is not inherently symmetric as in the classical Finite Element case. The degree of the unsymmetry is examined in the following section of this

Chapter (5.6) by forming the symmetric matrix $\underset{\sim}{K}^s$, whose elements are given by :

$$K^s_{ij} = \frac{1}{2}(K^u_{ij} + K^u_{ji}) \tag{5.5.19}$$

(which is simply the symmetric part of $\underset{\sim}{K}^u$) and comparing the relative performance of the two matrices for a series of examples:

The symmetry aspect of the formulation is discussed further in the following sections of this chapter, in the light of results given by the symmetric and unsymmetric 'equivalent' stiffness matrices, $\underset{\sim}{K}^s$ and $\underset{\sim}{K}^u$.

5.6 NUMERICAL EXAMPLES

5.6.1 Computer Programming

A computer program was written, using linear elements, implementing the Boundary Element Method, as described in section (3.4). The shape functions for the displacements and traction, $\underset{\sim}{\phi}$ and $\underset{\sim}{\psi}$ are taken to be the same, and for the linear case are given by :

$$\underset{\sim}{\phi} = [\phi_1 \quad \phi_2]$$

$$\phi_1 = \frac{1}{2}(1 - \xi) \tag{5.6.1}$$

$$\phi_2 = \frac{1}{2}(1 + \xi)$$

where ξ is a dimensionless local coordinate, along the element taking the values $\xi = -1$ at node 1 and $\xi = +1$ at node 2 (see Fig. 5.6.1).

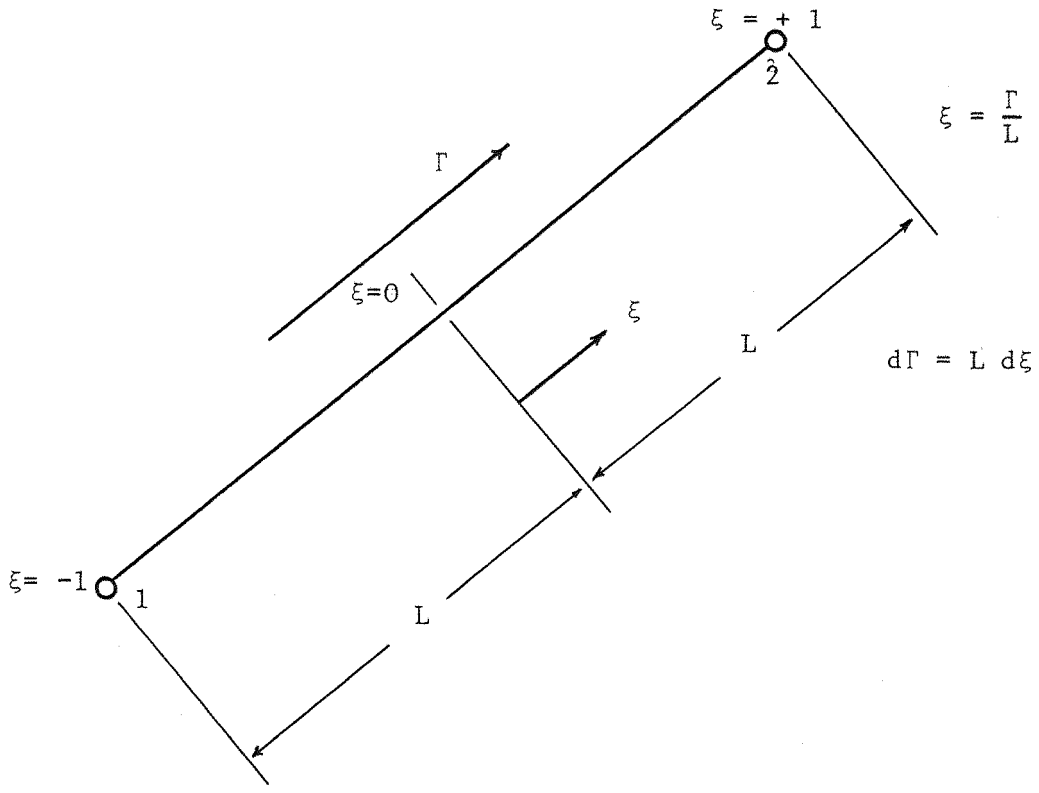

Figure 5.6.1 Linear element coordinates

The integrals of the fundamental solution, weighted by the shape functions, are carried out numerically in the general case, using a 4-point Gauss Quadrature integration scheme. The accuracy of a 4-point scheme was tested by experimenting with up to a 10-point scheme, and the differences in the numerical values of the integrals were found to be negligible.

The singular integrals which contribute to the diagonal sub-matrices of $\underset{\sim}{H}$ and $\underset{\sim}{G}$ are calculated as a special case. For the case of the $\underset{\sim}{H}$ matrix these terms are computed using rigid body motion considerations, as described in section (3.4) - see equation (3.4.15).

The diagonal terms of the $\underset{\sim}{G}$ matrix, which arise from the integration along an element which also contains the source node, are calculated analytically. This is relatively simple as the variable involved, r, lies along the element of integration,

The matrix $\underset{\sim}{M}$ linking the traction distribution along the boundary to the equivalent nodal forces is calculated using equation (3.6.4). The contribution from each element to the $\underset{\sim}{M}$ matrix is :

$$\underset{\sim}{M}_e = \int_{\Gamma_\ell} \underset{\sim}{\phi}\, \underset{\sim}{\phi}^T \, d\Gamma = L \int_{-1}^{+1} \begin{bmatrix} \phi_1^2 & \phi_1\phi_2 \\ \phi_2\phi_1 & \phi_2^2 \end{bmatrix} d\xi \qquad (5.6.2)$$

Taking into account the two coordinate directions and evaluating the integral in equation (5.6.2), we have,

$$\underset{\sim}{M}_e = \frac{L}{3}\begin{bmatrix} 2 & 0 & 1 & 0 \\ 0 & 2 & 0 & 1 \\ 1 & 0 & 2 & 0 \\ 0 & 1 & 0 & 2 \end{bmatrix} \qquad (5.6.3)$$

The contributions $\underset{\sim}{M}_e$ from each element may then be assembled into the global matrix $\underset{\sim}{M}$, in the usual way.

The rotation matrices which describe the 'Corner Condition' are simply set up, as described in the previous section, and the matrix operations, described by equations (5.5.9) - (5.5.19), are then performed to form the 'equivalent' stiffness matrices $\underset{\sim}{K}^u$ and $\underset{\sim}{K}^s$.

It is important to note that the whole process involves only one inversion (see equation (5.5.11)), which is required whether or not these 'Corner Conditions' are implemented. The remaining operations are either multiplication, addition or subtraction of matrices, and although there are a great deal of operations, most of these involve matrices which are predominantly null, containing terms in specified rows, or unity on the leading diagonals. As such, subroutines to perform these operations may be written taking into account these properties, substantially reducing the amount of computation involved.

The program developed for this work is very modular in structure using general routines to perform the matrix operations. The program was written this way largely for reasons of expediency, related to the period available for the development, implementation and testing of the formulation. As such, the efficiency of the existing program could be improved for this particular problem, but is perfectly adequate for performing a series of test examples. Further work in

this field could most certainly be directed towards the computational optimisation of the technique.

There are no particularly special or innovative techniques used in the actual programming, and as such, details of the program will not be included in this work. Such details would not provide any further insight into the formulations described, but would only serve as a translation into FORTRAN of the equations and matrices, fully described in previous sections of this chapter.

5.6.2 Testing the 'Corner Condition'

As a test on the validity of the 'Corner Condition' and of the techniques proposed for its implementation, the problem of a square plate with a circular hole, in tension was analysed. (Fig. 5.6.2a). Due to symmetry only one quarter of the plate need be considered, with the appropriate boundary conditions (Fig. 5.6.2b). The five points (A - E) in Fig. 5.6.2b are those at which there exists a traction discontinuity.

The analytical solution for the stresses in an infinite plate with a circular hole, is given by TIMOSHENKO [1]. This solution was integrated to derive expressions for the displacements in order to allow a full set of comparisons.

The problem was first analysed as a mixed value Boundary Element problem, using the discretisation shown in Fig. 5.6.2b. By defining a mixed set of boundary conditions, as shown in Fig. 5.6.2b , there is always only one unknown value in each coordinate direction at each of the corners. As such the situation at the corners is always one of the cases, (i) or (ii) described in section 5.4; hence the extra

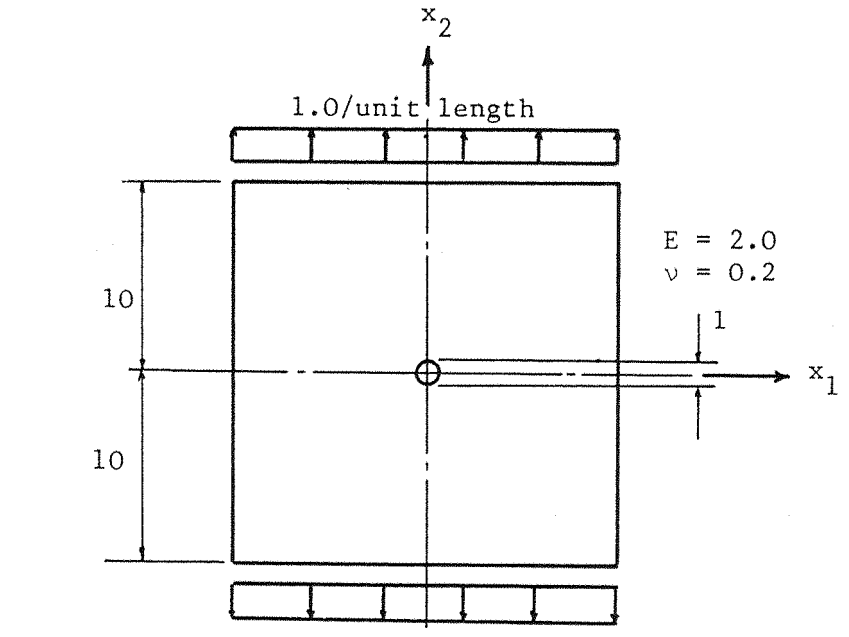

(a)

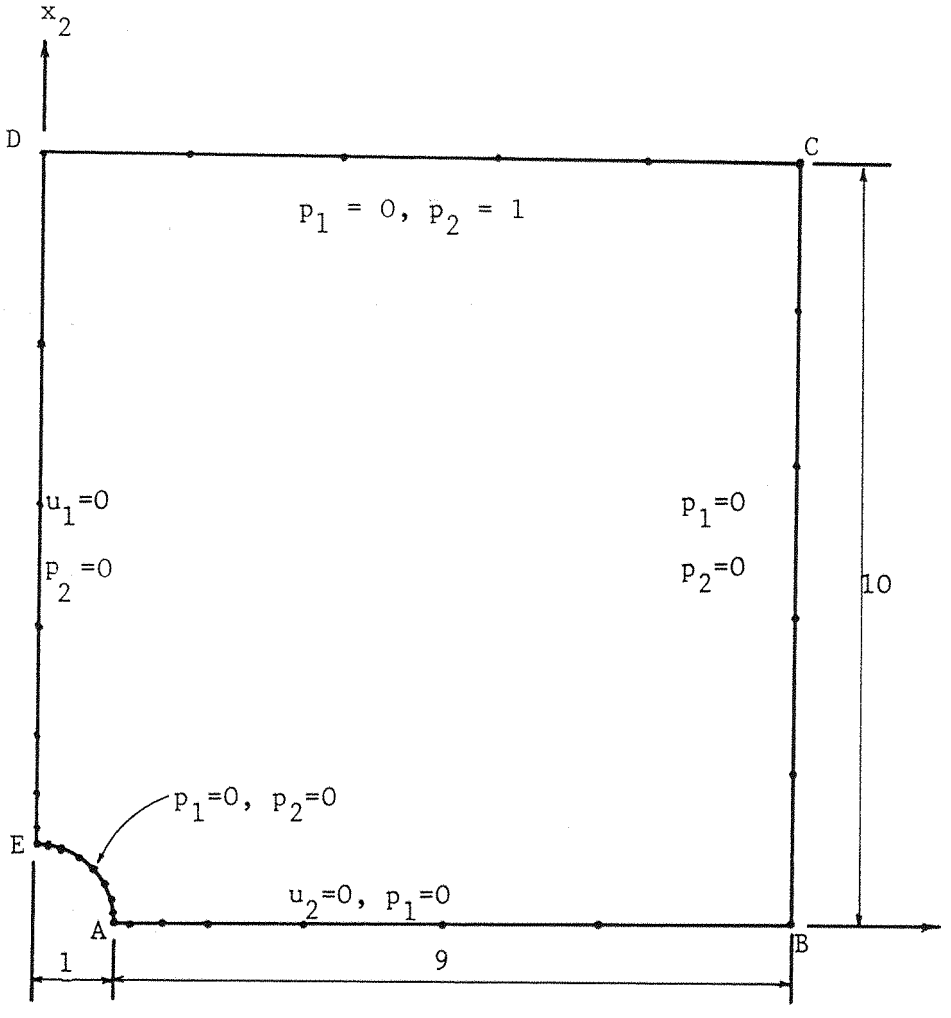

(b)

Figure 5.6.2 Plate with a circular hole. Problem definition and Boundary Element Mesh.

'Corner Condition' need not be implemented and the problem may be solved using a single node at the corners and assembling the equations as described in section 5.4.

The displacements and tractions along the lines of symmetry are compared to the analytical solution given by TIMOSHENKO [1] in Tables 5.6.1. The results are in good agreement and serve as a useful confirmation of the linear element program, and the integration scheme used. It should be remembered that the analytical solution is for a plate of infinite extent, and as such, a model of a finite plate with a free boundary results in a slight reduction of stiffness and hence yields slightly large displacements than the analytical solution.

The analytical solution was then used to calculate the displacements at all points, and these values used to define all the boundary conditions of the problem. At the discontinuous points (A - E, Fig. 5.6.2b), we now have a situation where there are two unknown sets of tractions, and the extra equations given by the 'Corner Condition' need to be implemented. This is done by modifying the contributions to the $\underset{\sim}{H}$ and $\underset{\sim}{G}$ matrices as described in section 5.4 - case (iii). The resulting stress distributions are shown in Table 5.6.2. This solution corresponds to a unit traction in the x_2 direction, along the top face, and the resulting tractions given by the program, along this face, vary between 0.994 and 1.001. The remaining tractions, which should all be zero, are mostly of the order 10^{-3} - 10^{-5}, the largest error occurring at the point of maximum stress concentration (point A, Fig. 5.6.2b), where the program gives a shear of 0.062, as opposed to zero.

RADIUS r	Displacements, u_2, along x_1 axis		Displacements, u_1, along x_2 axis	
	ANALYTICAL	B.E.M.	ANALYTICAL	B.E.M.
1.0	- 0.500	- 0.520	1.500	1.520
1.1	- 0.494	- 0.514	1.498	1.518
1.2	- 0.480	- 0.501	1.497	1.516
1.3	- 0.463	- 0.483	1.498	1.518
1.5	- 0.426	- 0.441	1.509	1.521
2.5	- 0.284	- 0.302	1.734	1.752
4.0	- 0.184	- 0.204	2.309	2.329

(a) Displacements along axes of symmetry.

RADIUS r	Stresses, σ_{22}, along x_1 axis		Stresses, σ_{11}, along x_2 axis	
	ANALYTICAL	B.E.M.	ANALYTICAL	B.E.M.
1.0	- 3.000	- 3.040	1.000	1.045
1.1	- 2.438	- 2.515	0.611	0.644
1.2	- 2.071	- 2.100	0.376	0.391
1.3	- 1.821	- 1.838	0.229	0.238
1.5	- 1.519	- 1.499	0.074	0.096
2.5	- 1.118	- 1.103	- 0.042	- 0.053
4.0	- 1.037	- 1.046	- 0.025	- 0.021

(b) Stresses along axes of symmetry.

Table 5.6.1 B.E.M. Solution for plate with circular hole with mixed boundary conditions.

Radius r	σ_{22} along x_1 axis		σ_{11} along x_2 axis	
	ANALYTICAL	B.E.M.*	ANALYTICAL	B.E.M.*
1.00	- 3.000	- 3.026	1.000	0.952
1.02	- 2.866	- 2.853	0.905	0.882
1.06	- 2.633	- 2.620	0.743	0.728
1.14	- 2.273	- 2.250	0.503	0.490
1.3	- 1.821	- 1.795	0.229	0.215
1.6	- 1.424	- 1.400	0.034	0.026
2.2	- 1.167	- 1.151	- 0.039	- 0.041
3.4	- 1.054	- 1.046	- 0.032	- 0.033
5.4	- 1.019	- 1.016	- 0.015	- 0.017
7.5	- 1.009	- 1.009	- 0.008	- 0.008
10.0	- 1.005	- 1.005	- 0.005	- 0.004

(* denotes the additional implementation of the 'Corner Condition' at geometric discontinuities).

Table 5.6.2 B.E.M. Solution for plate with circular hole, with displacement boundary conditions only.

5.6.3 Examples Using the 'Equivalent' Stiffness Approach

A series of examples were run using the formulation described in Section 5.5.2 to calculate the 'equivalent' stiffness matrix of the system. The problems were set up as Finite Element displacement type models and any boundary conditions imposed in the usual way. Resulting displacement profile given by both the unsymmetric and symmetrized 'equivalent' stiffness matrices, $\underset{\sim}{K}^{u}$ and $\underset{\sim}{K}^{s}$ (equation (5.5.18) and (5.5.19)) are compared to classical Finite Element and Boundary Element solutions, and to analytical solutions, when available.

EXAMPLE 1 : RECTANGULAR PLATE IN TENSION

The geometry of the problem is depicted in Fig. 5.6.3 below. The problem is solved for the case of plane strain with $E = 2.4$ $\nu = 0.2$, $G = 1.0$. The bottom of the plate is simply supported and the top is loaded with a uniformly distributed load of 1/unit length. The displacements in the x_2 direction at sample points A, B, C, D, E are compared using various discretisations, the results being shown in Table 5.6.3.

EXAMPLE 2 : DEEP CANTILEVER WITH END LOAD

A solution for problem (Fig. 5.6.4a) is presented by Timoshenko [1], giving a tip deflection of 15.2.

This, however, is not totally exact as the stress function used to calculate the solution does not exactly satisfy both the applied loading and boundary conditions. The loading requires a small correction to allow for the fact that the fixed end is not free to warp.

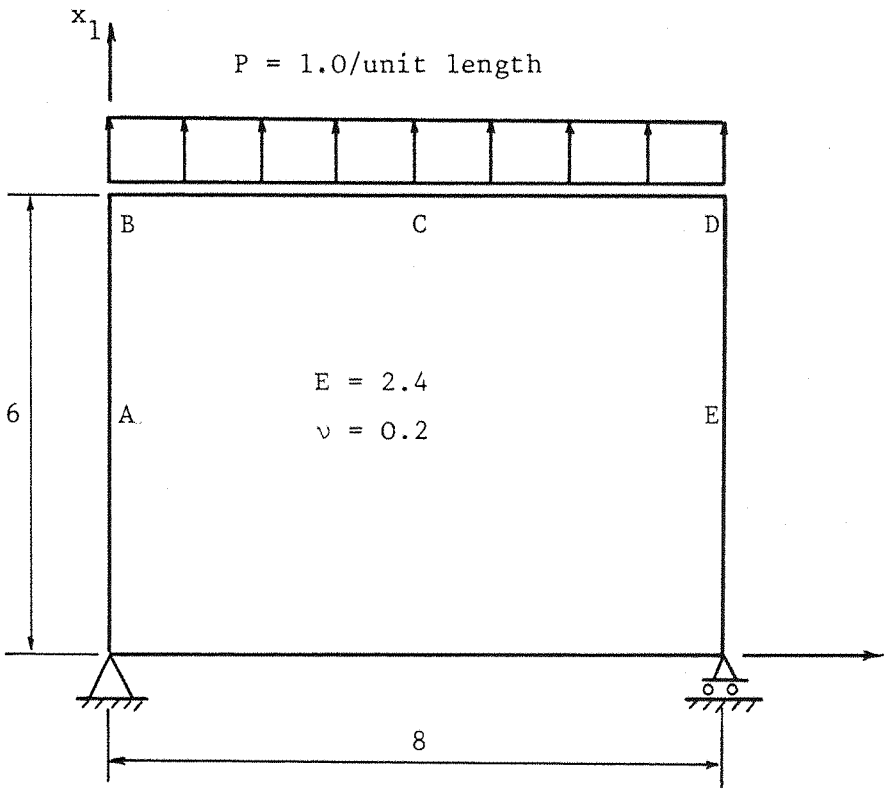

(a) Problem Definition

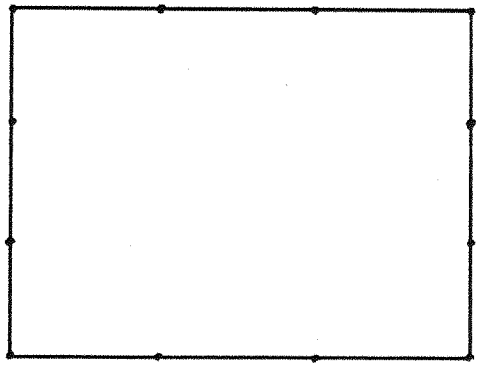

(b) 12 Element Mesh

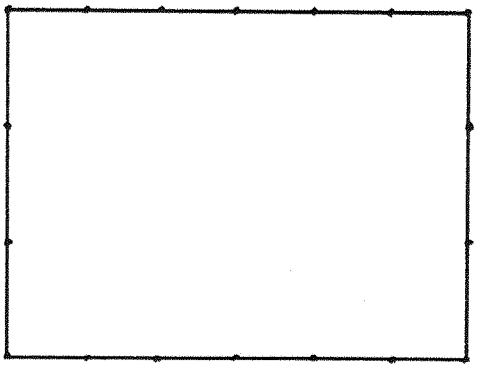

(c) 18 Element Mesh

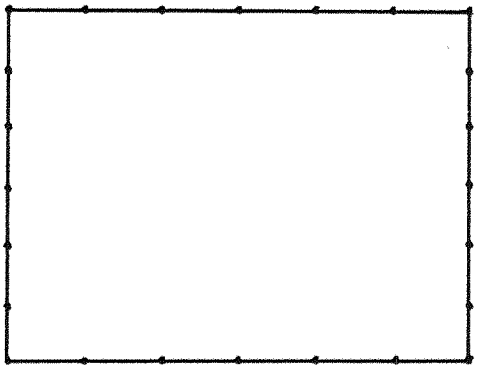

(d) 24 Element Mesh

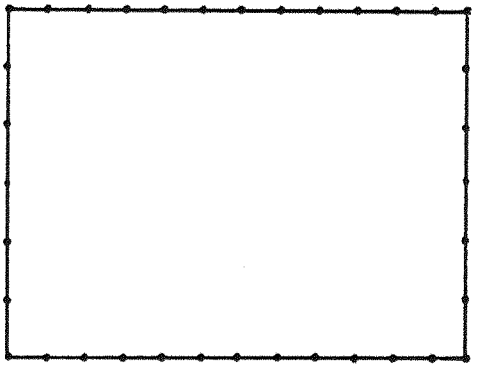

(e) 36 Element Mesh

Figure 5.6.3 Rectangular Plate in Tension.

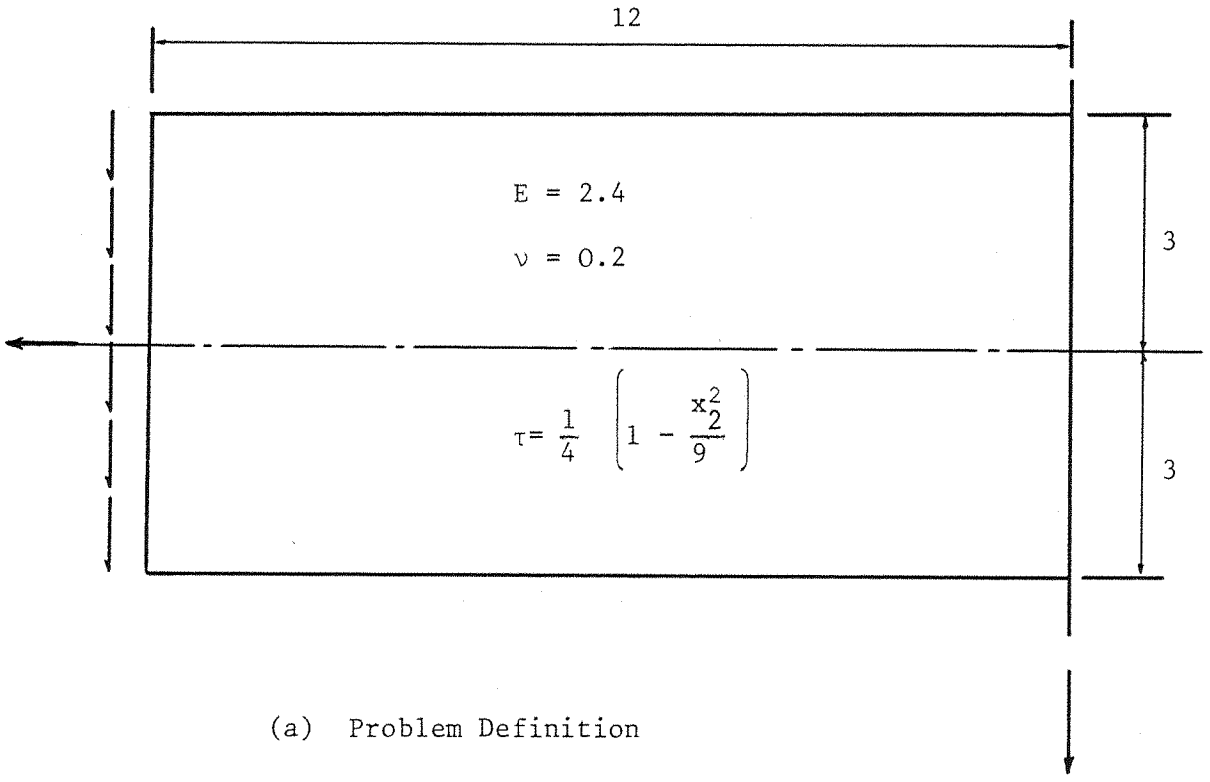

(a) Problem Definition

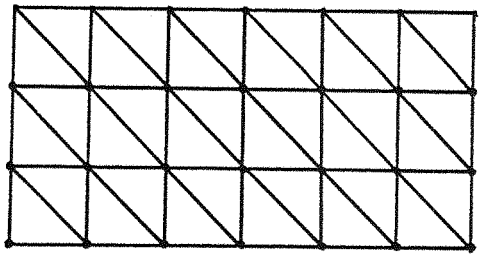

(b) Finite Element Mesh

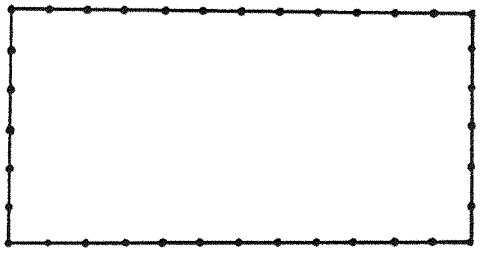

(c) Boundary Element Mesh

Figure 5.6.4 Deep Canitlever with End Load

Four solutions are compared in Table 5.6.4 below :

(i) A F.E.M. solution using 91 nodes and 36 linear strain triangles. (Mesh shown in Fig. 5.6.4b).

(ii) A B.E.M. solution using 36 linear elements (mesh shown in Fig. 5.6.4c).

(iii) A B.E.M. equivalent stiffness approach with $\underset{\sim}{K}^{u}$ and $\underset{\sim}{K}^{s}$ using the same discretisation as (ii).

EXAMPLE 3 : DEEP CANTILEVER WITH U.D.L.

The B.E.M. was employed to solve the problem (Fig. 5.6.5) using three different discretisations; 30, 48 and 96 elements. The same meshes were then used for the equivalent stiffness approach examining the solution for both $\underset{\sim}{K}^{u}$ and $\underset{\sim}{K}^{s}$. The solution was also compared to a F.E.M. run which used 54 linear strain triangles with 133 nodes. The discretisations used are shown in Figs. 5.6.5b - 5.6.5c.

A comparison of the results obtained for the horizontal displacement u_1 along the centre-line of the cantilever is given in Table 5.6.5. The analytical result for the tip deflection given by Timoshenko [1], is 396.1.

EXAMPLE 4 : THICK CYLINDER UNDER INTERNAL PRESSURE

Because of symmetry only one quarter of the problem need be considered. The geometry and boundary conditions are shown in Fig. 5.6.6: the radial displacements obtained using a B.E.M. method and an equivalent stiffness approach are compared to the exact solution in Table 5.6.6.

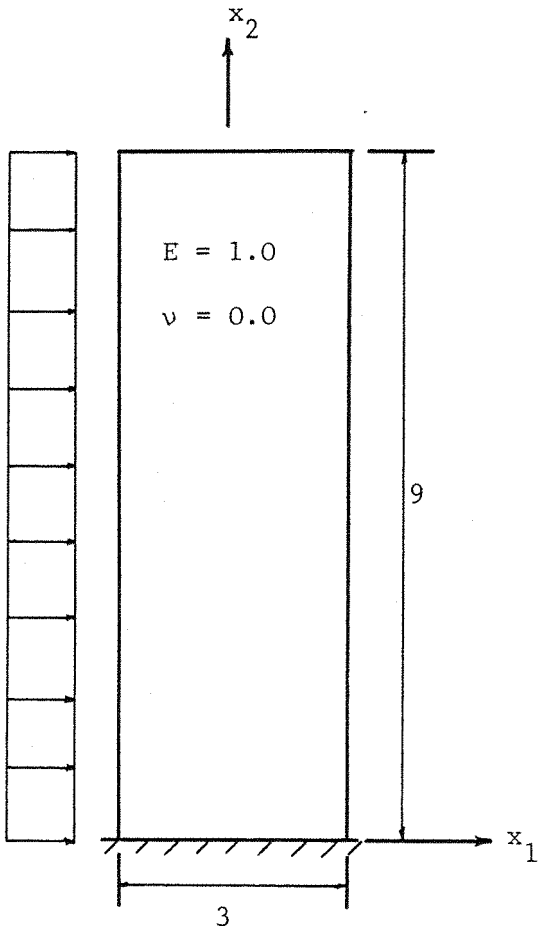

(a) Problem Definition

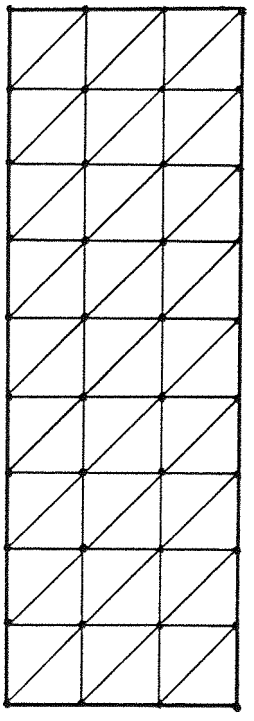

(b) Finite Element Mesh

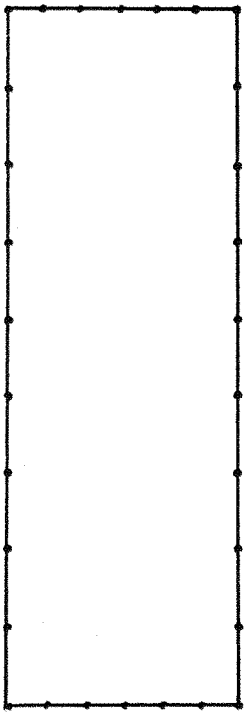

(c) 30 Boundary Elements

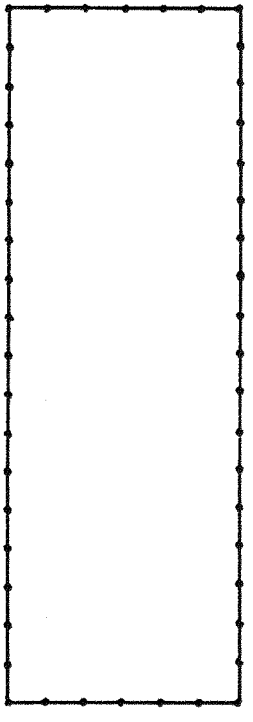

(d) 48 Boundary Elements

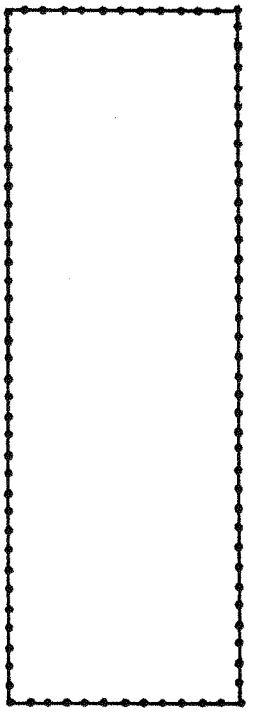

(e) 96 Boundary Elements

Figure 5.6.5. F.E.M. and B.E.M. Discretisations for deep cantilever with U.D.L.

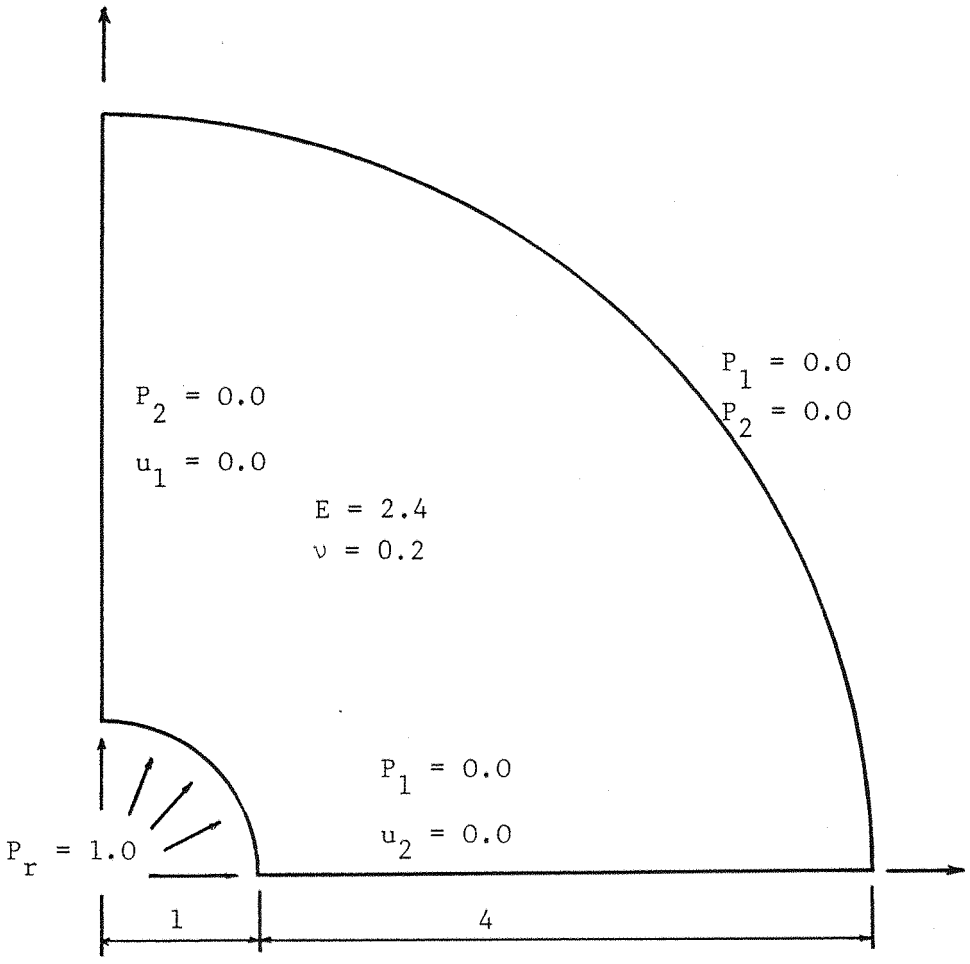

(a) Problem Definition

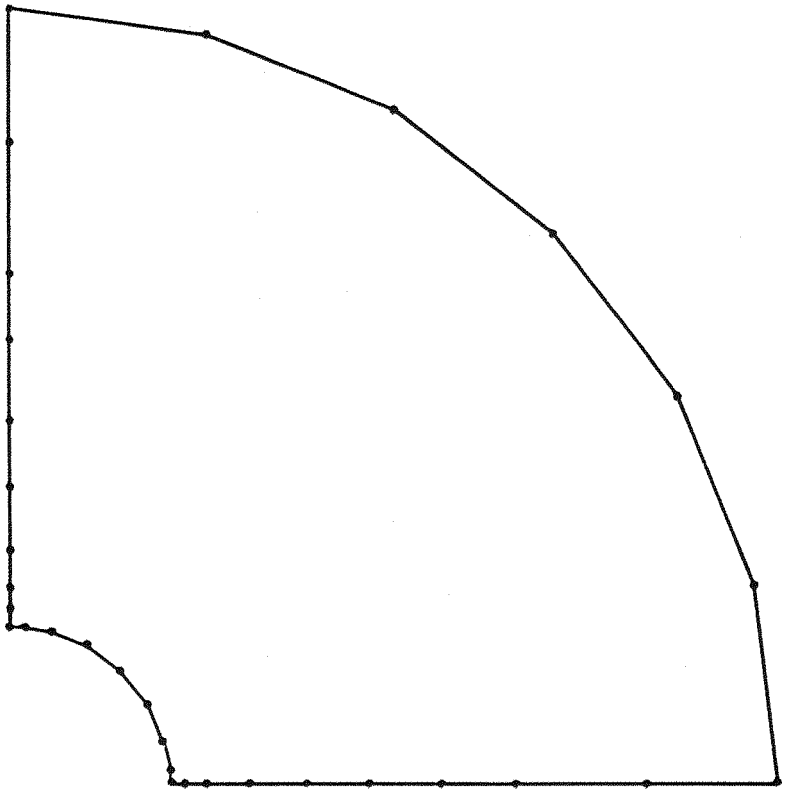

(b) Boundary Element Discretisation

Figure 5.6.6 Thick Cylinder under Internal Pressure.

POINT	EXACT SOLUTION	12 ELEMENTS		18 ELEMENTS	
		K^u	K^s	K^u	K^s
A	1.2	1.200	1.215	1.200	1.211
B	2.4	2.400	2.474	2.400	2.463
C	2.4	2.400	2.412	2.400	2.376
D	2.4	2.400	2.478	2.400	2.461
E	1.2	1.200	1.216	1.200	1.210

POINT	EXACT SOLUTION	24 ELEMENTS		36 ELEMENTS	
		K^u	K^s	K^u	K^s
A	1.2	1.200	1.203	1.200	1.201
B	2.4	2.400	2.446	2.400	2.432
C	2.4	2.400	2.399	2.400	2.400
D	2.4	2.400	2.446	2.400	2.433
E	1.2	1.200	1.203	1.200	1.201

Table 5.6.3 Displacements for a rectangular plate in tension.

	F.E.M. 36 Elements	B.E.M. 36 Elements	B.E.M. 'Equivalent' Stiffness Method 36 Elements	
			$\underset{\sim}{K}^{u}$	$\underset{\sim}{K}^{s}$
x_1	u_2	u_2	u_2	u_2
1.0	0.245	0.357	0.376	0.439
2.0	0.779	0.943	0.931	0.928
3.0	1.560	1.759	1.750	1.759
4.0	2.544	2.701	2.687	2.695
5.0	3.709	3.816	3.800	3.815
6.0	5.026	5.082	5.064	5.080
7.0	6.479	6.479	6.459	6.476
8.0	8.040	7.984	7.961	7.978
9.0	9.692	9.576	9.546	9.581
10.0	11.410	11.400	11.340	11.420
11.0	13.670	13.470	13.150	13.390
12.0	14.960	14.660	14.610	14.670

Table 5.6.4 Displacements along the centre line of a deep cantilever with an end load.

X_2	B.E.M. 30 Elements	B.E.M. 48 Elements	B.E.M. 96 Elements	F.E.M. 54, 6 noded Tr.
1.0	12.12	14.34	14.86	14.61
2.0	36.33	41.85	43.25	42.94
3.0	68.65	78.90	81.55	81.50
4.0	106.80	122.85	127.00	127.30
5.0	148.60	171.30	177.20	177.80
6.0	192.50	222.30	230.00	231.20
7.0	237.30	274.40	284.10	285.80
8.0	282.00	326.60	338.30	340.60
9.0	339.30	378.50	392.10	394.80

X_2	30 Elements		48 Elements		96 Elements	
	K^u	K^s	K^u	K^s	K^u	K^s
1.0	12.83	13.38	14.71	15.21	15.01	16.11
2.0	38.33	42.50	42.43	43.62	44.36	46.23
3.0	71.75	77.30	79.52	81.05	83.17	85.41
4.0	111.30	118.70	125.90	126.80	129.70	132.10
5.0	154.60	164.20	175.40	178.10	181.20	184.60
6.0	200.10	212.10	226.30	229.40	233.20	238.10
7.0	246.50	260.90	279.40	284.30	287.40	292.70
8.0	292.90	309.70	330.40	334.60	341.20	345.70
9.0	338.80	359.50	382.60	386.50	395.10	402.60

Table 5.6.5. Displacements for a cantilever with U.D.L.

r	Exact	B.E.M. 32 Elements	B.E.M. Equivalent Stiffness Approach K^u	K^s
1.0	0.5333	0.5295	0.5328	0.5364
1.1	0.4872	0.4824	0.4846	0.4938
1.2	0.4390	0.4445	0.4467	0.4436
1.35	0.4027	0.3987	0.4005	0.4009
1.8	0.3119	0.3089	0.3100	0.3055
2.3	0.2552	0.2528	0.2535	0.2554
3.4	0.1957	0.1940	0.1940	0.1921
4.2	0.1765	0.1746	0.1751	0.1783
5.0	0.1667	0.1645	0.1644	0.1635

Table 5.6.6. Radial displacements for thick cylinder under internal pressure.

5.7 THE SYMMETRY OF THE 'EQUIVALENT'STIFFNESS FORMULATION

5.7.1 General Observations

The 'equivalent' stiffness matrix, $\underset{\sim}{K}^{u}$, (equation(5.5.18)) is not quite symmetric, although the unsymmetric part only has a minor effect on the behaviour of the model, as is shown by the results of the examples of section 5.6.3. The results obtained using $\underset{\sim}{K}^{u}$ are always very close to the B.E.M. solution, for the same degree of discretisation. These results also compare favourably with Finite Element and analytical solutions; for the examples involving bending (examples 2 and 3) a relatively refined Boundary Element mesh is needed to approach the accuracy of the Finite Element solution. This is easily attributed to the fact that the Finite Elements used are linear strain triangles, allowing for quadratic variation of the displacement profile, (as opposed to the linear Boundary Elements) and these elements are known to perform much better in bending than elements allowing only linear displacement variations. A much more accurate solution, for a given discretisation, would be expected if quadratic Boundary Elements were used for these cases.

The important result to emerge is that the 'equivalent' stiffness matrix, $\underset{\sim}{K}^{u}$, provides a Finite Element type displacement model which is as accurate as the standard B.E.M. Furthermore, by discarding the unsymmetric part of the matrix, to form, $\underset{\sim}{K}^{s}$, the results do not significantly suffer, but there is clearly some error introduced; it is this symmetry aspect which will be discussed below.

5.7.2 Factors Pertaining to the Unsymmetry

The reason why the 'equivalent' stiffness matrix is not inherently symmetric is simply that the standard Direct Boundary Element method integration scheme is not a symmetric process, for similar reasons as those described for the constant elements in the previous chapters. This is demonstrated in Figs. 5.7.1 by considering two typical nodes, 'i' and 'j' ; for the system submatrices 'ij' , we apply a source at 'i' and integrate the fundamental solution, weighted by the shape functions, along the elements adjacent to 'j' , (Fig. 5.7.1a). Similarly for the submatrices 'ji' (Figs. 5.7.1b) Unless the elements are symmetrically oriented towards each other (e.g. Fig. 5.7.1c), then the submatrices 'ij' and 'ji' are clearly different, and we have an unsymmetric set of starting equations for the formulation. The degree of unsymmetry is clearly exaggerated if the elements differ greatly in length as one of a set of reciprocal terms will contain an integration along a much longer element. This property however, is greatly reduced when the $\underset{\sim}{M}$ matrix (equation 5.6.2) is introduced as it has the effect of scaling the terms in relation to the lengths of the corresponding elements. The resulting 'equivalent' stiffness matrix for the system will always exhibit some degree of unsymmetry, and in order to retain the overall symmetry savings from a Finite Element model, this matrix is "symmetrized". This "symmetrization" process, (in order to form $\underset{\sim}{K}^{S}$) is given by equation (5.5.19) - i.e. the unsymmetric part of the matrix is simply discarded.

The other important factor which affects the degree of symmetry is the way in which the corner discontinuity problem is included in the formulation. If this effect is simply ignored at the expense of accuracy at the points concerned, then the lack of symmetry is totally

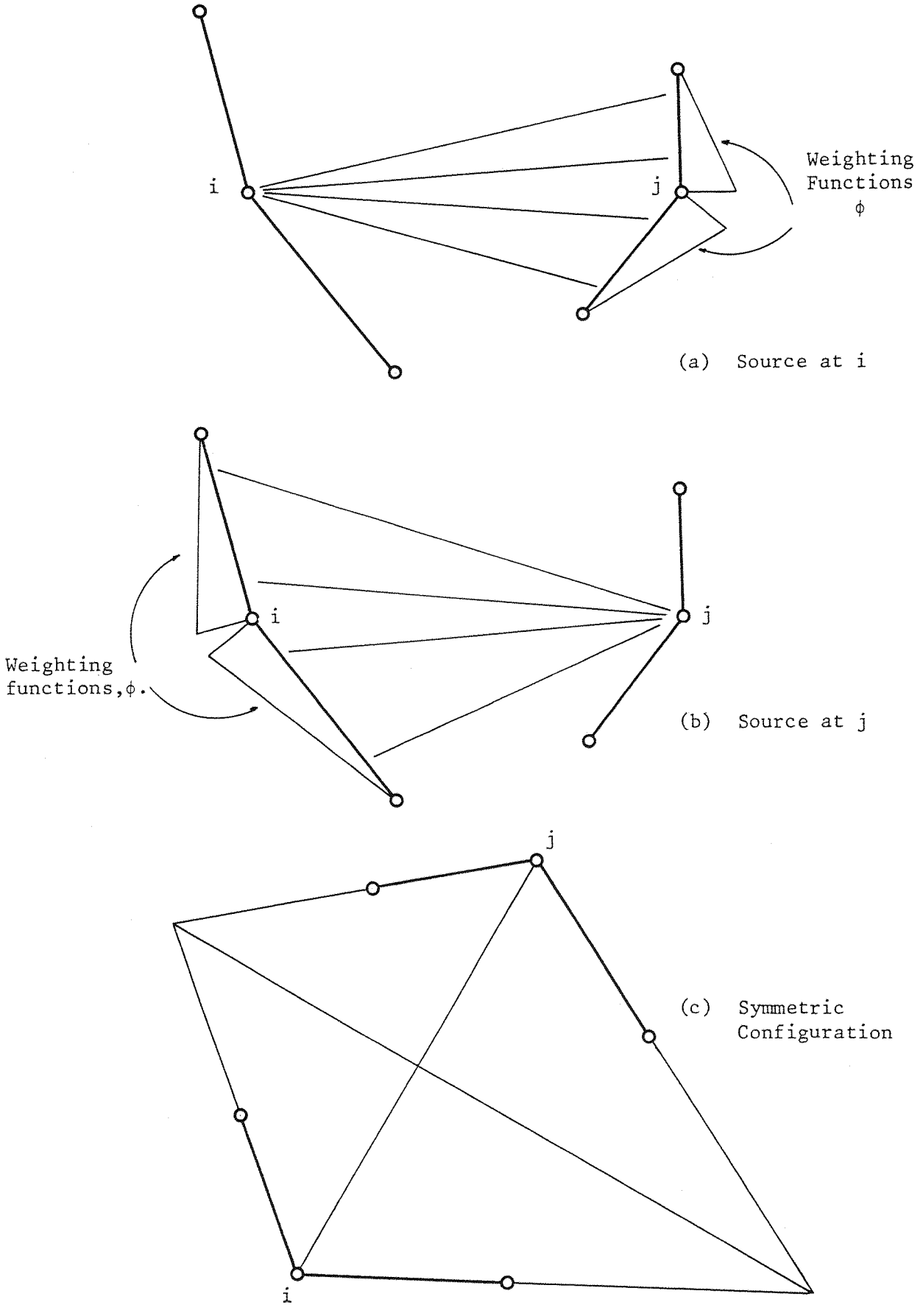

Figure 5.7.1 Reciprocal integration for two typical source points, 'i' and 'j'.

attributable to the integration processes, discussed above. The direct inclusion of any 'extra' equations will cause a large degree of unsymmetry and provide a totally erroneous solution if the 'symmetrisation' process is introduced; the formulation presented in section 5.5.2 introduces the 'extra' equations into the overall system in such a way as to provide a final system, which when symmetrised, yields a solution with an acceptable level of error.

5.7.3 Comments on the Symmetrisation Process

Brebbia and Georgiou [24] consider the symmetrisation process as a minimisation of the square of the errors in the non-symmetric off diagonal terms of $\underset{\sim}{K}^u$.

The error coefficient 'ij' can be written as the average difference between k^u_{ij} and k^u_{ji} and the still unknown coefficient k^s_{ij} , which is symmetric, i.e.

$$\varepsilon_{ij} = \frac{1}{2}\left\{ (k^s_{ij} - k^u_{ij}) - (k^s_{ij} - k^u_{ji}) \right\} \qquad (5.7.1)$$

The square of this error is now minimised with respect to the symmetric coefficient k^s_{ij} :

$$\frac{\partial}{\partial k_{ij}} (\varepsilon_{ij}) = 2k^s_{ij} - k^u_{ij} - k^u_{ji} = 0 \qquad (5.7.2)$$

Hence the new symmetric coefficient is given by :

$$k^s_{ij} = \frac{1}{2} (k^u_{ij} + k^u_{ji}) \qquad (5.7.3)$$

The above argument, however, assumes that there exists an error in $\underset{\sim}{K}^{u}$, by virtue of the fact that it is non-symmetric. This is not correct. A stiffness relation is not necessarily symmetric, as will be discussed later, and by using equation (5.7.3) to form our stiffness matrix, we are in fact introducing an error rather than minimising the effects of an existing one. However, we may think of the above technique as a 'minimisation of the error introduced by symmetrisation' as opposed to a'minimisation of an already existing error'.

Zienkiewicz et al. (e.g. [29], [30], [22]) presents an alternative approach to forming the 'equivalent' stiffness matrix, based on an energy formulation. The relationship between displacements and tractions is formed using the B.E.M., and then this equation is used in forming the energy functional (of the form of equation (2.3.22)) used as the starting expression of the Finite Element Method. The minimisation of this functional enables the derivation of the stiffness matrix for the system; the expression for this being of the form of equation (5.7.3).

The derivation of the BEM expressions requires the inclusion of an extra surface term in the energy functional (see equation (2.3.25)), as we do not assume that the displacement boundary conditions are identically satisfied. However this fact is neglected when performing the Finite Element part of the formulation.

The situation may be further clarified by considering the expressions of the Principle of Virtual Work. The extended general expression is given by equation (2.3.26) and includes surface terms from both parts of the boundary, and is the expression used to derive the Somigliana identity for the BEM (see Section 3.3); this is done

by considering the weighting functions, (alternatively interpreted as any virtual field), as the fundamental solutions for displacements and tractions. For the Finite Element formulation we do not impose this restriction on the virtual field, but assume it is of the same form as the real solution and can thus be made to identically satisfy the displacement boundary conditions. This enables the specialised form of the Principle of Virtual Work (equation (2.3.21)) to be used as the starting expression.

The effect of mixing the two formulations without examining the effect of this different interpretation of the weighting fields is suspect and requires much further investigation in a rigorous mathematical sense.

The lack of symmetry, in the general case, may also be examined by considering the nature of the arithmetic operations used to derive an expression for the stiffness matrix of an element, $\underset{\sim}{K}_e$. Consider a typical F.E. type stiffness matrix, which is usually written in the form

$$\underset{\sim}{K}_e = \int_\Omega \underset{\sim}{B}^T \underset{\sim}{D} \underset{\sim}{B} \, d\Omega \tag{5.7.4}$$

where $\underset{\sim}{D}$ is a matrix containing the coefficients of the stress-strain relations (symmetric) and $\underset{\sim}{B}$ describes the strain-displacement relations, using the derivatives of the shape functions used to model both the real and virtual displacements. $\underset{\sim}{K}_e$ is clearly symmetric, by virtue of the very nature of the arithmetic operations used to derive it, and the F.E. type relationship then exists :

$$\underset{\sim}{K}_e \underset{\sim}{U} = \underset{\sim}{F}_e \tag{5.7.5}$$

However, at this point, it is important to note that in the original integral statement of equilibrium,there are two functions :- the solution and its weighting (this weighting is equivalent to an arbitrary virtual field used in the Principle of Virtual Displacements). The Galerkin formulation, used in the classical F.E. technique requires that both these functions be described by polynomials of the same order and, hence, the same shape function is used for both.

It is this fact which eventually allows $\underset{\sim}{K}_e$ to be written as in equation (5.7.4). In principle, there is no reason why different approximations cannot be made for each of the functions, and although the ensuing matrix relationship would be perfectly valid, it would not necessarily be symmetric. This is the case in the B.E.M. formulation, where the weighting field is of a fixed form given by the fundamental solution.

In fact, by considering the problem of a set of linear algebraic equations, from a purely arithmetic point of view, it is possible to show that the coefficients of the influence matrix may undergo an infinite number of transformations and still retain uniqueness of solution for a given right hand side vector. Consider equation (5.7.5), where $\underset{\sim}{K}_e$ is symmetric, and consider a matrix $\underset{\sim}{A}$, the same order as $\underset{\sim}{K}_e$, which may be written in terms of its spectral decomposition as :

$$\underset{\sim}{A} = \underset{\sim}{V}\ \underset{\sim}{\Lambda}\ \underset{\sim}{V}^{-1} \qquad (5.7.6)$$

$\underset{\sim}{V}$ is a matrix whose columns are all eigenvectors of $\underset{\sim}{A}$ and $\underset{\sim}{\Lambda}$ is a diagonal matrix with the corresponding eigenvalues on the diagonal.

If we now choose any column of $\underset{\sim}{V}$ to equal $\underset{\sim}{F}_e$ (the right-hand-side vector of equation (5.7.5)) and the corresponding diagonal coefficient of $\underset{\sim}{\Lambda}$ to be unity, then $\underset{\sim}{F}_e$ is an eigenvector of $\underset{\sim}{A}$ with the corresponding eigenvalue equal to one. We may then write,

$$\underset{\sim}{A}\ \underset{\sim}{F}_e = \underset{\sim}{F}_e \tag{5.7.7}$$

and still allow an arbitrary choice of the remaining terms of $\underset{\sim}{V}$ and $\underset{\sim}{\Lambda}$, the only restriction being that $\underset{\sim}{V}$ is non-singular. Hence, an infinity of matrices $\underset{\sim}{A}$ exist which satisfy equation (5.7.7).

Now, premultiply equation (5.7.5) by the matrix $\underset{\sim}{A}$,

$$\underset{\sim}{A}\ \underset{\sim}{K}_e\ \underset{\sim}{U} = \underset{\sim}{A}\ \underset{\sim}{F}_e = \underset{\sim}{F}_e$$

or

$$\hat{\underset{\sim}{K}}_e\ \underset{\sim}{U} = \underset{\sim}{F}_e \tag{5.7.8}$$

where

$$\hat{\underset{\sim}{K}}_e = \underset{\sim}{A}\ \underset{\sim}{K}_e$$

If $\underset{\sim}{K}_e$ is symmetric, and as there are an infinity of possible matrices $\underset{\sim}{A}$, it is clearly possible to rewrite equations (5.7.5) in the form of (5.7.8) destroying the symmetry of the influence coefficients.

The natural question which follows from the above discussion is : 'given that a symmetric set of linear equations can be transformed to a non-symmetric form, is it possible to reverse the process?'. The answer must clearly be 'yes'; however, the problem is not a simple one. Consider a matrix $\underset{\sim}{B}$, with the same property as $\underset{\sim}{A}$ ($\underset{\sim}{B}\ \underset{\sim}{F}_e = \underset{\sim}{F}_e$), with the additional requirement that the product $\underset{\sim}{B}\ \hat{\underset{\sim}{K}}_e$ is symmetric; this does not uniquely define $\underset{\sim}{B}$, and in order to do so we may also impose symmetry on $\underset{\sim}{B}$. The restrictions on the nature of this matrix

are now enough to uniquely define each element of the matrix, but terms are interrelated, thus requiring the solution of a further set of linear equations. In fact, for an original system of order $\underset{\sim}{N}$, the solution of a system of order $\frac{N(N+1)}{2}$ is required to define the matrix $\underset{\sim}{B}$ above. This matrix may then be used to premultiply the unsymmetric equations (5.7.8), thus restoring symmetry. This process is clearly unsuitable for practical applications, but the whole problem of transforming sets of linear equations is certainly an interesting one, and warrants further investigation.

AN ALTERNATIVE APPROACH

An interesting technique for overcoming the symmetry problems arising from the form of the integration process is mentioned briefly by Zienkiewicz [29], and presented with further detail by Mustoe [49], for 2-Dimensional elastostatics. Silvester [32] presents an anologous formulation for the solution of magnetic field problems.

The technique is based on the further weighting of the Somigliana Identity by a general set of functions, W_i, say. The formulation presented in this work is the standard direct B.E.M. approach (e.g. Watson [33], Cruse [8], Rizzo [34]), where for each point 'i' we apply a unit load at that point and integrate around the boundary. This may be thought of as a Collocation Method using the more generalised form of the Somigliana Identity, and corresponds to taking W_i as a dirac function equal to 'one' at 'i' and 'zero' elsewhere.)

If we now choose W_i to be the same as the interpolation functions, used to describe the tractions and displacements, the integration process becomes symmetric, and symmetric system matrices ensue. This

is equivalent to applying a distributed load over the adjacent elements to each point 'i' (the form of which corresponds to the interpolation functions), as opposed to a point load; but this process very significantly increases the amount of numerical integration involved.

However, this technique seems to provide an elegant way of dealing with the surface traction discontinuity problem (see Mustoe [22]). For a node at which the traction is continuous, a continuous distributed source is applied to form the equation for that point. If a discontinuity exists, then the necessary extra set of equations is provided by applying 2 sets of discontinuous distributed sources :- one set on each element either side of the node concerned.

GENERAL CONSIDERATIONS RELATING TO SYMMETRY

Looking at the problems relating to the symmetry of a stiffness matrix from a more general viewpoint, there are certain apparent discrepancies which immediately spring to mind pertaining to the general reciprocal theorems of elastic behaviour, i.e. Betti's theorem, or Maxwell's reciprocal theorem.

These reciprocal theorems are often used as an argument for stating that any stiffness type relation must be symmetric, and hence any unsymmetry is due to some 'error' in the formulation. This is not necessarily true, as has been demonstrated by the examples of this chapter.

The reciprocal theorems of elasticity show that for a given body there does exist 'a' relation between displacements and applied forces such that the influence coefficients form a symmetric matrix. However, this does not mean that for a given system, 'no other' set of

influence coefficients can be written which yield a perfectly valid solution. This situation would arise, for example, in a Finite Difference Scheme where the collocation points for defining the derivatives were not placed symmetrically, or, in a Finite Element scheme where shape functions for the real and virtual fields were not chosen the same. The reasons why this situation arises with the Boundary Element based formulation have been fully discussed above.

The physical significance of the lack of perfect symmetry exhibited by the technique expounded in this work is easily explained : The Boundary Element Forumulation is based on the application of distributed surface tractions as opposed to point loads, and when forming the 'equivalent' stiffness matrix the equivalence between the tractions and nodal loads is represented by the matrix $\underset{\sim}{M}$ (equation (5.5.8)). This means that the final right hand side vector contains a set of nodal forces which have been weighted in such a way as to correspond to a required traction distribution, the form of which is given by equation (4.2.4) and depends on the local geometry of the element.

With a Boundary Element based formulation, the application of a point load cannot be represented exactly, i.e. placing a 'one' in the final right hand side vector (representing equivalent nodal forces) does not physically represent a unit load at that point, but some traction distribution around the node, the form of which is given by the inverse of equation (5.5.8). If a set of elements are symmetrically placed (i.e. Fig. 5.7.1c) then applying a unit load at 'i' will correspond to a traction distribution around 'i' , the same as that around 'j' , for a unit load at 'j' , and the computed stiffness coefficients 'ij' and 'ji' will be equal. However, in the

general case this reciprocal interpretation of a point source does not apply and hence the argument for a symmetric matrix is invalid (although the reciprocal theorems of elasticity are of course still true).

The easiest way of demonstrating this effect is to consider Maxwell's reciprocal theorem applied to a simple case (e.g. constant elements). Consider two points on a body, 'i' and 'j' and their respective elements of length ℓ_i and ℓ_j, as shown in Figs. 5.7.2. (The shape of the remaining body is irrelevant, and for convenience we will consider only one degree of freedom at each node). The inverse of the stiffness relation between the responses and the sources (i.e. displacements and forces for elastiticy problems) may be written:

$$\underset{\sim}{U} = \underset{\sim}{S}\ \underset{\sim}{F} \tag{5.7.9}$$

where

$$\underset{\sim}{S} = \underset{\sim}{K}^{-1} \tag{5.7.10}$$

(remember, the inverse of a symmetric matrix is also symmetric).

If we apply a unit load at 'i', then the response at 'j', given by equation (5.7.9), will be $u_j = s_{ji}$. (Fig. 5.7.2a(i)). Now for $F_j = 1$, $u_i = s_{ij}$, (Fig. 5.7.2a(ii)). Maxwell's reciprocal theorem says that these two responses are equal, hence the matrix $\underset{\sim}{S}$ is symmetric, as is its inverse $\underset{\sim}{K}$. However, with a Boundary Element representation, applying $F_i = 1$, physically represents a traction along element 'i' of $P_i = 1/\ell_i$ (Fig. 5.7.2b(i)), and again the response at 'j' is s_{ji}. Similarly for $F_j = 1$, $u_i = s_{ij}$. (Fig. 5.7.2b(ii)).

As can readily be seen, the two sets of applied tractions are not exactly equivalent and the reciprocal theorem does not apply.

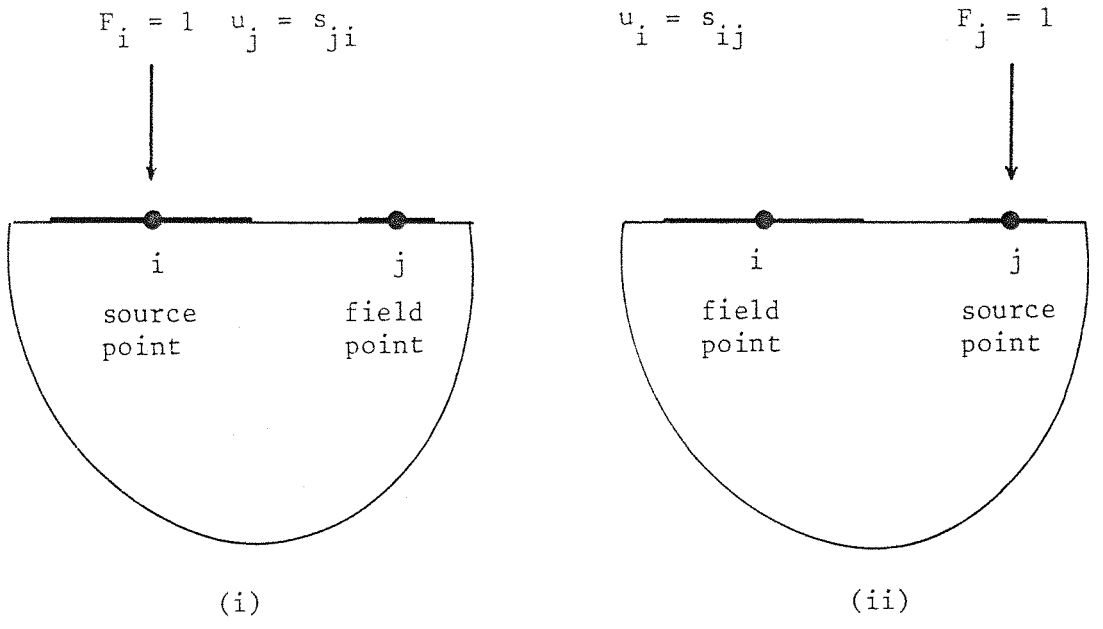

(a)

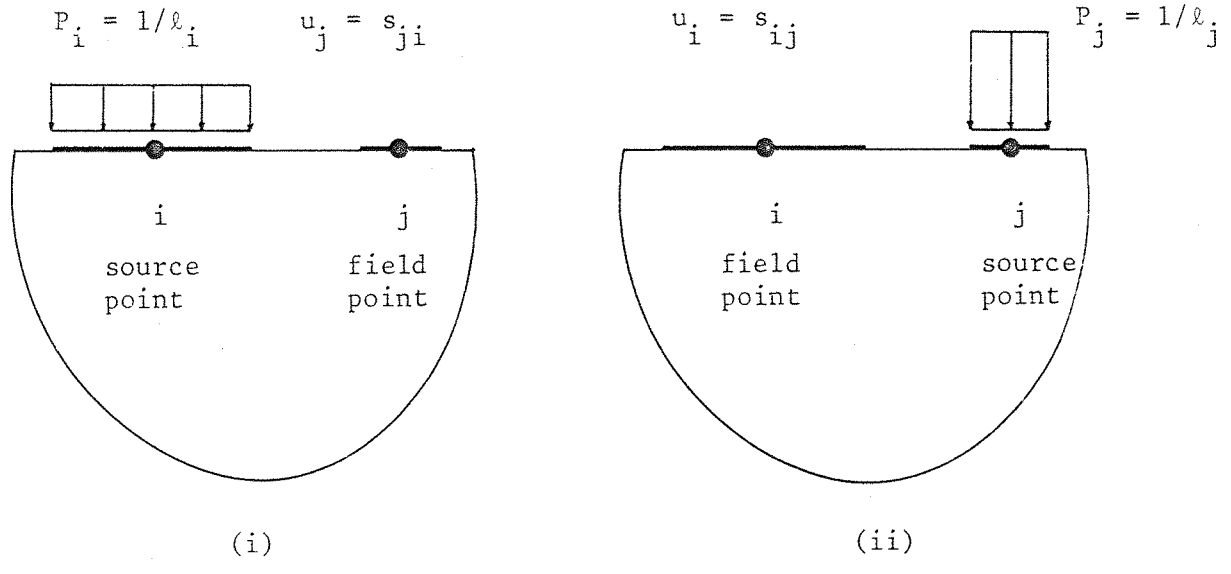

(b)

Figure 5.7.2 Physical interpretation of Maxwell's reciprocal theorem.

Hence the coefficients s_{ij} and s_{ji} are not equal, and $\underset{\sim}{S}$ (hence $\underset{\sim}{K}$) is not symmetric.

(Note that if the elements were of the same length, then Maxwell's theorem is applicable, and symmetric coefficients would be expected. This would in fact arise, due to the symmetry of the integration process involved in forming the two terms).

The same argument applies to higher order discretisations, but it should be noted that the two sets of applied tractions are almost equivalent in the 'average'sense, as the same total load is being applied in each case. (The only difference being in the local distribution of the load, depending on the local geometry). This is the reason why the matrices are 'almost' symmetric, and that when the 'unsymmetric' part is discarded, only relatively small errors are introduced.

An interesting academic point worth noting, is that if we continually refine the Boundary Element mesh such that the element lengths tend to zero, then the applied tractions will tend to point loads, and the Finite Element interpretation of the applied sources would give rise to symmetric matrices.

Another important observation is that for two nodes 'i' and 'j' which are far apart (in relation to the size of their adjacent elements), by St. Venant's principle, the local distribution of the source at 'i' , say, will have very little effect on the response at 'j' , and vice-versa. For this situation the influence coefficients are almost identical, and any difference has a negligible effect as the terms will be several orders of magnitude lower than the principal diagonal coefficients.

5.8 EXAMPLES OF COMBINATION PROBLEMS

The examples of this section are run as Finite Element displacement models. The Finite Element region is discretised using linear strain triangles (6-noded), and the 'equivalent' stiffness matrix for the Boundary Element region is formed in the manner described in section 5.5 i.e. $\underset{\sim}{K}^{S}$, as given by equations (5.5.18) and (5.5.19)

The element stiffnesses are then assembled together and the equations solved in the usual Finite Element manner. (i.e. making use of the symmetry in the storage and solution schemes).

EXAMPLE 1. DEEP CANTILEVER (with parabolically varying end load)

This is the same problem as example 2 of section 5.6.3. Two degrees of discretisation are used, and in each case a Finite Element, Boundary Element, and Combination run is made. The overall problem is again depicted here, (for easy reference) in Fig. 5.8.1 and the meshes used are shown in Figs. 5.8.2, 5.8.3 and 5.8.4.

Table 5.8.1 shows the deformation along the centre line of the cantilever, in the direction of the load. The exact solution given by Timoshenko [1], for the tip deflection is 15.1.

Table 5.8.2 shows the shear stress distribution over a cross-section, half way along the cantilever, corresponding to the interface of the Combination run, (i.e. along the line $x_1 = 6.0$). As we approach the fixed end of the cantilever, the shear stress becomes unbounded at the edges, and an analytical solution is not available unless special boundary conditions are imposed to allow the fixed end to warp. (See [1]). However, this effect is quite localised, and at a reasonable distance from the fixed end the stress distribution is the same as that applied at the loaded end. (St. Vennant's Principle).

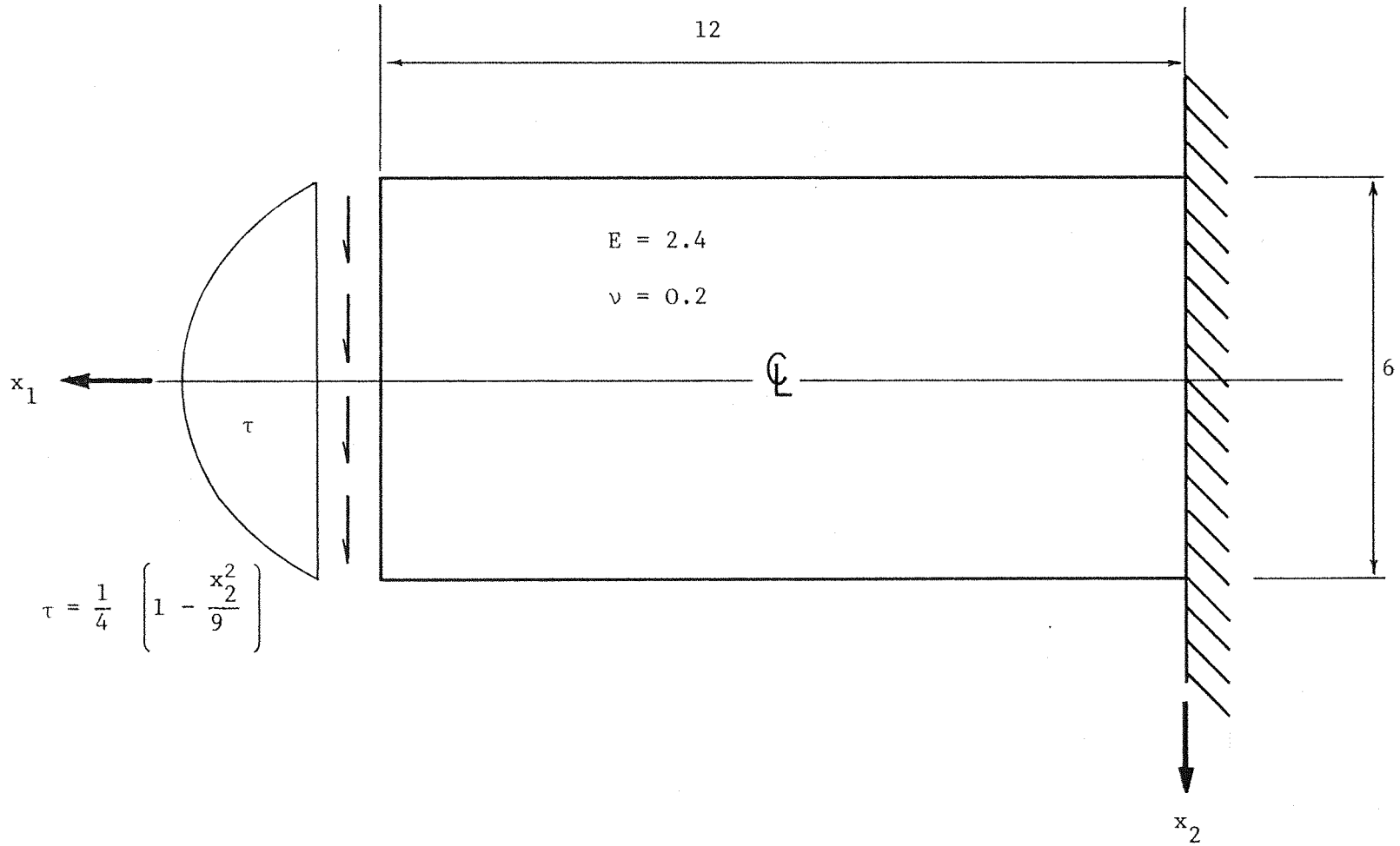

Figure 5.8.1 Cantilever. Problem Definition.

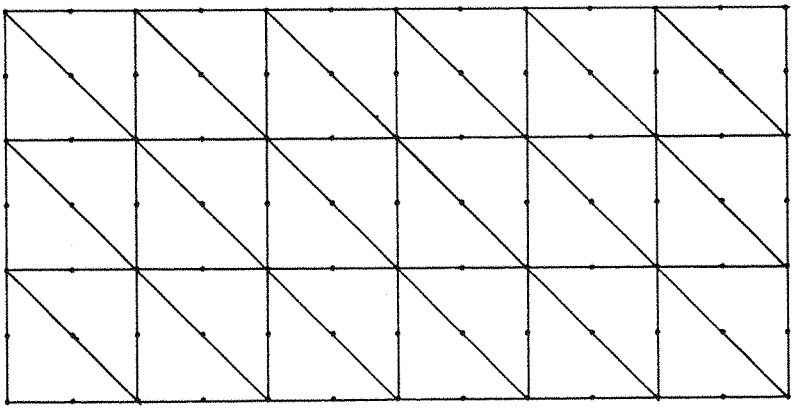

(a) Mesh 1F, 36 Finite Elements

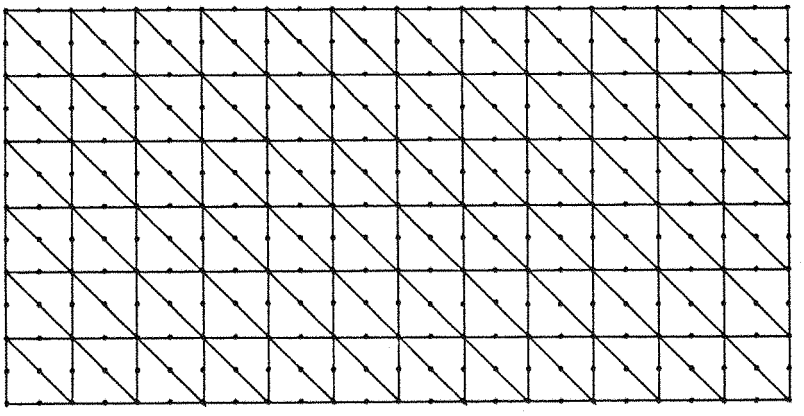

(b) Mesh 2F, 144 Finite Elements

Figure 5.8.2 Deep Cantilever. F.E.M. Discretisations.

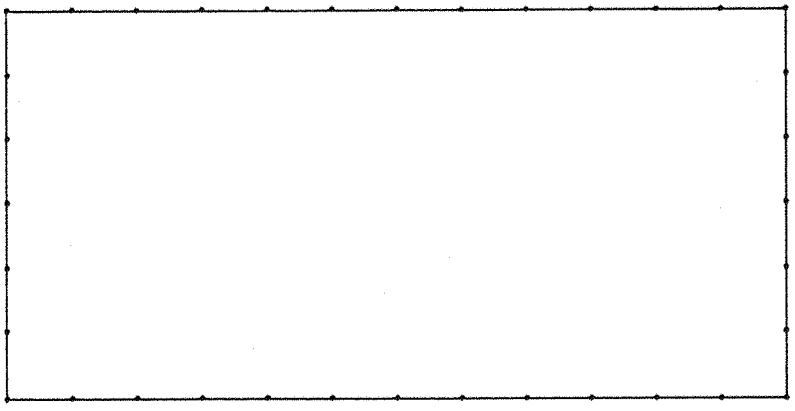

(a) Mesh 1B, 36 Linear Boundary Elements.

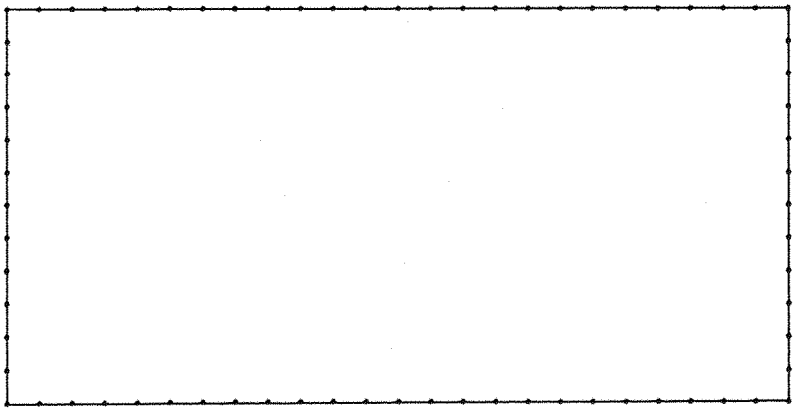

(b) Mesh 2B, 72 Linear Boundary Elements.

Figure 5.8.3. Boundary Element Discretisation.

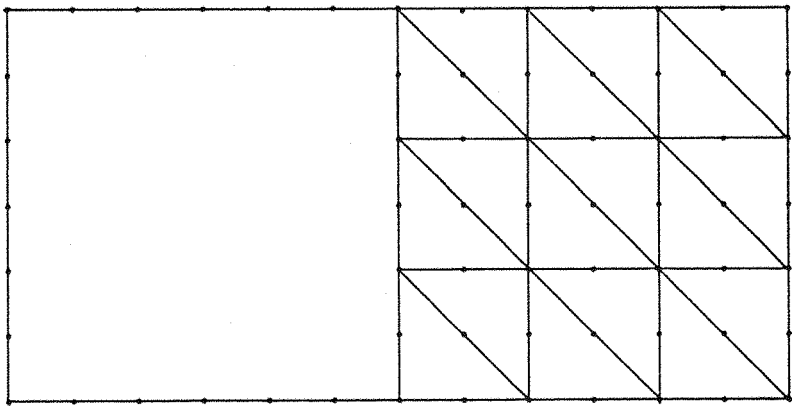

(a) Mesh 1C, 18 Finite Elements, 24 Boundary Elements.

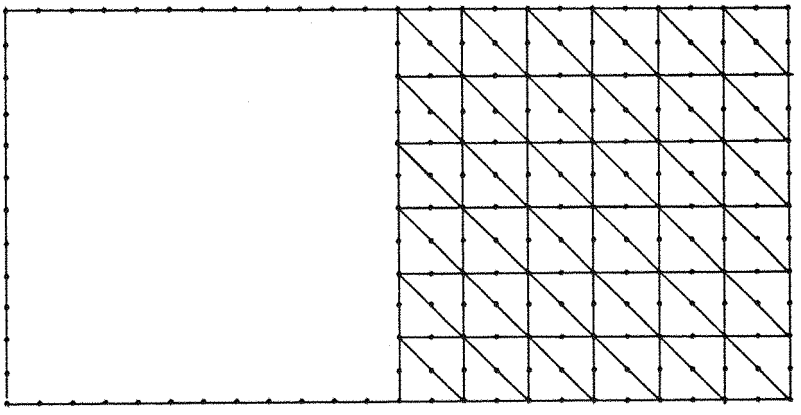

(b) Mesh 2C, 72 Finite Elements, 48 Boundary Elements.

Figure 5.8.4 Deep Canitlever. COMBINATION Discretisations.

x_1	Finite Element Method		Boundary Element Method		Combination Method	
	MESH 1F	MESH 2F	MESH 1B	MESH 2B	MESH 1C	MESH 2C
1.0	0.245	0.252	0.357	0.362	0.326	0.315
2.0	0.779	0.813	0.943	1.004	0.892	0.962
3.0	1.560	1.594	1.759	1.862	1.623	1.614
4.0	2.544	2.579	2.701	2.831	2.694	2.603
5.0	3.709	3.755	3.816	3.942	3.771	3.672
6.0	5.026	5.076	5.082	5.204	5.142	5.113
7.0	6.479	6.503	6.479	6.613	6.501	6,572
8.0	8.040	8.104	7.984	8.115	8.022	8.156
9.0	9.692	9.742	9.576	9.776	9.604	9.736
10.0	11.410	11.901	11.400	11.635	11.408	11.817
11.0	13.670	13.734	13.270	13.510	13.236	13.715
12.0	14.960	15.110	14.660	14.973	14.815	15.062

Table 5.8.1 Displacements along the centre line of a deep cantilever with an end load.

x_2		FEM		BEM		COMBINATION	
	EXACT SOLUTION	MESH 1F	MESH 2F	MESH 1B	MESH 2B	MESH 1C	MESH 2C
-3.0	0.0000	0.0187	0.0047	0.0000	0.0000	0.0000	0.0000
-2.0	0.1389	0.1389	0.1409	0.1352	0.1396	0.1334	0.1405
-1.0	0.2222	0.2402	0.2232	0.2356	0.2227	0.2516	0.2234
0.0	0.2500	0.2487	0.2508	0.2491	0.2504	0.2479	0.2511
1.0	0.2222	0.2402	0.2234	0.2355	0.2227	0.2518	0.2234
2.0	0.1389	0.1344	0.1410	0.1355	0.1394	0.1329	0.1406
3.0	0.0000	0.0192	0.0048	0.0000	0.0000	0.0000	0.0000

Table 5.8.2 Shear Stress distribution along the mid-section/ interface of a deep cantilever.

EXAMPLE 2. HOLLOW BEAM

The overall problem is depicted in Fig. 5.8.5a; However, due to symmetry, only half of the domain need be considered, with the appropriate boundary conditions, as shown in Fig. 5.8.5b. This problem was run using Finite Element (linear strain triangles) by Vasilopoulos [38], and his results are compared against a Boundary Element and a Combination run. The discretisations used, for the three solutions, are shown in Figs. 5.8.6, 5.8.7 and 5.8.8.

The combination runs were performed using both the unsymmetrised and symmetrised 'equivalent' stiffness matrices, $\underset{\sim}{K}^{u}$ and $\underset{\sim}{K}^{s}$, for the Boundary Element region.

Comparisons of the displacements at all the corner points on the boundary of the problem (points 1 - 10, Figs. 5.8.6 - 5.8.8) are shown in Table 5.8.3.

Table 5.8.4 shows the displacement profile along the internal axis AA (Figs. 5.8.6 - 5.8.8), which also corresponds to part of the interface of the combination problem.

The stresses along this interface are calculated, for the combination problem, by substituting the final solution for the displacements into BEM equations for this region. These values are compared to the FEM and BEM solutions in Table 5.8.5.

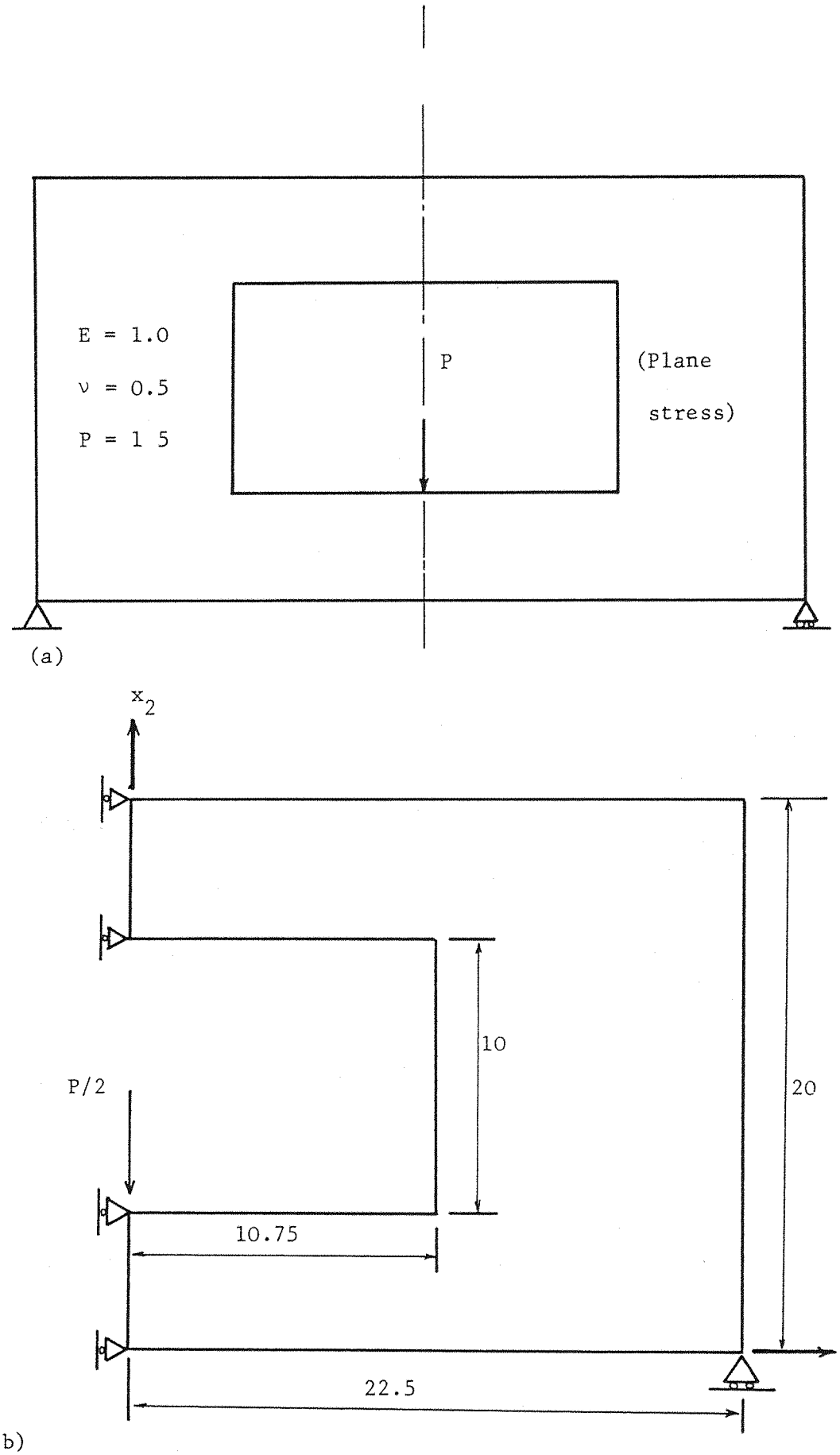

Figure 5.8.5 Hollow Beam Example Problem Definition.

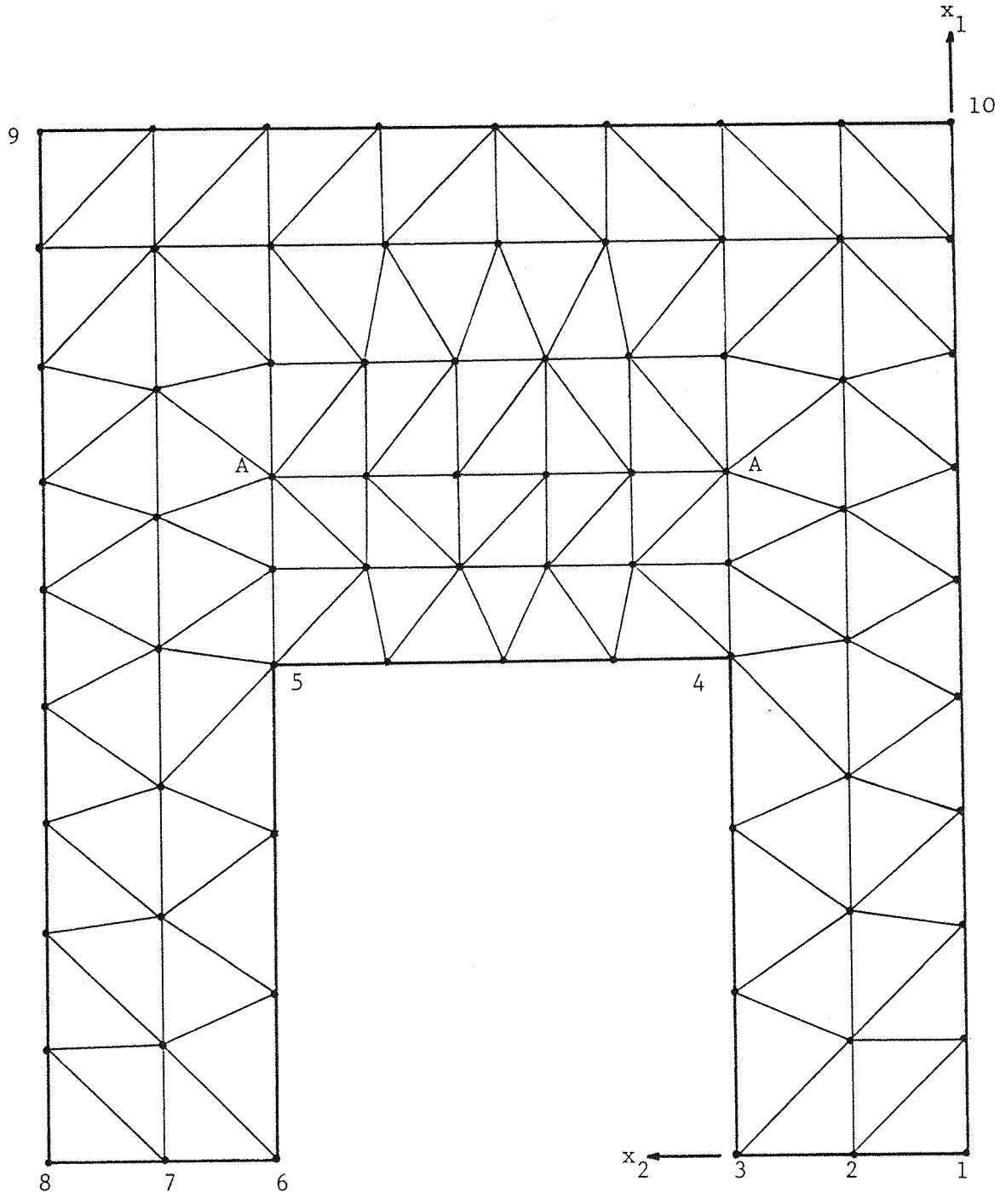

Figure 5.8.6 Hollow Beam, Finite Element Mesh.

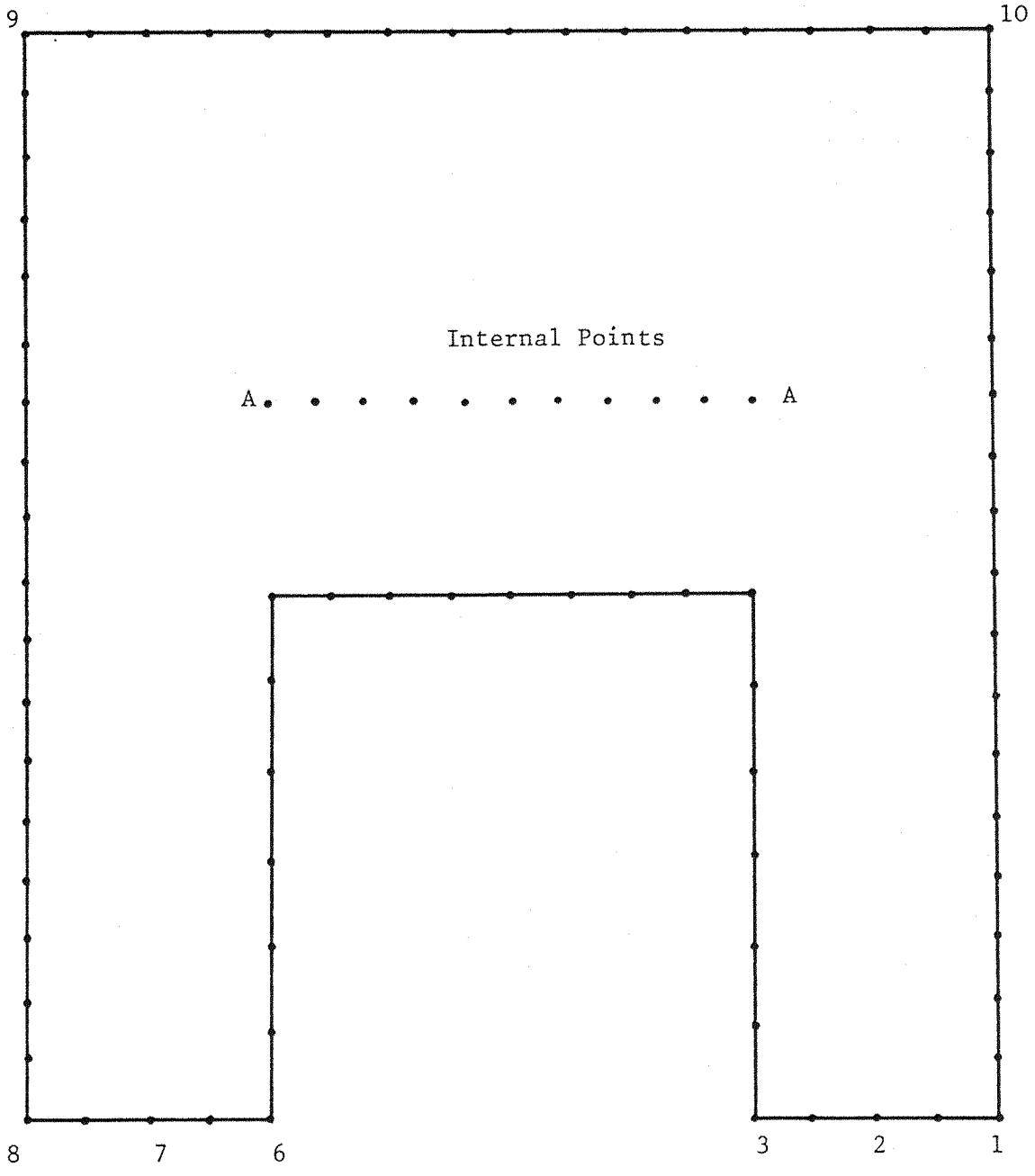

Figure 5.8.7 Hollow Beam, Boundary Element Mesh.

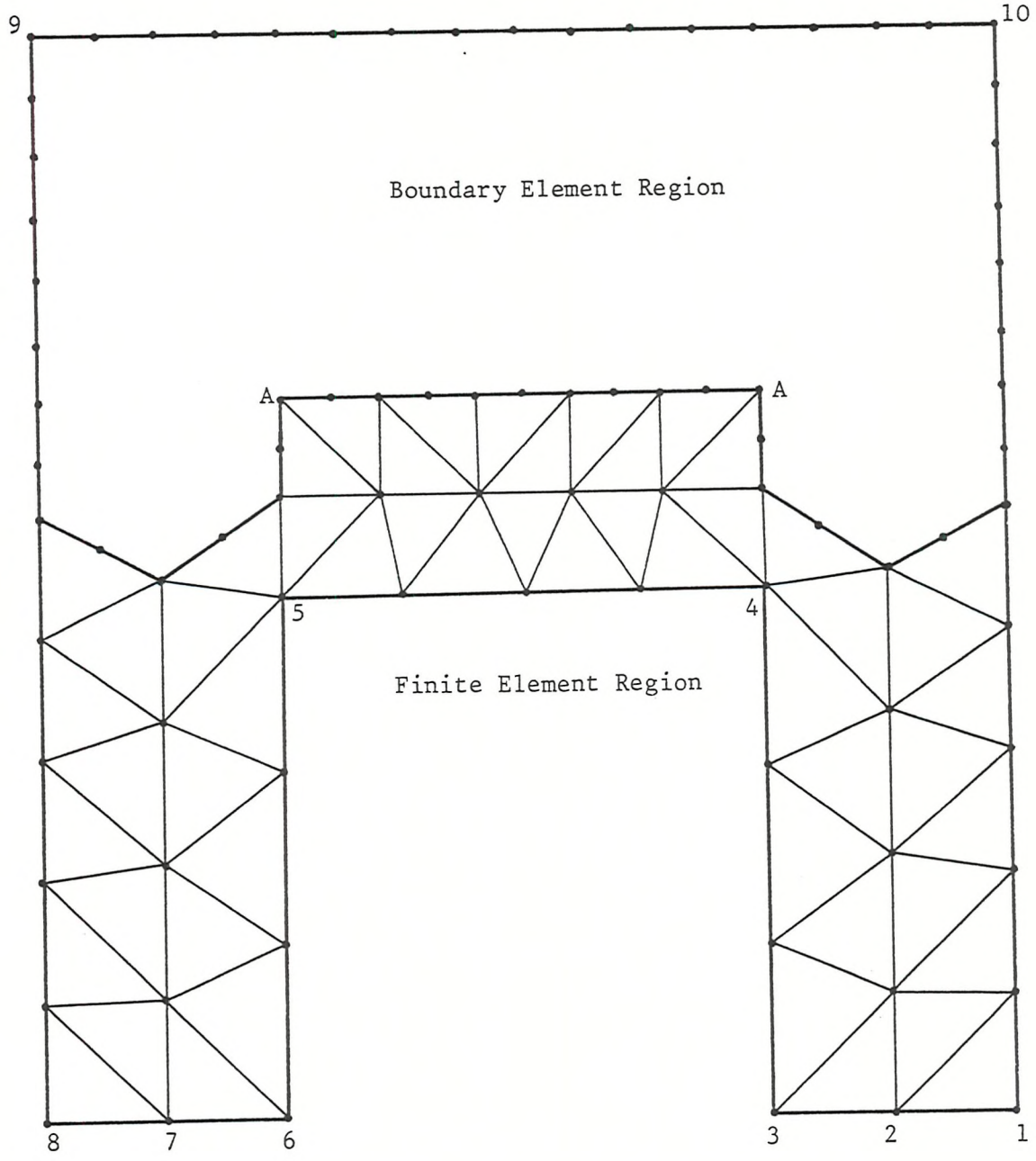

Figure 5.8.8 Hollow Beam. Combination Mesh.

Point	FEM		BEM		COMBINATION using K^u		COMBINATION using K^s	
u_1	u_1	u_2	u_1	u_2	u_1	u_2	u_1	u_2
1		-304.75		-303.3		-305.5		-306.4
2		-313.80		-311.7		-315.6		-317.2
3		-333.54		-331.1		-335.4		-338.9
4	-10.47	-119.89	-11.80	-124.8	-11.10	-121.32	-12.04	-124.3
5	-16.86	-87.53	-17.11	-93.27	-17.53	-90.75	-17.44	-92.94
6		-88.20		-94.17		-91.37		-93.56
7		-86.87		-92.84		-88.82		-91.02
8		-85.50		-91.46		-87.63		-89.83
9	-28.27	-65.63	-29.05	-70.02	-28.62	-68.35	-29.29	-71.73
10	-56.69		-60.15		-56.72		-58.11	

(position of points 1 - 10 are shown in Figs. 5.8.6 - 5.8.8)

Table 5.8.3. Hollow Beam example. Displacements at geometric discontinuities on the boundary

x_2	FEM		BEM		COMBINATION using $\underset{\sim}{K}^u$		COMBINATION using $\underset{\sim}{K}^s$	
	u_1	u_2	u_1	u_2	u_1	u_2	u_1	u_2
15.0	-20.89	-82.39	-21.13	-87.48	-23.27	-91.88	-22.89	-93.13
14.0	-20.68	-82.81	-20.84	-87.90	-22.82	-92.33	-22.54	-93.73
13.0	-20.35	-83.23	-20.84	-88.32	-22.21	-92.66	-22.06	-94.01
12.0	-19.84	-83.66	-19.83	-88.75	-21.49	-93.27	-21.36	-94.59
11.0	-18.99	-84.14	-18.89	-89.23	-20.35	-93.61	-20.23	-94.52
10.0	-17.82	-84.68	-17.57	-89.74	-19.01	-94.30	-18.93	-95.61
9.0	-15.96	-85.03	-15.80	-90.25	-17.03	-94.68	-16.97	-96.00
8.0	-13.81	-85.62	-13.47	-90.68	-14.68	-95.23	-14.70	-96.61
7.0	-10.98	-85.89	-10.40	-90.94	-11.36	-95.37	-11.41	-96.90
6.0	-6.97	-85.85	-6.29	-90.95	-7.22	-95.38	-8.04	-97.17
5.0	-1.67	-85.6	-0.85	-90.70	-1.24	-95.55	-2.62	-96.49

Table 5.8.4 Hollow Beam. Displacement profile along an internal axis (x_1 = 15.05) (corresponding to interface Combination problem).

x_2	FEM		BEM		COMBINATION using $\underset{\sim}{K}^u$		COMBINATION using $\underset{\sim}{K}^s$	
	σ_{11}	σ_{12}	σ_{11}	σ_{12}	σ_{11}	σ_{12}	σ_{11}	σ_{12}
15.0	-0.504	0.866	-0.517	0.842	-0.532	0.942	-0.539	0.951
14.0	-0.323	0.908	-0.329	0.908	-0.352	0.981	-0.356	0.991
13.0	-0.151	0.954	-0.163	0.934	-0.178	1.040	-0.184	1.056
12.0	-0.022	0.962	-0.027	0.940	-0.031	1.058	-0.039	1.061
11.0	0.109	0.969	0.093	0.945	0.104	1.046	0.108	1.058
10.0	0.276	0.973	0.224	0.953	0.246	1.061	0.252	1.065
9.0	0.442	0.976	0.398	0.954	0.431	1.054	0.441	1.057
8.0	0.714	0.932	0.637	0.913	0.672	1.016	0.679	1.023
7.0	1.003	0.813	0.929	0.773	0.987	0.870	1.014	0.881
6.0	1.207	0.412	1.194	0.471	1.283	0.494	1.304	0.506
5.0	1.316	-0.044	1.289	0.015	1.379	-0.021	1.392	-0.032

Table 5.8.5 Hollow Beam. Stress Profile along an internal axis (x_1 = 15.05) (corresponding to interface of Combination Problem).

EXAMPLE 3. RETAINING WALL-FOUNDATION PROBLEM

A large rectangular shaped foundation with its perimeter (other than the free surface) fixed, supports a cantilever- retaining wall type structure, which is inset into the foundation, as shown in Fig. 5.8.9. The retaining wall is descretised using 48 Finite Elements (linear strain triangles), Fig. 5.8.10, and the stiffness of the foundation is computed using both the Boundary Element based formulation and classical Finite Elements. (The meshes used are shown in Figs. 5.8.11 and 5.8.12, respectively).

The combination runs were performed using both the unsymmetric and symmetrised 'equivalent' stiffness matrices, $\underset{\sim}{K}^{u}$ and $\underset{\sim}{K}^{s}$. The displacement profiles, thus obtained, are compared to the Finite Element results. Table 5.8.6 shows the displacement profiles along the length (centre line) of the cantilever; and Table 5.8.7 shows the displacements at the wall - foundation interface (which also corresponds to the interface for the combination problem).

The results are in excellent agreement, again confirming the validity of the 'equivalent' stiffness approach, and also the fact that the symmetrisation of the 'equivalent' stiffness matrix introduces a very negligible error in the formulation.

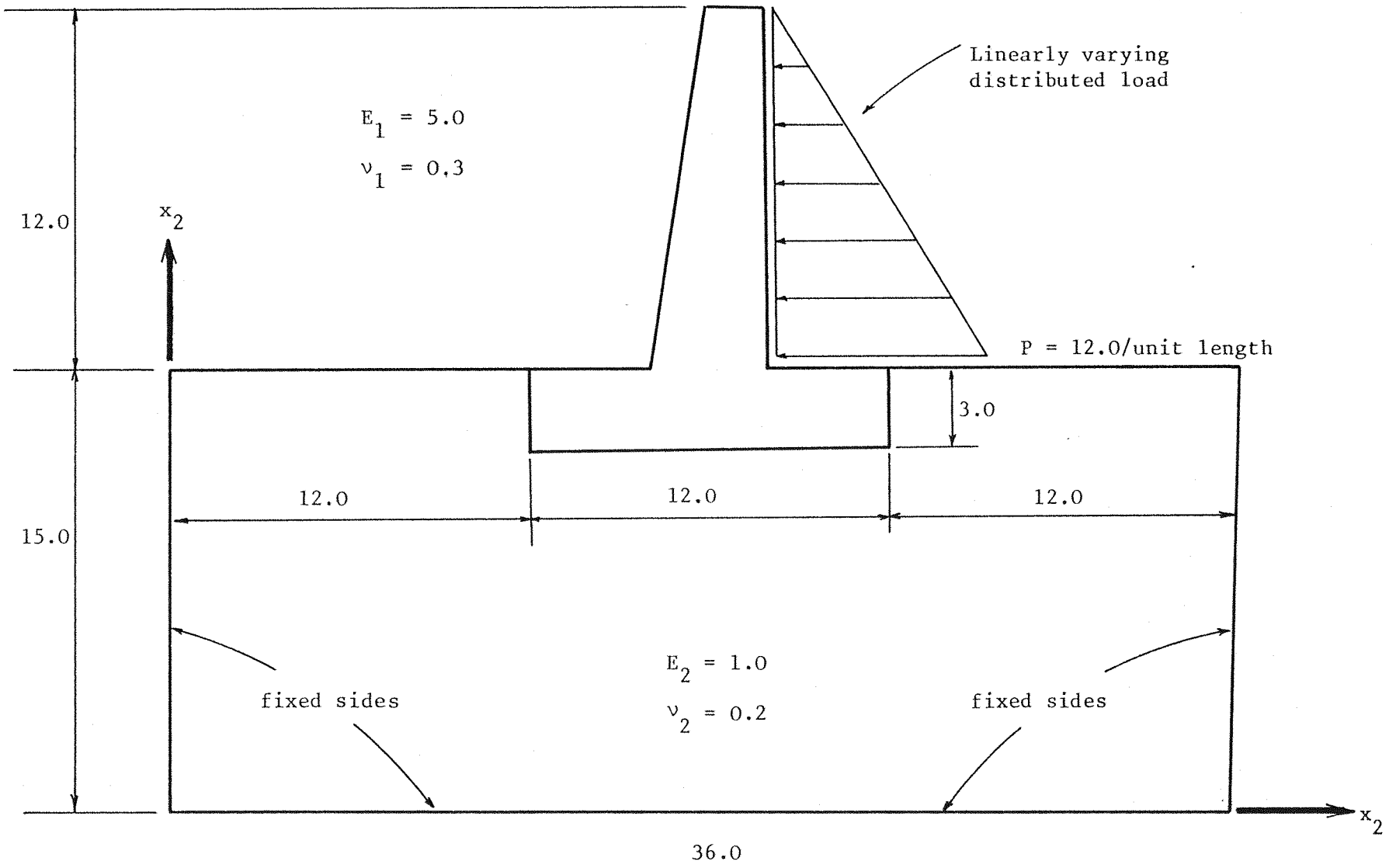

Figure 5.8.9 Retaining Wall-Foundation. Problem Definition.

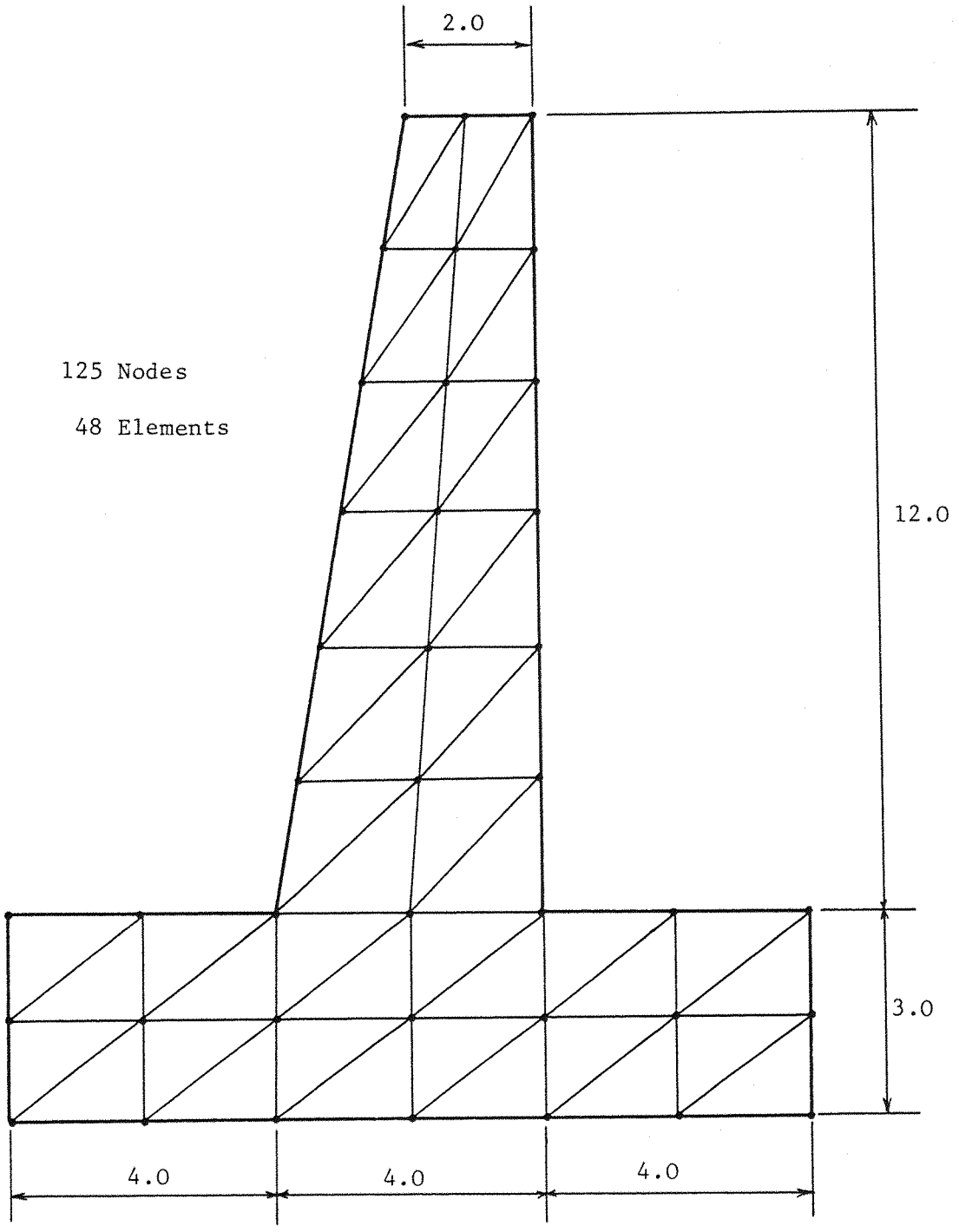

Figure 5.8.10 Finite Element Mesh, for retaining Wall part of the problem. (mid-side nodes not shown).

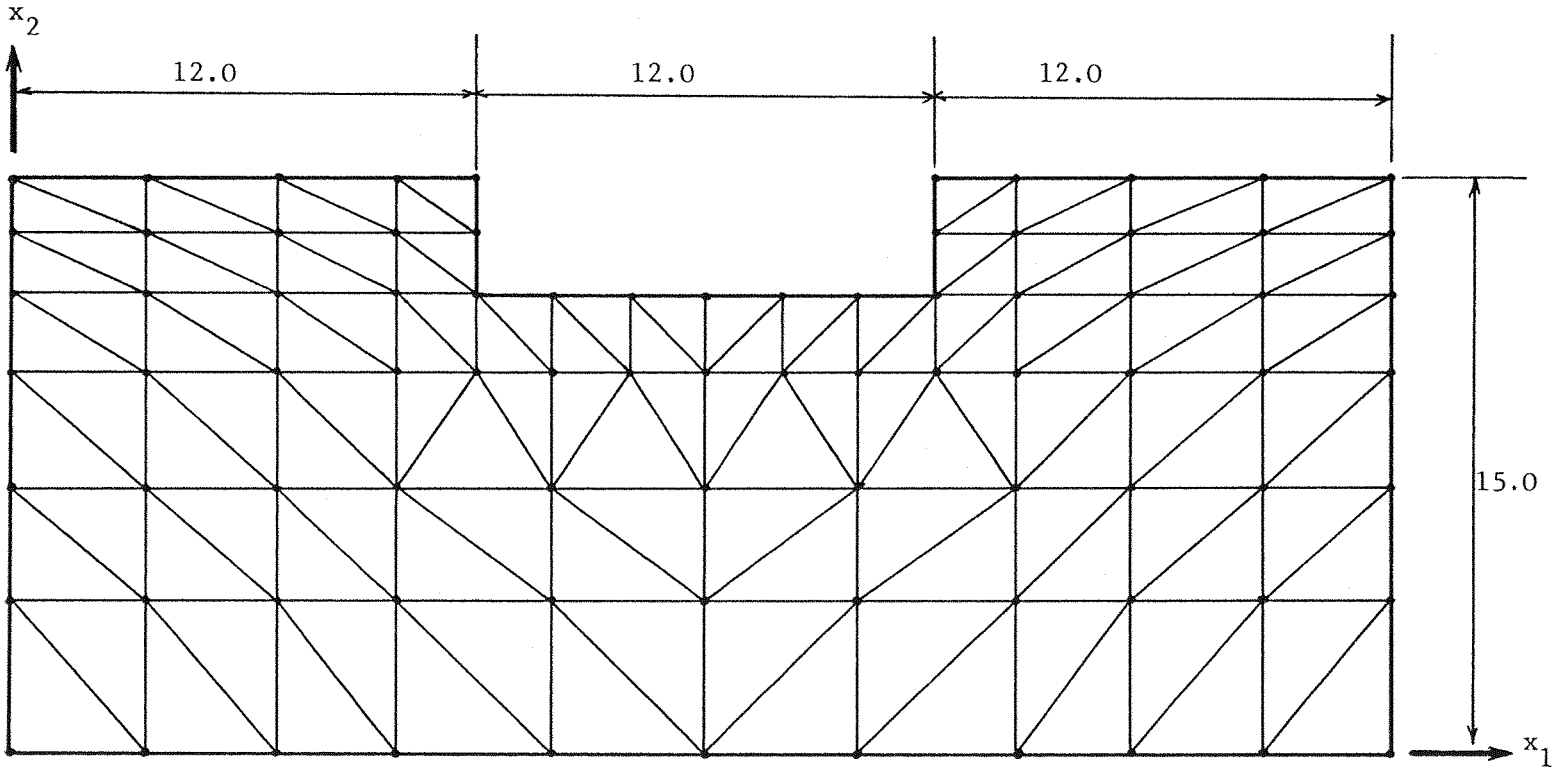

289 Nodes, 124 Elements

Figure 5.8.11 Finite Element Mesh for Foundation of Retaining Wall
(mid-side nodes not shown)

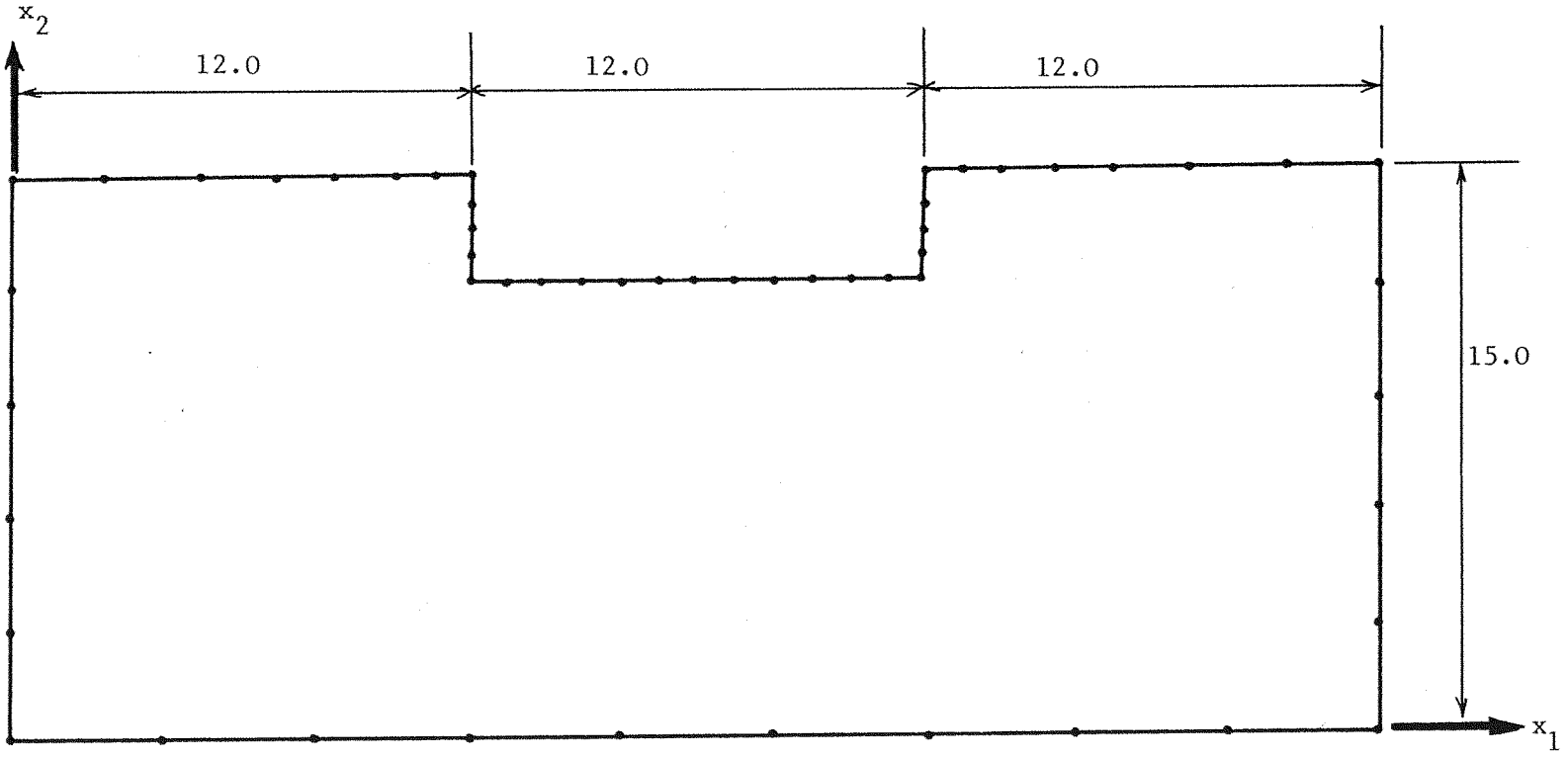

53 Nodes, 53 Elements

Figure 5.8.12 Boundary Element Mesh for Foundation of Retaining Wall.

x_2	FINITE ELEMENTS		COMBINATION using K^u		COMBINATION using K^s	
	u_1	u_2	u_1	u_2	u_1	u_2
15.0	-813.7	60.28	-837.6	59.32	-838.2	59.62
16.0	-744.4	54.47	-766.3	53.34	-766.8	53.76
17.0	-674.9	48.62	-694.8	47.33	-695.3	47.46
18.0	-605.2	42.76	-623.1	41.31	-623.6	41.44
19.0	-535.6	36.91	-551.4	35.30	-552.0	35.42
20.0	-466.6	31.04	-480.5	29.26	-480.9	29.38
21.0	-398.8	25.30	-410.9	23.36	-411.2	23.48
22.0	-333.3	19.69	-343.3	17.59	-343.7	17.70
23.0	-270.8	14.38	-279.0	12.11	-279.3	12.22
24.0	-212.7	9.32	-218.9	6.95	-219.2	7.01
25.0	-160.0	4.71	-164.3	2.17	-164.5	2.28
26.0	-114.8	1.61	-117.2	-0.92	-117.4	-0.81
27.0	-80.99	-0.97	- 81.56	-3.33	-81.78	-3.23

Table 5.8.7 Displacement profile along centre line of Cantilever.

Coordinates of point		Finite Elements		Combination using $\underset{\sim}{K}^u$		Combination using $\underset{\sim}{K}^s$	
x_1	x_2	u_1	u_2	u_1	u_2	u_1	u_2
12.0	15.0	-50.27	-39.69	-49.22	-40.17	-49.62	-40.14
12.0	13.5	-49.58	-41.81	-49.35	-42.07	-49.45	-42.26
12.0	12.0	-44.75	-40.97	-45.33	-41.28	-45.43	-41.40
14.0	12.0	-45.43	-41.65	-46.24	-42.88	-46.30	-42.95
16.0	12.0	-36.94	-31.63	-38.44	-32.52	-38.53	-32.50
18.0	12.0	-32.01	0.26	-31.38	-0.69	-31.50	-0.61
20.0	12.0	-37.32	31.31	-36.55	30.94	-36.71	31.06
22.0	12.0	-45.44	41.14	-44.48	42,36	-44.73	42.43
24.0	12.0	-45.62	40.51	-46.30	41.04	-46.76	40.69
24.0	13.5	-49.71	41.78	-48.94	43.02	-49.02	42.85
24.0	15.0	-50.01	39.12	-49.86	40.81	-49.65	40.89

Table 5.8.6 Displacements around the Retaining Wall-Foundation Interface

CHAPTER 6 A 2-DIMENSIONAL HALF-SPACE FORMULATION

6.1 INTRODUCTION

In this chapter, formulations are developed for a 2-Dimensional semi-infinite domain loaded on the free surface. For this case the 2-D Boussinesq solution is applicable (see section 3.2.2) and only requires discretisation of the loaded segment. As such, all the primary influences and effects are defined on the free boundary, and once these have been established, solutions for internal displacements and stresses are readily obtainable. As the boundary segment under consideration now has a consistent and simple geometry, the integrals involved in the Boundary Element Method may be performed analytically, for the general case, thus allowing explicit definition of the algebraic, discretised form of the governing equations.

This chapter presents formulations for constant, linear and quadratic Boundary Elements, and compares their performances for a series of test problems.

The 'equivalent' stiffness matrix is then formed, for each type of element, and its performance is examined with respect to both its accuracy and symmetric properties. Finally a problem combining Finite Elements with the above formed 'equivalent' stiffness matrix is run, in order to demonstrate the applicability of the technique.

There is an important point worth a mention here; As the fundamental solution for the B.E.M. yields a traction on the surface which is zero, the left hand side, $\underset{\sim}{H}$, matrix is null, other than the free term, (see Chapter 4, for the analogous situation in 3-D). This

means that no interpolation for the displacements is required, and if the interpolation for the applied tractions is of high enough order to represent these tractions exactly, then the solution for the displacements should also be exact, as the use of analytic integration introduces no approximations in the formulation.

It should also be remembered that the displacements cannot be calculated absolutely, as there are arbitrary constants involved in the fundamental solution (See Section 3.2.2). This means that the displacements can only be defined in relation to some datum, and it is their relative magnitude which is important. For consistency, all the examples presented in this Chapter were run using the same values for the constants involved.

6.2 IMPLEMENTATION OF THE BOUNDARY ELEMENT METHOD.

6.2.1 General Features of the Formulation.

Consider the loaded segment of the free surface of a 2-Dimensional half-space which we divide into a number of elements, as depicted in Figure 6.2.1. An interpolation of the variables along each element is achieved with the usual dimensionless, normalised shape functions, $\underset{\sim}{\Phi}^T$, linking the variables to their nodal values; see Equations (3.4.4).

Referring to the discretised form of the Boundary Integral equations (3.4.5), in order to obtain the equations for each point , 'i', we apply a set of unit tractions at 'i' , and then require the evaluation, on each element, e , of the integrals,

$$\int_{\Gamma_e} \underset{\sim}{u}^* \, \underset{\sim}{\Phi}^T \, d\Gamma \qquad (6.2.1)$$

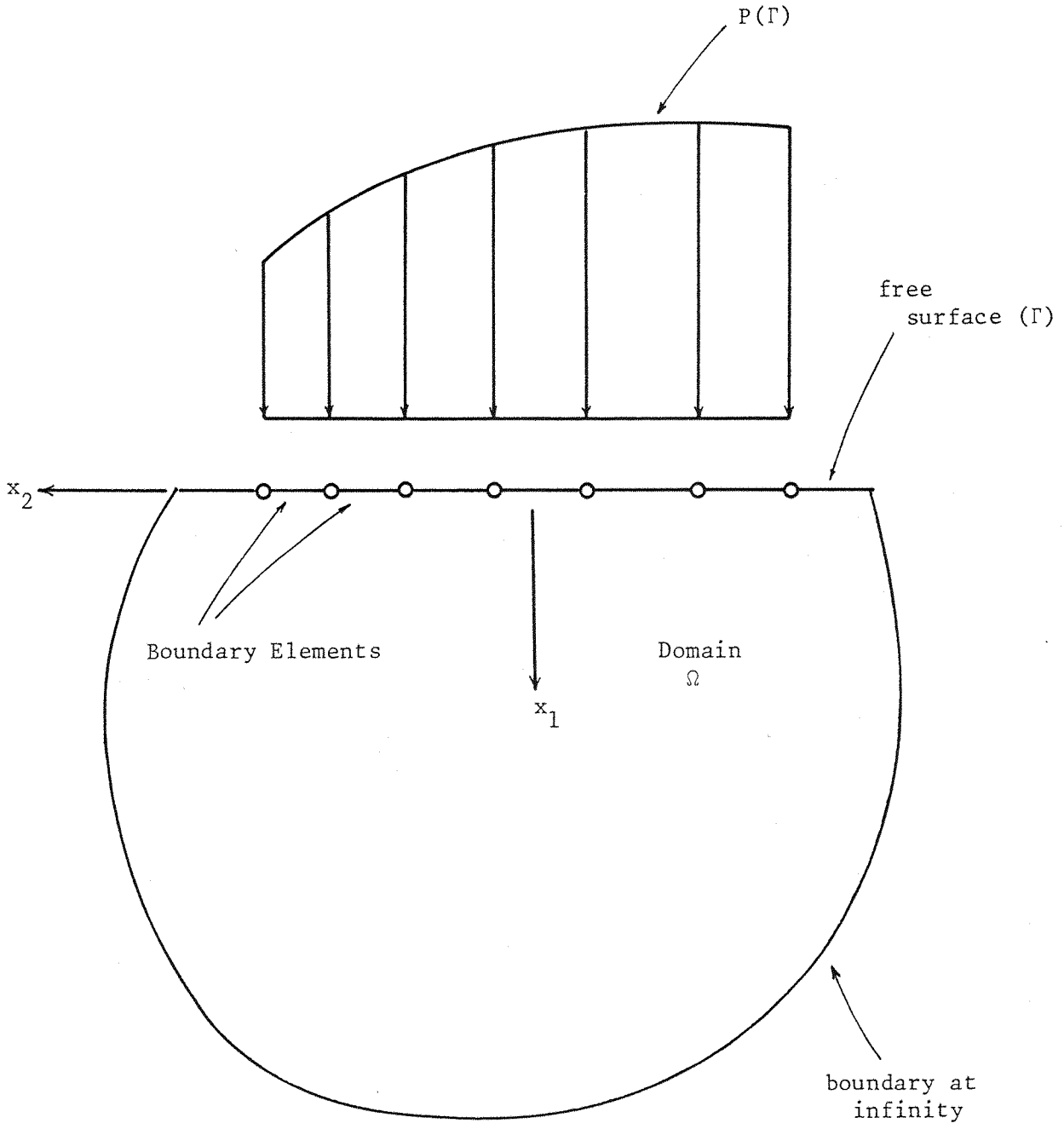

Figure 6.2.1 2-D Half Space, with loaded segment discretised using Boundary Elements.

If there are 'n' nodes on each element, (n = 1, for constant elements, n = 2, for linear elements, etc. See Figures 6.2.3) then there will be 'n' 2×2 contributions to the $\underset{\sim}{G}$ matrix, corresponding to rows 'i' , i.e.

$$g^{ij}_{\ell k} = \int_{\Gamma_e} u^*_{\ell k} \, \phi_j \, d\Gamma \qquad (j = 1, n) \tag{6.2.2}$$

(Γ_e refers to the element containing node 'j')

and, $u^*_{\ell k}$ is the fundamental solution for the problem, discussed in detail in section 3.2.2. The form of the solution is repeated here for easy reference, and expressed in terms of the local coordinates, ξ , (see Figure 6.2.2).

$$\begin{aligned} u^*_{11} &= \alpha_1 - \alpha_2 \, \ell n(r_3 + \lambda \, L\xi) \\ u^*_{12} &= - \alpha_3 \, \lambda \\ u^*_{21} &= + \alpha_3 \, \lambda \\ u_{22} &= \alpha_4 - \alpha_2 \, \ell n(r_3 + \lambda \, L \, \xi) \end{aligned} \tag{6.2.3}$$

where $\lambda = + 1$ for the field point on positive x_2 side.

$\lambda = - 1$ for the field point on negative x_2 side.

and $\alpha_i (i = 1, 4)$ are defined in equations (3.2.13).

The left hand side integral of the Somigliana identity (3.4.5) does not contribute, as $p^*_{\ell k}$ is identically zero on the free surface, (by definition). As a result, the $\underset{\sim}{H}$ matrix, is null, other than the diagonal submatrices arising from the $c^i_{\ell k}$ term. This term is in fact the unit matrix of order 2 (see Chapter 3), making $\underset{\sim}{H}$ the identity matrix, (of the same order as $\underset{\sim}{G}$). An alternative argument for concluding the

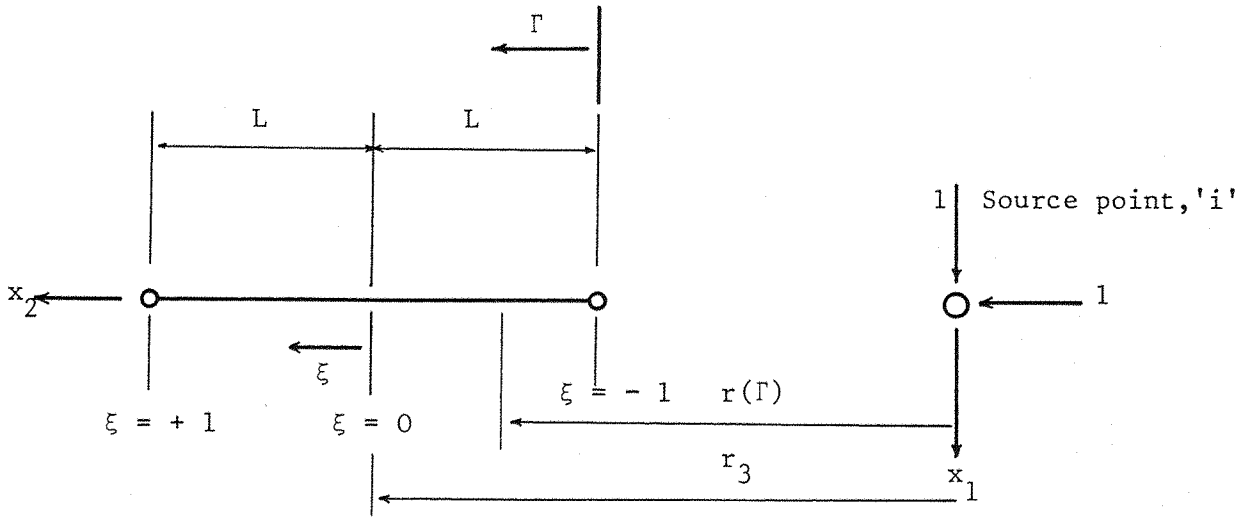

Figure 6.2.2 Geometry and local geometry of typical Boundary Element.

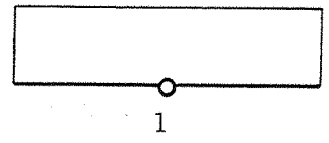

(a) CONSTANT Variation

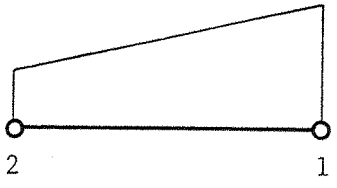

(b) LINEAR Variation

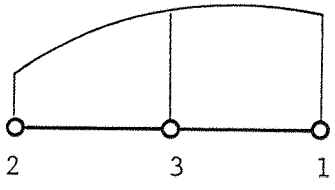

(c) QUADRATIC Variation

Figure 6.2.3 Nodal points on Boundary Elements.

form of $\underset{\sim}{H}$, is to develop the discretised form of the equations by applying the principle of superposition. Consider the point 'i' , and apply a load p_1, p_2 at some point S on the boundary. The displacements at 'i' will be given by:

$$\begin{aligned} u_1^i &= \bar{u}^*_{11}\, p_1 + \bar{u}^*_{21}\, p_2 \\ u_2^i &= \bar{u}^*_{12}\, p_1 + \bar{u}^*_{22}\, p_2 \end{aligned} \tag{6.2.4}$$

where the $\bar{u}^*_{\ell k}$ denotes the fundamental solution, at 'i' for a source at the field point, S . Now, $\bar{u}^*_{\ell k}$ differs from $u^*_{\ell k}$ (equation 6.2.3) only by a sign change of u^*_{12} and u^*_{21} , (as the sign of these terms depends on which side of the source the effect is being measured).

Hence

$$\bar{u}^*_{21} = - u^*_{21} = u^*_{12}$$

and

$$\bar{u}^*_{12} = - u^*_{12} = u^*_{21} \tag{6.2.5}$$

Equation (6.2.4) may then be written:

$$\begin{aligned} u_1^i &= u^*_{11}\, p_1 + u^*_{12}\, p_2 \\ u_2^i &= u^*_{21}\, p_1 + u^*_{22}\, p_2 \end{aligned} \tag{6.2.6}$$

If a continuous loading is applied, we may introduce an interpolation function for p_k , and integrate equations (6.2.6) along the loaded segment, to find the displacement at 'i' . Summing these integrals on each element,

$$\underset{\sim}{u}^i = \sum_{\ell=1}^{NE} \left\{ \int_{\Gamma_\ell} \underset{\sim}{u}^* \, \underset{\sim}{\Phi}^T \, d\Gamma \right\} \underset{\sim}{P} \tag{6.2.7}$$

Repeating this process for each point 'i' on the boundary, equations (6.2.7) result in,

$$\underset{\sim}{U} = \underset{\sim}{G}\ \underset{\sim}{P} \tag{6.2.8}$$

where the contributions to $\underset{\sim}{G}$ are given by equation (6.2.2), and (6.2.8) now corresponds to the BEM equations, with $\underset{\sim}{H}$ equal to the identity matrix.

When evaluating the terms given by equation (6.2.2), certain integrals involving products of algebraic and logarithmic terms will commonly arise. In order to keep the final expressions as compact as possible, these standard integrals will be referred to as I_i (i = 1, 6) and are defined and explicitly evaluated in Appendix A.

6.2.2 BEM - Constant Elements

With constant elements, the shape function is trivial (being equal to unity), and the integral of expression (6.2.2) produces only one 2×2 submatrix for each element (i.e. $g^{ij}_{\ell k}$, 'j' is the node corresponding to the element under consideration).

For each source node 'i' , and field point 'j' , the 2×2 submatrix of $\underset{\sim}{G}$ is given by ,

$$g^{ij}_{\ell k} = \int_{\Gamma_\ell} u^*_{\ell k}\, d\Gamma = L \int_{-1}^{+1} u^*_{\ell k}\,(\xi)\, d\xi \tag{6.2.9}$$

and upon evaluation yields

(i) For $i \neq j$

$$\begin{aligned} g^{ij}_{11} &= L(2\alpha_1 - \alpha_2\, I) \\ g^{ij}_{12} &= -\,2\,\alpha_3\,\lambda L \\ g^{ij}_{21} &= +\,2\,\alpha_3\,\lambda L \\ g^{ij}_{22} &= L(2\alpha_4 - \alpha_2\, I) \end{aligned} \tag{6.2.10}$$

where $\alpha_i (i = 1, 4)$ are defined by equations (3.2.13), and we define

$$I = I(r_3, \lambda L) = \int_{-1}^{+1} \ln(r_3 + \lambda L\xi) d\xi \qquad (6.2.11)$$

which is readily integrable, giving,

$$I = \left(1 + \frac{r_3}{\lambda L}\right) \ln(r_3 + \lambda L) + \left(1 - \frac{r_3}{\lambda L}\right) \ln(r_3 - \lambda L) - 2 \qquad (6.2.12)$$

(ii) For $i = j$, we must split the integral into two parts (as there are sign changes in the fundamental solution when passing from one side of the source to the other), and upon evaluation, equations (6.2.2) yield:

$$\begin{aligned} g_{11}^{ii} &= 2L\left[\alpha_1 - \alpha_2\left(\ln(L) - 1\right)\right] \\ g_{12}^{ii} &= 0 \\ g_{21}^{ii} &= 0 \\ g_{22}^{ii} &= 2L\left[\alpha_4 - \alpha_2\left(\ln(L) + 1\right)\right] \end{aligned} \qquad (6.2.13)$$

6.2.3. B.E.M. Linear Elements

The geometry and node numbering is shown in Figures 6.2.2 and 6.2.3.b. The relevant shape functions corresponding to nodes 1 and 2 are :

$$\begin{aligned} \phi_1 &= \frac{1}{2}(1 - \xi) \\ \phi_2 &= \frac{1}{2}(1 + \xi) \end{aligned} \qquad (6.2.14)$$

There will now be two 2×2 submatrices corresponding to each element. Consider the term g_{11}^{il} for a typical element :

$$g_{11}^{i1} = \int_{\Gamma} u_{11}^{*} \, \phi_1 \, d\Gamma = L \int_{-1}^{+1} u_{11}^{*} \, (\xi) \, \phi_1(\xi) \, d\xi \qquad (6.2.15)$$

Substituting from equations (6.2.3) and (6.2.14), we have:

$$g_{11}^{i1} = \frac{L}{2} \left\{ \alpha_1 \int_{-1}^{+1} (1 - \xi) \, d\xi - \alpha_2 \int_{-1}^{+1} \ln(r_3 + \lambda L \xi) d\xi + \alpha_2 \int_{-1}^{+1} \xi \, \ln(r_3 + \lambda L \xi) \, d\xi \right\} \qquad (6.2.16)$$

or

$$g_{11}^{i1} = \frac{L}{2} \left\{ 2 \, \alpha_1 - \alpha_2 \left[I_1(r_3, \lambda L) - I_2(r_3, \lambda L) \right] \right\} \qquad (6.2.17)$$

where I_1 and I_2 are given in Appendix A.

Consider the term g_{12}^{i1} for a typical element:

$$g_{12}^{i1} = L \int_{-1}^{+1} u_{12}^{*}(\xi) \, \phi_1(\xi) \, d\xi$$

$$g_{12}^{i1} = - \alpha_3 \, \lambda \, \frac{L}{2} \int_{-1}^{+1} (1 - \xi) \, d\xi = - \alpha_3 \, L \, \lambda \qquad (6.2.18)$$

All other terms can immediately be written using the form of equations (6.2.17) and (6.2.18). The $g_{\ell k} (\ell \neq k)$ terms differ by a sign change, and the $g_{\ell k}$ $(\ell = k)$ terms differ by the value of the first constant. The ϕ_2 terms simply differ by a sign change of the I_2 integral. Hence we may express all the $g_{\ell k}$ submatrices as follows

<u>for $\ell = k$</u> $$g_{\ell k}^{ij} = \frac{L}{2} \left\{ 2\beta - \alpha_2 \left[I_1(r_3, \lambda L) - \gamma I_2(r_3, \lambda L) \right] \right\} \qquad (6.2.19)$$

where, $\beta = \alpha_1$ for $\ell = k = 1$

$\beta = \alpha_4$ for $\ell = k = 2$

$\gamma = +1$ for $j = 1$

$\gamma = -1$ for $j = 2$

for $\ell \neq k$ $$g^{ij}_{\ell k} = - \gamma \alpha_3 \lambda L \quad j = 1, 2 \tag{6.2.20}$$

and $$\gamma = + 1 \quad \text{for} \quad \ell = 1, k = 2$$

$$\gamma = - 1 \quad \text{for} \quad \ell = 2, k = 1$$

There is a special case when the element under consideration contains the source node. In this instance, the integrals I_1 and I_2 are indeterminate as $r_3 \to L$, but may be evaluated in the limiting sense using L'Hopital's rule. (see Appendix A).

6.2.4 B.E.M. Quadratic Elements

The relevant shape functions corresponding to the 3 nodes of the element, (see Figure 6.2.3. c), are given by,

$$\phi_1 = \frac{1}{2} (\xi^2 - \xi)$$

$$\phi_2 = \frac{1}{2} (\xi^2 + \xi) \tag{6.2.21}$$

$$\phi_3 = (1 - \xi^2)$$

We now require the evaluation of the 3 $g^{ij}_{\ell k}$ $(j = 1, 3)$ terms given by equation (6.2.2). Consider the term g^{i1}_{11} :

$$g^{i1}_{11} = \frac{L}{2} \int_{-1}^{+1} u^*_{11}(\xi) \, \phi_1 \, (\xi) \, d\xi \tag{6.2.22}$$

Substituting from equations (6.2.3) and (6.2.21), we have,

$$g^{i1}_{11} = \frac{\alpha_2 L}{2} \int_{-1}^{+1} (\xi^2 - \xi) \, d\xi - \frac{\alpha_2 L}{2} \int_{-1}^{+1} \xi^2 \ln(r_3 + \lambda L \xi) \, d\xi$$

$$+ \frac{\alpha_2 L}{2} \int_{-1}^{+1} \xi \ln(r_3 + \lambda L \xi) \, d\xi \tag{6.2.23}$$

or

$$g_{11}^{i1} = \frac{\alpha_1 L}{3} - \frac{\alpha_2 L}{2} \left[I_3(r_3, \lambda L) - I_2(r_3, \lambda L) \right] \tag{6.2.24}$$

Consider the term g_{12}^{i1} :

$$g_{12}^{i1} = -\frac{\alpha_3 \lambda L}{2} \int_{-1}^{+1} (\xi + \xi^2)\, d\xi$$

or

$$g_{12}^{i1} = -\frac{\alpha_3 \lambda L}{3} \tag{6.2.25}$$

As ϕ_1 and ϕ_2 are of the same form (with a change of sign of the ξ term), we may express all the $g_{\ell k}^{ij} (j = 1, 2)$ terms as follows

<u>for $\ell = k$</u> $\quad g_{\ell k}^{ij} = \frac{\beta L}{3} - \frac{\alpha_2 L}{2} \left[I_3(r_3, \lambda L) - \gamma I_2(r_3, \lambda L) \right]$ (6.2.26)

$\beta = \alpha_1$ for $\ell = k = 1$

$\beta = \alpha_4$ for $\ell = k = 2$

$\gamma = +1$ for $j = 1$

$\gamma = -1$ for $j = 2$

<u>for $\ell \neq k$</u>

$$g_{\ell k}^{ij} = -\gamma \frac{\alpha_3 \lambda L}{3} \tag{6.2.27}$$

where,

$\gamma = +1$ for $\ell = 1, k = 2$

$\gamma = -1$ for $\ell = 2, k = 1$

Consider the terms $g_{\ell k}^{i3}$. Equation (6.2.2) gives,

<u>for $\ell = k$</u>

$$g_{\ell k}^{i3} = \beta L \int_{-1}^{+1} (1 - \xi^2)\, d\xi - \alpha_2 L \int_{-1}^{+1} \ln(r_3 + \lambda L \xi) d\xi$$
$$+ \alpha_2 L \int_{-1}^{+1} \xi^2 \ln(r_3 + \lambda L \xi)\, d\xi \tag{6.2.26}$$

or

$$g_{\ell k}^{i3} = \frac{4}{3}\beta L - \alpha_2 L\left[I_1(r_3, \lambda L) - I_3(r_3, \lambda L)\right] \qquad (6.2.27)$$

where $\beta = \alpha_1$ for $\ell = k = 1$

$\beta = \alpha_4$ for $\ell = k = 2$

for $\ell \neq k$

$$g_{\ell k}^{i3} = -\gamma\,\alpha_3\,\lambda L \int_{-1}^{+1} (1 - \xi^2)\, d\xi$$

or

$$g_{\ell k}^{i3} = -\gamma\,\frac{4}{3}\,\alpha_3\,\lambda\,L \qquad (6.2.28)$$

where $\gamma = +1$ for $\ell = 1,\ k = 2$

$\gamma = -1$ for $\ell = 2,\ k = 1$

Again, when the source node, 'i' , is coincident with either of the end nodes of the element $(j = 1, 2)$, I_1, I_2, I_3 must be evaluated using L'Hopital's rule as the limiting case for $r_3 \to L$. (See Appendix A).

There now remains only one special case; when the source node, 'i', is coincident with the centre node of the element under consideration. In this instance, the source point lies within the integration limits, and in order to keep track of the sign changes involved in the local coordinate and the cross terms of the $u^*_{\ell k}$, it is convenient to divide the element into 2 parts.

(i) the left side, (denoted by superscript, ^{L})

(ii) the right side, (denoted by superscript, ^{R})

On the right side we define $\eta = -\xi$, write u^{*R}_k and ϕ^R_j in terms of η . (See Figure 6.2.4), and then divide the integral into two parts. For any function $f(\xi)$ we have,

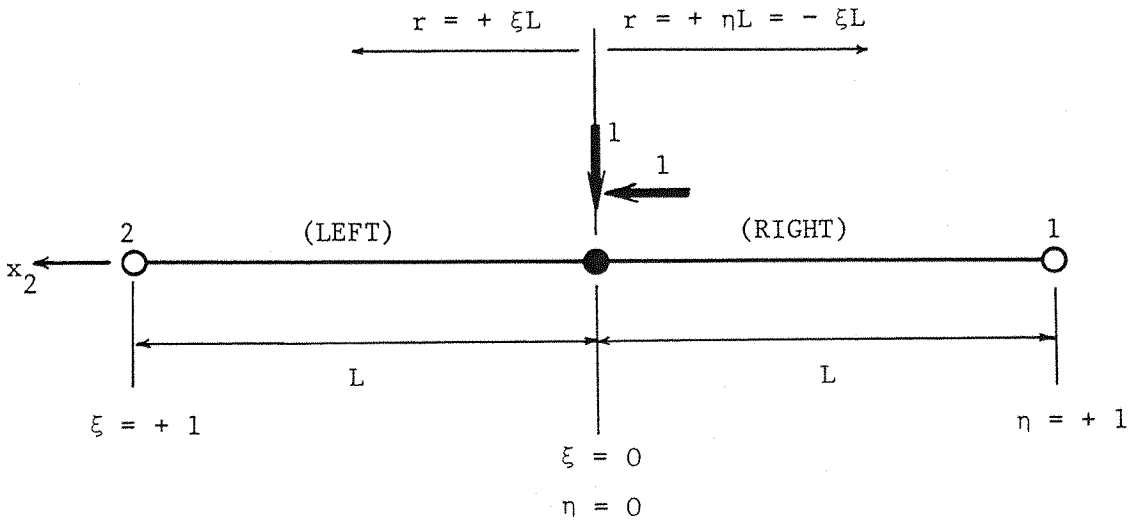

$$\phi_1 = \frac{1}{2}(\xi^2 - \xi) \qquad \phi_1 = \frac{1}{2}(\eta^2 + \eta)$$

$$\phi_2 = \frac{1}{2}(\xi^2 + \xi) \qquad \phi_2 = \frac{1}{2}(\eta^2 - \eta)$$

$$\phi_3 = (1 - \xi^2) \qquad \phi_3 = (1 - \eta^2)$$

$$u^L_{11} = \alpha_1 - \alpha_2 \ln(\xi L) \qquad u^R_{11} = \alpha_1 - \alpha_2 \ln(\eta L)$$

$$u^L_{12} = -\alpha_3 \qquad u^R_{12} = +\alpha_3$$

$$u^L_{21} = +\alpha_3 \qquad u^R_{21} = -\alpha_3$$

$$u^L_{22} = \alpha_5 - \alpha_2 \ln(\xi L) \qquad u^R_{22} = \alpha_5 - \alpha_2 \ln(\eta L)$$

Figure 6.2.4 Source at Centre of Element.

$$\int_{-1}^{+1} f(\xi)\, d\xi = \int_{0}^{+1} f(\xi)\, d\xi + \int_{-1}^{0} f(\xi)\, d\xi \qquad (6.2.29)$$

Now,

$$\int_{-1}^{0} f(\xi)\, d\xi = -\int_{+1}^{0} f(\eta)\, d\eta = \int_{0}^{1} f(\eta)\, d\eta \qquad (6.2.30)$$

For the general case, we have,

$$g_{\ell k}^{ij} = L \int_{-1}^{+1} u_{\ell k}^{*} (\xi)\ \phi_j(\xi)\, d\xi$$

or

$$g_{\ell k}^{ij} = L \int_{-1}^{0} u_{\ell k}^{*R} (\xi)\ \phi_j^{R}(\xi)\, d\xi + L \int_{0}^{1} u_{\ell k}^{*L}(\xi)\ \phi_j^{L}(\xi)\, d\xi \qquad (6.2.31)$$

using equation (6.2.30) for the first term, equation (6.2.31) may be written as,

$$g_{\ell k}^{ij} = L \int_{0}^{1} u^{*R}_{k} (\eta)\ \phi_j^{R} (\eta)\, d\eta + L \int_{0}^{1} u^{*L}_{k}(\xi)\ \phi_j^{L}(\xi)\, d\xi \qquad (6.2.32)$$

The terms $u_{\ell k}^{*R}$, $u_{\ell k}^{*L}$, ϕ_j^{L} , ϕ_j^{R} are given on Figure 6.2.4, and the expressions given by equation (6.2.32) may be readily evaluated.

For the terms containing ϕ_1 and ϕ_2 , we have the following result: ($j = 1, 2$)

<u>for $\ell = k$</u>

$$g_{\ell k}^{ij} = L \left[\frac{\beta}{3} - \alpha_2\ I_6(L) \right] \qquad (6.2.33)$$

where $\beta = \alpha_1$ for $\ell = 1, k = 1$

$\beta = \alpha_4$ for $\ell = 2, k = 2$

for $\ell \neq k$

$$g^{ij}_{\ell k} = - \gamma_1 \gamma_2 \frac{L\alpha_3}{2} \tag{6.2.34}$$

$$\gamma_1 = - 1 \quad \text{for} \quad j = 1$$
$$\gamma_1 = + 1 \quad \text{for} \quad j = 2$$
$$\gamma_2 = + 1 \quad \text{for} \quad \ell = 1, \; k = 2$$
$$\gamma_2 = - 1 \quad \text{for} \quad \ell = 2, \; k = 1$$

And, for the terms containing ϕ_3 $(j = 3)$, we have

for $\ell = k$

$$g^{i3}_{\ell k} = 2L \left\{ \frac{2\beta}{3} - \alpha_2 \left[I_4(L) - I_6(L) \right] \right\} \tag{6.2.35}$$

for $\ell \neq k$

$$g^{i3}_{\ell k} = 0 \tag{6.2.36}$$

6.2.5 Stresses at Internal Points

Given a particular distribution of tractions on the surface, the stresses at any internal point within the domain may be calculated by numerical integration.

The stresses due to a point load at the surface are given by a simple radial distribution (See [1]). Referring to Figure 6.2.5, and denoting σ^{*k}_{ij} as the stress component σ^{*}_{ij}, at q, due to a point load in the 'k' direction at S, the fundamental solution for the stress components is given by :

$$\sigma^{*1}_{11} = - \frac{2}{\pi A_1} \cos^4\theta \; ; \; \sigma^{*2}_{11} = - \frac{2}{\pi A_2} \sin^2\theta \cos^2\theta$$
$$\sigma^{*1}_{22} = - \frac{2}{\pi A_1} \sin^2\theta \cos^2\theta \; ; \; \sigma^{*2}_{22} = - \frac{2}{\pi A_2} \sin^4\theta \tag{6.2.37}$$
$$\sigma^{*1}_{12} = - \frac{2}{\pi A_1} \sin\theta \cos^3\theta \; ; \; \sigma^{*2}_{12} = - \frac{2}{\pi A_2} \sin^3\theta \cos\theta$$

For a general load p_1, p_2 at the surface, the stress at q is given by

$$\sigma_{ij}(q) = \sigma^{*k}_{ij}(S, q)\ p_k(S) \qquad (6.2.38)$$

Given the interpolation for p_k, over each element, equation (6.2.38) may be integrated to yield the stress at q due to some arbitrary load on the surface.

$$\sigma_{ij}(q) = \left\{ \sum^{NE} L_e \int_{\xi=1}^{\xi=+1} \sigma^{*k}_{ij}\left(\theta(\xi)\right)\ \underset{\sim}{\phi}^T(\xi)\ d\xi \right\} \underset{\sim}{P} \qquad (6.2.39)$$

A simple Gauss Quadrature numerical integration scheme may be used to evaluate the above expression. For 'n' sample points on each element, with weightings W_n, and at a local coordinate along the element, ξ_n, equation (6.2.39) becomes:

$$\sigma_{ij}(q) = \left[\sum_{e=1}^{NE} L_e \sum^{n} \left\{ W_n\ \sigma^{*k}_{ij}\left(\theta(\xi_n)\right)\ \underset{\sim}{\phi}^T(\xi_n) \right\} \right] \underset{\sim}{P} \qquad (6.2.40)$$

where NE is the number of elements

and L_e is (the length of element e)/2

6.3 FORMATION OF AN 'EQUIVALENT' STIFFNESS MATRIX

The final discretised formed of the B.E.M. equations, (6.2.8) may be written:

$$\underset{\sim}{G}^{-1}\ \underset{\sim}{U} = \underset{\sim}{P} \qquad (6.3.1)$$

Premultiplying by the $\underset{\sim}{M}$ matrix, relating the traction distribution to the equivalent nodal forces, (see equation (3.6.4)), we have

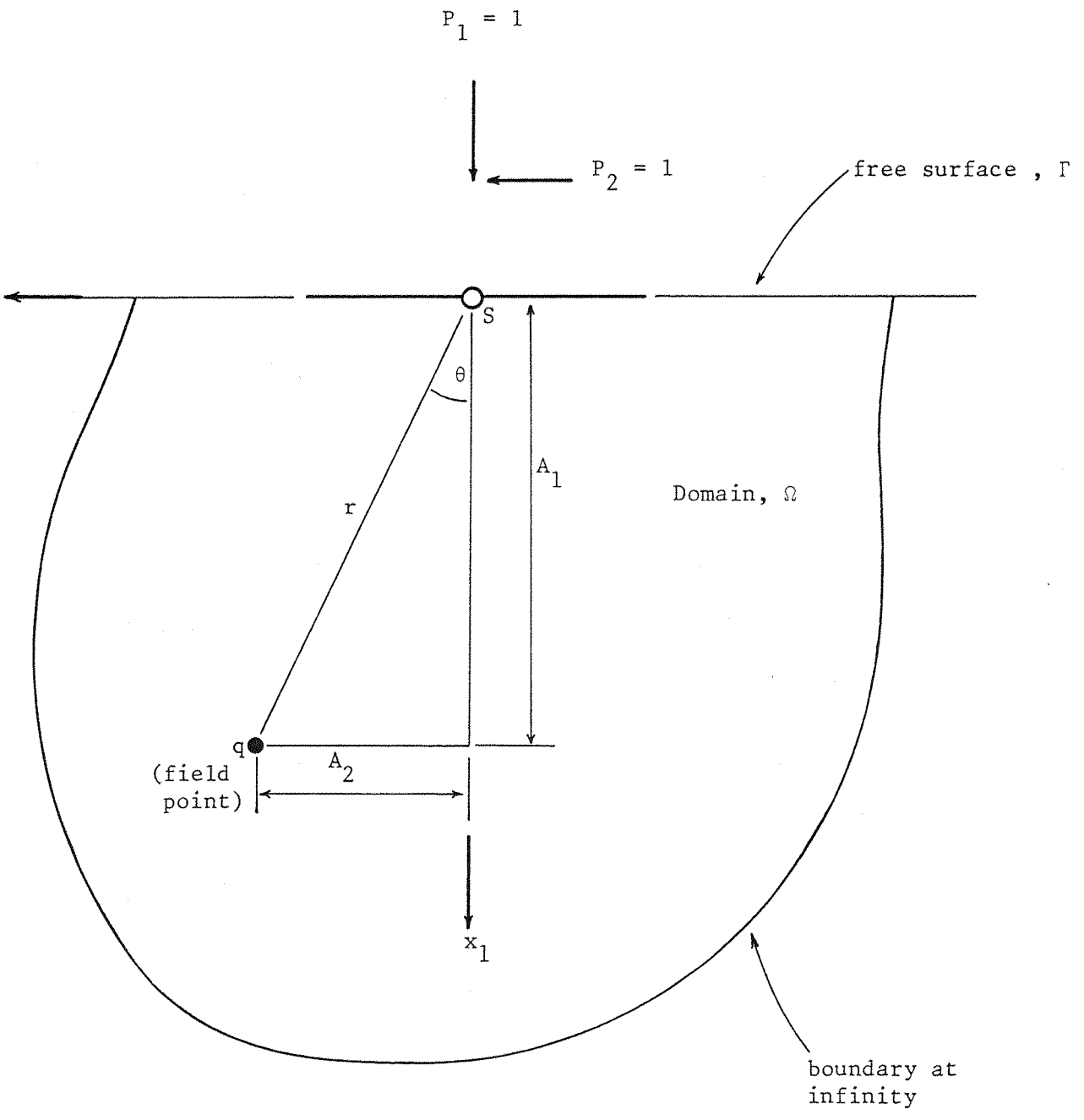

Figure 6.2.5 Geometry of problem for the calculation of the internal stresses.

$$(\underset{\sim}{M}\ \underset{\sim}{G}^{-1})\ \underset{\sim}{U} = \underset{\sim}{M}\ \underset{\sim}{P} = \underset{\sim}{F} \tag{6.3.2}$$

or

$$\underset{\sim}{K}^{u}\ \underset{\sim}{U} = \underset{\sim}{F} \tag{6.3.3}$$

Assuming the same interpolation for displacements and tractions, $\underset{\sim}{\Phi}^{T}$, the matrix $\underset{\sim}{M}$ is given by, (see section 4.2)

$$\underset{\sim}{M} = \sum_{e=1}^{NE} \left\{ L \int \underset{\sim}{\Phi}\ \underset{\sim}{\Phi}^{T}\, d\xi \right\} \tag{6.3.4}$$

The integral may be evaluated for each element, forming the submatrix $\underset{\sim e}{M}$, which can then be assembled into $\underset{\sim}{M}$ in the usual manner. Evaluating the integral yields the following results:

(i) For Constant Elements

$$\underset{\sim e}{M} = L \begin{vmatrix} 1 & 0 \\ 0 & 1 \end{vmatrix} \tag{6.3.5}$$

(ii) For Linear Elements

$$\underset{\sim e}{M} = \frac{L}{6} \left[\begin{array}{cc:cc} 2 & 0 & 1 & 0 \\ 0 & 2 & 0 & 1 \\ \hdashline 1 & 0 & 2 & 0 \\ 0 & 1 & 0 & 2 \end{array}\right] \begin{matrix} \\ \\ N1 \\ \\ \\ N2 \end{matrix} \qquad \begin{matrix} \\ \\ - - \\ \\ \\ \end{matrix} \tag{6.3.6}$$

$$\begin{matrix} N1 & & N2 \end{matrix}$$

(iii) For Quadratic Elements

$$\underset{\sim e}{M} = \frac{L}{15} \left[\begin{array}{cc:cc:cc} 2 & 0 & -\frac{1}{2} & 0 & 1 & 0 \\ 0 & 2 & 0 & -\frac{1}{2} & 0 & 1 \\ \hdashline -\frac{1}{2} & 0 & 2 & 0 & 1 & 0 \\ 0 & -\frac{1}{2} & 0 & 2 & 0 & 1 \\ \hdashline 1 & 0 & 1 & 0 & 8 & 0 \\ 0 & 1 & 0 & 1 & 0 & 8 \end{array}\right] \begin{matrix} \\ \\ N1 \\ \\ \\ N2 \\ \\ \\ N3 \end{matrix} \qquad \begin{matrix} \\ \\ - - \\ \\ \\ - - \\ \\ \\ \end{matrix} \tag{6.3.7}$$

$$\begin{matrix} N1 & & N2 & & N3 \end{matrix}$$

where, L is the length of the element, e , and N1, N2, N3 refer to nodes 1, 2, 3 of the element.

For reasons, which have been discussed at length in Chapters 4 and 5, the 'equivalent' stiffness matrix, $\underset{\sim}{K}^{u}$, is not inherently symmetric in the general case. The usual symmetisation process is adopted, i.e.

$$\underset{\sim}{K}^{s} = \frac{1}{2} (\underset{\sim}{K}^{u} + \underset{\sim}{K}^{u,T}) \qquad (6.3.8)$$

The behaviour of the symmetric 'equivalent' stiffness matrix is examined, upon implementation, in the following section.

6.4 NUMERICAL TESTING OF THE FORMULATIONS

6.4.1 Examples

A series of examples were run, implementing the B.E.M. and 'equivalent' stiffness formulations described in the preceding sections. The examples run are all of the form depicted by Figure 6.2.1, with the distribution of the applied load taken to be of the same order as the shape functions used in the formulation. As such, we expect the model to yield the analytic solution for the deformed shape.

Each of the three problems were run by discretising the loaded segment into 4 elements. (It should be noted that as the shape functions, in each case, can represent the traction distribution exactly, the solution is independent of the number of elements used. This was in fact found to be the case, and was used as one of the first tests on the program. However, using one element, only implements the special cases of the integrals described in Section 6.2, and the use of more elements not only enables solution at more points, but will serve as a better illustration of the general behaviour of the model). For each problem, 2 discretisations

were used; firstly dividing the loaded segment into elements of equal length, (Mesh A, Figure 6.4.1.a), and secondly employing elements of varying lengths (Mesh B, Figure 6.4.1.b).

In each case, the $\underset{\sim}{G}$ matrix was calculated (equation (6.2.8)), from which the displacements are immediately available (B.E.M.). Following this, the 'equivalent' stiffness matrices, $\underset{\sim}{K}^{u}$ and $\underset{\sim}{K}^{s}$ were formed and the tractions weighted in the appropriate manner to calculate the equivalent nodal forces for each type of traction distribution. The equations were then solved as a stiffness problem. The solution using $\underset{\sim}{K}^{u}$ and the B.E.M. give exactly the same results as the same equations are being solved in both cases, (and this served as a useful check on the 'equivalent' stiffness program). Also, the fundamental solution may in fact be integrated along the loaded segment to yield the analytic solution. (This is in fact what the B.E.M. formulation presented in this chapter does, but employs a segmented integration process).

In order to facilitate comparisons, all calculations were performed using identical values of the arbitrary constants of integration involved in the fundamental solution i.e. all displacements in the direction of the load are effectively being measured from the same datum.

In all cases it was found that, as expected, the analytic solution, the B.E.M. solution, and the $\underset{\sim}{K}^{u}$ solution were in exact agreement. Comparisons of this solution with that obtained using the symmetrised 'equivalent' stiffness matrix, $\underset{\sim}{K}^{s}$, is given in tables 6.4.1 - 6.4.3.

The same series of examples were also used as a basis for further examination of the behaviour of the 'equivalent' stiffness matrices, $\underset{\sim}{K}^{u}$ and $\underset{\sim}{K}^{s}$. The resulting displacement profile was substituted back into the B.E.M. equations (6.3.1), in order to obtain the corresponding starting form of the traction distribution. This serves as a useful

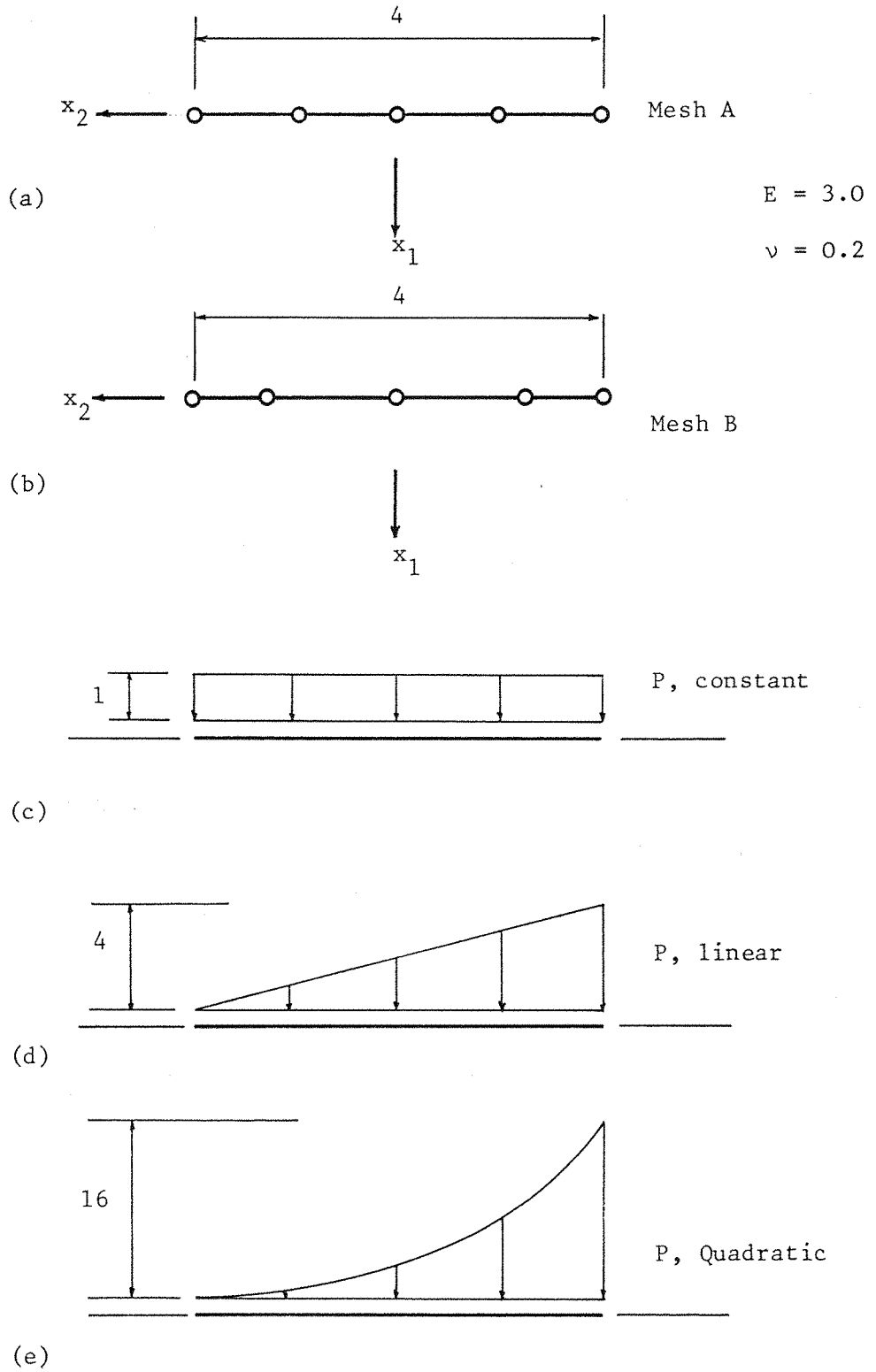

Figure 6.4.1 Boundary Element discretisations and load distributions.

x_2	Analytic, B.E.M., and $\underset{\sim}{K}^u$		$\underset{\sim}{K}^s$	
	u_1	u_2	u_1	u_2
- 1.50	3.800	0.360	3.800	0.360
- 0.50	4.032	0.120	4.032	0.120
0.50	4.032	- 0.120	4.032	- 0.120
1.50	3.800	- 0.360	3.800	- 0.360

(a) MESH A

x_2	Analytic, B.E.M., and $\underset{\sim}{K}^u$		$\underset{\sim}{K}^s$	
	u_1	u_2	u_1	u_2
- 1.50	3.800	0.360	3.801	0.360
- 0.60	4.021	0.144	4.012	- 0.108
0.45	4.037	- 0.108	4.045	- 0.108
1.55	3.780	- 0.372	3.775	- 0.372

(b) MESH B

Table 6.3.1 Displacement Profile for Constant Traction using Constant Elements.

x_2	Analytic, B.E.M., and $\underset{\sim}{K}^u$		$\underset{\sim}{K}^s$	
- 2.00	u_1	u_2	u_1	u_2
- 2.00	6.172	0.960	6.157	0.956
- 1.00	7.160	0.840	7.167	0.838
0.00	8.116	0.480	8.107	0.491
1.00	8.646	- 0.120	8.680	- 0.165
2.00	7.802	- 0.960	7.778	- 0.810

(a) MESH A

x_2	Analytic, B.E.M., and $\underset{\sim}{K}^u$		$\underset{\sim}{K}^s$	
	u_1	u_2	u_1	u_2
- 2.00	6.172	0.960	6.147	0.944
- 1.00	7.160	0.840	7.198	0.860
- 0.20	7.946	0.571	7.926	0.532
1.10	8.655	- 0.193	8.663	- 0.167
2.00	7.802	- 0.960	7.809	- 0.861

(b) MESH B

Table 6.3.2. Displacement Profile for Linear Traction Distribution using Linear Elements.

x_2	Analytic, B.E.M., and $\underset{\sim}{K}^u$		$\underset{\sim}{K}^s$	
	u_1	u_2	u_1	u_2
- 2.00	22.253	2.560	21.959	2.405
- 1.50	24.335	0.867	24.564	0.931
- 1.00	23.819	- 0.400	23.505	- 0.470
- 0.50	22.510	- 1.310	22.636	- 1.276
0.00	20.919	- 1.920	20.782	- 1.959
0.50	19.320	- 2.290	19.367	- 2.272
1.00	17.874	- 2.480	17.830	- 2.500
1.50	16.670	- 2.550	16.681	- 2.543
2.00	15.734	- 2.560	15.728	- 2.566

(a) MESH A

x_2	Analytic, B.E.M., and $\underset{\sim}{K}^u$		$\underset{\sim}{K}^s$	
	u_1	u_2	u_1	u_2
- 2.00	22.253	2.560	21.962	2.410
- 1.50	24.337	0.867	24.566	0.927
- 1.00	23.819	- 0.400	23.502	- 0.457
- 0.60	22.810	- 1.153	22.944	- 1.125
- 0.20	21.574	- 1.708	21.429	- 1.764
0.45	19.479	- 2.262	19.538	- 2.233
1.10	17.615	- 2.502	17.563	- 2.528
1.55	16.567	- 2.553	16.578	- 2.546
2.00	15.737	- 2.560	15.728	- 2.567

(b) MESH B

Table 6.3.3. Displacement Profile for Quadratic Traction Distribution using Quadratic Elements.

of the sensitivity of the respective formulations in obtaining a solution for the tractions at the surface, once the displacements have been established by some overall F.E.M. displacement technique. The same problems as those depicted in Figures 6.4.1 were run using the formulations based on constant, linear and quadratic elements. The loaded segment was discretised using (i) 4 equal length elements (as shown in Figure 6.4.1.a, Mesh A), and, (ii) 8 unequal length elements (as shown in Figure 6.4.1.b, with each element divided into 2-Mesh B).

As no approximations are introduced when using $\underset{\sim}{K}^{u}$, then the tractions given by equation 6.3.1 should be exactly equal to the original distributions (Figures 6.4.1, c, d, e), and this was simply used as a check on the programming. Comparisons of the traction distributions obtained using the displacements derived after the symmetrisation process of $\underset{\sim}{K}^{u}$ (i.e. using $\underset{\sim}{K}^{s}$) as shown in Figures 6.4.2 - 6.4.4.

6.4.2 Discussion of Results

The B.E.M., or alternatively, the 'equivalent' stiffness approach, using $\underset{\sim}{K}^{u}$, always yield the exact deformed shape of the free surface. In general, therefore, the accuracy of the solution for some arbitrary loading will only depend on how closely the chosen interpolation functions can model the actual traction distribution at the surface. This is of course to be expected, and the improvement of accuracy with increasing orders of approximating functions, is a feature true for all numerical approximation techniques; but the powerful aspect of the present formulation is the fact that there is no approximation for displacements, and the solution is exact for the given loading.

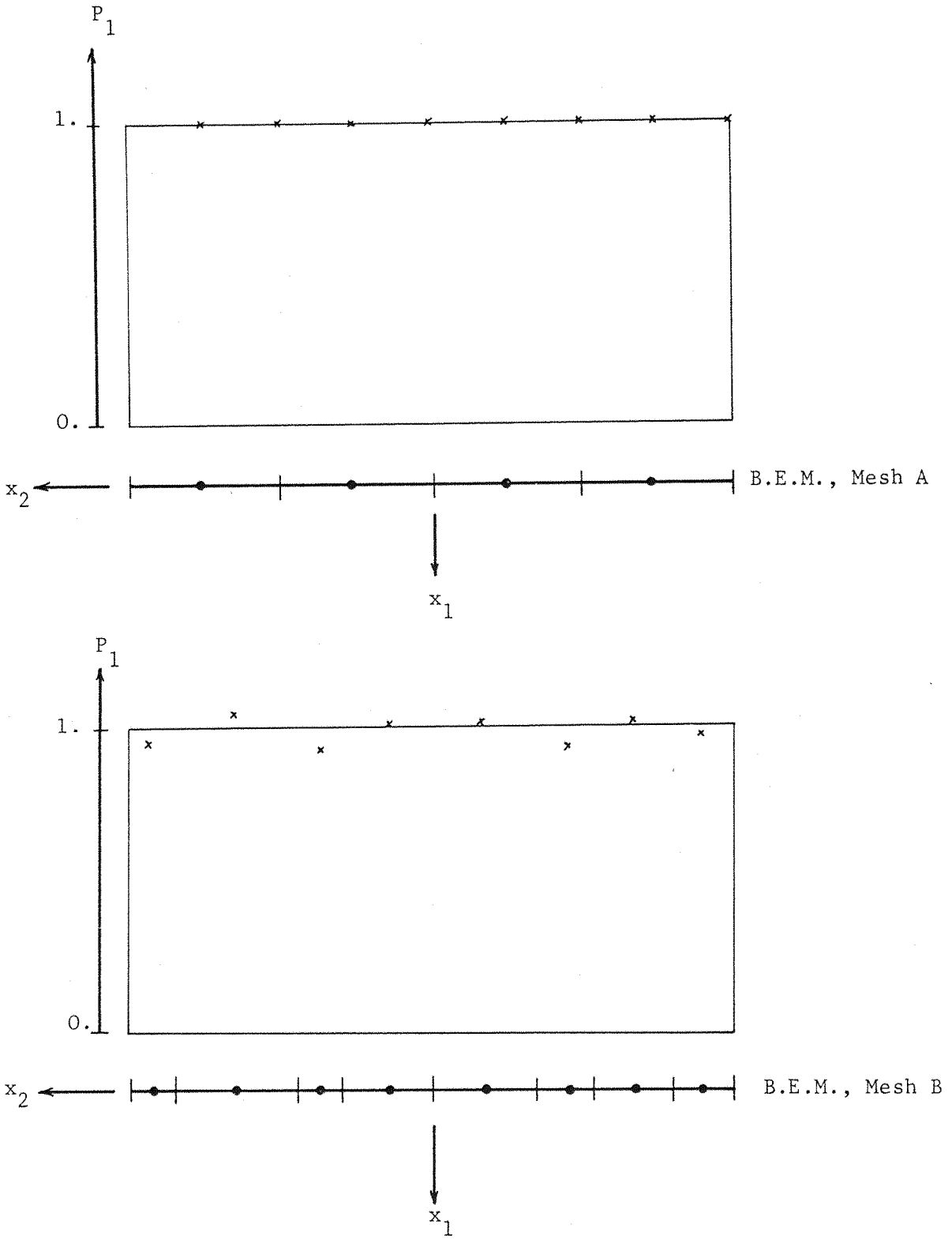

Figure 6.4.2 Traction Distibution for Constant Element Run.

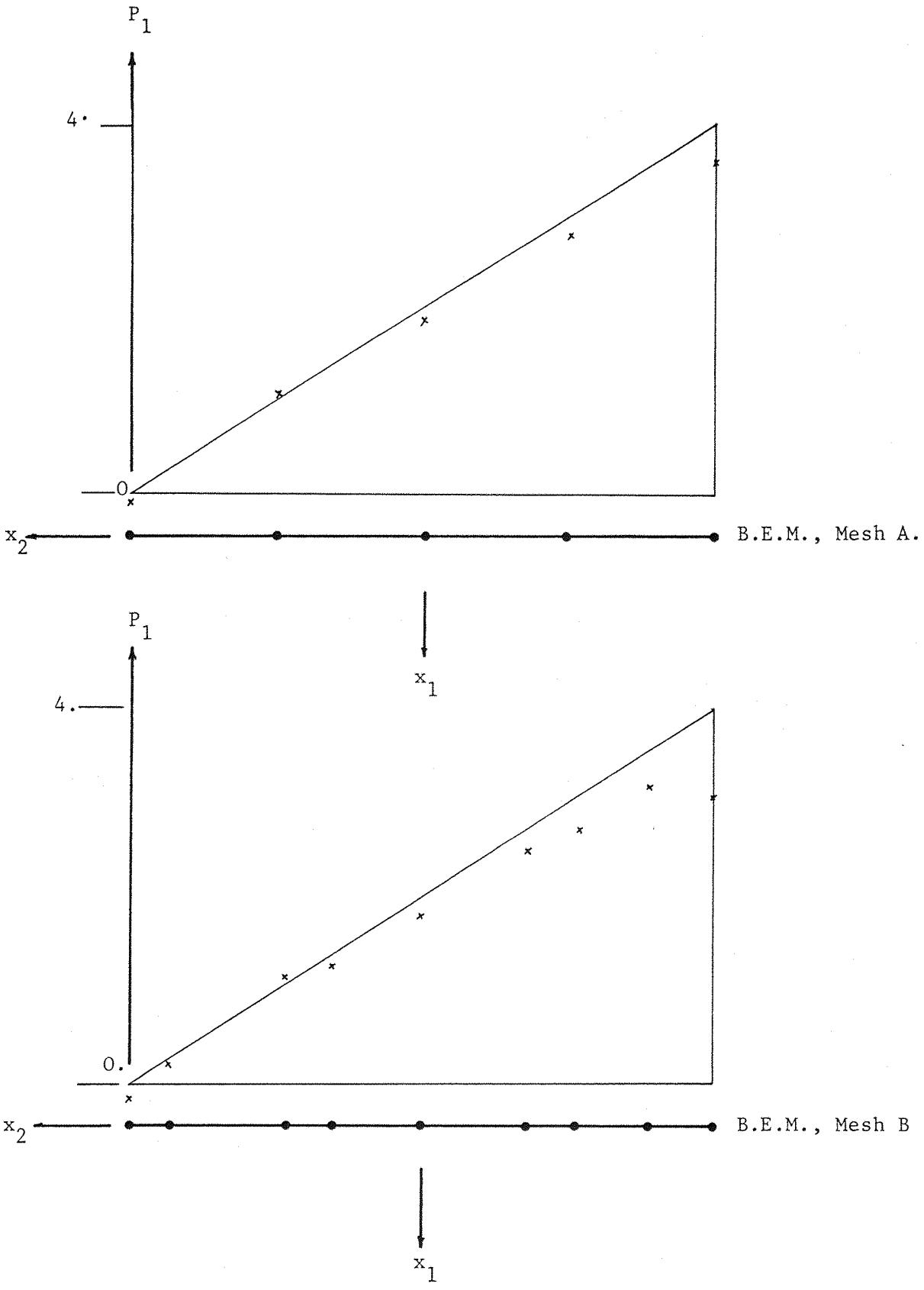

Figure 6.4.3 Traction Distribution for Linear Element Run.

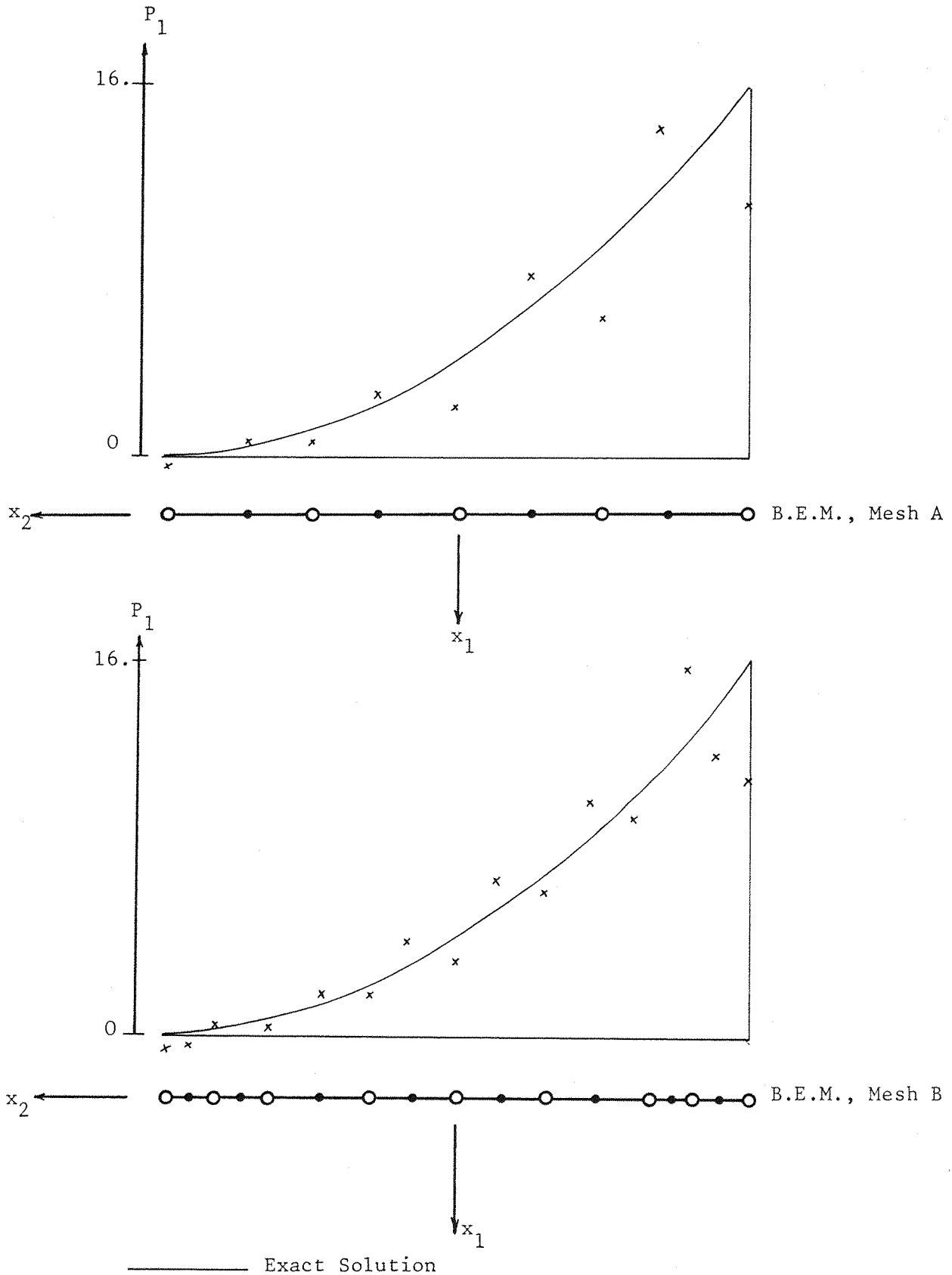

Figure 6.4.4 Traction distribution for Quadratic Element Run.

The behaviour of solutions obtained using the symmetrised form of the 'equivalent' stiffness matrix, $\underset{\sim}{K}^{s}$, follows the established pattern, shown by the examples of the previous chapters. The level of error introduced by the symmetrisation process is of an acceptable magnitude for most practical engineering applications, but it is interesting to note that the higher the order of the elements, the larger the error; especially for the case of obtaining the traction distribution from a given set of 'approximate' displacements. This is an important aspect of the formulation and requires further discussion.

In this case, the unsymmetry in $\underset{\sim}{K}^{u}$ arises due to the differing sizes of the elements and differing forms of interpolation functions associated with particular points. As before, the effect of the differing lengths is largely scaled out by the $\underset{\sim}{M}$ matrix, and as can be seen by tables 6.3.1 - 6.3.3, the degree of error is not generally increased by having an unsymmetric discretisation (i.e. varying the lengths of the elements). The exception is of course the case of constant elements, which form a perfectly symmetric matrix, if all the lengths are the same.

For higher order elements, there is an additional factor involved in the lack of symmetry: Consider the case of linear elements, and 2 nodes i, j, one of which is one of the end nodes (Figure 6.4.5.a). When forming the subelement $g_{\ell k}^{ji}$, a source is applied at 'j' and the integral performed over both the elements adjacent to the 'i' , and their contributions added. However, there is only one contribution for the term $g_{\ell k}^{ij}$, as there is only one element adjacent to 'j' . (See Figures 6.4.5.b, c). For the use of quadratic elements there is still a further factor involved. The shape functions associated with midside nodes are of a different form to those associated with nodes

at the end of the element, and this introduces a further lack of symmetry in the integration process. (See Figure 6.4.6).

It is perfectly clear, therefore, that the symmetrisation process introduces an error into the solution, but does not seem to greatly affect the displacement profile, in the general case. However, when using this 'erroneous' displacement profile to calculate the traction distribution, the sensitivity of the system to the degree of 'error' in the displacements increases as does the order of the elements: The constant element solution (Figure 6.4.2) is very good, and this is to be expected as the formulation exhibits the least problems with regards to symmetry. The linear element solution is again in good agreement, most of the error occurring at the end of the segment, which again is to be expected due to the unsymmetric effect of the end nodes. The quadratic element solution is comparatively poor in this aspect. and is due to the combined unsymmetry effects described above, which make the system very sensitive to differences in displacements.

However, it should be noted, that in a combined problem, where the surface nodes are joined to some Finite Element model, the degree of the unsymmetry effect will be diminished. This is due to the fact that the terms of $\underset{\sim}{K}^{u}$ will be assembled into a global stiffness matrix, and will be added to the terms of the Finite Element stiffness matrices corresponding to the nodes on the interface. These terms will be symmetric, and as such the relative error introduced by the symmetisation process will be reduced. The degree of this 'reduction' in the error will depend on the relative stiffness of the two regions, which is the determining factor governing the orders of the terms involved. This aspect is discussed in greater detail, following the combination examples of the following section.

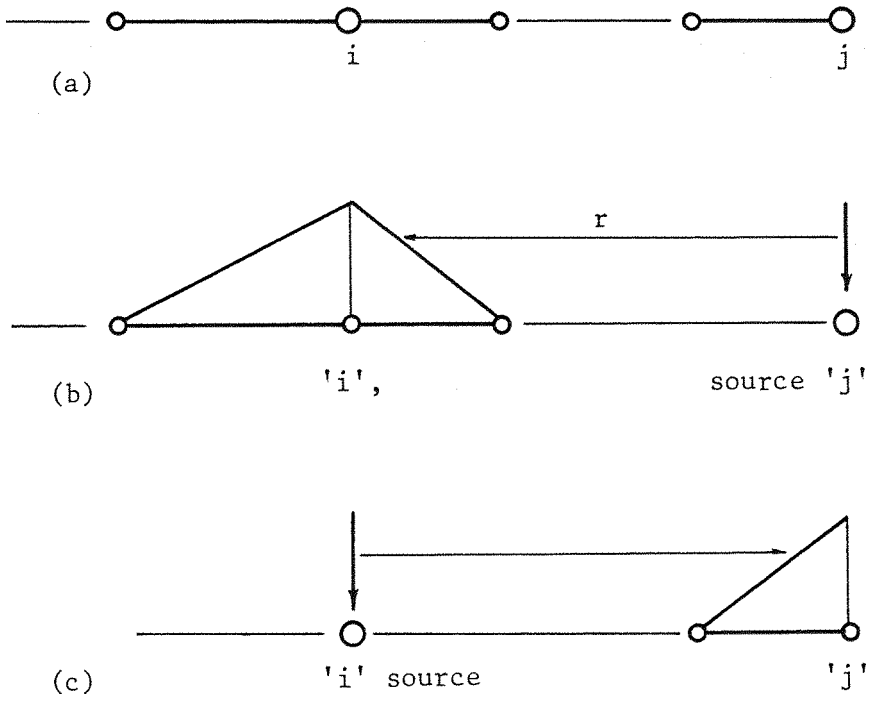

Figure 6.4.5 Linear Elements Reciprocal integration.

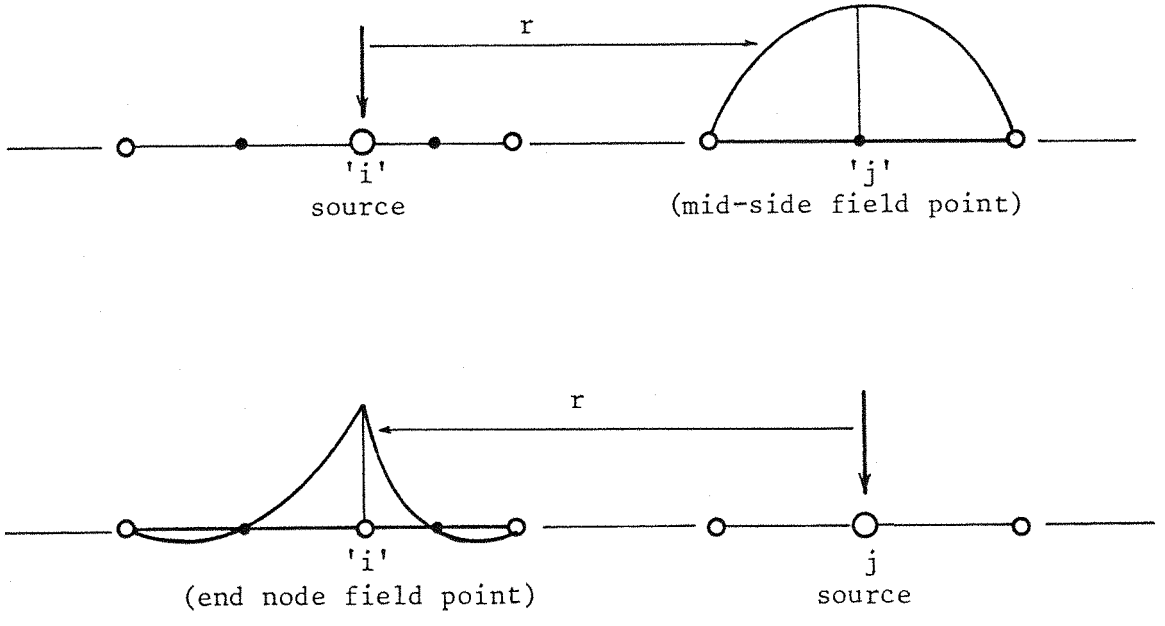

Figure 6.4.6 Quadratic Elements. Reciprocal Integration.

6.5 COMBINATION PROBLEMS

6.5.1 General Remarks

The equivalent stiffness matrix which models the behaviour of the semi-infinite half space, may now be incorporated in a Finite Element package in order to model a structure resting on a semi inifinite foundation, (Figure 6.5.1). The Finite Elements employed, are 6-noded linear strain triangles, and are used to form an overall displacement type model,

$$\underset{\sim}{K}\,\underset{\sim}{U} = \underset{\sim}{F} \qquad (6.5.1)$$

Solution of (6.5.1) yields all unknown displacements; the stresses in the Finite Element domain Ω_2 may then be calculated in the normal way. The tractions at the interface may now be computed using equation (6.3.1) for the semi-infinite region. Integration of these tractions yield the internal stresses at any points in Ω_2 . (See Section 6.2.5).

A Finite Element program was written which also forms the additional stiffness matrices ($\underset{\sim}{K}^u$ and $\underset{\sim}{K}^s$) representing the semi-infinite foundation, and assembles the extra contributions into the global stiffness matrix in the usual manner. The program was written with the option of using linear or quadratic elements to model the half-space, and also solved each problem twice : firstly using $\underset{\sim}{K}^u$ and secondly $\underset{\sim}{K}^s$. The constant element formulation was omitted due to its inability to make a good approximation of an arbitrary load variation, without a very fine discretisation. For reasons of expediency in performing the tests, the program developed, stored the whole of the stiffness matrix, when using $\underset{\sim}{K}^u$, and used a solver which took no account of any symmetry. This is in fact very uneconomical especially in a problem where the

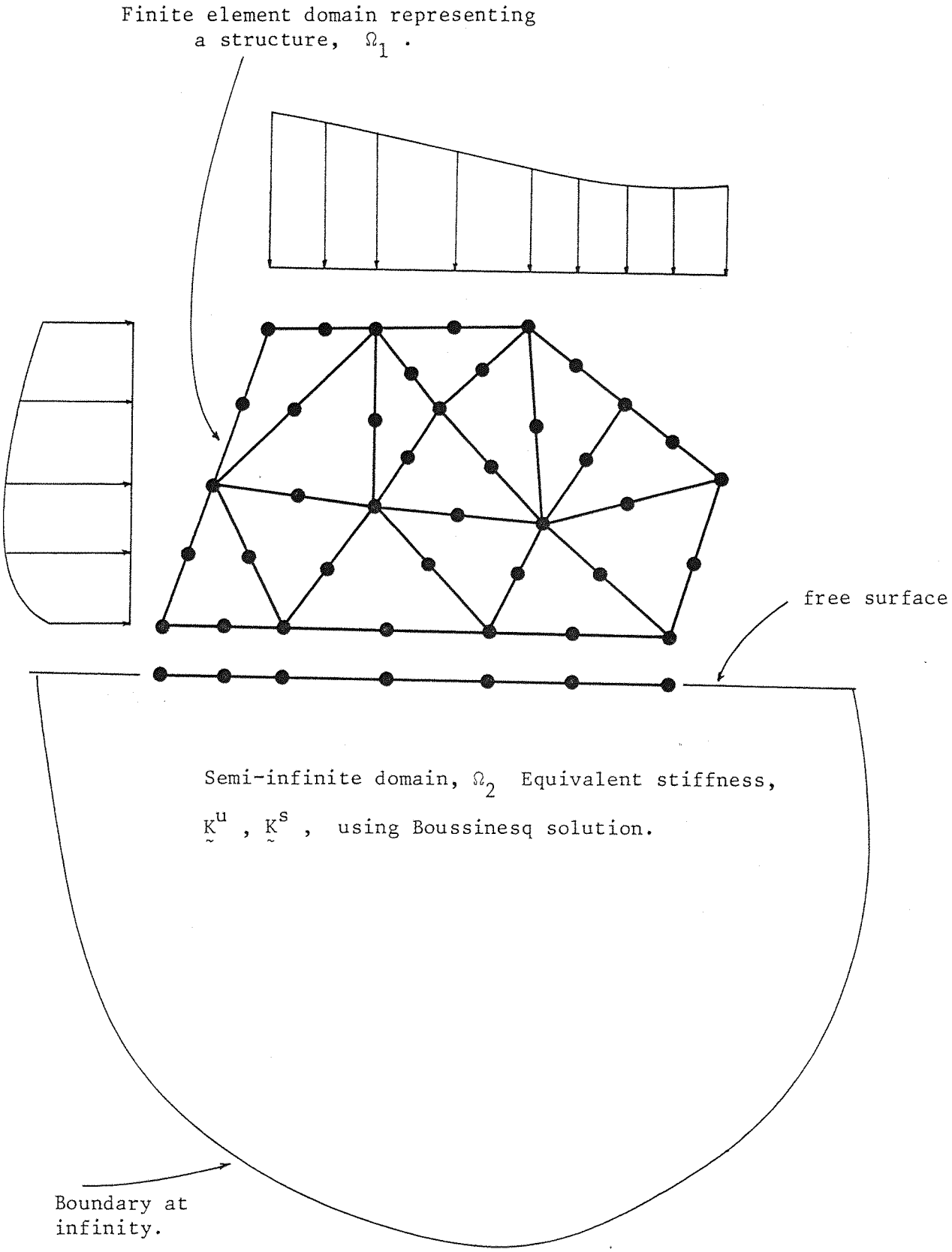

Figure 6.5.1 Semi-infinite domain combination problem.

unsymmetric part is relatively small, but the efficiency may be greatly improved by partitioning the solution : Consider the general combination problem shown in Figure 6.5.2 (a). All contributions to $\underset{\sim}{K}$ from the Finite Element part, ($\underset{\sim}{K}_{II}$, $\underset{\sim}{K}_{IJ}$, $\underset{\sim}{K}_{JI}$) , are symmetric, ($\underset{\sim}{K}_{IJ} = \underset{\sim}{K}_{JI}^{T}$) , and the only unsymmetric part is $\underset{\sim}{K}_{JJ}$. (See Figure 6.5.2.(b)). We may now write the equations as follows:

$$\underset{\sim}{K}_{II}\ \underset{\sim}{U}_{I} + \underset{\sim}{K}_{IJ}\ \underset{\sim}{U}_{J} = \underset{\sim}{F}_{I} \tag{6.5.1}$$

$$\underset{\sim}{K}_{JI}\ \underset{\sim}{U}_{I} + \underset{\sim}{K}_{JJ}\ \underset{\sim}{U}_{J} = \underset{\sim}{F}_{J} \tag{6.5.2}$$

Equation (6.5.1) may be written

$$\underset{\sim}{U}_{I} = \underset{\sim}{K}_{II}^{-1}\ (\underset{\sim}{F}_{I} - \underset{\sim}{K}_{IJ}\ \underset{\sim}{U}_{J}) \tag{6.5.3}$$

Substituting equation (6.5.3) in equation (6.5.2),

$$\underset{\sim}{K}_{JJ}\ \underset{\sim}{U}_{J} = \underset{\sim}{F}_{J} - \underset{\sim}{K}_{JI}\ \underset{\sim}{K}_{II}^{-1}\ (\underset{\sim}{F}_{I} - \underset{\sim}{K}_{IJ}\ \underset{\sim}{U}_{J}) \tag{6.5.4}$$

or

$$\hat{\underset{\sim}{K}}_{JJ}\ \underset{\sim}{U}_{J} = \hat{\underset{\sim}{F}}_{J} \tag{6.5.5}$$

where

$$\begin{aligned} \hat{\underset{\sim}{K}}_{JJ} &= \underset{\sim}{K}_{JJ} - \underset{\sim}{K}_{JI}\ \underset{\sim}{K}_{II}^{-1}\ \underset{\sim}{K}_{IJ} \\ \hat{\underset{\sim}{F}}_{J} &= \underset{\sim}{F}_{J} - \underset{\sim}{K}_{JI}\ \underset{\sim}{K}_{II}^{-1}\ \underset{\sim}{F}_{I} \end{aligned} \tag{6.5.6}$$

This process is more efficient than storing the full band of the equations and not making use of any symmetry during solution , - especially if the 'JJ' part of the equations is relatively small. The inversion of the K_{II} part of the matrix is performed independently and full use of symmetry may be made in both the storage and solution

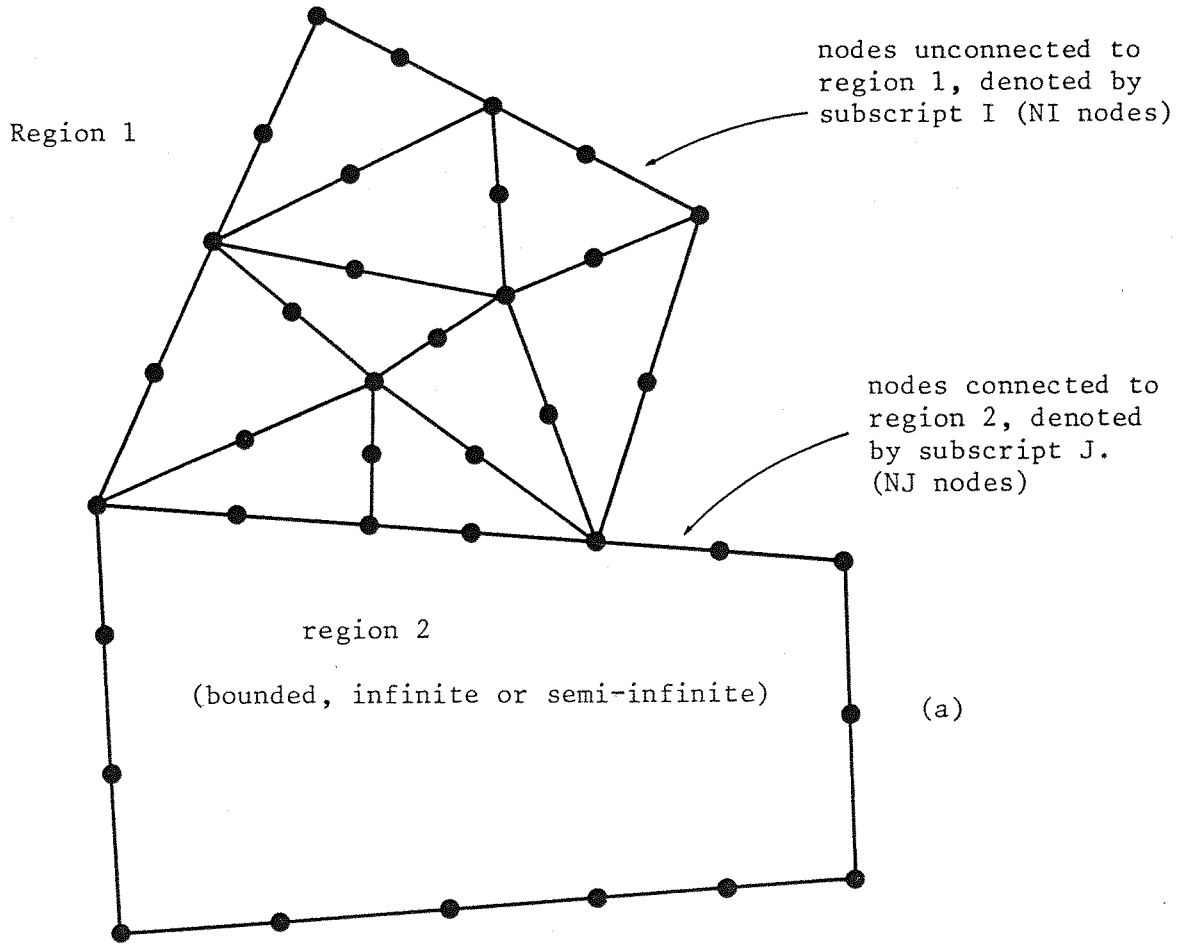

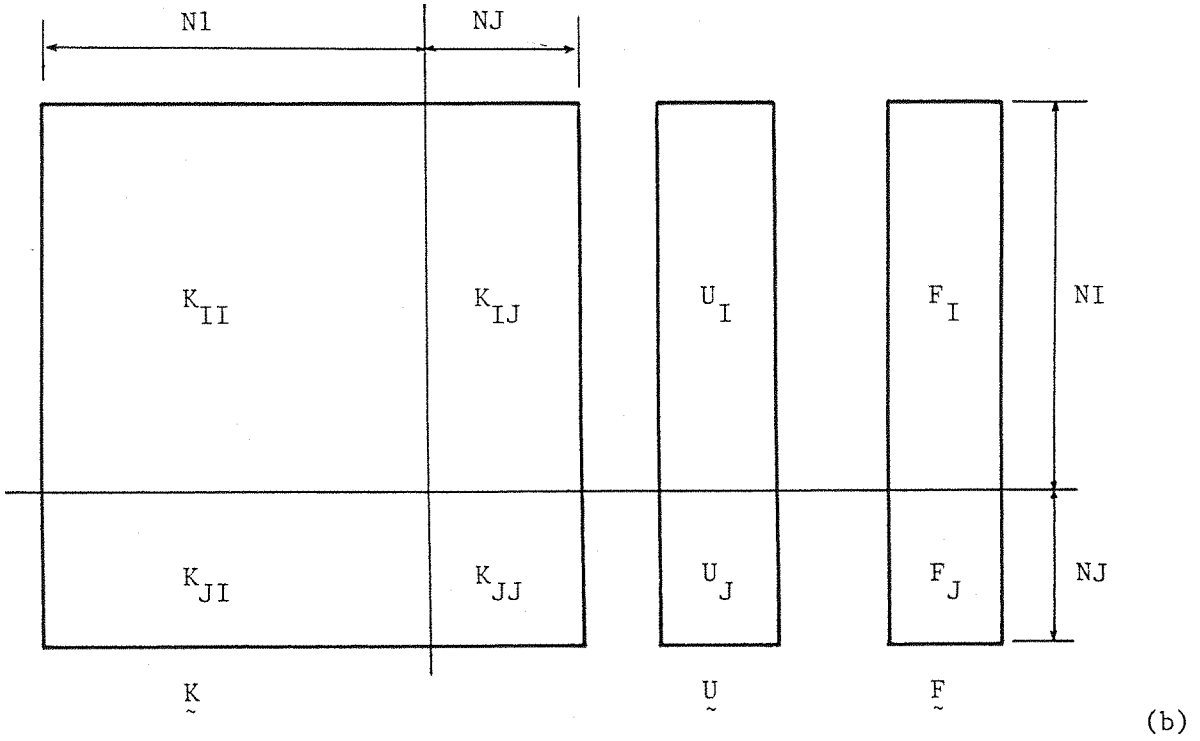

Figure 6.5.2 Partitioning of the system of equations for the combination problem.

schemes. The relatively small unsymmetric equations (6.5.5) may now be solved for $\underset{\sim}{U}_J$ and the solution substituted in equations (6.5.3) to yield the remaining unknowns, $\underset{\sim}{U}_I$.

6.5.2 Examples

A series of examples were run for a deep beam, axially loaded, resting on a semi-infinite foundation, which may be used to demonstrate a typical soil structure interaction problem. The deep beam represents a structure and is modelled using Finite Elements to discretise its domain, whereas, the semi-infinite foundation is modelled using a Boundary Element discretisation of the interface segment. Due to the expected stress concentrations at the bottom corners of the beam, the mesh is quite refined in that neighbourhood. The Finite and Boundary element discretisations employed, are shown in Figure 6.5.3.

The series of examples were run for a point load of 6.0 acting at the top of the beam, in the direction of its length, and solutions were obtained for varying values of the relative stiffness of the beam and foundation. The Young's Modulus of the semi-infinite space was kept constant at $E_2 = 2.4$, and E_1 took the values 2.4, 24, 240, 2400, in turn; each problem was run using, firstly, 16 linear, and secondly, 8 quadratic Boundary Elements for the interface segment (the nodal points, of course, corresponding to those of the Finite Element mesh). Also, each case was run using both $\underset{\sim}{K}^u$ and $\underset{\sim}{K}^s$, to represent the stiffness of the foundation.

Tables 6.5.1 - 6.5.4 show the traction profile (in the direction of the load) along the interface, for each case, and these results demonstrate some interesting features of the behaviour of the technique :-

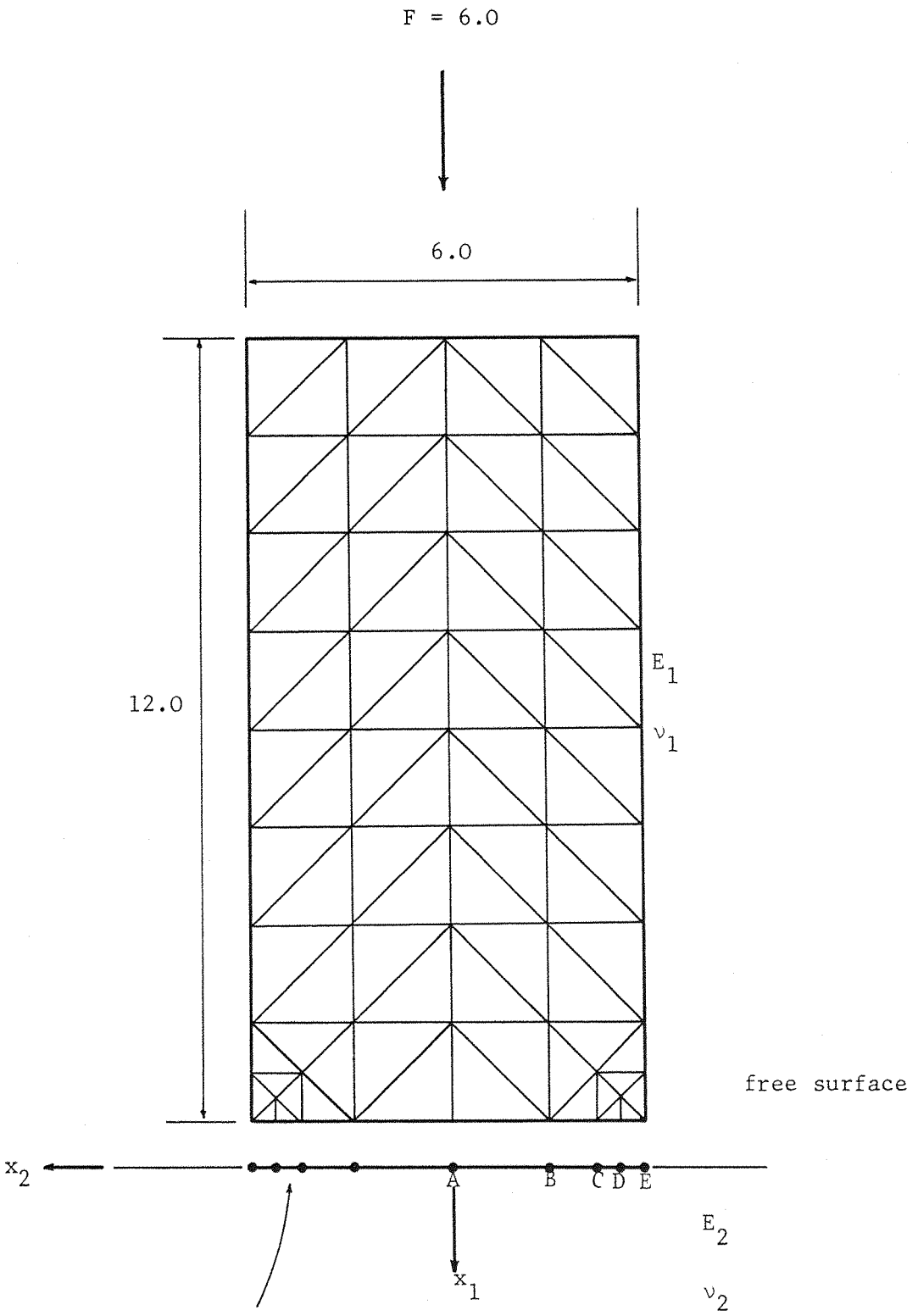

Figure 6.5.3 Deep Beam supported on a semi-infinite half-space.

x_2	Linear Boundary Elements		Quadratic Boundary Elements	
	$\underset{\sim}{K}^u$	$\underset{\sim}{K}^s$	$\underset{\sim}{K}^u$	$\underset{\sim}{K}^s$
0.0	0.623	0.624	0.800	0.730
0.75	0.985	0.986	0.802	0.836
1.5	0.650	0.626	0.852	0.753
1.875	1.077	1.114	0.886	0.948
2.25	7.697	7.459	0.962	0.843
2.435	1.283	1.316	1.087	1.155
2.625	0.824	0.816	1.200	0.956
2.8125	1.518	1.850	1.366	1.684
3.0	3.859	3.226	4.676	3.818

$$E_1 = 2.4$$

Table 6.5.1 Interface Tractions for Deep Beam resting on a semi-infinite foundation, with axial load. (relative foundation/structure stiffness 1/1)

x_2	Linear Boundary Elements		Quadratic Boundary Elements	
	$\underset{\sim}{K}^u$	$\underset{\sim}{K}^s$	$\underset{\sim}{K}^u$	$\underset{\sim}{K}^s$
0.0	0.706	0.706	0.727	0.720
0.75	0.763	0.764	0.745	0.750
1.5	0.779	0.777	0.808	0.797
1.875	0.889	0.896	0.872	0.883
2.25	0.961	0.965	0.959	0.953
2.435	1.128	1.139	1.137	1.147
2.625	0.961	1.004	0.774	0.774
2.8125	2.348	2.452	2.307	2.387
3.00	3.087	2.734	3.154	2.752

$E_1 = 24$

Table 6.5.2 Interface Tractions for Deep Beam resting on a semi-infinite foundation, with axial load. (Relative foundation/structure stiffness 1/10).

	Linear Boundary Elements		Quadratic Boundary Elements	
x_2	$\underset{\sim}{K}^u$	$\underset{\sim}{K}^s$	$\underset{\sim}{K}^u$	$\underset{\sim}{K}^s$
0.0	0.724	0.726	0.730	0.729
0.75	0.749	0.749	0.751	0.752
1.5	0.817	0.817	0.824	0.823
1.875	0.898	0.899	0.900	0.901
2.25	1.025	1.026	1.006	1.006
2.4375	1.160	1.162	1.180	1.181
2.625	1.110	1.117	0.806	0.808
2.8125	2.647	2.658	2.519	2.528
3.00	1.711	1.662	1.497	1.442

$E_1 = 240$

Table 6.5.3 Interface Tractions for Deep Beam resting on a semi-infinite foundation, with axial load. (Relative Foundation/Structure stiffness 1/100).

x_2	Linear Boundary Elements		Quadratic Boundary Elements	
	$\underset{\sim}{K}^u$	$\underset{\sim}{K}^s$	$\underset{\sim}{K}^u$	$\underset{\sim}{K}^s$
0.0	0.727	0.727	0.731	0.731
0.75	0.748	0.748	0.752	0.753
1.5	0.822	0.822	0.827	0.827
1.875	0.900	0.901	0.905	0.905
2.25	1.035	1.036	1.014	1.014
2.4375	1.167	1.168	1.188	1.188
2.625	1.133	1.134	0.816	0.817
2.8125	2.682	2.683	2.540	2.541
3.0	1.495	1.490	1.244	1.239

$E_1 = 2400$

Table 6.5.4 Interface Tractions for Deep Beam resting on a semi-infinite foundation, with axial load. (Relative Foundation/Structure stiffness 1/1000).

As the relative stiffness of the structure increases, the actual traction profile becomes more and more singular at the ends of the loaded segment, the numerical results exhibit an oscillation from the true path in this vicinity. This is to be expected, as it is a common feature of many numerical techniques. However, in these cases, the results obtained using linear and quadratic elements are in excellent agreement, and the symmetrisation process introduces very negligible differences in the results. This is because the contributions to the overall stiffness arising from the boundary element part are of a much lower order of magnitude, and hence the differences due to the lack of symmetry in this part of the system do not produce a significant effect when they are removed. (e.g. see results in Tables 6.5.3 and 6.5.4, where the stiffness of the structure is 100 and 1000 times greater than that of the foundation,respectively). The very good agreement between the linear and quadratic element formulation is due to the fact that for a very stiff structure, the interface traction distribution approaches a form of $(9 - x_2^2)^{-\frac{1}{2}}$ (see TIMOSHENKO [1]), and although this is singular as $x_2 \to 3$ -hence the oscillation of the results mentioned above-, there are no sign changes in the function or its derivative, in the region $0 < x_2 < 3$. This means that linear elements can provide almost as good an approximation to the form of the solution as can the quadratic elements.

The situation changes, however, when the structure and foundation have stiffnesses of similar magnitudes. The effects of this are most marked in the results in Table 6.5.1, which represent the situation of a 1/1 ratio in the relative stiffness.

We do not know the expected form of the solution from analytical

techniques, but there is no reason to expect the real solution, and its derivative to be as well behaved in this situation. This is confirmed by the greater differences obtained by using linear or quadratic elements. Furthermore, the structure and foundation stiffnesses provide terms of the same order of magnitude in the global stiffness matrix and hence the symmetisation process of the foundation terms have a much more pronounced effect on the overall solution.

In conclusion, it must be remembered that for typical soil-structure interaction problems, the structure is usually about one order of magnitude stiffer than the soil. As such, the errors introduced by the symmetisation process are relatively small, (e.g. see Table 6.5.2), and $\underset{\sim}{K}^S$ may confidently be used to represent the stiffness of the foundation. As to the choice of the type of Boundary Elements, clearly the quadratic elements will always provide a better model, although the difference between these and linear elements may not be very marked if the actual variation of the interface tractions is of relatively low order. However, as the number of nodes on the surface is determined by the Finite Element mesh to which they must be joined, quadratic elements may as well be employed as no extra work is required in doing so (other than slightly longer expressions for the terms of the $\underset{\sim}{G}$ matrix, which in relation to the overall solution represents a negligible amount of computation).

CHAPTER 7 GENERAL DISCUSSION AND SUMMARY

After presenting the basic principles leading to the Direct Boundary Element formulation, this work has been predominantly concerned with the development, implementation, and testing of an 'equivalent' Finite Element stiffness matrix, derived using a boundary discretisation, for the region under consideration.

The simple transformation of the final set of equations from their Boundary Element form to the form of a Finite Element stiffness type relation is shown in Chapter 4, and the technique was implemented for 2 and 3-Dimensional problems using constant elements. This avoided many of the problems, generally incurred at geometric discontinuities and served as a useful check on the basic formulation. The 'equivalent' stiffness matrix, thus derived, was always found to give the same solution as the Direct B.E.M. which is to be expected, as the same equations are being solved in a different form, without introducing any further approximations than those originally contained in the Boundary Element formulation.

The interesting feature to emerge from this initial part of the work was the general lack of symmetry of the 'equivalent' stiffness matrix, $\underset{\sim}{K}^{u}$. Upon consideration it was evident that the way in which the original B.E.M. equations are set up (i.e. evaluating the $\underset{\sim}{H}$ and $\underset{\sim}{G}$ matrices) involves an integration process around the boundary which is not symmetric, unless all elements are placed in such a way that they are all reflections of each other about some symmetry axis or plane. As such the starting equations are unsymmetric, and there is no reason to expect any final set of equations, based on these, to be exactly symmetric.

This explained the numerical reason for the lack of symmetry but immediately lead to questions relating to the general symmetry properties of a stiffness type relation. The current school of thought, generally expressed in the literature, was that due to the fundamental reciprocal theorems of elasticity (Maxwell's theorem, Betti's theorem), any stiffness type set of equations, relating nodal values of displacement and forces, should have symmetric coefficients, as does the classical Finite Element technique. As such the stiffness matrix $\underset{\sim}{K}^u$ is 'symmetrised' to form $\underset{\sim}{K}^s$. Several arguments are used to justify this, usually based on some 'error minimisation' or on a variational approach; but the 'symmetrisation' process always takes the form of discarding the unsymmetric part of $\underset{\sim}{K}^u$, by adding it to its transpose and taking the average value of all terms. This in fact was the technique implemented here, and examples were run comparing the behaviour of the two 'equivalent' stiffness matrices, $\underset{\sim}{K}^u$ and $\underset{\sim}{K}^s$. However, before we discuss the relative merits and behaviour of $\underset{\sim}{K}^u$ and $\underset{\sim}{K}^s$, some further discussion on the lack of symmetry of $\underset{\sim}{K}^u$ is warranted.

To facilitate further understanding of the lack of symmetry of $\underset{\sim}{K}^u$, the classical Finite Element Galerkin formulation, which does inherently produce symmetric matrices, was considered. (At this stage, it should be remembered that both the F.E.M. and B.E.M., - as well as other numerical techniques, such as Finite Differences - can all be derived from the same starting expression of the general Weighted Residual Technique - see Chapter 2). The differential equations of equilibrium are expressed in an integral form using the Weighted Residual Technique (also shown to be equivalent to the general statement of the Principle of Virtual Work), and this integral form always

contains terms which are products of the 'actual solution' and some 'weighting function'. In the classical Finite Element Galerkin approach, we interpret this 'weighting function' to be any virtual stress-strain-displacement field, and then make the assumption that this field has the same variation as the 'approximate' solution. It is this assumption that allows the same shape functions to be used for both fields, and this choice of identical shape functions is the fact that leads to symmetric matrices. There is however no reason why some other choice of shape functions cannot be made, still retaining the validity of the formulation.

When comparing this procedure to the B.E.M. formulation, we immediately see the discrepancy which destroys the symmetric properties of the final set of equations in the general case. With the B.E.M., we interpret the 'weighting function' of our original statement of equilibrium as a fundamental solution of the problem (thus eliminating the domain integral). This is of a fixed form and varies completely independently of the actual solution. Thus, the property of the method which leads to symmetric matrices in the Finite Element technique, is not exhibited in the Boundary Element formulation.

The lack of symmetry of $\underset{\sim}{K}^{u}$ is now well explained from numerical and analytical considerations. However, we are now faced with reconciling this lack of symmetry with the physical requirements imposed on the system by the fundamental reciprocal theorems of elasticity. This is easily done by considering the physical interpretation of the relevant terms. A stiffness relation (for the elasticity problems considered in this work) links a set of displacements to a set of nodal forces. These nodal forces are equivalent to some traction distribution and are obtained by the appropriate weighting of this traction distribution,

around the boundary. So, applying a nodal load of one, say, at any point does not physically represent a point source, but some localised traction distribution depending on the local geometry and shape functions. Therefore, by applying a load equal to one, say, at different points, the physical interpretation of the total loads applied, is the same, but the way in which these loads are distributed can be different. It is this difference in the physical interpretation of the exact form of the load state which does not allow the reciprocal theorems to be applied, and explains the lack of symmetry of $\underset{\sim}{K}^{u}$. (This is discussed in greater detail, with reference to an example in Chapters 5 and 6). The important point, however, is that as the physical magnitude of the load is the same, we do not expect the differences in its effect (especially at a distance) to be very marked; and thus do not expect the lack of symmetry of $\underset{\sim}{K}^{u}$ to be very pronounced. This is, in fact, the behaviour found when comparing results obtained using $\underset{\sim}{K}^{u}$ and $\underset{\sim}{K}^{s}$.

Chapter 4 describes several exaples, in 2 and 3 dimensions, using constant elements, and the results obtained using the symmetrised matrix $\underset{\sim}{K}^{s}$ were always close to the answers given by the B.E.M., for the same discretisation, and the degree of the differences were such as to make the use of $\underset{\sim}{K}^{s}$ quite acceptable for most engineering applications.

There are however situations when the tractions on the Boundary Element region surface obtained using $\underset{\sim}{K}^{s}$ can be misleading, especially in the following circumstances : If the solution for displacements is such that on a particular part of the surface of the Boundary Element region the magnitude of these displacements is of much lower order than the dominant terms of the solution, then these values will be much

more susceptable to numerical instability. It is the rate of change of these values which define the stresses in that region and if the errors are quite large in relation to their absolute values, then the errors in calculating the stresses can also be significant. However, this boils down to numerical problems involved in the solution of linear equations and in this context could warrant further investigation in its own right.

The behaviour of linear elements was also investigated, in Chapter 5, and their behaviour with regards to the symmetry properties of the 'equivalent' stiffness matrix, was found to be similar to the constant elements, used in the examples of Chapter 4. The important feature of the work presented in Chapter 5 is the way in which the discontinuity problem is dealt with. This problem arises at geometric discontinuities, where the tractions have different values either side of the node concerned. Additional equations are required for these points, in order to uniquely define the problem, and following the work of CHAUDONERRET [23], a technique was developed for dealing with this problem. It was found that the straight forward inclusion of any extra equations completely destroyed the 'almost' symmetric properties of $\underset{\sim}{K}^{u}$, although the solutions obtained were quite correct. A method for introducing these extra 'Corner Conditions' into the global system of equations was developed, which sets up these equations as a set of rotation matrices; these are then included in the overall formulation in a manner similar to the inclusion of a set of linearly dependent constraints on a Finite Element model.

The process is more complicated, as the 'Corner Condition' is expressed as a linear dependence of neighbouring displacements and tractions. The process involves a great deal of matrix multiplication; however, the rotation matrices contain a very large proportion of null terms, and the non-zero terms appear in positions well defined by the overall nodal numbering system. As such, specialised routines could be written, would take full advantage of this property, thus considerably reducing the computational effort involved.

The technique was implemented for several examples, and found to work very well. The solutions obtained using $\underset{\sim}{K}^{u}$ were almost the same as the standard B.E.M., for the same discretisation. The differences are attributable to numerical errors, which arise in the matrix manipulations involved. Upon symmetrisation, the solutions obtained using $\underset{\sim}{K}^{s}$ were also in good agreement, exhibiting small discrepancies, usually of the order of 3 - 5%.

An interesting general feature of the 'equivalent' stiffness approach is that the differences in the displacments obtained using $\underset{\sim}{K}^{u}$ and $\underset{\sim}{K}^{s}$ are greater for the displacment components which are of lesser magnitude (compared to the dominant values). This could be a numerical problem due to the differing orders of the terms in the solution.

Once the validity of the 'equivalent' stiffness approach had been demonstrated, several combination examples were run, which coupled a classical Galerkin Finite Element Displacement type model, with the 'equivalent' stiffness matrix, obtained using the Boundary Element formulation. The combination results were always in good agreement with the F.E.M. or B.E.M. results obtained using the same degree of discretisation.

Comparisons were also made of results using both $\underset{\sim}{K}^{u}$ and $\underset{\sim}{K}^{s}$, and any differences occurring due to the symmetrisation process were always found to again be of the order of 3 - 5% in the dominant terms.

A formulation for a 2-Dimensional half-space, loaded at the free surface was presented in Chapter 6, employing the Bousinesq fundamental solution, and performing the necessary intergrations analytically. Constant, Linear and Quadratic elements were used, and their behaviour with regards to symmetry properties of the 'equivalent' stiffness matrix thus formed, was found to be consistent with the previous work. The important feature of the formulation is that no numerical integration is necessary and that there is no interpolation of displacements on the surface. The governing factor, therefore, in the performance of each type of element is the degree to which the chosen interpolation for the surface tractions can adequately approximate the real loading. However, very little extra computation is necessary when employing the higher order elements, and as such their use is recommended.

In conclusion, the following areas are recommended for further investigation :

(i) The development and programming of higher order isoparametric elements, with the provision for corner discontinuities. This work does not indicate that any additional problems would arise in forming an 'equivalent' stiffness matrix using such elements, and their generally better performance would greatly improve the efficiency of the method.

(ii) The 2-Dimensional half-space solution presented in Chapter 6 could be generalised for influences acting in the criterior of the domain (i.e. using the Melan solution). This would of course necessitate the use of numerical integration procedures, but there is no reason to expect any additional problems in this case, and it would enable the application of the technique to a wider class of practical problems.

(iii) A general investigation into the numerical problems associated with solving large sets of linear equations could prove quite fruitfull. In certain cases such solutions are very sensitive, especially in situations where material properties differ significantly, producing ill-conditioned matrices. Also, there are situations where high stress concentrations occur at such interfaces and when using the approximate solution for displacements (obtained using $\underset{\sim}{K}^{s}$) to calculate the stresses at such an interface, significant errors may ensue. (see 6.4.1). For such cases it would be advisable to use the more 'exact' form of the 'equivalent' stiffness matrix, $\underset{\sim}{K}^{u}$, and in order to optimise the solution procedure, a partitioning scheme (see 6.5.1) should be built into the program.

Following the demonstration of the validity and applicability of the 'equivalent' stiffness formulation presented in this work, the algorithm may now readily be incorporated into standard finite element packages as an additional type of element in the library. This will enable great savings in the solution of problems, large parts of which are amenable to a boundary element treatment.

APPENDIX A

QUADRATIC INTERPOLATION FUNCTIONS, AND SOME USEFUL INTEGRALS

For a quadratic interpolation of a function over an element we require three nodes at which the value of the function is to be defined. A local system of coordinates (ξ) along the element length allow the problem to be non-dimensionalised. (See Figure A.1). The variation of a function, F, along the element may now be expressed in terms of its nodal values, F_i, $(i = 1, 2, 3)$.

$$F = \sum_{i=1}^{3} \Phi_i F_i \tag{A.1}$$

The following integrals will be useful:

$$\int_{-1}^{+1} \Phi_1 \, d\xi = \frac{1}{3} ; \quad \int_{-1}^{+1} \xi \, \Phi_1 \, d\xi = -\frac{1}{3}$$

$$\int_{-1}^{+1} \Phi_2 \, d\xi = \frac{1}{3} ; \quad \int_{-1}^{+1} \xi \, \Phi_2 \, d\xi = +\frac{1}{3} \tag{A.2}$$

$$\int_{-1}^{+1} \Phi_3 \, d\xi = \frac{4}{3} ; \quad \int_{-1}^{+1} \xi \, \Phi_3 \, d\xi = 0$$

When dealing with logarithmic functions the following integrals will appear.

$$I_1(a, b) = \int_{-1}^{+1} \ln(a + bx) \, dx \tag{A.3}$$

$$I_2(a, b) = \int_{-1}^{+1} x \ln(a + bx) \, dx \tag{A.4}$$

$$I_3(a, b) = \int_{-1}^{+1} x^2 \ln(a + bx) \, dx \tag{A.5}$$

where, a and b are constants.

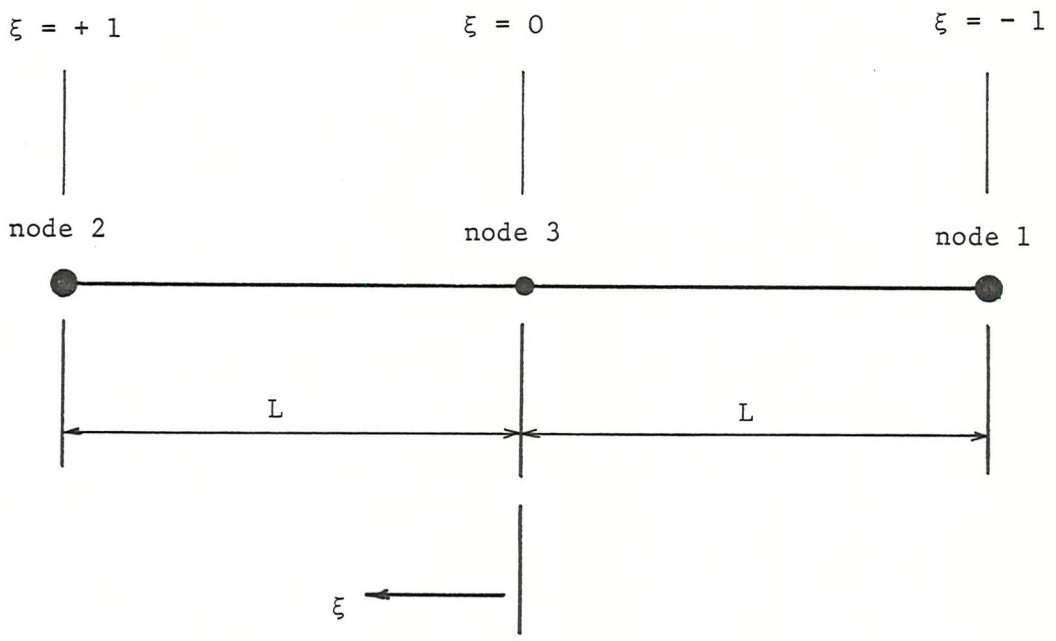

$$\phi_1 = \frac{1}{2}(\xi^2 - \xi)$$

$$\phi_2 = \frac{1}{2}(\xi^2 + \xi)$$

$$\phi_3 = (1 - \xi^2)$$

Figure A.1 Quadratic interpolation functions

These may readily be evaluated using integration by parts. The integrals are then given by:

$$I_1(a, b) = \left| \left(x + \frac{a}{b}\right) \ln(a + bx) - x \right|_{-1}^{+1}$$

$$I_1(a, b) = \left[\left(1 + \frac{a}{b}\right) \ln(a + b) + \left(1 - \frac{a}{b}\right) \ln(a - b) - 2 \right] \qquad (A.6)$$

$$I_2(a, b) = \left| \frac{1}{2}\left(x^2 - \frac{a^2}{b^2}\right) \ln(a + bx) - \frac{1}{2}\left(\frac{x^2}{2} - \frac{ax}{b}\right) \right|_{-1}^{+1}$$

$$I_2(a, b) = \left[\frac{1}{2}\left(1 - \frac{a^2}{b^2}\right) \ln\left(\frac{a+b}{a-b}\right) + \frac{a}{b} \right] \qquad (A.7)$$

$$I_3(a, b) = \left| \frac{1}{3}\left(x^3 + \frac{a^3}{b^3}\right) \ln(a + bx) - \frac{1}{3}\left(\frac{x^3}{3} - \frac{ax^2}{2b} + \frac{a^2x}{b^2}\right) \right|_{-1}^{+1}$$

$$I_3(a, b) = \frac{1}{3}\left[\left(1 + \frac{a^3}{b^3}\right) \ln(a + b) + \left(1 - \frac{a^3}{b^3}\right) \ln(a - b) - \frac{2a^2}{b^2} - \frac{2}{3} \right] \qquad (A.8)$$

When dealing with singular nodes, the following limiting cases of the integrals $I_i(a, b)$ $(i = 1, 2, 3)$ will appear.

$$\lim_{a \to L} I_i(a, \lambda L), \quad \lambda = \pm 1 \qquad (A.9)$$

These limits may readily be evaluated by differentiating the products in equations (A.6 - A.8) and applying L'Hopitals rule.

Consider $\lim_{a \to L} I_1(a, -L)$ $\quad (\lambda = -1)$

$$\lim_{a \to L} I_1(a, -L) = \lim_{a \to L} \left[\left(1 - \frac{a}{L}\right) \ln(a - L) + \left(1 + \frac{a}{L}\right) \ln(a + L) - 2 \right] \qquad (A.10)$$

using L'Hopitals rule on the first term

$$\lim_{a\to L}\left[\frac{\ln(a-L)}{\frac{L}{(L-a)}}\right] = \lim_{a\to L}\left[\frac{\frac{1}{(a-L)}}{\frac{L}{(L-a)^2}}\right] = \lim_{a\to L}\left[\frac{-1}{(L-a)}\,\frac{(L-a)^2}{L}\right] = 0 \qquad (A.11)$$

Hence,

$$\lim_{a\to L} I_1(a-L) = 2\,\ln(2L) - 2 \qquad (A.12)$$

The remaining integrals may be evaluated in the same manner, and the resulting values are:

$$\lim_{a\to L} I_1(a, \lambda L) = 2\,\ln(2L) - 2 \qquad (A.13)$$

$$\lim_{a\to L} I_2(a, \lambda L) = \lambda \qquad (A.14)$$

$$\lim_{a\to L} I_3(a, \lambda L) = \frac{1}{3}\left[2\,\ln(2L) - \frac{8}{3}\right] \qquad (A.15)$$

When the source (which produces a response given by the function, F), is at the centre of the element under consideration, additional integrals will appear.

$$I_4(L) = \int_0^1 \ln(Lx)\,dx$$

$$I_4(L) = \Big|x\,\ln(Lx) - x\Big|_0^1 \qquad (A.16)$$

$$I_4(L) = \left[\ln(L) - 1\right]$$

$$I_5(L) = \int_0^1 x\,\ln(Lx)\,dx$$

$$I_5(L) = \left|\frac{x^2}{2}\left(\ln(Lx) - \frac{1}{2}\right)\right|_0^1 \qquad (A.17)$$

$$I_5(L) = \frac{1}{2}\left[\ln(L) - \frac{1}{2}\right]$$

$$I_6(L) = \int_0^1 x^2 \ln(Lx)\, dx$$

$$I_6(L) = \frac{1}{3}\left[\ln(L) - \frac{1}{3}\right] \qquad (A.18)$$

APPENDIX B

THE MINDLIN FUNDAMENTAL SOLUTION

The formulas quoted here were originally derived by MINDLIN [7]. For more details on the solution's behaviour on implementation with the Boundary Element method, see NAKAGUMA [10].

The notation refers to Figure B.1.

$$r = (r_i r_i)^{\frac{1}{2}}$$

$$R = (R_i R_i)^{\frac{1}{2}}$$

$$r_i = Y_i - X_i$$

$$R_i = Y_i - X'_i$$

$$C = X_3 > 0$$

$$Z = Y_3 > 0$$

$$K_d = \frac{1 + \nu}{8\pi E(1-\nu)}$$

$$K_s = \frac{1}{8\pi(1-\nu)}$$

The fundamental displacements are given by:

$$u^*_{11} = K_d \left\{ \frac{3-4\nu}{r} + \frac{1}{R} + \frac{r_1^2}{r^3} + \frac{(3-4\nu)r_1^2}{R^3} + \frac{2CZ}{R^3}\left(1 - \frac{3r_1^2}{R^2}\right) + \right.$$

$$\left. + \frac{4(1-\nu)(1-2\nu)}{R + R_3}\left[1 - \frac{r_1^2}{R(R + R_3)}\right] \right\}$$

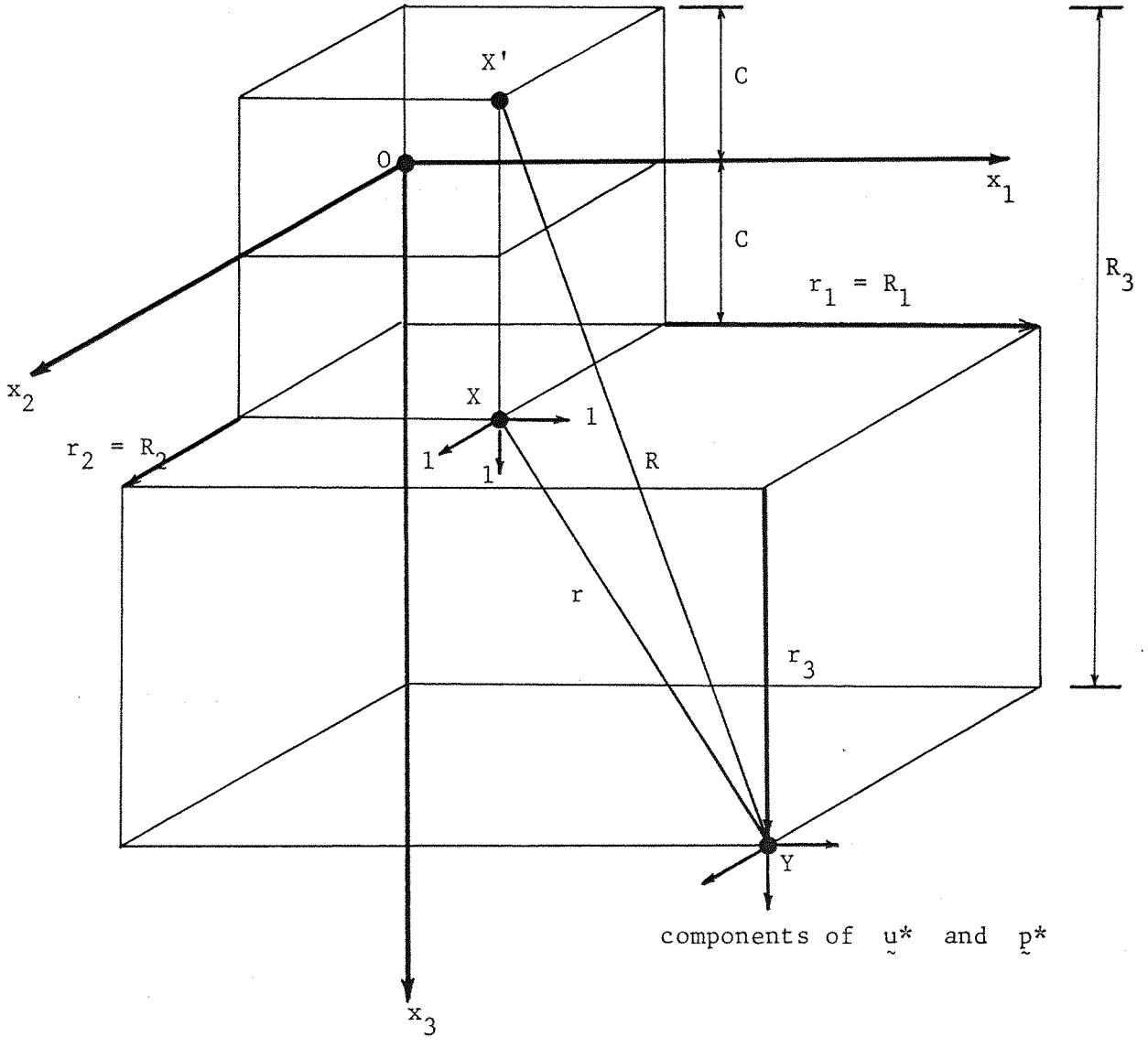

Ω : Semi-infinite space

X : load point

Y : field point

Figure B.1 Mindlin Fundamental Problem.

$$u^*_{12} = K_d r_1 r_2 \left\{ \frac{1}{r^3} + \frac{3-4\nu}{R^3} - \frac{6CZ}{R^5} - \frac{4(1-\nu)(1-2\nu)}{R(R+R_3)^2} \right\}$$

$$u^*_{13} = K_d r_1 \left\{ \frac{r_3}{r^3} + \frac{(3-4\nu)r_3}{R^3} - \frac{6CZR_3}{R^5} + \frac{4(1-\nu)(1-2\nu)}{R(R+R_3)} \right\}$$

$$u^*_{21} = u^*_{12}$$

$$u^*_{22} = K_d \left\{ \frac{3-4\nu}{r} + \frac{1}{R} + \frac{r_2^2}{r^3} + \frac{(3-4\nu)r_2^2}{R^3} + \frac{2CZ}{R^3} \left[1 - \frac{3r_2^2}{R^2} \right] + \right.$$

$$\left. + \frac{4(1-\nu)(1-2\nu)}{R+R_3} \left[1 - \frac{r_2^2}{R(R+R_3)} \right] \right\}$$

$$u^*_{23} = \frac{r_2}{r_1} u^*_{13}$$

$$u^*_{31} = K_d \, r_1 \left\{ \frac{r_3}{r^3} + \frac{(3-4\nu)r_3}{R^3} - \frac{4(1-\nu)(1-2\nu)}{R(R+R_3)} + \frac{6CZ \, R_3}{R^5} \right\}$$

$$u^*_{32} = \frac{r_2}{r_1} u^*_{31}$$

$$u^*_{33} = K_d \left\{ \frac{3-4\nu}{r} + \frac{8(1-\nu)^2 - (3-4\nu)}{R} + \frac{r_3^2}{r^3} + \frac{(3-4\nu)R_3^2 - 2CZ}{R \quad R^3} + \right.$$

$$\left. + \frac{6CZR_3^2}{R^5} \right\} \qquad \text{(B.1)}$$

The components of the fundamental tractions p^*_{ij} are given by:

$$p^*_{ij} = \sigma^{*i}_{jk}\, n_k \qquad (B.2)$$

where the index 'i' refers to the direction of the source load.

The expressions for the stresses σ^{*i}_{jk} are written below, so that the fundamental tractions p^*_{ij} can be evaluated using equation (B.2).

The fundamental stresses are given by:

$$\sigma^{*1}_{11} = K_s r_1 \left\{ -\frac{1-2\nu}{r^3} + \frac{(1-2\nu)(5-4\nu)}{r^3} - \frac{3r_1^2}{r^5} - \frac{3(3-4\nu)r_1^2}{R^5} + \right.$$

$$\left. - \frac{4(1-\nu)(1-2\nu)}{R(R+R_3)^2}\left[3 - \frac{r_1^2(3R+R_3)}{R^2(R+R_3)}\right] + \frac{6C}{R^5}\left[3C - (3-2\nu)R_3 + \frac{5r_1^2 Z}{R^2}\right]\right\}$$

$$\sigma^{*1}_{12} = K_s r_2 \left\{ -\frac{1-2\nu}{r^3} + \frac{1-2\nu}{R^3} - \frac{3r_1^2}{r^5} - \frac{3(3-4\nu)r_1^2}{R^5} + \right.$$

$$\left. - \frac{4(1-\nu)(1-2\nu)}{R(R+R_3)^2}\left[1 - \frac{r_1^2(3R+R_3)}{R^2(R+R_3)}\right] - \frac{6CZ}{R^5}\left[1 - \frac{5r_1^2}{R^2}\right]\right\}$$

$$\sigma^{*1}_{13} = K_s \left\{ -\frac{(1-2\nu)r_3}{r^3} + \frac{(1-2\nu)r_3}{R^3} - \frac{3r_1^2 r_3}{r^5} - \frac{3(3-4\nu)r_1^2 R_3}{R^5} + \right.$$

$$\left. - \frac{6C}{R^5}\left[ZR_3 - (1-2\nu)r_1^2 - \frac{5r_1^2 Z R_3}{R^2}\right]\right\}$$

$$\sigma^{*1}_{22} = K_s r_1 \left\{ \frac{1-2\nu}{r^3} + \frac{(1-2\nu)(3-4\nu)}{R^3} - \frac{3r_2^2}{r^5} - \frac{3(3-4\nu)r_2^2}{R^5} + \right.$$

$$\left. - \frac{4(1-\nu)(1-2\nu)}{R(R+R_3)^2}\left[1 - \frac{r_2^2(3R+R_3)}{R^2(R+R_3)}\right] + \frac{6C}{R^5}\left[C - (1-2\nu)R_3 + \frac{5r_2^2 Z}{R^2}\right]\right\}$$

$$\sigma^{*1}_{23} = K_s r_1 r_2 \left\{ - \frac{3r_3}{r^5} - \frac{3(3-4\nu)R_3}{R^5} + \frac{6C}{R^5}\left[1-2\nu + \frac{5ZR_3}{R^2}\right]\right\}$$

$$\sigma^{*1}_{33} = K_s r_1 \left\{ \frac{1-2\nu}{r^3} - \frac{1-2\nu}{R^3} - \frac{3r_3^2}{r^5} - \frac{3(3-4\nu)R_3^2}{R^5} + \right.$$

$$\left. + \frac{6C}{R^5}\left[C + (1-2\nu)R_3 + \frac{5ZR_3^2}{R^2}\right]\right\}$$

$$\sigma^{*2}_{11} = K_s r_2 \left\{ \frac{1-2\nu}{r^3} + \frac{(1-2\nu)(3-4\nu)}{R^3} - \frac{3r_1^2}{r^5} - \frac{3(3-4\nu)r_1^2}{R^5} + \right.$$

$$\left. - \frac{4(1-\nu)(1-2\nu)}{R(R+R_3)^2}\left[1 - \frac{r_1^2(3R+R_3)}{R^2(R+R_3)}\right] + \frac{6C}{R^5}\left[C - (1-2\nu)R_3 + \frac{5r_1^2 Z}{R^2}\right]\right\}$$

$$\sigma^{*2}_{12} = K_s r_1 \left\{ - \frac{1-2\nu}{r^3} + \frac{1-2\nu}{R^3} - \frac{3r_2^2}{r^5} - \frac{3(3-4\nu)r_2^2}{R^5} + \right.$$

$$\left. - \frac{4(1-\nu)(1-2\nu)}{R(R+R_3)^2}\left[1 - \frac{r_2^2(3R+R_3)}{R^2(R+R_3)}\right] - \frac{6CZ}{R^5}\left[1 - \frac{5r_2^2}{R^2}\right]\right\}$$

$$\sigma^{*2}_{13} = \sigma^{1}_{23}$$

$$\sigma^{*2}_{22} = K_s r_2 \left\{ -\frac{(1-2\nu)}{r^3} + \frac{(1-2\nu)(5-4\nu)}{R^3} - \frac{3r_2^2}{r^5} - \frac{3(3-4\nu)r_2^2}{R^5} + \right.$$

$$\left. - \frac{4(1-\nu)(1-2\nu)}{R(R+R_3)^2}\left[3 - \frac{r_2^2(3R+R_3)}{R^2(R+R_3)}\right] + \frac{6C}{R^5}\left[3C - (3-2\nu)R_3 + \frac{5r_2^2 Z}{R^2}\right]\right\}$$

$$\sigma^{*2}_{23} = K_s \left\{ -\frac{(1-2\nu)R_3}{r^3} + \frac{(1-2\nu)R_3}{R^3} - \frac{3r_2^2 r_3}{r^5} - \frac{3(3-4\nu)r_2^2 R_3}{R^5} + \right.$$

$$\left. - \frac{6C}{R^5}\left[ZR_3 - (1-2\nu)\, r_2^2 - \frac{5r_2^2 Z R_3}{R^2}\right]\right\}$$

$$\sigma^{*2}_{33} = \frac{r_2}{r_1}\,\sigma^{*1}_{33}$$

$$\sigma^{*3}_{11} = K_s \left\{ \frac{(1-2\nu)r_3}{r^3} - \frac{3r_1^2 r_3}{r^5} + \frac{(1-2\nu)(3r_3 - 4\nu R_3)}{R^3} + \right.$$

$$- \frac{3(3-4\nu)r_1^2 R_3 - 6CR_3\left[(1-2\nu)Z - 2\nu C\right]}{R^5} - \frac{30Cr_1^2 Z R_3}{R^7} +$$

$$\left. - \frac{4(1-\nu)(1-2\nu)}{R(R+R_3)}\left|1 - \frac{r_1^2}{R(R+R_3)} - \frac{r_1^2}{R^2}\right|\right\}$$

$$\sigma^{*3}_{12} = K_s r_1 r_2 \left\{ -\frac{3r_3}{r^5} - \frac{3(3-4\nu)r_3}{R^5} + \frac{4(1-\nu)(1-2\nu)}{R^2(R+R_3)}\left(\frac{1}{R+R_3} + \frac{1}{R}\right) + \right.$$

$$\left. - \frac{30CZR_3}{R^7}\right\}$$

$$\sigma^{*3}_{13} = K_s r_1 \left\{ -\frac{1-2\nu}{r^3} + \frac{1-2\nu}{R^3} - \frac{3r_3}{r^5} - \frac{3(3-4\nu)ZR_3 - 3C(3Z + C)}{R^5} + \right.$$

$$\left. - \frac{30CZR_3^2}{R^7} \right\}$$

$$\sigma^{*3}_{22} = K_s \left\{ \frac{(1-2\nu)r_3}{r^3} - \frac{3r_2^2 r_3}{r^5} + \frac{(1-2\nu)(3r_3 - 4\nu R_3)}{R^3} + \right.$$

$$- \frac{3(3-4\nu)r_2^2 r_3 - 6CR_3\left[(1-2\nu)Z - 2\nu C\right]}{R^5} - \frac{30Cr_2^2\, ZR_3}{R^7} +$$

$$\left. - \frac{4(1-\nu)(1-2\nu)}{R(R + R_3)} \left\{ 1 - \frac{r_2^2}{R(R + R_3)} - \frac{r_2^2}{R^2} \right\} \right\}$$

$$\sigma^{*3}_{23} = K_s r_2 \left\{ -\frac{1-2\nu}{r^3} + \frac{1-2\nu}{R^3} - \frac{3r_3^2}{r^5} - \frac{3(3-4\ )ZR_3 - 3C(3Z + C)}{R^5} + \right.$$

$$\left. - \frac{30CZR_3^2}{R^7} \right\}$$

$$\sigma^{*3}_{33} = K_s \left\{ -\frac{(1-2\nu)r_3}{r^3} + \frac{(1-2\nu)r_3}{R^3} - \frac{3r_3^3}{r^5} + \right.$$

$$\left. - \frac{3(3-4\nu)ZR_3^2 - 3CR_3(5Z-C)}{R^5} - \frac{30CZR_3^3}{R^7} \right\} \qquad \text{(B.3)}$$

REFERENCES

[1] TIMOSHENKO, S., 'Theory of Elasticity'. (New York, 1934).

[2] LOVE, A.E.H., 'Teatise on the Mathematical Theory of Elasticity', 1944.

[3] FUNG Y.C. 'Foundations of Solid Mechanics', Prentic Hall, 1965.

[4] BREBBIA,C.A., and WALKER, S., 'Introduction to Boundary Element Methods', published in [21].

[5] BREBBIA., 'The Boundary Element Method for Engineers' Pentech Press, 1978.

[6] FINLAYSON, B.A. 'The Method of Weighted Residuals and Variational Principles'. Academic Press (1972).

[7] MINDIN, R.D., 'Force at a Point in the Interior of a Semi-infinite Solid', in 'Journal of Applied Physics', Vol. 7. (1936).

[8] CRUSE, T.A. 'Application of the Boundary Integral Equation Solution Method in Solid Mechanics', published in [17], Vol. 2.

[9] TOTTENHAM, H., BREBBIA, C.A., 'Finite Element Techniques in Structural Mechanics', Hobbs, 1970.

[10] NAKAGUMA, R.K., 'Three Dimensional Elastostatics using the Boundary Element Method', Ph.D. thesis, Southampton University, 1979.

[11] BREBBIA, C.A., 'Weighted Residual Classification of Approximate Methods'. Applied Mathematical Modelling, Vol. 2, No.3, September, 1978.

[12] BREBBIA, C.A., WALKER, S., 'General Formulation of Approximating Techniques in Engineering Sciences'. Chapter in the Book 'System STructures in Engineering'. Tapir, Trondheim, 1978.

[13] CRUSE, T.A., 'Numerical Solutions in three Dimensional Elastostatics', Int. J. Solids Structure, Vol. 5, 1969.

[14] MELAN, E., 'Der Spannugszustand der Durch eine Einzelkraft im Innern Beanspruchten Halbscheibe', Zeits. f. angew. Math. und Mech. 12, 1932.

[15] FLAMANT., 'Compt. Rend., Vol. 114, p. 1465, Paris, 1892.

[16] BOUSSINESQ., 'Conpt. Rend., Vol. 114, p. 1510, Paris,1892.

[17] BREBBIA, C.A., TOTTENHAM, H., (Editors), 'Variational Methods in Engineering', Southampton University Press, 1972.

[18] BREBBIA, C.A. (Editor), Recent Advances in Boundary Element Methods, Pentech Press, 1978.

[19] ZIENKIEWICZ, O.C. 'The Finite Element Method', 3rd Edition, McGraw-Hill.

[20] BREBBIA, C.A., CONNOR, J.J., 'Fundamentals of Finite Element Techniques for Structural Engineers', Butterworths, 1973.

[21] BREBBIA, C.A., (Editor) 'Recent Advances in Boundary Element Methods', Pentech Press, 1978.

[22] MUSTOE, G., 'A Symmetric Boundary Integral Equation Method for Two-Dimensional Elastostatics', to be published.

[23] CHAUDONNERET, M., 'On the Discontinuity of the Stress Vector in the Boundary Integral Equation Method for Elastic Analysis', published in [21].

[24] BREBBIA, C.A., GEORGIOU, P., 'Combination of Boundary and Finite Elements in Elastostatics', Applied Mathematical Modelling, Vol. 3. June, 1979.

[25] WARDLE, L.J., CROTTY, J.M., 'Two Dimensional Boundary Integral Equation Analysis for Non-Homogeneous Mining Applications'. Published in [21].

[26] LACHAT, J.C., WATSON, J.O., 'Progress in the use of Boundary Integral Equations, Illustrated by Examples', Computer Methods in Appl. Mech. and Eng., 10, North Holland Publ. Co., 1977.

[27] WATSON, J.O., 'The Solution of Boundary Integral Equations of Three-Dimensional Elastostatics for Infinite Regions', in [7], 1978.

[28] CRUSE, T.A., 'An Improved Boundary-Integral Equation Method for Three Dimensional Elastic Stress Analysis', Computers and Structures, Vol. 4, pp. 741-754; Pergamon Press 1974.

[29] ZIENKIEWICZ, KELLY, BETTESS, 'The Coupling of the Finite Element Method and Boundary Solution Procedures', in International Journal for Numerical Methods in Engineering', Vol. 11, pp. 355-375, 1977.

[30] ZIENKIEWICZ, O.C., 'The Finite Element Method', Chapter 23, 3rd Edition, McGraw-Hill.

[31] ZIENKIEWICZ, KELLY, BETTESS, 'Mariage a la Mode", Finite Elements and Boundary Integrals', in Proc. Conf. Innovative Numerical Analysis in Engineering Science, CETIM, Paris, 1977.

[32] SILVESTER, P., HSIEH, M.S., 'Projective Solution of Integral Equations Arising in Electric and Magnetic Field Problems', J. Comp. Phys., Vol. 8. pp. 73-82 (1971).

[33] WATSON, J.O. 'Advanced Implementation of the Boundary Element Method for 2 and 3-Dimensional Elastostatics', published in [35], Chapter 3.

[34] RIZZO, F.J., 'An Integral Equation Approach to Boundary Value Problems of Classical Elastostatics', Quart. Appl. Math., 25, pp. 83-95, 1967.

[35] BANERJEE, P.K., BUTTERFIELD, R., (Editors) 'Developments in Boundary Element Methods - 1', Applied Science Publishers Ltd., 1979.

[36] KELLY, D.W., MUSTOE, G.G.W., ZIENKIEWICZ, O. C., 'Coupling Boundary Element Methods with other Numerical Methods', published in [35], Chapter 10.

[37] ABRAMOWITZ, M., STEGUN, I.A., 'Handbook of Mathematical Functions', Dover Publications, New York, 1965.

[38] VASILOPOULOS, D., 'A Finite Element Package for Medium Size Systems', M.Sc. thesis, Southampton University, 1979.

[39] TOTTENHAM, H., 'Boundary Element Methods - A General Introduction', Course Notes - Boundary Element Methods, Southampton, September, 1977.

[40] CRUSE, T.A., and RIZZO, F.J., (eds), 'Boundary Integral Equation Method : Computational Applications in Applied Mechanics', AMD-Vol. 11, ASME, NYC., 1975.

[41] ZIENKIEWICZ, O. C., and CHUNG, Y.K., 'Finite Elements in the Solution of Field Problems', The Engineer, Vol. 220, pp. 507-510, 1965.

[42] FUSCO, F.B. Jr., 'A Unified Formutation of the Finite and Boundary Element Methods, Starting by the Energy Method' - (to be published).

[43] GEORGIOU, P., 'The Combination of Finite and Boundary Elements', M.Sc. thesis, Southampton University, 1977.

[44] GEORGIOU, P., and BREBBIA, C.A., 'On the Symmetry of an 'Equivalent' Stiffness Formulation, Based on the Direct Boundary Element Method'. (To be published).

[45] CRUSE, T.A., and RIZZO, F.J., 'A Direct Formulation and Numerical Solution of the General Transient Elastodynamic Problem' - I.J. Math. Analysis Applic. Vol. 22. pp. 244, 1968.

[46] KUPRADZE, V.D. 'Potential methods in the theory of elasiticity', (1965) D. Davey.

[47] MUSKHELISHVILI, N.I. 'Singualr integral equations', Noordoff, Groningen, 1953.

[48] LACHAT, J.C. 'Further development of boundary integral techniques for elastostatics', Ph.D. Thesis, Southampton University, 1975.

[49] MUSTOE, G.G.W., 'Symmetric variational boundary integral and finite element procedures in continuum mechanics'. Thesis, University of Wales, Swansea, 1980.

[50] SOMIGLIANA, C. 'Sopra l'equillibrio di un corpo elastico isotropo'; 1885.

[51] BREBBIA, C.A., and BUTTERFIELD, R. 'Formal equivalence of direct and indirect boundary element methods', Appl. Math. Modelling, 1978, 2, 132.

[52] SHAW, R.P. 'Coupling boundary integral equation method to other numerical techniques'. Int. Symp. on recent advances in boundary element methods, Southampton, July, 1978.

[53] SHAW, R.P. and FALBY, W. 'FEBIE - A combined finite element - boundary integral equation approach', CETIM, Senlis, France, pp. 1. 97-1.101. Also, 'Computers and Fluids', (1978) Vol. 6, (1978)., pp. 153-60.

BIBLIOGRAPHY

BREBBIA, C.A., and NAKAGUMA, R., 'Boundary Elements in stress analysis', J. Eng. Mech. Div., Feb. 1979.

BREBBIA, C.A. and DOMINGUEZ, J., "Application of the Boundary Element Method for Potential Problems," Applied Mathematical Modelling, Vol. 1, No.7, 1977.

BUTTERFIELD, R. 'The Application of the integral equation methods to continuum problems in soil mechanics', Stress-strain behaviour of soils, Roscoe Memorial Symposium, Cambridge, Poulis, pp.573-587, (1972).

BUTTERFIELD, R. and BANERJEE, P.K. 'The elastic analysis of compressible piles and pile groups', Geotechnique, Vol. 21, (No. 1), Vol. 21, (No. 1), pp.43-60, 1971.

BUTTERFIELD, R. and TOMLIN, G.R. 'Integral techniques for solving zoned anisotropic continuum problems', Int. Conf. Var. Meth. in Engng. Southampton, (9), pp. 31-51, 1972.

TOMLIN, G.R. 'Numerical analysis of continuum problems in zoned anisotropic media', Ph.D. Thesis, Southampton University, 1973.

SYMM, G.T. 'Integral equation methods in potential theory II' Proc. Roy. Soc. (A), Vol. 275, pp.33-46, 1963.

SYMM, G.T. 'Integral equation methods in elasticity and potential theory', Ph.D. Thesis, Imperial College, University of London,1964.

TELLES, J.C.F. and BREBBIA, C.A. 'The boundary element method in plasticity', Int. Symp. on new developments in boundary elements, Southampton, March, 1980.

JASWON, M.A. 'Integral equation methods in potential theory I', Proc. Roy. Soc. (A), Vol. 275, pp.23-32. 1965.

JASWON, M.A. and SYMM, G.T. 'Integral equation methods in potential theory and elastostatics', Academic Press, 1977.

CRUSE, T.A. 'Mathematical foundations of the boundary integral equation method in solid mechanics', Report by Pratt and Whitney Aircraft Group, United Technologies Corp., East Hartford, Connecticut, PWA-5539. Prepared for the U.S. Airforce Office of Scientific Research, 1977.

WEXLER, A. 'Some applications of boundary element method to electrical engineering', Int. Symp.on recent advances in boundary element methods, Southampton, July, 1978.

RIZZO, F.J. 'An integral equation approach to boundary value problems of classical elastostatics', Quart. Appl. Math., Vol. 25, No.1. 1967.

MENDELSON, A. and ALBERS, L.V. 'Application of boundary integral equation method to elastoplastic problems', Proc. A.S.M.E. Conf. on Boundary integral equation methods, A.M.D., Vol. 11, Eds. Cruse, T.A. and Rizzo, F.J., New York. 1975.

ZIENKIEWICZ, O.C. 'The finite element method and boundary solution procedures as general approximation methods for field problems', Proc. of the World Cong. on Finite Element Methods in Struct. Mech., Bournemouth, 1975.

RICARDELLA, P. 'An implementation of the boundary integral technique, for planar problems of elasticity and elastoplasticity', Ph.D. Thesis, Carnegie Mellon University, Pittsburg, U.S.A., 1973.

ARGYRIS, J.H. 'Energy theorems and structural analysis', Butterworth (reprinted from Aircraft Eng., 1954-55). (1960).

CRUSE, T.A. and WILSON, R.B. 'Advanced applications of boundary integral equation methods', Nucl. Eng. Des., Vol. 46, pp.223-234.

CRUSE, T.A., SNOW, D.W. and WILSON, R.B. 'Numerical solutions and axisymmetric elasticity', Computers and Structures, Vol. 7, pp.445-451, (1977).

CRUSE, T.A. 'Application of the boundary integral equation method to 3-D stress analysis', J. Comp. Struct. Vol. 3, pp.509-27, 1973.

McDONALD, B.H., FRIEDMAN, M. and WEXLER, A. 'Variational Solution of integral equations', IEEE Trans. Microwave Theory and TEchniques, MTT-22, pp.237-48,1974.

FREDHOLM, I. 'Sur un classe d'equations fonctionelles', Acta Math., Vol. 27, pp.365-390, 1903.

BREBBIA, C.A. and WALKER, S. 'Simplified boundary elements for radiation problems', Appl. Math. Modelling, Vol. 2., pp. 135-137. (Short note), 1978.

MIKHLIN,S.G. 'Multidimensional singular integrals and integral equations', Pergamon Press, 1965.

TOMLIN, G.R.and BUTTERFIELD, R. 'Elastic analysis of zoned orthotropic continua', Proc., A.S.C.E. Mech. Div. EM3, pp.511-529, 1974.

MIKHLIN, S.G. 'Variational Methods in Mathematical Physics', Macmillan, New York, 1964.

SHAW, R.P. 'An integral equation qpproach to acoustic radiation and scattering', In : Topics in Ocean Engineering II, Ed. C. Bretschneider, Gulf Publ. Co., Houston, Texas, pp.143-163, 1970.

SHAW, R.P. 'Boundary integral equation methods applied to water waves', In : Boundary Integral Equation Method - Computational Applications in Applied Mechanics, Eds. T. Cruse and F. Rizzo, AMD Vol. 11, ASME, N.Y.C., pp. 7-14, 1975.

RIZZO, F.J. and SHIPPY, D.J. 'An advanced boundary integral equation method for three dimensional thermoelasticity', Dept. Engineering Mechanics, University of Kentucky, Internal Report, 1977.

BREBBIA, C.A., and CHANG, O.V., 'Boundary elements applied to seepage problems in zoned anisotropic soils', Adavance in Eng. Soft. Vol. 1, No.3, 1979.

TELLES, J.C.F., and BREBBIA, C.A., 'On the application of the boundary element method to plasticity'. Appl. Math. Modelling, Vol.3, Dec, 1979.